Year : 2020

Genetics of IDDCA syndrome

De Nittis Pasquelena

UNIL | Université de Lausanne
Faculté de biologie
et de médecine

Centre Intégratif de Génomique

Genetics of IDDCA syndrome

Thèse de doctorat ès sciences de la vie (PhD)

présentée à la

Faculté de biologie et de médecine
de l'Université de Lausanne

par

Pasquelena DE NITTIS

Diplômé en Biotechnologie Médicale à l'Université de Bologna, Italie, 2013

Jury

Prof. Robinson-Rechavi Marc, Président
Prof. Alexandre Reymond, Directeur de thèse
Prof. Jacques Beckmann, Expert
Prof. Frank Kooy, Expert

Lausanne 2020

UNIL | Université de Lausanne
Faculté de biologie
et de médecine

Centre Intégratif de Génomique

Genetics of IDDCA syndrome

Thèse de doctorat ès sciences de la vie (PhD)

présentée à la

Faculté de biologie et de médecine
de l'Université de Lausanne

par

Pasquelena DE NITTIS

Diplômé en Biotechnologie Médicale à l'Université de Bologna, Italie, 2013

Jury

Prof. Robinson-Rechavi Marc, Président
Prof. Alexandre Reymond, Directeur de thèse
Prof. Jacques Beckmann, Expert
Prof. Frank Kooy, Expert

Lausanne 2020

UNIL | Université de Lausanne
Faculté de biologie et de médecine

Ecole Doctorale
Doctorat ès sciences de la vie

Imprimatur

Vu le rapport présenté par le jury d'examen, composé de

Président·e	Monsieur	Prof.	Marc	**Robinson-Rechavi**
Directeur·trice de thèse	Monsieur	Prof.	Alexandre	**Reymond**
Expert·e·s	Monsieur	Prof.	Jacques	**Beckmann**
	Monsieur	Prof.	Frank	**Kooy**

le Conseil de Faculté autorise l'impression de la thèse de

Madame Pasquelena De Nittis

Master of Science in medical biotechnology, Università degli Studi di Bologna, Italie

intitulée

Genetics of IDDCA syndrome

Lausanne, le 28 février 2020

pour le Doyen
de la Faculté de biologie et de médecine

Prof. Marc Robinson-Rechavi

Acknowledgments

I found myself rewinding the tape of this 5-year-long journey, and I depicted it as a feature film where I have not been the only protagonist; it could not have been achieved without a good script, a worthy director and without the other actors, all playing a very important role.

I would like to start this piece of acknowledgments by thanking Jacques Beckman and Frank Kooy for accepting to be part of the jury who will evaluate my work and for finding the time to be at my PhD defense. I am grateful for the encouragement, insightful comments and fruitful discussion we exchanged in the occasions we had to meet. I thank the Faculty of Biology and Medicine, and Marc Robinson-Rechavi for presiding this evaluation committee.

A special thank goes to my Thesis Director, Prof. Alexandre Reymond, who convincingly offered me guidance and trust. From the time I started to the end, he has always been there providing me challenges, as well as opportunities to grow and improve myself. He encouraged me to be professional and do the right thing even when the road got tough. I am extremely thankful to this wonderful person and master of life who taught me – scientifically and non - in every conversation we had.

I wish to thank all the people whose assistance was a milestone in the completion of this project.

Foremost, I feel to thank every single person of the Reymond's group, present and past members, (and Nico, Adriana, and Mariana) that made my journey unforgettable. I am proud to have been part of the group. Thanks for having opened my horizon and for giving me the opportunity to learn a lot from each of you. In particular, my thanks have to be addressed to: Eleonora (Ele), Giuliana (Giuli), Adriana (Adri), and Nicolas (Nico).
Ele, thank you for your overwhelming enthusiasm, for the patience in explaining the difficult and incomprehensible (to me) scripts I had to face with, for sharing your statistical knowledge and visions. Thanks for the car rides with the *Topotaxi*, and more importantly for being a friend, before than a colleague. Even when somebody literally tried to hit us, we have always been there for each other and ready to be a Cric&Croc sparkling duo having crazy ideas and lots of fun.
Giuli, the two of us have shared the 3039 office since my arrival, you have been the constant presence in these 5 years. Thank you for having been there, in the beautiful days and in the difficult ones, for the professional and non-professional discussions, for your competence, for having involved me in your projects and for having stimulated my scientific inspiration. Thank you for the time we shared outside the lab; I am sure that you will always be part of the circle of people that I wish to have alongside - after all, Milan is not so far away.
Adri, Nico, I had the privilege of overlapping with you for a limited amount of time during this journey. The amount of commitment, expertise, and efficiency but also of joy, positivity, and friendship that you have been able to convey are invaluable to me. Not just colleagues, but friends of the lab 3039 (plus Ele).
Once, I read that "*Nella vita ti renderai conto che c'è una ragione per tutti quelli che incontrerai. Alcuni ti metteranno alla prova, altri ti utilizzeranno e pochi ti insegneranno qualcosa. Ma i più importanti saranno quelli che tireranno fuori il meglio di te, rispettandoti ed accettandoti per quello che sei. Questi sono quelli che vale la pena tenere come amici.*" Grazie a voi quattro per aver tirato fuori il meglio di me in questo periodo!

Thanks to the Secretaries, and to the facilities for their willingness to share assistance, competences, enthusiasm, and that in some cases "forced" me to learn a bit of French. It has been amazing to be part of the CIG community.

Last, but not least, I wish to acknowledge the support and great love of my family, my brother and my nephews, my boyfriend, Filippo and his family, my Italian friends Martina, Serena, Maria, Wanda, Marianna, and Rossana, among the many, and Iris and Nicla. They kept me going on and this work would not have been possible without their input.

Content

Abstract (English)

Genetics of IDDCA syndrome

Pasquelena De Nittis, PhD student in the lab of Professor Alexandre Reymond, Center for Integrative Genomics, University of Lausanne

Intellectual disability (ID) is a complex neurodevelopmental disorder involving intellectual and adaptive functioning. With a frequency of 1-3% in the general population, this disorder is highly heterogeneous in terms of clinical manifestations and etiology. Hundreds of different genes have been associated with ID; the recent discovery of rare genetic variants in genes encoding the G-protein β subunits, and associated to genetic disorders with variable brain and heart involvement, has expanded the repertoire of causal genes involved in neurodevelopmental conditions. G-protein β subunits, together with α and γ subunits constitute the heterotrimeric G-proteins, molecular switches that mediate key signal transduction cascades. They associate with G-protein-coupled receptors (GPCRs) and modulate essential cellular functions involved, among others, in neuronal communication and homeostatic regulation of multiple organs, through mediation of the antagonistic effects of the autonomic nervous system branches.

During my doctorate, we identified the genetic cause responsible for the phenotype of patients presenting with a new syndrome characterized by ID, early-onset sinus node dysfunction, hypotonia, seizures and retinopathy. We reported that bi-allelic germline mutations in *GNB5* (Gβ5) cause this ultra-rare Intellectual Developmental Disorder with Cardiac Arrhythmia syndrome (IDDCA, MIM #617173). After the description of the first patients, other and we reported additional cases, enlarging the IDDCA cohort to a total of 33 ascertained individuals. Despite the paucity of patients, genotype-phenotype correlation shows that homozygous or compound heterozygous missense variants are associated with an attenuated phenotype with mild ID and sinus node dysfunction, while homozygous null alleles cause severe ID, epileptic encephalopathy, hypotonia and sinus node dysfunction. We engineered *gnb5* knockout zebrafish and found that they showed impaired swimming activity, abnormal ocular response, and reduced heart rate, thus recapitulating IDDCA clinical manifestations. Additionally, we characterized the cardiac manifestation of the *Gnb5* knockout (*Gnb5*$^{-/-}$) mouse model. We observed that these mice had a smaller heart, a feature compensated by increased contractile capacities. Concordantly, we detected modified expression levels of genes involved in muscle contraction. We also unearthed a higher number of sinus arrhythmias in *Gnb5*$^{-/-}$ animals that presented an enhanced parasympathetic stimulation, resulting in strong bradycardia.

A hallmark of GNB5 is its ability to form complexes with members of the R7 group of regulators of G-protein signaling (RGS). Overall, these data reveal that lack of GNB5 destabilizes the corresponding GNB5-RGS macromolecular complex with ion channels (e.g. the G protein-coupled inwardly rectifying potassium channels) involved in the GPCR-mediated autonomic nervous system activities.

Résumé (Français)

La génétique du syndrome IDDCA

Pasquelena De Nittis, doctorante dans le laboratoire du Professeur Alexandre Reymond,
Centre Intégratif de Génomique de l'Université de Lausanne

La déficience intellectuelle (DI) est un trouble du neurodéveloppement impliquant une altération du fonctionnement cognitif et adaptatif. Avec une fréquence de 1-3% dans la population générale, ce trouble est très hétérogène dans son étiologie et ses manifestations cliniques. Des centaines de gènes différents ont été associés à la DI; la découverte récente de variantes génétiques rares dans des gènes codant pour les sous-unités β de la protéine G a élargi le répertoire des gènes associés. Les sous-unités β, ainsi que les sous-unités α et γ, constituent les protéines G, qui assurent la médiation des cascades de transduction de signaux. Ils s'associent aux récepteurs couplés aux protéines G (GPCR) et modulent les fonctions cellulaires impliquées dans la communication neuronale et la régulation homéostatique de nombreux organes, par modulation des effets antagonistes du système nerveux autonome. Pendant mon doctorat, nous avons identifié la cause génétique de nouveau syndrome caractérisé par une DI, un dysfonctionnement précoce du nœud sinusal, une hypotonie, des convulsions et une rétinopathie. Nous avons démontré que des mutations germinales dans le gène *GNB5* (Gβ5) provoquent ce syndrome nommé «Intellectual Developmental Disorder with Cardiac Arrhythmia» (IDDCA, MIM # 617173). Après la description des premiers patients, nous et d'autres laboratoires avons découverts des cas supplémentaires, élargissant la cohorte IDDCA à 33 individus au total. La corrélation génotype-phénotype montrent que les variantes faux sens homozygotes ou hétérozygotes composites sont associés à un phénotype atténué du syndrome avec une légère DI et un dysfonctionnement du nœud sinusal, tandis que les porteurs d'allèles nuls homozygotes présentent une DI sévère, une encéphalopathie épileptique, une hypotonie et un dysfonctionnement cardiaque. Nous avons créé un poisson zèbre knockout pour *gnb5* et avons constaté qu'il présentait une altération de l'activité natatoire, une réponse oculaire anormale et une fréquence cardiaque réduite, des symptômes qui rappellent les manifestations cliniques du IDDCA syndrome. Nous avons caractérisé les phénotypes cardiaques de la souris *Gnb5* knockout (*Gnb5*$^{-/-}$). Nous avons observé que ces souris avaient un cœur plus petit que leurs consœurs et des capacités contractiles accrues, en accord avec une expression modifiée des gènes impliqués dans la contraction musculaire. Nous avons aussi découvert un nombre plus élevé d'arythmies sinusales chez les animaux *Gnb5*$^{-/-}$. Ils présentaient une stimulation parasympathique améliorée, entraînant une forte bradycardie. La protéine GNB5 à la capacité de former des complexes avec des membres du groupe R7 de régulateurs de la signalisation des protéines G (RGS). Dans l'ensemble, ces données révèlent que la perte de GNB5 déstabilise les complexes macromoléculaires GNB5-RGS avec des canaux ioniques (p. ex., les canaux potassiques rectificateurs couplés aux protéines G) impliqués dans les activités du système nerveux autonome médiées par le GPCR.

Introduction

1. Genome, genetic variation and genetic disease

The genome represents the complete set of hereditary material (DNA) present in all nucleated cells of an organism. Human genomes consist among others of both protein coding-DNA (genes) and non-coding DNA sequences (e.g. unstranslated regions at the end of the genes, intronic regions within genes, and intergenic regions between genes), as well as mitochondrial DNA. The genome of each individual is different due to variations occurring in the DNA sequence, named *genetic variation*, and making each individual's genome unique. Whereas most of these differences between individual human genomes seem to have no effect, other differences affect the phenotype, the disease state and/or the disease risk. There are different sources through which genetic variation is introduced, some of these being errors during DNA replication, environmental DNA damage, independent segregation and crossing over.

Genetic variations can be classified as large- or small-scale on the basis of their size. Conventionally, small-scale variants are those smaller than one kilobase (kb), compared to large-scale structural variations that span more than 1kb.

Small-scale variants include:

- **Single Nucleotide Variants** (SNVs): base-pair substitutions at a given DNA position. SNVs occurring in the coding part of the genome are broadly classified as *synonymous*, if the substitution is silent and does not alter the protein sequence, and *non-synonymous*, when the base-pair change impacts the protein sequence. The latter are further categorized into *missense* substitutions with alteration of a single amino-acid and *nonsense* variations whit anomalies in the frame of the protein or with creation of a stop codon, both resulting in premature termination of the entire protein. Furthermore, mutations that change the canonical splice sites are known as *splice-site variants* and are most of the time damaging to protein function, since they prevent the recognition of the site by the spliceosome, thus affecting splicing accuracy and resulting in alternatively spliced transcripts. Often these type of mutations also result in premature termination of the translated peptides and non-sense mediate decay (NMD).

- **In-dels:** insertion or removal of one or more nucleotides. Coding in-dels are divided into *non-frameshift* when they do not change the translational reading frame, and *frameshift* if they disrupt the reading frame and thus result in a truncated product or degradation of the transcript via nonsense mediated decay (NMD).

Large-scale variants include:

- **Copy Number Variations** (CNVs): a type of structural variation characterized by loss or amplification of stretches of genomic DNA, commonly named *deletion* and *duplication*, respectively. They can affect gene dosage as well as genome architecture.
- **Chromosomal rearrangements**: chromosome abnormalities characterized by anomalies in the original structure of the chromosomes. They include *translocations* (balanced or unbalanced rearrangements occurring between two chromosomes or even within one chromosome), and *inversions* (end to end reversion of the segment of a chromosome).

The human genome contains at least 20,000 protein-coding genes[1], unevenly distributed between and within chromosomes. When the genome is altered by one or more abnormalities, a *genetic disorder* may arise. Most genetic disorders said to be rare, i.e. if they affect < 1 person per 2000 (European guidelines)[2,3] or, according to American guidelines, they are conditions with < 200,000 people diagnosed[4,5]. Genetic disorders can be *hereditary* or non-*hereditary* depending on whether they are transmitted from the parental genome or not. When inherited, they can be transmitted according to five basic modes, known as *Mendelian pedigree patterns*:

- **Autosomal dominant**: when only one mutated allele on the autosomes is necessary to pass down the mutation to the offspring;
- **Autosomal recessive**: when both parental disruptive autosomal alleles have to be transmitted to the progeny;
- **X-linked dominant**: when a dominant allele is carried on the X-chromosome;
- **X-linked recessive**: when the mutation in a gene on the X-chromosome causes the phenotype to be expressed in males (hemizygous) and in females homozygous or compound heterozygous for the gene mutation;
- **Y-linked**: refers to the inheritance of a gene on the Y chromosome (father to son transmission).

These basic patterns are further complicated by additional factors, such as:

- clinical heterogeneity: when mutations in the same gene produce two or more different phenotypes in different individuals;
- intra-familial genetic heterogeneity;
- non-complete penetrance: when some individuals who carry the pathogenic variant express the associated trait while others do not;
- age-related penetrance;
- variable expression: refers to the degree in which a genotype is phenotypically expressed;
- anticipation: a phenomenon whereby as a genetic disorder is passed on to the next generation, the symptoms of the genetic disorder become apparent at an earlier age with each generation and with increased severiyt;
- imprinting: phenomenon that causes genes to be expressed in a parent-of-origin-specific manner;
- mosaicism: when two or more populations of cells with different genotypes co-exist in one individual who has developed from a single fertilized egg;
- chimeras: an organism or tissue that contains at least two different sets of genome sets, most often originating from the fusion of different zygotes (fertilized eggs).

Finding a link between disease phenotypes and molecular alterations is a challenging task. Despite the great effort to identify the causal variant and gene of different conditions, the genetic bases of congenital disorders are still largely unknown. In recent years, the advent of Next-Generation Sequencing (NGS) technologies, including whole exome and whole genome sequencing, have enabled the reliable detection of millions of variants within the genome. Furthermore, NGS has emerged as a new tool for the identification of genes involved in rare and complex genetic conditions. In the next section, I will emphasize the use of NGS technologies together with its advantages and challenges.

2. Next-Generation sequencing (NGS)

Next generation sequencing (NGS) refers to a DNA sequencing technology, which has positively influenced genomics research. Compared to the previous Sanger sequencing technology, it allows a larger sequencing volume in a much shorter amount of time.

With its implementation in 2010, NGS technologies have represented a turning point in the discovery of genetic disorders (GDs) causes[6-8]. The pace of detection of genes underlying GDs has increased the proportion of discoveries made by NGS compared to conventional approaches (**Figure 1**); by 2013, NGS had uncovered nearly three times as many genes as conventional approaches. The rate of discovery appears to be declining[7]. However, this decline might be temporary and reflecting a drop in publication rate[9,10]; e.g. while obvious cases were quickly solved, more complex ones will require more investigation time.

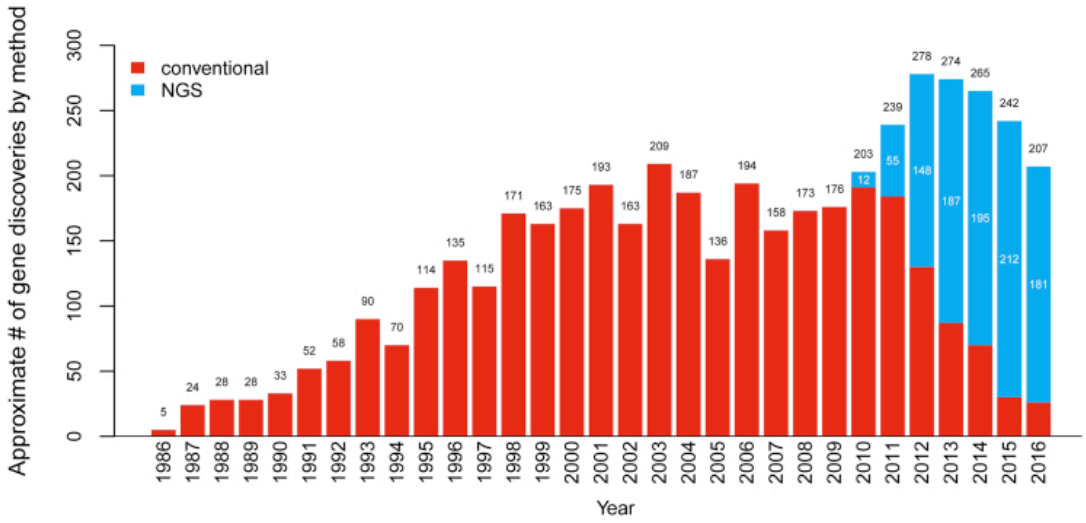

Figure 1. Number of gene discoveries by NGS (blue) compared to conventional approaches (red) (adapted from Boycott K.M. *et al.* 2017)

There are three main high-throughput NGS-based tests used in the field of GDs; they include *gene panels*, where exons of a group of genes (up to 300) associated to similar or overlapping phenotypes are sequenced; *whole exome sequencing* (WES), a genomic technology for sequencing all of the protein-coding regions of genes in a genome (representing ~2% of the human genome); and *whole genome-sequencing* (WGS) which analyzes the entire genome. The first difference among the three approaches is

represented, as intrinsic in their names, by the amount of information that is investigated, and consequently, where variants could be detected; the second one is related to their cost, while targeted panels are cheap, WES is more cost-effective compared to WGS even if the gap is shrinking. **Figure 2** summarizes the features of each approach, as well as their advantages and limitations.

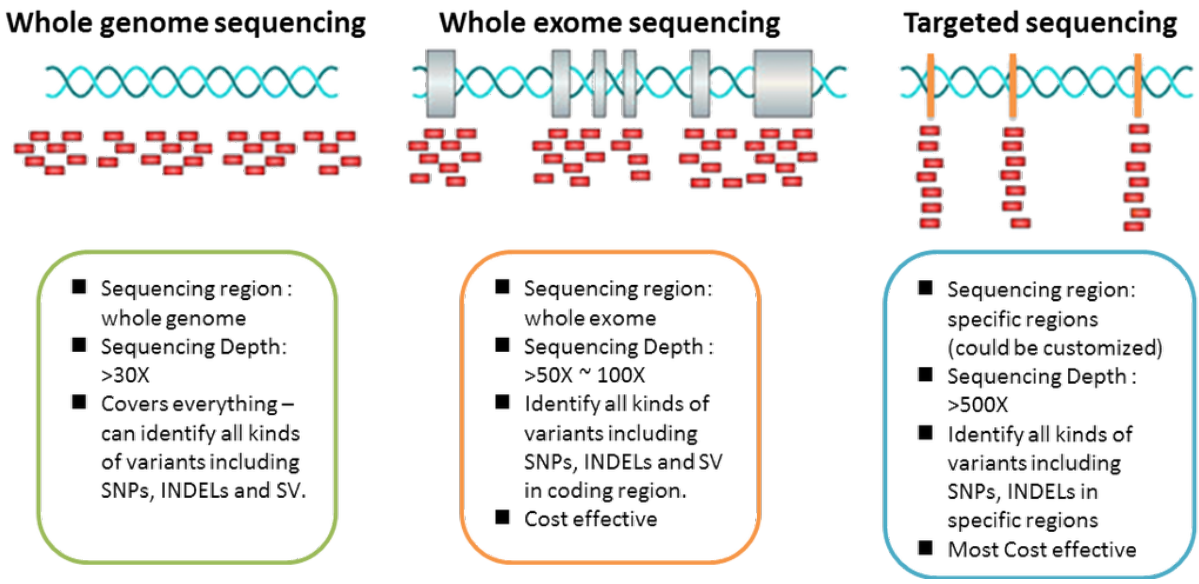

Figure 2. Comparison among WGS, WES and targeted sequencing (adapted from http://www.genomesop.com/somatic-mutations/).

The power of NGS is expressed, for example, by important outcomes achieved in the diagnosis of many unknown GDs. Neurodevelopmental disorders, including Intellectual Disability (ID), experienced a rapid increase in the number of newly unraveled genes[11].

The grouping of individuals sharing overlapping phenotypic manifestations and the possibility to ascertain them through NGS has represented the starting point towards the identification of a common mutated gene; an example is the discovery of *KMT2D* (*MLL2*) as the genetic cause of Kabuki Syndrome[12]. On the other hand, NGS has also been used in an unbiased manner (e.g. regardless of phenotypic information), in a "genotype-first approach", widely implemented for non-syndromic forms of ID, that gathers patients based on the underlying genetic etiology[13-18].

Recently another approach, RNA-sequencing, was used in the interpretation of variance of unknown significance[19-21]. RNA-sequencing provides information on the expression level of

a gene or transcript, sometimes even outside of its physiological range. The advantage of this approach is in the interpretation and detection of splicing events and in the ability to link regulatory events to diseases. However, one disadvantage lays in the fact that many genes have a tissue-specific profile that may confound the variants' interpretation. In this context, new databases based on large-scale studies, such as the one established by the GTEx (Genotype-Tissue Expression) project[22], have been collecting and integrating information focused on the relationships between genes, isoforms, and tissues. They are used in the tissue selection based on the clinical case, or at least on the best possible proxy.

General drawbacks related to NGS technologies are linked to the enormous amount of information generated and to the interpretation of the large number of novel variants in known Mendelian and newly associated genes.

When pathogenicity of a given variant cannot be established nor ecluded, it is labeled as *variant of unknown significance* (VUS).

For variant interpretation, characteristics such as allele frequency (extracted from databases like ExAC[23], and GnomAD[24] that catalog variation in the normal population across multiple ethnicities, position in the genome and evolutionary conservation gauged by anticipated severity calculated by several prediction tools (SIFT[25], Polyphen[26], Mutation Taster[27], Provean[28], GERP[29,30], CADD[31]), help the classification of the detected variants as *benign* or *pathogenic*, as well as their prioritization in the list of possibly causative variants.

Concerning gene involvement in a given phenotype, data mining on its expression profile, related protein function, and phenotyping information in model organisms (attainable from IMPC[32], ZFIN[33], and FlyBase[34] among others), in combination with literature-based evidences provides indication for considering them as good candidate genes. Similar to VUS, identification of a pathogenic variant in a gene never associated to a given phenotypic trait, defines it as a *gene of unknown significance* (GUS). Web tools such as GeneMatcher[35,36] facilitate the identification of additional individuals sharing similar phenotypes and/or candidate variants within the same gene. Subsequently, functional validation through *in silico*, *in vitro* and *in vivo* modeling are of great support towards the association of variants and/or genes to the observed phenotypes.

3. Neurodevelopmental disorders and intellectual disability

Neurodevelopmental disorders are a group of conditions characterized by early onset of developmental deficits that produce impairments of personal, social, academic, or occupational functioning[37]. The phenotypic spectrum of neurodevelopmental disorders ranges from limitations of learning or control of executive functions to global impairment of social skills or intelligence.

Intellectual Disability (ID) is a complex neurodevelopmental disorder which is defined by limited mental abilities (e.g. reasoning, problem solving, planning, learning from experience) and deficits in adaptive functioning diagnosed by 18 years of age[37]. It has a worldwide prevalence estimated at 1%[38]. However, considering the heterogeneity of its causes, estimation of the frequency is highly variable, for example ID prevalence varies according to age[39].

ID is a human trait that like brain morphology, anthropometric traits and immune functions is associated with sex differences in prevalence, outcome and/or progression[40-50]. A higher ratio in males compared to females has been reported. There are many factors possibly contributing to phenotypic sex differences. Sex chromosomes, genetic variation and genome architecture are included among the genetic components, but biological differences between sexes can stem from exogenous (e.g. environmental exposures) and endogenous (e.g. hormones and reproductive events) factors as well. Moreover, levels and patterns of gene expression in combination with the complexity of gene networks of both sexual and autosomal genes, might account for sex dimorphism related to many traits[51].

The diagnosis of ID is based on medical evaluation and individualized testing of the intellectual and adaptive capacities, i.e. intelligence quotient (IQ) test scores. IQ categories define different severity levels of ID: i) an IQ ranging between 50-69 classifies the mild ID forms, ii) moderate ID is featured by an IQ of 36-49, and iii) severe and iv) profound IDs are characterized by IQ ranges of 20-35 and <20, respectively. ID can be classified further into syndromic intellectual disability (S-ID) and non-syndromic intellectual disability (NS-ID). Individuals with S-ID exhibit additional clinical manifestations along with ID, whereas NS-ID patients only present intellectual impairment with or without additional neurological anomalies and psychiatric disorders. Concordantly, comorbidity between ID and various neuropsychiatric disorders such as schizophrenia and autism, has been reported.

The etiology of ID can be either from environmental (e.g. exposure to certain teratogens, viruses or radiation) or genetic origin. Chromosomal abnormalities, single and multi-genic defects, mitochondrial disorders, Copy Number Variations (CNVs), epigenetic defects, repeat expansion diseases and single gene impairments have been reported to be among genetic causes of ID[52]. D*e novo* and/or inherited single nucleotide variants represent a common genetic cause of ID; overall thousands of genes have been identified to be involved in the pathogenesis of syndromic and non-syndromic conditions with ID[11,39,53]. In case of autosomal recessive ID there are 1062 known causal genes (SysID, update June 2018[54]); 903 autosomal recessive intellectual disability genes have been identified by the most recent evaluation of the DDD study[55] as clarifying half of the observed excess of damaging bi-allelic genotypes, suggesting that the second half would be clarified by more (potentially rarer) genes to be discovered yet[53].

Understanding the pathogenesis of ID is challenging because of its high clinical and genetic heterogeneity. Despite the great technology advancement, molecular and cellular mechanisms underlying the pathophysiology of ID are indeed still limited.

4. G-protein β subunits: expansion of the repertoire of genes involved in intellectual disability and cardiac dysfunction

Neurodevelopmental and ID genes typically convey into similar functional modules. Genes encoding for presynaptic components, proteins for postsynaptic density, and members of the cytoskeleton dynamics are commonly affected in ID. Typical examples are: *GRIN2A* (MIM: 138253) and *GRIN2B* (MIM: 138252), *SHANK2* (MIM: 603290) and *SHANK3* (MIM: 606230) genes, whose mutations have been associated to neurodevelopmental conditions and ID pathogenesis. *GRIN2A* and *GRIN2B* encode for the N-methyl-D-aspartate (NMDA) receptors, members of the ionotropic glutamate receptor superfamily, mediating the excitatory synaptic transmission in the central nervous system. The early expression of these genes during development suggests an important role in brain formation, circuit expansion, synaptic plasticity, and cellular migration and differentiation. Disruption within *GRIN2A* gene is associated with focal epilepsy and speech disorder with or without cognitive disability[56-67] as well as with a non-epileptic neurodevelopmental disorder[68]. Similarly, *GRIN2B* mutations cause neurodevelopmental disorders including autism spectrum disorder

(ASD), attention deficit hyperactivity disorder (ADHD), epilepsy, and schizophrenia[57,69-73]. *SHANK2* and *SHANK3* are part of the Shank gene family; encoded Shank proteins are scaffold proteins of the postsynaptic density connecting neurotransmitter receptors and ion channels to the actin cytoskeleton and G-protein-coupled signaling pathways, thus regulating processes such as synapse formation and spine maturation[74]. *SHANK2* genetic alteration results in ASD and ID diseases[75], while mutations of *SHANK3* are linked to Phelan-McDermid syndrome (OMIM: #606232), a condition characterized by developmental delay, seizures and moderate-severe ID, among other signs[76-83]; additionally, mutations in this gene were also found in individuals affected by schizophrenia combined with ID[84].

Cytoskeleton dynamics are essential for events determining dendritic spine development and morphology in neuronal cells. Multiple evidences have linked regulators of proteins involved in cytoskeleton remodeling, such as members of the RhoGTPases, to ID[85]. The cytoplasmic FMRP-interacting protein 1 (CYFIP1) links the Rho GTPase signaling to the FMR1 protein disrupted in fragile X syndrome (OMIM: #300624). Mutations in the *OPHN1* gene, encoding the Rho-GTPase-activating protein that promotes GTP hydrolysis are responsible for OPHN1-related-X-linked cognitive disability (OMIM: #300486) with cerebellar hypoplasia and facial dysmorphisms[86-88]. Another member of the RhoGTPases family, *FGD1*[89,90], causes the facio-genital dysplasia in Aarskog-Scott syndrome (OMIM: #300546) and syndromic ID[91] when mutated.

Disruption of cellular signaling cascades - Ras signaling pathway *inter alia* - plays a fundamental role in the etiology of conditions including neurologic, cardiac and facial abnormalities. Costello syndrome (OMIM: #218040), LEOPARD syndrome (OMIM: #613707), neurofibromatosis (OMIM: #162200), Cowden disease (OMIM: #158350), Tuberous sclerosis 1 and 2 (OMIMs: #191100, #613254) are only some of a large group of disorders. They are caused by alteration of the Ras/MAPK/ERK and PI3K/Akt/mTOR networks. All the conditions associate with the ID phenotype.

Another group of genes, acting as transcription regulators or co-regulators, and whose disruption had a proven link with ID, thus expanding the spectrum of genes linked to this condition, are those found in epigenetic protein complexes. Major examples of epigenetic readers and writers associated with ID are: *CHD7*, *MECP2*, *MED12*, and *KMT2D* genes. Mutations in these genes are respectively responsible of CHARGE syndrome (OMIM:

#214800), Rett syndrome (OMIM: #312750), FG/Opitz-Kaveggia syndrome (OMIM: #305450), and Kabuki syndrome (OMIM: #147920).

Finally, defects in many genes encoding for ion channels result into abnormal brain activity, ID, seizures and developmental delay. Given that ion channels conducting sodium, calcium, or potassium ions are the major determinants of neuronal firing patterns, it is not surprising that genetic mutations of such channels in humans can lead to early-onset epilepsies. Moreover, defective ion channels alter further essential aspects of neuronal function. Loss- and gain-of function variations in *SCN2A* gene, encoding for a voltage-dependent sodium channel, cause epilepsy in humans[92,93] and gene protein-truncation bears considerable risk of developing ASD[94]. Altered dendritic excitability and synaptic function was found in mice lacking *Scn2a*, highlighting that those deficits might be consequential for ASD and ID etiology[95]. *De novo* missense mutations in the potassium channel gene, *KCNK4*, leading to aberrant gain of function of the channel sensitivity, cause a neurodevelopmental disorder featured by global developmental delay, ID, epilepsy, facial dysmorphisms, hypertrichosis and gingival overgrowth (FHEIGH syndrome, OMIM: #618381)[96]. Defective *CACNA1G*, producing one subunit of the calcium channels (the $Ca_v3.1$ T-type) with impaired channel inactivation, has been discovered in individuals displaying severe motor and cognitive impairment, cerebellar atrophy, epilepsy, and variable features including digital anomalies, facial dysmophisms and microencephaly[97].

Inherited ion channels mutations are not only crucial in ID and other neurodevelopmental conditions, but they are also an important cause of sinoatrial node dysfunction in young[98]. *HCN4* locus, belonging to the hyperpolarization-activated cyclic nucleotide-gates channels superfamily, has been linked to heart rate modulation in a genome-wide association study (GWAS)[99] and to lower heart rate in mouse models of heart failure[100] and in a rat model of aging[101]. *HCN1* and *HCN2* mice present a sick sinus syndrome phenotype[102,103], a sign of the sinoatrial node inadequacy to rule out its pacemaker function. Other ion channels genes important in cardiac automaticity are: *CACNA1D*, encoding the pore forming subunit of the $Ca_v1.2$ voltage-gated L-type calcium channels, found in two consanguineous families with bradycardia and congenital deafness[104]; and *SCN5A*, encoding the cardiac sodium channel $Na_v1.5$, causes Brugada Syndrome 1 (OMIM: #601144) - a disorder of the electric activity of the heart -, sick sinus syndrome 1 (OMIM: #608567) and *Scn5a* null-mouse models present bradycardia, sinus node conduction block and augmented sinus node conduction time[105].

The recent identification of rare genetic variants in genes encoding the G-protein β subunits has expanded the repertoire of causal genes involved in neurodevelopmental disorders and sinus node dysfunction, beyond the previously described genes[106-124].

G-proteins regulate one of the most common type of cell signaling transduction network that controls, for example, synaptic transmission, visual photoreception, hormone and growth factors release, regulation of cell contraction and migration, as well as cell growth and differentiation. G-proteins are activated by G-protein-coupled receptors (GPCRs) and transmit signals from hormones, neurotransmitters, and other signaling factors. G-proteins mainly act as heterotrimeric complexes, composed of alpha, beta, and gamma subunits. In the following paragraph, I will focus on the G-protein β subunits and their contribution to the etiology of genetically inherited rare diseases in humans.

5. The emerging role of Gβ subunits in human genetic diseases

(This paragraph is entirely extracted from a review I co-wrote and recently published in *Cells*, doi: 10.3390/cells8121567)

The G-Protein-Coupled Receptor (GPCR) superfamily includes over 800 members in humans[125] and is the largest group of cell-surface seven-transmembrane receptors[126]. They translate the signal from extracellular ligands into intracellular responses[127]. The GPCRs have a ligand-binding pocket, with seven motif α-helices, in the extracellular region, and a cytoplasmic domain engaged in G-proteins binding, guanosine triphosphate (GTP)-binding heterotrimers, consisting of α, β, and γ subunits[128,129].

When inactive, the G-protein α subunit is linked to guanosine diphosphate (GDP). Ligand-activated GPCRs catalyze the exchange of GDP with GTP on Gα, promoting its dissociation from Gβγ (**Figure 3**). The Gαβγ dissociation, in turn, promotes the activation of the Gα and Gβγ units that activate downstream factors, thus regulating an array of cellular functions such as cell contraction, excitability, migration, cell growth, and differentiation[130,131]. Notably, the combinatorial association of the distinct G-protein subunit subtypes, comprising at least 20 Gα, 5 Gβ, and 13 Gγ subunits[124,132], provides the level of selectivity that is needed to generate the wide range of signals governed by G-proteins and their cognate GPCRs (**Figure 3**)[133-135].

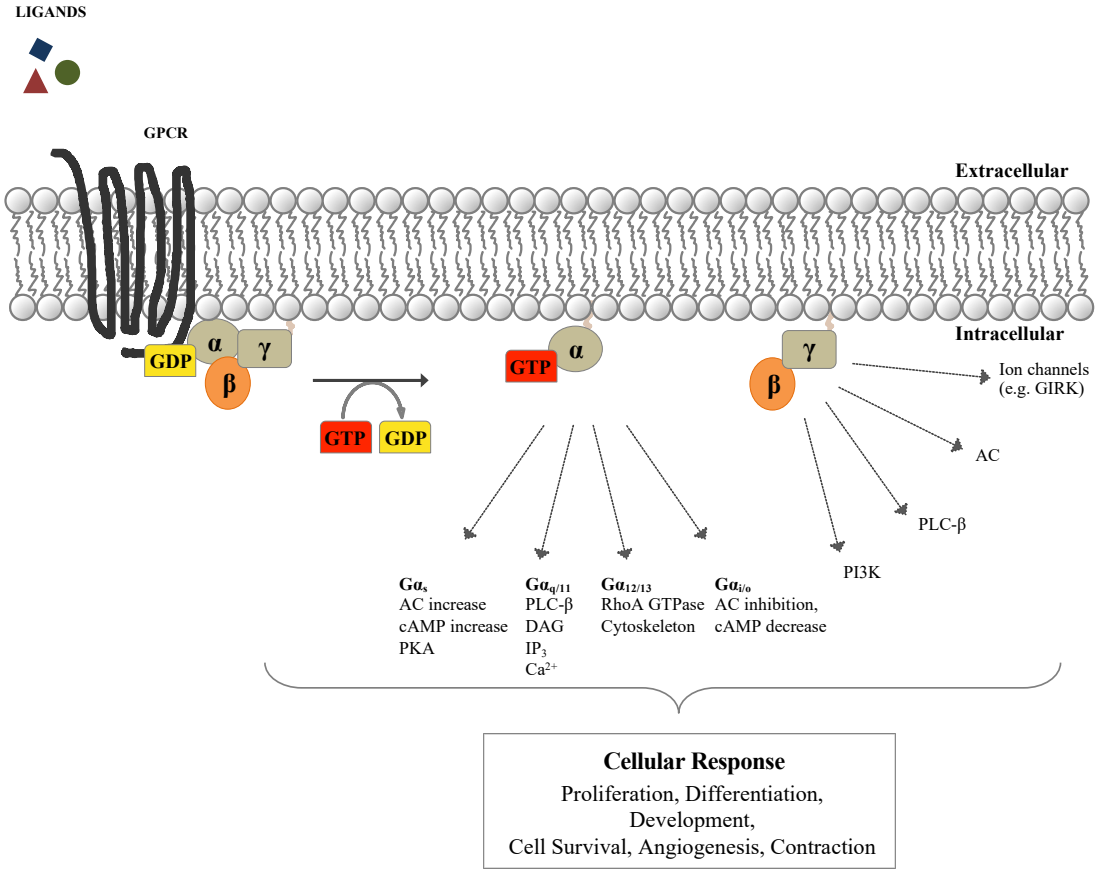

Figure 3. G-protein-coupled receptors signalosome. In the resting state, G-proteins are heterotrimers of alpha bound to guanosine diphosphate (GDP, yellow), beta, and gamma subunits. When activated by an extracellular ligand through G-protein coupled receptors (GPCRs, black), they undergo a conformational change that permits the GDP exchange with GTP (red) on Gα, which then dissociates from Gβγ. In the active state, Gα-GTP and Gβγ regulate various effectors. According to functional and structural homologies of their α subunit, heterotrimeric G-proteins are divided into four types (Gαs, Gαi/o, Gαq/11, and Gα12/13). Each Gα defines the unique Gαβγ mediated cellular responses[125,136-139]. Gαs and Gαi subfamily members are involved in the modulation of the intracellular second-messenger cAMP levels, either stimulating (Gs) or inhibiting (Gi) the production of cAMP by AC activity. Gαq/11 induces the activation of PLC-β, promoting the production of the intracellular messenger DAG and IP3 which activate the PKC and calcium signaling. Gα12/13 plays a role in the activation of the RhoA GTPase and of phospholipase D in regulating cell shape and motility[139-141]. Adenylyl cyclase (AC); cyclic adenosine monophosphate (cAMP); protein kinase A (PKA); phospholipase Cβ (PLC-β); diacylglycerol (DAG); inositol (1,4,5) trisphosphate (IP3); protein kinase C (PKC); intracellular concentration of free Ca2+ (Ca2+); Ras homolog family member A GTPase (RhoA GTPase); phosphatidylinositol-3-kinase (PI3K); G-protein–gated inwardly rectifying potassium channels (GIRK).

The propagation of the GPCR signaling cascade is restricted by the Regulators of G-protein Signaling (RGS) proteins, which limit the active Gα subunit lifetime and accelerate its GTP hydrolysis with a consequent re-association with the Gβγ dimer[142-147].

Here, we review the Gβ subunits and their contribution to the etiology of rare human genetic conditions. In the last six years, the outbreak of Next Generation Sequencing (NGS) technologies has assisted us to reach the description of a tapestry of human genetic conditions caused by pathogenic variants in Gβ subunits, and disease manifestations mainly involving neuronal and cardiac systems associated with ophthalmic pathology.

The human genome contains five paralogous genes (*GNB1* to *GNB5*) encoding the different Gβ subunits[148]. Chromosomal locations, genes structure and exons content of each of the five subunits are summarized in **Table 1**. The $G\beta_{1-4}$ subunits share between 80 and 90% sequence identity and are widely expressed throughout the tissues[149,150], whereas the $G\beta_5$ exhibits much less homology (~50%) and is preferentially expressed in the brain and nervous system[151]. Of note the alternatively spliced $G\beta_5$ longer isoform, $G\beta_5L$, expression is restricted to retinal photoreceptor outer segments[132,152].

At the protein level, iconic is the beta-propeller structure of the Gβ subunits, characterized by seven regular WD40-repeats[153] and a coiled coil domain at the N-terminus end. The WD40 domain is one of the most abundant and interacting moieties of the eukaryotic proteome; each domain is approximately 40 amino acids long and is characterized by a conserved tryptophan (W)-aspartic (D) acid pair, hence the name WD40[152,154]. With its β-propeller architecture, the WD40 domain provides extensive surface exposure for protein-protein or protein-DNA interactions, that coordinate downstream cellular events including signal transduction, autophagy, and apoptosis[155].

Gene Name (HGNC)	Description	Ensembl ID	RefSeq ID	Ensembl Transcript ID	Transcritp Length (bp)	Protein length (aa)	Uniprot	Cytogenetic Location	Genomic Coordinates (GRCh38, from Ensembl)	Strand	Nr. of Exons	Nr. of Coding Exons	MIM ID	Phenotype MIM Number(s)
GNB1	G protein subunit beta 1	ENSG00000078369.18	NM_002074	ENST00000378609.9	3163	340	P62873	1p36.33	1:1,785,285-1,891,117	reverse strand	12	9	*139380	#616973
GNB2	G protein subunit beta 2	ENSG00000172354.10	NM_005273	ENST00000303210.9	1664	340	Q6FHM2	7q22.1	7:100,673,567-100,679,174	forward strand	10	9	*139390	-
GNB3	G protein subunit beta 3	ENSG00000111664.10	NM_002075	ENST00000229264.7	1923	340	P16520	12p13.31	12:6,840,211-6,847,393	forward strand	11	9	*139130	#617024
GNB4	G protein subunit beta 4	ENSG00000114450.10	NM_021629	ENST00000232564.8	6315	340	Q9HAV0	3q26.33	3:179,396,088-179,451,476	reverse strand	10	9	*610863	#615185
GNB5	G protein subunit beta 5	ENSG00000069966.18	NM_006578	ENST00000358784.11	1735	353	O14775	15q21.2	15:52,122,206-52,180,001	reverse strand	11	11	*604447	#617173, #617182

Table 1. Gene content and major features of the five genes encoding the Gβ subunits. Gene names are reported according to the Hugo Gene Nomenclature Committee (HGNC[156]); Ensembl gene and transcript IDs, information on transcript/protein length as well as number of exons were retrieved to the Ensembl 97 and Ensembl Genomes 44 release, and, finally, genomic coordinates are specified on the GRCh38.p13 genome assembly. Uniprot identifiers rely on the UniProt release 2019_06 (published July 3, 2019)[157]. MIM IDs and phenotype MIM numbers are as in OMIM (Online Mendelian Inheritance in Men) database.

- *G Protein Subunit Beta 1 (GNB1, Gβ$_1$)*

In humans, *GNB1* (MIM 139380) missense, splice-site and frameshift pathogenic variants cause an autosomal dominant neurodevelopmental disorder, named MRD42 (Mental Retardation, Autosomal Dominant 42; MIM#616973). The phenotype observed across individuals with MRD42 include global developmental delay/intellectual disability (ID), hypotonia often associated with limb hypertonia, various types of seizures, and poor overall growth[107,120,158]. Strabismus, nystagmus, cortical visual impairment, attention deficit hyperactivity disorder, and autistic features may also be present[117]. Less frequent and variable symptoms are ataxia, dystonia, hydronephrosis, acute lymphoblastic leukemia[110,113,117,120,158], and cutaneous mastocytosis[109,121].

GNB1 was found as one of five genes deleted in five patients with 200 to 823-kb overlapping interstitial deletions of chromosome 1p36.33 (MIM#607872) affected by ID, developmental delay, seizures and muscular hypotonia together with characteristic dysmorphic features, and behavior abnormalities[159,160]. Functional evidence of *GNB1* involvement in neurodevelopmental delay is also corroborated by the study of homozygous *Gnb1* mutant mice that showed that *Gnb1* is essential for normal embryonic neurogenesis. Forty percent of *Gnb1* knock-out embryos died before birth. They showed defects in neural tube closure and neural progenitor cell proliferation associated to exencephaly (Table 2). The rest of the embryos presented microencephaly and died after birth[161]. *Gnb1* heterozygous mice

exhibited abnormal retina morphology with progressive degeneration (http://www.informatics.jax.org/marker/MGI:95781), thus supporting the ophthalmic manifestations reported in MRD42 affected individuals. To date, twenty-eight *de novo* and four with undefined inheritance *GNB1* variants have been reported in 53 affected individuals; of these 28 are missense, 2 frame-shift, and 2 splice-site variants (**Figure 4**)[107,109,110,113,117,120,121,158].

Overall, 23/32 (~74%) *GNB1* variants affect residues encoded by exon 6 (10/23) or exon 7 (13/23) (**Figure 4**). This small part of the gene encodes for a protein region forming the Gα and Gβγ interaction surface[162]. Accordingly, three *GNB1* likely benign missense variants (c.88C>T, p.(Leu30Phe); c.272A>G, p.(His91Arg); c.1009A>C, p.(Lys337Gln) are located distantly from the interaction site and no impaired $G\beta_1$ functionality has been shown[113].

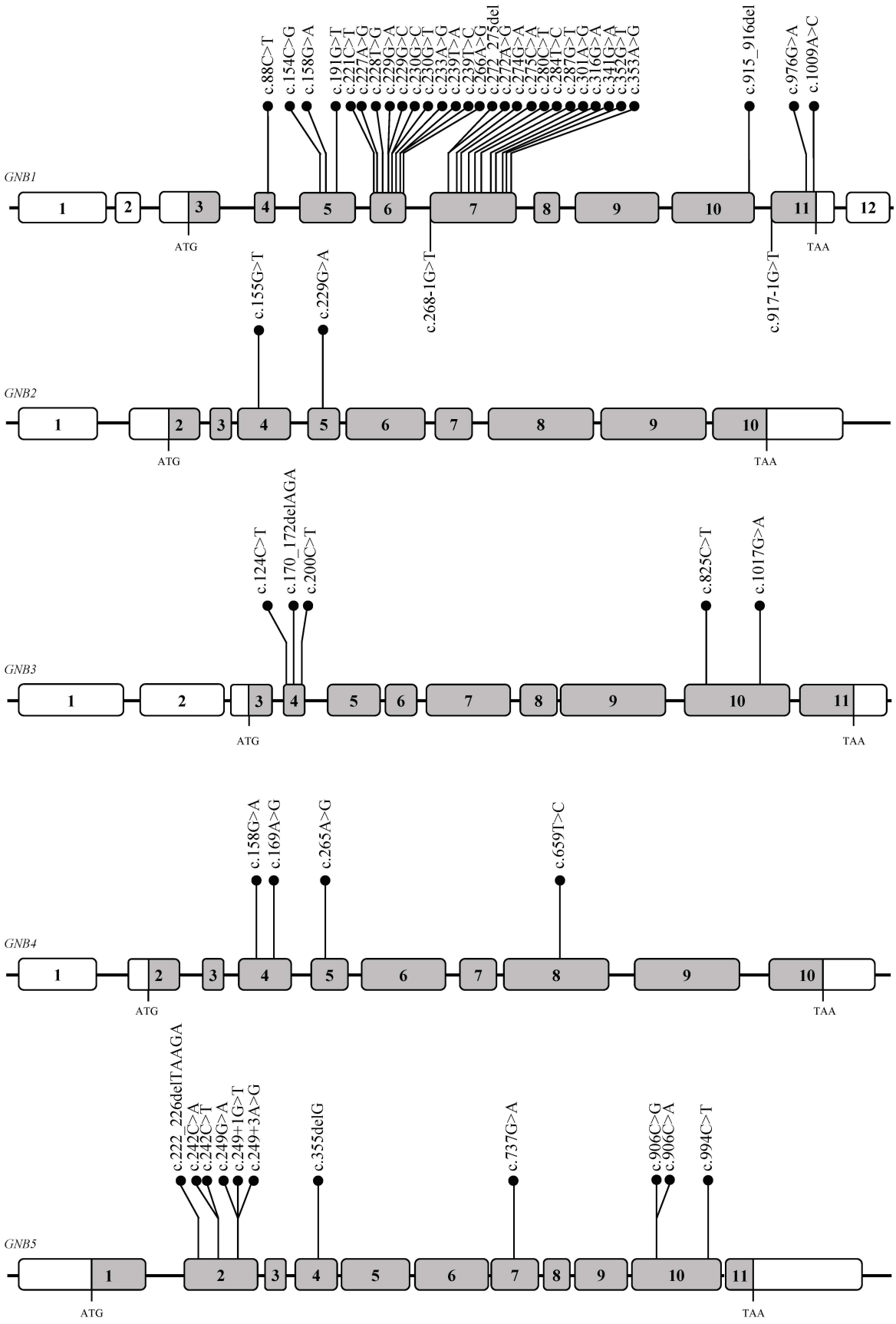

Figure 4. Variants distribution across the entire *GNB1-GNB5* genes. Genomic coordinates are specified on the GRCh37.p13 genome assembly. Coding exons are indicated by grey boxes, while untranslated regions are

displayed in white. Variants annotations refer to NM_002074 for *GNB1*, NM_005273 for *GNB2*, NM_002075 for *GNB3*, NM_021629 for *GNB4*, NM_006578 for *GNB5*.

- *G Protein Subunit Beta 2 (GNB2, Gβ$_2$)*

GNB2 (MIM 139390) c.155G>T, p.(Arg52Leu) (**Figure 4**) missense variant has been identified in 11 individuals of a family composed of 25 members. Carriers were affected by an autosomal dominant form of Sinus Node Dysfunction (SND) combined with atrioventricular conduction dysfunction and atrial fibrillation, in the absence of heart structural problems[163]. Crystal structure model of the mammalian G-protein–coupled inwardly rectifying potassium channel 2 (GIRK2) with $\beta_1\gamma_2$ G-protein complex, showed that Arg52 lays at the binding interface with GIRK[164], a data confirmed also for GIRK1/4 and Gβ_2[163]. The presence of the mutant residue is predicted to decrease the steric interaction at the GIRK-Gβ_2 surface. Functional studies revealed that the variant has an impact on the rectification of the GIRK channel with a consequent increase of ACh-activated K^+ current ($I_{K,ACh}$)[163], thus displaying a gain-of-function effect. Of note, the cardiac GIRK channels are directly switched on by the Gβγ units and are involved in the negative chronotropic effect of the parasympathetic nervous system, thus controlling heart rate and cellular electrical excitability[165,166]. A recent study of 52 unrelated patients with idiopathic SND uncovered a nonsynonymous substitution (c.303G>C, p.(Trp101Cys)) in the *KCNJ5* gene, encoding the Kir3.4 subunit of the GIRK channel. The mutation leads to a sustained activation of the cardiac GIRK channel[167]. Finally, further examples of the connection between *GNB2* and heart disease are provided by the *Gnb2* knock-out mice, generated by the International Mouse Phenotyping Consortium (IMPC; https://www.mousephenotype.org/data/genes/MGI:95784)[32]. Null *Gnb2* mice showed an increased heart rate, and abnormal electrocardiogram with shortened RR interval, PQ interval, and ST segment (**Table 2**)**.**

Additionally, an individual with global developmental delay, intellectual disability, muscle hypotonia and dysmorphisms carrying a *de novo GNB2* missense variant (c.229G>A, p.(Gly77Arg)) (**Figure 4**), predicted to impair protein function, was recently described in[108]. This study highlights that *GNB2* variants are not only associated with cardiac manifestations, but also with developmental delay[108].

Gene name (HGNC)	Annotated terms in animal models			
	M. Musculus	*Zebrafish*	*D. Melanogaster*	*C. elegans*
GNB1	(***Gnb1***): abnormal brain morphology and size (KO)[32]	(***gnb1a/gnb1b***): altered regulation of neutrophil migrations and posterior lateral line neuromast primordium migration (KD)[168]	(***CG10545***): abnormal spindle size (KD and overexpression)[169]	(***gpb1***): essential for embryo development (50-80% embryonic lethality); uncoordinated phenotype in surviving adult worms; functions in establishment of mitotic spindle orientation; expressed in alimentary system, body wall musculature, epithelial system, nervous system and reproductive organs (KD)[170,171]
GNB2	(***Gnb2***): abnormal behavioral response to light, increased heart rate, shortened PQ interval, shortened RR interval, shortened ST segment (KO)[32]	NA		
GNB3	(***Gnb3***): abnormal eye electrophysiology, mild bradycardia (KO); weight gain (Dup)[172-174]	(***gnb3a***): expressed throughout development; (***gnb3b***) expressed in the cones of the dorsal and medial retina (KD)[175]		
GNB4	(***Gnb4***): enlarged heart and spleen (KO)[32]	NA		
GNB5	(***Gnb5***): pre-weaning lethality with incomplete penetrance, decreased body size, slow post-natal weigh gain and abnormal vision (KO); increased body weight, adiposity, insulin resistance and liver steatosis (HET)[176-179]	(***gnb5a/gnb5b***): abnormal heart contraction, optokinetic behavior and swimming behavior (KO)[112]	(***CG10763***): pain responsive defective (KD)[34]	(***gpb-2***): behavioral defects, e.g. delayed egg laying, locomotion, and pharingeal pumping (KO and overexpression)[180]

Table 2. GNB genes have been studied in different model organisms. The table lists phenotypic manifestations resulting from complete (knock-out, KO) or partial (knock-down, KD) lack of each of the five GNB genes. "HET" refers to mouse models carrying only one functional copy of the gene, and "Dup" concerns the presence of three copies. Of note, in Zebrafish each of the genes has two paralogs, as a result of an ancient genome duplication event. In *Drosophila melanogaster* and *C. elegans* only two definite homologues have been identified, one corresponding to human *GNB1-4* and one corresponding to human *GNB5*, in each species. NA indicates "Not Available" model.

- *G Protein Subunit Beta 3 (GNB3, Gβ$_3$)*

Homozygous and compound heterozygous *GNB3* (MIM 139130) disease-causing variants were described in three individuals of a large Lebanese–Armenian family affected by Congenital Stationary Night Blindness type 1H (CSNB1H, MIM#617024)[124] and in a fourth sporadic case[106]. CSNB refers to a group of clinically heterogeneous retinal disorders caused by genetic defects of the retinoid metabolism in the retinal pigment epithelium (RPE), phototransduction, or signal transmission through the bipolar cells (BCs)[181,182]. Based on BCs ability to either initiate or terminate light stimuli, BCs can be either ON- or OFF-type. Specifically, while cone photoreceptors can connect both ON- and OFF-BCs, the rods are served largely by the ON-BCs[181].

The three first identified *GNB3* variants lie in the first (c.170_172delAGA, p.(Lys57del); c.200C>T, p.(Ser67Phe)) and seventh (c.1017G>A, p.(Trp339*)) WD40 repeat of the encoded Gβ$_3$ protein, respectively (**Figure 4**). Homology model studies of Gβ$_3$ protein structure, pointed out that each variant would impact interactions abilities as well as the formation of effective G-protein complexes[124]. A fourth *GNB3* variant (c.124C>T, p.(Arg42Ter)) was found in a patient with distinct early-onset inherited retinal disease, characterized by nystagmus, normal funduscopic exam, full-field electroretinography abnormalities, and mild disturbance of the central macula[106]. The Arg42 variant, located in exon 4 of the gene, gives rise to a premature stop codon, which is expected to be a substrate of the nonsense–mediate decay pathway[106].

Gβ$_3$ is expressed at higher levels in the eyes, in particular in the cone photoreceptors and ON-BCs of the retina in mammals and additional species[183-185]. In the eye, Gβ$_3$ modulates cone transducing function and cone and rod ON-bipolar signaling[124]. Similar to humans[124], abnormal light ON bipolar response and reduced cone sensitivity was found in the *Gnb3* knock-out mouse model[186,187], while retinopathy globe enlarged *(rge)* phenotype was reported in chickens carrying a 3-bp homozygous deletion of the *GNB3* homolog[188]. Interestingly, ablation of the *Gnb3* gene in mice causes mild bradycardia[174], thus suggesting a possible additional role of *GNB3* in heart rate regulation.

Beyond the role of *GNB3* pathogenic variants in the etiology of CSNB1H[124], Siffert and colleagues[189], described the c.825C>T (rs5443) polymorphism in exon 10 of the gene as linked to the expression of a shortened splice variant, Gβ$_3$s, whose translated protein is

characterized by the deletion of 41 amino acids, responsible of enhanced G-proteins signal transduction[189]. The c.825C>T polymorphism is associated with an increased risk of hypertension[189-192] obesity[173,193], diabetes[194], metabolic syndrome component[195,196], depression[197,198], seasonal variations in mood and behaviors[199], functional dyspepsia[200,201], stroke[202,203], arrhythmia[204], coronary artery disease[205,206], and other cardiovascular phenotypes[207-210]. In addition, duplication and overexpression of *GNB3* gene is responsible for a syndromic form of childhood obesity[173,211].

- *G Protein Subunit beta (GNB4, Gβ$_4$)*

Pathogenic variants in *GNB4* gene (MIM 610863) (**Figure 4**) have been reported as causative of intermediate Charcot–Marie–Tooth disease F (CMTDIF, MIM#615185), an autosomal dominant form of CMT. CMT is a neurologic disorder characterized by progressive distal muscle atrophy and weakness and variable nerve conduction velocities ranging from the demyelinating to the axonal range[212]. The missense variant c.158G>A, p.(Gly53Asp) in *GNB4* gene was reported in six affected family members. An unrelated case carried the c.265A>G; p.(Lys89Glu) *de novo* missense variant[212]. The pathogenicity of the variants and the importance of GPCR signaling in peripheral-nerve function in humans were supported by the reduced Gβ$_4$ immunostaining in the axon and Schwann cells of peripheral nerves of affected individuals. Moreover, *in vitro* studies demonstrated that both variants altered the bradykinin induced GPCR signaling[212]. More recently, the description of a Czech patient carrying the c.169A>G, p.(Lys57Glu) variant[111], and one Japanese family, for which axonal neuropathy has been reported, and segregating with c.659T>C, p.(Gln220Arg)[213], confirmed the pathogenic role of *GNB4* as the causal gene of CMTIDF.

All the *GNB4* pathogenic variants described so far are located in the first (p.(Gly53Asp) and p.(Lys57Glu))[111,212], in the second (p.(Lys89Glu))[212], and in the fifth WD40 domain (p.(Gln220Arg))[213], respectively (**Figure 4**). The Gly53 and Lys89 are important residues for the architecture of the WD40 β-propeller structure[214]. Functional characterization of p.(Gly53Asp) and p.(Lys89Glu) showed an impaired GPCR signaling via a dominant-negative effect, and resulting in reduced PLCβ$_2$ activity[214,215] followed by inhibition of IP_3 production and moderate increase in cytosolic calcium (Ca^{2+}) level[212,216], a universal second messenger that regulates the transmission of the depolarizing signal and neuronal synaptic activity.

Similar to $G\beta_2$, $G\beta_4$ is known to influence the activity of the cardiac GIRK channel, which regulates the heart rhythm through the acetylcholine-dependent activation of the muscarinic M2-receptor present in the sinoatrial node[217-220]. Although this gene has been reported in human hereditary neuropathy, genome-wide association studies have revealed association of the *GNB4* locus with variation in heart rate[99,163,221]. This suggests that *GNB4* variation may also impact heart rate.

- *G protein Subunit Beta (GNB5, Gβ5)*

The *GNB5* gene (MIM 604447), encoding the subunit β5 of the heterotrimeric G-proteins, is a divergent member of the Gβ family with distinct biochemical properties. Differently from $G\beta_{1-4}$, $G\beta_5$ forms irreversible dimer with the G-protein γ-like (GGL) domain[222] present in the R7 regulator group of G-protein signaling proteins (R7 RGS)[177,223-228]. Interaction of the GGL domain and the atypical $G\beta_5$ is a general requirement for stabilization of the whole R7 protein subfamily.

Homozygous and compound heterozygous variants in *GNB*5 have been associated with either IDDCA (Intellectual Developmental Disorder with Cardiac Arrhythmia, MIM#617173) or the milder LADCI (Language delay and ADHD/Cognitive Impairment with or without cardiac arrhythmia, MIM#617182) human syndromes[112,115,118,119,122,123,229]. Homozygous carriers of the recurrent missense variant c.242C>T, p.(Ser81Leu), present with LADCI syndrome, characterized by mild intellectual disability in combination with language delay, attention-deficit/hyperactivity disorder, with or without cardiac arrhythmia[112,119]. The substitution of the evolutionary conserved Serine 81 with the hydrophobic Leucine was predicted to compromise protein folding and/or stability as well as impair the binding kinetics of RGS proteins[112] and their capacity to deactivate G-protein signaling initiated by dopamine receptors[119]. By contrast, homozygous or compound heterozygous carriers of *GNB5* Loss of Function alleles presented with IDDCA, whose phenotypic spectrum includes epileptic seizures, severe intellectual disability, drastic impairment in speech and language skills, vision problems (which mainly include nystagmus and retinal abnormalities), hypotonia, and sick sinus syndrome[112,114,118,122,123,229]. Among the *GNB5* pathogenic variants described so far[112,114,118,122,123,229], a mutational hot spot in exon 2, encoding the first WD40 domain and containing 55% of described variants, has been identified (**Figure 4**). The evidence of the *GNB5* involvement in neuronal and cardiac signaling was confirmed in *Gnb5*-

null zebrafish and mouse models that resulted in neuronal and cardiac phenotypes reminiscent of those of IDDCA patients[112,178,230,231].

Gnb5-null mouse models displayed marked neurobehavioral abnormalities, impaired gait and motor learning, hyperactivity[176-179], defective visual adaptation with perturbed development and functioning of retinal bipolar cells[231-233]. Moreover, targeted deletion of one or two copies of the *Gnb5* gene had distinct effects on body weight and behavior in mice[176]. Although the cardiac phenotype of *Gnb5*-null mouse has never been studied, it is interesting to observe that bradycardia and heart rate responses to the cholinergic stimulation were exhibited by mice lacking *Rgs6*, the *Gnb5*-dependent RGS protein in the heart[234-236]. The *gnb5* knock-out zebrafish model also recapitulated the phenotypic spectrum of affected individuals, highlighting the involvement of *GNB5* in the control of motor capacity, vision and heart rate[112]. Several model organisms have been characterized regarding *GNB5*; information of additional animal models is included in **Table 2**.

References

1. Clamp, M. *et al.* Distinguishing protein-coding and noncoding genes in the human genome. *Proc Natl Acad Sci U S A* **104**, 19428-33 (2007).
2. Baldovino, S., Moliner, A.M., Taruscio, D., Daina, E. & Roccatello, D. Rare Diseases in Europe: from a Wide to a Local Perspective. *Isr Med Assoc J* **18**, 359-63 (2016).
3. EURORDIS, R.D.E.
4. Orphan Drug Act of 1983; Pub L. No. 97-414, 96 Stat. 2049.
5. Rare Disease Act of 2002; Pub L. 107-280. (Nov. 6, 2002).
6. Fernandez-Marmiesse, A., Gouveia, S. & Couce, M.L. NGS Technologies as a Turning Point in Rare Disease Research , Diagnosis and Treatment. *Curr Med Chem* **25**, 404-432 (2018).
7. Boycott, K.M. *et al.* International Cooperation to Enable the Diagnosis of All Rare Genetic Diseases. *Am J Hum Genet* **100**, 695-705 (2017).
8. Gilissen, C. *et al.* Genome sequencing identifies major causes of severe intellectual disability. *Nature* **511**, 344-7 (2014).
9. Bamshad, M.J., Nickerson, D.A. & Chong, J.X. Mendelian Gene Discovery: Fast and Furious with No End in Sight. *Am J Hum Genet* **105**, 448-455 (2019).
10. Posey, J.E. *et al.* Insights into genetics, human biology and disease gleaned from family based genomic studies. *Genet Med* **21**, 798-812 (2019).
11. Vissers, L.E., Gilissen, C. & Veltman, J.A. Genetic studies in intellectual disability and related disorders. *Nat Rev Genet* **17**, 9-18 (2016).
12. Ng, S.B. *et al.* Exome sequencing identifies MLL2 mutations as a cause of Kabuki syndrome. *Nat Genet* **42**, 790-3 (2010).
13. Abou Jamra, R. *et al.* Homozygosity mapping in 64 Syrian consanguineous families with non-specific intellectual disability reveals 11 novel loci and high heterogeneity. *Eur J Hum Genet* **19**, 1161-6 (2011).
14. Carvill, G.L. & Mefford, H.C. Next-Generation Sequencing in Intellectual Disability. *J Pediatr Genet* **4**, 128-35 (2015).
15. Deciphering Developmental Disorders, S. Large-scale discovery of novel genetic causes of developmental disorders. *Nature* **519**, 223-8 (2015).
16. Helbig, I. & Tayoun, A.A. Understanding Genotypes and Phenotypes in Epileptic Encephalopathies. *Mol Syndromol* **7**, 172-181 (2016).
17. Ng, S.B. *et al.* Exome sequencing identifies the cause of a mendelian disorder. *Nat Genet* **42**, 30-5 (2010).
18. Riazuddin, S. *et al.* Exome sequencing of Pakistani consanguineous families identifies 30 novel candidate genes for recessive intellectual disability. *Mol Psychiatry* **22**, 1604-1614 (2017).
19. Cummings, B.B. *et al.* Improving genetic diagnosis in Mendelian disease with transcriptome sequencing. *Sci Transl Med* **9**(2017).
20. Kremer, L.S. *et al.* Genetic diagnosis of Mendelian disorders via RNA sequencing. *Nat Commun* **8**, 15824 (2017).
21. Marco-Puche, G., Lois, S., Benitez, J. & Trivino, J.C. RNA-Seq Perspectives to Improve Clinical Diagnosis. *Front Genet* **10**, 1152 (2019).
22. Mele, M. *et al.* Human genomics. The human transcriptome across tissues and individuals. *Science* **348**, 660-5 (2015).

23. Karczewski, K.J. *et al.* The ExAC browser: displaying reference data information from over 60 000 exomes. *Nucleic Acids Res* **45**, D840-D845 (2017).
24. Karczewski, K.J., Francioli, L.C., Tiao, G., Cummings, B.B., Alföldi, J., Wang, Q., Collins, R.L., Laricchia, K.M., Ganna, A., Birnbaum, D.P., et al. Variation across 141,456 human exomes and genomes reveals the spectrum of loss-of-function intolerance across human protein-coding genes. *bioRxiv* **531210**(2019).
25. Vaser, R., Adusumalli, S., Leng, S.N., Sikic, M. & Ng, P.C. SIFT missense predictions for genomes. *Nat Protoc* **11**, 1-9 (2016).
26. Adzhubei, I., Jordan, D.M. & Sunyaev, S.R. Predicting functional effect of human missense mutations using PolyPhen-2. *Curr Protoc Hum Genet* **Chapter 7**, Unit7 20 (2013).
27. Schwarz, J.M., Cooper, D.N., Schuelke, M. & Seelow, D. MutationTaster2: mutation prediction for the deep-sequencing age. *Nat Methods* **11**, 361-2 (2014).
28. Choi, Y. & Chan, A.P. PROVEAN web server: a tool to predict the functional effect of amino acid substitutions and indels. *Bioinformatics* **31**, 2745-7 (2015).
29. Davydov, E.V. *et al.* Identifying a high fraction of the human genome to be under selective constraint using GERP++. *PLoS Comput Biol* **6**, e1001025 (2010).
30. Cooper, G.M. *et al.* Distribution and intensity of constraint in mammalian genomic sequence. *Genome Res* **15**, 901-13 (2005).
31. Rentzsch, P., Witten, D., Cooper, G.M., Shendure, J. & Kircher, M. CADD: predicting the deleteriousness of variants throughout the human genome. *Nucleic Acids Res* **47**, D886-D894 (2019).
32. Dickinson, M.E. *et al.* High-throughput discovery of novel developmental phenotypes. *Nature* **537**, 508-+ (2016).
33. Ruzicka, L. *et al.* The Zebrafish Information Network: new support for non-coding genes, richer Gene Ontology annotations and the Alliance of Genome Resources. *Nucleic Acids Res* **47**, D867-D873 (2019).
34. Thurmond, J. *et al.* FlyBase 2.0: the next generation. *Nucleic Acids Res* **47**, D759-D765 (2019).
35. Sobreira, N., Schiettecatte, F., Boehm, C., Valle, D. & Hamosh, A. New tools for Mendelian disease gene identification: PhenoDB variant analysis module; and GeneMatcher, a web-based tool for linking investigators with an interest in the same gene. *Hum Mutat* **36**, 425-31 (2015).
36. Sobreira, N., Schiettecatte, F., Valle, D. & Hamosh, A. GeneMatcher: a matching tool for connecting investigators with an interest in the same gene. *Hum Mutat* **36**, 928-30 (2015).
37. *Diagnostic and Statistical Manual of Mental Disorders*, (American Psychiatry Association, 2013).
38. Maulik, P.K., Mascarenhas, M.N., Mathers, C.D., Dua, T. & Saxena, S. Prevalence of intellectual disability: a meta-analysis of population-based studies. *Res Dev Disabil* **32**, 419-36 (2011).
39. Chiurazzi, P. & Pirozzi, F. Advances in understanding - genetic basis of intellectual disability. *F1000Res* **5**(2016).
40. Frazier, T.W., Georgiades, S., Bishop, S.L. & Hardan, A.Y. Behavioral and Cognitive Characteristics of Females and Males With Autism in the Simons Simplex Collection. *Journal of the American Academy of Child and Adolescent Psychiatry* **53**, 329-340 (2014).

41. Heid, I.M. *et al.* Meta-analysis identifies 13 new loci associated with waist-hip ratio and reveals sexual dimorphism in the genetic basis of fat distribution. *Nature Genetics* **42**, 949-U160 (2010).
42. Jacquemont, S. *et al.* A Higher Mutational Burden in Females Supports a "Female Protective Model" in Neurodevelopmental Disorders. *American Journal of Human Genetics* **94**, 415-425 (2014).
43. Klein, S.L. & Flanagan, K.L. Sex differences in immune responses. *Nature Reviews Immunology* **16**, 626-638 (2016).
44. Lai, M.C. *et al.* Cognition in Males and Females with Autism: Similarities and Differences. *Plos One* **7**(2012).
45. Randall, J.C. *et al.* Sex-stratified Genome-wide Association Studies Including 270,000 Individuals Show Sexual Dimorphism in Genetic Loci for Anthropometric Traits. *Plos Genetics* **9**(2013).
46. Ruigrok, A.N.V. *et al.* A meta-analysis of sex differences in human brain structure. *Neuroscience and Biobehavioral Reviews* **39**, 34-50 (2014).
47. Volkmar, F.R., Szatmari, P. & Sparrow, S.S. Sex-Differences in Pervasive Developmental Disorders. *Journal of Autism and Developmental Disorders* **23**, 579-591 (1993).
48. Wells, J.C.K. Sexual dimorphism of body composition. *Best Practice & Research Clinical Endocrinology & Metabolism* **21**, 415-430 (2007).
49. Werling, D.M. & Geschwind, D.H. Sex differences in autism spectrum disorders. *Current Opinion in Neurology* **26**, 146-153 (2013).
50. Zwaigenbaum, L. *et al.* Sex Differences in Children with Autism Spectrum Disorder Identified Within a High-Risk Infant Cohort. *Journal of Autism and Developmental Disorders* **42**, 2585-2596 (2012).
51. Khramtsova, E.A., Davis, L.K. & Stranger, B.E. The role of sex in the genomics of human complex traits. *Nature Reviews Genetics* **20**, 173-190 (2019).
52. Khan, M.A. *et al.* The Molecular Genetics of Autosomal Recessive Nonsyndromic Intellectual Disability: a Mutational Continuum and Future Recommendations. *Ann Hum Genet* **80**, 342-368 (2016).
53. Jamra, R. Genetics of autosomal recessive intellectual disability. *Med Genet* **30**, 323-327 (2018).
54. Kochinke, K. *et al.* Systematic Phenomics Analysis Deconvolutes Genes Mutated in Intellectual Disability into Biologically Coherent Modules. *American Journal of Human Genetics* **98**, 149-164 (2016).
55. Hilary C. Martin, W.D.J., James Stephenson, Juliet Handsaker, Giuseppe Gallone, Jeremy F. McRae, Elena Prigmore, Patrick Short, Mari Niemi, Joanna Kaplanis, Elizabeth Radford, Nadia Akawi, Meena Balasubramanian, John Dean, Rachel Horton, Alice Hulbert, Diana S. Johnson, Katie Johnson, Dhavendra Kumar, Sally Ann Lynch, Sarju G. Mehta, Jenny Morton, Michael J. Parker, Miranda Splitt, Peter D. Turnpenny, Pradeep C. Vasudevan, Michael Wright, Caroline F. Wright, David R. FitzPatrick, Helen V. Firth, Matthew E. Hurles, Jeffrey C. Barrett. Quantifying the contribution of recessive coding variation to developmental disorders. *bioRxiv* **201533. 10.1101/201533**
(2018).
56. Lesca, G. *et al.* Update on the genetics of the epilepsy-aphasia spectrum and role of GRIN2A mutations. *Epileptic Disord* **21**, 41-47 (2019).

57. Li, J. *et al.* De novo GRIN variants in NMDA receptor M2 channel pore-forming loop are associated with neurological diseases. *Hum Mutat* **40**, 2393-2413 (2019).
58. Strehlow, V. *et al.* GRIN2A-related disorders: genotype and functional consequence predict phenotype. *Brain* **142**, 80-92 (2019).
59. Yang, X. *et al.* GRIN2A mutations in epilepsy-aphasia spectrum disorders. *Brain Dev* **40**, 205-210 (2018).
60. Sculier, C. *et al.* Acquired epileptic opercular syndrome related to a heterozygous deleterious substitution in GRIN2A. *Epileptic Disord* **19**, 345-350 (2017).
61. Gao, K. *et al.* A de novo loss-of-function GRIN2A mutation associated with childhood focal epilepsy and acquired epileptic aphasia. *PLoS One* **12**, e0170818 (2017).
62. von Stulpnagel, C. *et al.* Epilepsy in patients with GRIN2A alterations: Genetics, neurodevelopment, epileptic phenotype and response to anticonvulsive drugs. *Eur J Paediatr Neurol* **21**, 530-541 (2017).
63. Marwick, K., Skehel, P., Hardingham, G. & Wyllie, D. Effect of a GRIN2A de novo mutation associated with epilepsy and intellectual disability on NMDA receptor currents and Mg(2+) block in cultured primary cortical neurons. *Lancet* **385 Suppl 1**, S65 (2015).
64. Lesca, G. *et al.* GRIN2A mutations in acquired epileptic aphasia and related childhood focal epilepsies and encephalopathies with speech and language dysfunction. *Nat Genet* **45**, 1061-6 (2013).
65. Lemke, J.R. *et al.* Mutations in GRIN2A cause idiopathic focal epilepsy with rolandic spikes. *Nat Genet* **45**, 1067-72 (2013).
66. Carvill, G.L. *et al.* GRIN2A mutations cause epilepsy-aphasia spectrum disorders. *Nat Genet* **45**, 1073-6 (2013).
67. Endele, S. *et al.* Mutations in GRIN2A and GRIN2B encoding regulatory subunits of NMDA receptors cause variable neurodevelopmental phenotypes. *Nat Genet* **42**, 1021-6 (2010).
68. Fernandez-Marmiesse, A. *et al.* A novel missense mutation in GRIN2A causes a nonepileptic neurodevelopmental disorder. *Mov Disord* **33**, 992-999 (2018).
69. Sharawat, I.K., Yadav, J. & Saini, L. Novel GRIN2B mutation: A rare cause of severe epileptic encephalopathy. *Neurol India* **67**, 562-563 (2019).
70. Kyriakopoulos, P. *et al.* Atypical Rett Syndrome and Intractable Epilepsy With Novel GRIN2B Mutation. *Child Neurol Open* **5**, 2329048X18787946 (2018).
71. O'Roak, B.J. *et al.* Multiplex targeted sequencing identifies recurrently mutated genes in autism spectrum disorders. *Science* **338**, 1619-22 (2012).
72. Platzer, K. *et al.* GRIN2B encephalopathy: novel findings on phenotype, variant clustering, functional consequences and treatment aspects. *J Med Genet* **54**, 460-470 (2017).
73. Lemke, J.R. *et al.* GRIN2B mutations in West syndrome and intellectual disability with focal epilepsy. *Ann Neurol* **75**, 147-54 (2014).
74. Scheefhals, N. *et al.* Shank Proteins Couple the Endocytic Zone to the Postsynaptic Density to Control Trafficking and Signaling of Metabotropic Glutamate Receptor 5. *Cell Rep* **29**, 258-269 e8 (2019).
75. Berkel, S. *et al.* Mutations in the SHANK2 synaptic scaffolding gene in autism spectrum disorder and mental retardation. *Nat Genet* **42**, 489-91 (2010).
76. De Rubeis, S. *et al.* Delineation of the genetic and clinical spectrum of Phelan-McDermid syndrome caused by SHANK3 point mutations. *Mol Autism* **9**, 31 (2018).

77. Zhu, W. *et al.* Two de novo novel mutations in one SHANK3 allele in a patient with autism and moderate intellectual disability. *Am J Med Genet A* **176**, 973-979 (2018).
78. Holder, J.L., Jr. & Quach, M.M. The spectrum of epilepsy and electroencephalographic abnormalities due to SHANK3 loss-of-function mutations. *Epilepsia* **57**, 1651-1659 (2016).
79. Yi, F. *et al.* Autism-associated SHANK3 haploinsufficiency causes Ih channelopathy in human neurons. *Science* **352**, aaf2669 (2016).
80. Betancur, C. & Buxbaum, J.D. SHANK3 haploinsufficiency: a "common" but underdiagnosed highly penetrant monogenic cause of autism spectrum disorders. *Mol Autism* **4**, 17 (2013).
81. Boccuto, L. *et al.* Prevalence of SHANK3 variants in patients with different subtypes of autism spectrum disorders. *Eur J Hum Genet* **21**, 310-6 (2013).
82. Moessner, R. *et al.* Contribution of SHANK3 mutations to autism spectrum disorder. *Am J Hum Genet* **81**, 1289-97 (2007).
83. Durand, C.M. *et al.* Mutations in the gene encoding the synaptic scaffolding protein SHANK3 are associated with autism spectrum disorders. *Nat Genet* **39**, 25-7 (2007).
84. Gauthier, J. *et al.* De novo mutations in the gene encoding the synaptic scaffolding protein SHANK3 in patients ascertained for schizophrenia. *Proc Natl Acad Sci U S A* **107**, 7863-8 (2010).
85. Zamboni, V. *et al.* Rho GTPases in Intellectual Disability: From Genetics to Therapeutic Opportunities. *Int J Mol Sci* **19**(2018).
86. Schwartz, T.S. *et al.* Expanding the phenotypic spectrum associated with OPHN1 variants. *Eur J Med Genet* **62**, 137-143 (2019).
87. Moortgat, S. *et al.* Expanding the phenotypic spectrum associated with OPHN1 mutations: Report of 17 individuals with intellectual disability but no cerebellar hypoplasia. *Eur J Med Genet* **61**, 442-450 (2018).
88. Bedeschi, M.F. *et al.* Association of syndromic mental retardation with an Xq12q13.1 duplication encompassing the oligophrenin 1 gene. *Am J Med Genet A* **146A**, 1718-24 (2008).
89. Ge, Y., Li, N., Wang, Z., Wang, J. & Cai, H. Novel variant in the FGD1 gene causing Aarskog-Scott syndrome. *Exp Ther Med* **13**, 2623-2628 (2017).
90. Orrico, A. *et al.* A mutation in the pleckstrin homology (PH) domain of the FGD1 gene in an Italian family with faciogenital dysplasia (Aarskog-Scott syndrome). *FEBS Lett* **478**, 216-20 (2000).
91. Lebel, R.R. *et al.* Non-syndromic X-linked mental retardation associated with a missense mutation (P312L) in the FGD1 gene. *Clin Genet* **61**, 139-45 (2002).
92. Begemann, A. *et al.* Further corroboration of distinct functional features in SCN2A variants causing intellectual disability or epileptic phenotypes. *Mol Med* **25**, 6 (2019).
93. Wolff, M. *et al.* Genetic and phenotypic heterogeneity suggest therapeutic implications in SCN2A-related disorders. *Brain* **140**, 1316-1336 (2017).
94. Ben-Shalom, R. *et al.* Opposing Effects on NaV1.2 Function Underlie Differences Between SCN2A Variants Observed in Individuals With Autism Spectrum Disorder or Infantile Seizures. *Biol Psychiatry* **82**, 224-232 (2017).
95. Spratt, P.W.E. *et al.* The Autism-Associated Gene Scn2a Contributes to Dendritic Excitability and Synaptic Function in the Prefrontal Cortex. *Neuron* **103**, 673-685 e5 (2019).

96. Bauer, C.K. *et al.* Mutations in KCNK4 that Affect Gating Cause a Recognizable Neurodevelopmental Syndrome. *Am J Hum Genet* **103**, 621-630 (2018).
97. Chemin, J. *et al.* De novo mutation screening in childhood-onset cerebellar atrophy identifies gain-of-function mutations in the CACNA1G calcium channel gene. *Brain* **141**, 1998-2013 (2018).
98. Verkerk, A.O. & Wilders, R. Pacemaker activity of the human sinoatrial node: an update on the effects of mutations in HCN4 on the hyperpolarization-activated current. *Int J Mol Sci* **16**, 3071-94 (2015).
99. den Hoed, M. *et al.* Identification of heart rate-associated loci and their effects on cardiac conduction and rhythm disorders. *Nat Genet* **45**, 621-31 (2013).
100. Zicha, S., Fernandez-Velasco, M., Lonardo, G., L'Heureux, N. & Nattel, S. Sinus node dysfunction and hyperpolarization-activated (HCN) channel subunit remodeling in a canine heart failure model. *Cardiovasc Res* **66**, 472-81 (2005).
101. Huang, X., Yang, P., Du, Y., Zhang, J. & Ma, A. Age-related down-regulation of HCN channels in rat sinoatrial node. *Basic Res Cardiol* **102**, 429-35 (2007).
102. Fenske, S. *et al.* Sick sinus syndrome in HCN1-deficient mice. *Circulation* **128**, 2585-94 (2013).
103. Ludwig, A. *et al.* Absence epilepsy and sinus dysrhythmia in mice lacking the pacemaker channel HCN2. *EMBO J* **22**, 216-24 (2003).
104. Baig, S.M. *et al.* Loss of Ca(v)1.3 (CACNA1D) function in a human channelopathy with bradycardia and congenital deafness. *Nat Neurosci* **14**, 77-84 (2011).
105. Lei, M. *et al.* Sinus node dysfunction following targeted disruption of the murine cardiac sodium channel gene Scn5a. *J Physiol* **567**, 387-400 (2005).
106. Arno, G. *et al.* Recessive Retinopathy Consequent on Mutant G-Protein beta Subunit 3 (GNB3). *JAMA Ophthalmol* **134**, 924-7 (2016).
107. Endo, W. *et al.* Phenotype-genotype correlations in patients with GNB1 gene variants, including the first three reported Japanese patients to exhibit spastic diplegia, dyskinetic quadriplegia, and infantile spasms. *Brain Dev* (2019).
108. Fukuda, T. *et al.* Exome reports A de novo GNB2 variant associated with global developmental delay, intellectual disability, and dysmorphic features. *Eur J Med Genet*, 103804 (2019).
109. Hemati, P. *et al.* Refining the phenotype associated with GNB1 mutations: Clinical data on 18 newly identified patients and review of the literature. *Am J Med Genet A* **176**, 2259-2275 (2018).
110. Jones, H.F. *et al.* Myoclonus-dystonia caused by GNB1 mutation responsive to deep brain stimulation. *Mov Disord* **34**, 1079-1080 (2019).
111. Lassuthova, P. *et al.* Confirmation of the GNB4 gene as causal for Charcot-Marie-Tooth disease by a novel de novo mutation in a Czech patient. *Neuromuscul Disord* **27**, 57-60 (2017).
112. Lodder, E.M. *et al.* GNB5 Mutations Cause an Autosomal-Recessive Multisystem Syndrome with Sinus Bradycardia and Cognitive Disability. *Am J Hum Genet* **99**, 786 (2016).
113. Lohmann, K. *et al.* Novel GNB1 mutations disrupt assembly and function of G protein heterotrimers and cause global developmental delay in humans. *Hum Mol Genet* **26**, 1078-1086 (2017).
114. Malerba, N., De Nittis, P. & Merla, G. The Emerging Role of Gbeta Subunits in Human Genetic Diseases. *Cells* **8**(2019).

115. Malerba, N. *et al.* A NGS-Targeted Autism/ID Panel Reveals Compound Heterozygous GNB5 Variants in a Novel Patient. *Front Genet* **9**, 626 (2018).
116. Peng, J. *et al.* Novel West syndrome candidate genes in a Chinese cohort. *CNS Neurosci Ther* **24**, 1196-1206 (2018).
117. Petrovski, S. *et al.* Germline De Novo Mutations in GNB1 Cause Severe Neurodevelopmental Disability, Hypotonia, and Seizures. *Am J Hum Genet* **98**, 1001-1010 (2016).
118. Poke, G. *et al.* The epileptology of GNB5 encephalopathy. *Epilepsia* **60**, e121-e127 (2019).
119. Shamseldin, H.E. *et al.* GNB5 mutation causes a novel neuropsychiatric disorder featuring attention deficit hyperactivity disorder, severely impaired language development and normal cognition. *Genome Biol* **17**, 195 (2016).
120. Steinrucke, S. *et al.* Novel GNB1 missense mutation in a patient with generalized dystonia, hypotonia, and intellectual disability. *Neurol Genet* **2**, e106 (2016).
121. Szczaluba, K. *et al.* Novel GNB1 de novo mutation in a patient with neurodevelopmental disorder and cutaneous mastocytosis: Clinical report and literature review. *Eur J Med Genet* **61**, 157-160 (2018).
122. Turkdogan, D., Usluer, S., Akalin, F., Agyuz, U. & Aslan, E.S. Familial early infantile epileptic encephalopathy and cardiac conduction disorder: A rare cause of SUDEP in infancy. *Seizure* **50**, 171-172 (2017).
123. Vernon, H. *et al.* Intellectual developmental disorder with cardiac arrhythmia syndrome in a child with compound heterozygous GNB5 variants. *Clin Genet* **93**, 1254-1256 (2018).
124. Vincent, A. *et al.* Biallelic Mutations in GNB3 Cause a Unique Form of Autosomal-Recessive Congenital Stationary Night Blindness. *Am J Hum Genet* **98**, 1011-1019 (2016).
125. Fredriksson, R., Lagerstrom, M.C., Lundin, L.G. & Schioth, H.B. The G-protein-coupled receptors in the human genome form five main families. Phylogenetic analysis, paralogon groups, and fingerprints. *Mol Pharmacol* **63**, 1256-72 (2003).
126. Kamato, D., Burch, M.L., Osman, N., Zheng, W. & Little, P.J. Therapeutic implications of endothelin and thrombin G-protein-coupled receptor transactivation of tyrosine and serine/threonine kinase cell surface receptors. *J Pharm Pharmacol* **65**, 465-73 (2013).
127. de Oliveira, P.G., Ramos, M.L.S., Amaro, A.J., Dias, R.A. & Vieira, S.I. Gi/o-Protein Coupled Receptors in the Aging Brain. *Front Aging Neurosci* **11**, 89 (2019).
128. Lagerstrom, M.C. & Schioth, H.B. Structural diversity of G protein-coupled receptors and significance for drug discovery. *Nat Rev Drug Discov* **7**, 339-57 (2008).
129. Pierce, K.L., Premont, R.T. & Lefkowitz, R.J. Seven-transmembrane receptors. *Nat Rev Mol Cell Biol* **3**, 639-50 (2002).
130. Gilman, A.G. G proteins: transducers of receptor-generated signals. *Annu Rev Biochem* **56**, 615-49 (1987).
131. Smrcka, A.V. G protein betagamma subunits: central mediators of G protein-coupled receptor signaling. *Cell Mol Life Sci* **65**, 2191-214 (2008).
132. Watson, A.J., Aragay, A.M., Slepak, V.Z. & Simon, M.I. A novel form of the G protein beta subunit Gbeta5 is specifically expressed in the vertebrate retina. *J Biol Chem* **271**, 28154-60 (1996).

133. Dupre, D.J., Robitaille, M., Rebois, R.V. & Hebert, T.E. The role of Gbetagamma subunits in the organization, assembly, and function of GPCR signaling complexes. *Annu Rev Pharmacol Toxicol* **49**, 31-56 (2009).
134. Khan, S.M. *et al.* The expanding roles of Gbetagamma subunits in G protein-coupled receptor signaling and drug action. *Pharmacol Rev* **65**, 545-77 (2013).
135. Robishaw, J.D. & Berlot, C.H. Translating G protein subunit diversity into functional specificity. *Curr Opin Cell Biol* **16**, 206-9 (2004).
136. Azzi, M. *et al.* Beta-arrestin-mediated activation of MAPK by inverse agonists reveals distinct active conformations for G protein-coupled receptors. *Proc Natl Acad Sci U S A* **100**, 11406-11 (2003).
137. Rajagopal, S. *et al.* Beta-arrestin- but not G protein-mediated signaling by the "decoy" receptor CXCR7. *Proc Natl Acad Sci U S A* **107**, 628-32 (2010).
138. Rosenbaum, D.M., Rasmussen, S.G. & Kobilka, B.K. The structure and function of G-protein-coupled receptors. *Nature* **459**, 356-63 (2009).
139. Yudin, Y. & Rohacs, T. Inhibitory Gi/O-coupled receptors in somatosensory neurons: Potential therapeutic targets for novel analgesics. *Mol Pain* **14**, 1744806918763646 (2018).
140. Milligan, G. & Kostenis, E. Heterotrimeric G-proteins: a short history. *Br J Pharmacol* **147 Suppl 1**, S46-55 (2006).
141. Nobles, M., Benians, A. & Tinker, A. Heterotrimeric G proteins precouple with G protein-coupled receptors in living cells. *Proc Natl Acad Sci U S A* **102**, 18706-11 (2005).
142. Berman, D.M., Wilkie, T.M. & Gilman, A.G. GAIP and RGS4 are GTPase-activating proteins for the Gi subfamily of G protein alpha subunits. *Cell* **86**, 445-52 (1996).
143. De Vries, L., Zheng, B., Fischer, T., Elenko, E. & Farquhar, M.G. The regulator of G protein signaling family. *Annu Rev Pharmacol Toxicol* **40**, 235-71 (2000).
144. Hepler, J.R., Berman, D.M., Gilman, A.G. & Kozasa, T. RGS4 and GAIP are GTPase-activating proteins for Gq alpha and block activation of phospholipase C beta by gamma-thio-GTP-Gq alpha. *Proc Natl Acad Sci U S A* **94**, 428-32 (1997).
145. Hunt, T.W., Fields, T.A., Casey, P.J. & Peralta, E.G. RGS10 is a selective activator of G alpha i GTPase activity. *Nature* **383**, 175-7 (1996).
146. Kozasa, T. *et al.* p115 RhoGEF, a GTPase activating protein for Galpha12 and Galpha13. *Science* **280**, 2109-11 (1998).
147. Neer, E.J. Heterotrimeric G proteins: organizers of transmembrane signals. *Cell* **80**, 249-57 (1995).
148. Downes, G.B. & Gautam, N. The G protein subunit gene families. *Genomics* **62**, 544-52 (1999).
149. Gautam, N., Downes, G.B., Yan, K. & Kisselev, O. The G-protein betagamma complex. *Cell Signal* **10**, 447-55 (1998).
150. Lindorfer, M.A. *et al.* Differential activity of the G protein beta5 gamma2 subunit at receptors and effectors. *J Biol Chem* **273**, 34429-36 (1998).
151. Howlett, A.C., Gray, A.J., Hunter, J.M. & Willardson, B.M. Role of molecular chaperones in G protein beta5/regulator of G protein signaling dimer assembly and G protein betagamma dimer specificity. *J Biol Chem* **284**, 16386-99 (2009).
152. Watson, A.J., Katz, A. & Simon, M.I. A fifth member of the mammalian G-protein beta-subunit family. Expression in brain and activation of the beta 2 isotype of phospholipase C. *J Biol Chem* **269**, 22150-6 (1994).

153. Li, D. & Roberts, R. WD-repeat proteins: structure characteristics, biological function, and their involvement in human diseases. *Cell Mol Life Sci* **58**, 2085-97 (2001).
154. Sondek, J., Bohm, A., Lambright, D.G., Hamm, H.E. & Sigler, P.B. Crystal structure of a G-protein beta gamma dimer at 2.1A resolution. *Nature* **379**, 369-74 (1996).
155. Jain, B.P. & Pandey, S. WD40 Repeat Proteins: Signalling Scaffold with Diverse Functions. *Protein J* **37**, 391-406 (2018).
156. Yates, B. *et al.* Genenames.org: the HGNC and VGNC resources in 2017. *Nucleic Acids Res* **45**, D619-D625 (2017).
157. UniProt, C. UniProt: a worldwide hub of protein knowledge. *Nucleic Acids Res* **47**, D506-D515 (2019).
158. Brett, M. *et al.* Acute lymphoblastic leukemia in a child with a de novo germline gnb1 mutation. *Am J Med Genet A* **173**, 550-552 (2017).
159. Rosenfeld, J.A. *et al.* Refinement of Causative Genes in Monosomy 1p36 Through Clinical and Molecular Cytogenetic Characterization of Small Interstitial Deletions. *American Journal of Medical Genetics Part A* **152a**, 1951-1959 (2010).
160. Shaffer, L.G. & Lupski, J.R. Molecular mechanisms for constitutional chromosomal rearrangements in humans. *Annual Review of Genetics* **34**, 297-329 (2000).
161. Okae, H. & Iwakura, Y. Neural tube defects and impaired neural progenitor cell proliferation in Gbeta1-deficient mice. *Dev Dyn* **239**, 1089-101 (2010).
162. Ford, C.E. *et al.* Molecular basis for interactions of G protein betagamma subunits with effectors. *Science* **280**, 1271-4 (1998).
163. Stallmeyer, B. *et al.* A Mutation in the G-Protein Gene GNB2 Causes Familial Sinus Node and Atrioventricular Conduction Dysfunction. *Circ Res* **120**, e33-e44 (2017).
164. Whorton, M.R. & MacKinnon, R. X-ray structure of the mammalian GIRK2-betagamma G-protein complex. *Nature* **498**, 190-7 (2013).
165. Gehrmann, J. *et al.* Impaired parasympathetic heart rate control in mice with a reduction of functional G protein betagamma-subunits. *Am J Physiol Heart Circ Physiol* **282**, H445-56 (2002).
166. Logothetis, D.E., Kurachi, Y., Galper, J., Neer, E.J. & Clapham, D.E. The Beta-Subunit and Gamma-Subunit of Gtp-Binding Proteins Activate the Muscarinic K+ Channel in Heart. *Nature* **325**, 321-326 (1987).
167. Kuss, J. *et al.* Familial Sinus Node Disease Caused by a Gain of GIRK (G-Protein Activated Inwardly Rectifying K(+) Channel) Channel Function. *Circ Genom Precis Med* **12**, e002238 (2019).
168. Ke, W. *et al.* Gbeta1 is required for neutrophil migration in zebrafish. *Dev Biol* **428**, 135-147 (2017).
169. Fuse, N., Hisata, K., Katzen, A.L. & Matsuzaki, F. Heterotrimeric G proteins regulate daughter cell size asymmetry in Drosophila neuroblast divisions. *Curr Biol* **13**, 947-54 (2003).
170. Dubaj Price, M. & Hurd, D.D. WormBase: A Model Organism Database. *Med Ref Serv Q* **38**, 70-80 (2019).
171. Simmer, F. *et al.* Genome-wide RNAi of C. elegans using the hypersensitive rrf-3 strain reveals novel gene functions. *PLoS Biol* **1**, E12 (2003).
172. Goldlust, I.S. *et al.* Mouse model implicates GNB3 duplication in a childhood obesity syndrome. *Proceedings of the National Academy of Sciences of the United States of America* **110**, 14990-14994 (2013).

173. Ozdemir, A.C. *et al.* GNB3 overexpression causes obesity and metabolic syndrome. *Plos One* **12**(2017).
174. Ye, Y.C. *et al.* Ablation of the GNB3 gene in mice does not affect body weight, metabolism or blood pressure, but causes bradycardia. *Cellular Signalling* **26**, 2514-2520 (2014).
175. Lagman, D., Callado-Perez, A., Franzen, I.E., Larhammar, D. & Abalo, X.M. Transducin duplicates in the zebrafish retina and pineal complex: differential specialisation after the teleost tetraploidisation. *PLoS One* **10**, e0121330 (2015).
176. Wang, Q. *et al.* Targeted deletion of one or two copies of the G protein beta subunit G beta 5 gene has distinct effects on body weight and behavior in mice. *Faseb Journal* **25**, 3949-3957 (2011).
177. Xie, K.Q. *et al.* G beta 5-RGS complexes are gatekeepers of hyperactivity involved in control of multiple neurotransmitter systems. *Psychopharmacology* **219**, 823-834 (2012).
178. Zhang, J.H. *et al.* Knockout of G protein beta5 impairs brain development and causes multiple neurologic abnormalities in mice. *J Neurochem* **119**, 544-54 (2011).
179. Chen, C.K. *et al.* Instability of GGL domain-containing RGS proteins in mice lacking the G protein beta-subunit Gbeta5. *Proc Natl Acad Sci U S A* **100**, 6604-9 (2003).
180. Robatzek, M., Niacaris, T., Steger, K., Avery, L. & Thomas, J.H. eat-11 encodes GPB-2, a G beta(5) ortholog that interacts with G(o)alpha and G(q)alpha to regulate C-elegans behavior. *Current Biology* **11**, 288-293 (2001).
181. Das, R.G. *et al.* Genome-wide association study and whole-genome sequencing identify a deletion in LRIT3 associated with canine congenital stationary night blindness. *Sci Rep* **9**, 14166 (2019).
182. Zeitz, C., Robson, A.G. & Audo, I. Congenital stationary night blindness: an analysis and update of genotype-phenotype correlations and pathogenic mechanisms. *Prog Retin Eye Res* **45**, 58-110 (2015).
183. Lee, R.H., Lieberman, B.S., Yamane, H.K., Bok, D. & Fung, B.K. A third form of the G protein beta subunit. 1. Immunochemical identification and localization to cone photoreceptors. *J Biol Chem* **267**, 24776-81 (1992).
184. Peng, Y.W., Robishaw, J.D., Levine, M.A. & Yau, K.W. Retinal Rods and Cones Have Distinct G-Protein Beta-Subunit and Gamma-Subunit. *Proceedings of the National Academy of Sciences of the United States of America* **89**, 10882-10886 (1992).
185. Ritchey, E.R. *et al.* THE PATTERN OF EXPRESSION OF GUANINE NUCLEOTIDE-BINDING PROTEIN beta 3 IN THE RETINA IS CONSERVED ACROSS VERTEBRATE SPECIES. *Neuroscience* **169**, 1376-1391 (2010).
186. Dhingra, A. *et al.* G beta(3) Is Required for Normal Light ON Responses and Synaptic Maintenance. *Journal of Neuroscience* **32**, 11343-11355 (2012).
187. Nikonov, S.S. *et al.* Cones respond to light in the absence of transducin beta subunit. *J Neurosci* **33**, 5182-94 (2013).
188. Tummala, H. *et al.* Mutation in the guanine nucleotide-binding protein beta-3 causes retinal degeneration and embryonic mortality in chickens. *Investigative Ophthalmology & Visual Science* **47**, 4714-4718 (2006).
189. Siffert, W. *et al.* Association of a human G-protein beta 3 subunit variant with hypertension. *Nature Genetics* **18**, 45-48 (1998).

190. Hengstenberg, C. *et al.* Association between a polymorphism in the G protein beta 3 subunit gene (GNB3) with arterial hypertension but not with myocardial infarction. *Cardiovascular Research* **49**, 820-827 (2001).
191. Rong, S.L. *et al.* Association of G-protein beta3 subunit C825T polymorphism with essential hypertension: evidence from 63 729 subjects. *J Hum Hypertens* **31**, 511-514 (2017).
192. Sousa, A.C. *et al.* The genetic variant C825T of the beta 3 subunit of G protein is associated with hypertension in a Portuguese population. *Revista Portuguesa De Cardiologia* **37**, 499-507 (2018).
193. Moselhy, S.S. *et al.* Analysis of SNPs of MC4R, GNB3 and FTO gene polymorphism in obese Saudi subjects. *African Health Sciences* **17**, 1059-1069 (2017).
194. Rizvi, S., Raza, S.T., Rahman, Q. & Mahdi, F. Role of GNB3, NET, KCNJ11, TCF7L2 and GRL genes single nucleotide polymorphism in the risk prediction of type 2 diabetes mellitus. *3 Biotech* **6**, 255 (2016).
195. Chen, P.S. *et al.* A longitudinal study of the association between the GNB3 C825T polymorphism and metabolic disturbance in bipolar II patients treated with valproate. *Pharmacogenomics Journal* **17**, 155-161 (2017).
196. Prystupa, L.N., Moiseyenko, I.O., Garbuzova, V.Y., Kmyta, V.V. & Dudchenko, I.A. Association of metabolic syndrome components with the genotypes of the capital ES, Cyrillic825capital TE, Cyrillic polymorphism in the g protein beta3-subunit gene (GNB3). *Wiad Lek* **71**, 1242-1249 (2018).
197. Ma, J. *et al.* GNB3 and CREB1 gene polymorphisms combined with negative life events increase susceptibility to major depression in a Chinese Han population. *PLoS One* **12**, e0170994 (2017).
198. Zill, P. *et al.* Evidence for an association between a G-protein beta3-gene variant with depression and response to antidepressant treatment. *Neuroreport* **11**, 1893-7 (2000).
199. Nam, Y.J., Cho, C.H., Kim, L. & Lee, H.J. Association of G-Protein beta3 Subunit C825T Polymorphism with Seasonal Variations in Mood and Behavior. *Psychiatry Investig* **15**, 200-204 (2018).
200. Song, Y.Z. *et al.* The C825T Polymorphism of the G-Protein beta3 Gene as a Risk Factor for Functional Dyspepsia: A Meta-Analysis. *Gastroenterol Res Pract* **2016**, 5037254 (2016).
201. Triantafyllou, K., Kourikou, A., Gazouli, M., Karamanolis, G.P. & Dimitriadis, G.D. Functional dyspepsia susceptibility is related to CD14, GNB3, MIF, and TRPV1 gene polymorphisms in the Greek population. *Neurogastroenterol Motil* **29**(2017).
202. Morrison, A.C. *et al.* G-protein beta3 subunit and alpha-adducin polymorphisms and risk of subclinical and clinical stroke. *Stroke* **32**, 822-9 (2001).
203. Zhang, L. *et al.* The 825C/T polymorphism of G-protein beta3 subunit gene and risk of ischaemic stroke. *J Hum Hypertens* **19**, 709-14 (2005).
204. Schreieck, J. *et al.* C825T polymorphism of the G-protein beta3 subunit gene and atrial fibrillation: association of the TT genotype with a reduced risk for atrial fibrillation. *Am Heart J* **148**, 545-50 (2004).
205. Eba, A. *et al.* Association of SDF1beta (G801A) and GNB3 (C825T) polymorphisms with the incidence and severity of coronary artery disease. *Br J Biomed Sci* **76**, 49-51 (2019).

206. Zhu, W., Li, J., Sun, X. & Hua, Q. Association of G-protein beta3 subunit gene C825T polymorphism with cardiac and cerebrovascular events in Chinese hypertensive patients. *Clin Exp Hypertens* **39**, 80-84 (2017).
207. Casiglia, E. *et al.* The C825T GNB3 polymorphism, independent of blood pressure, predicts cerebrovascular risk at a population level. *Am J Hypertens* **25**, 451-7 (2012).
208. Frey, U.H. *et al.* GNB3 gene 825 TT variant predicts hard coronary events in the population-based Heinz Nixdorf Recall study. *Atherosclerosis* **237**, 437-42 (2014).
209. Nakao, R. *et al.* GNB3 C825T polymorphism is associated with postural tachycardia syndrome in children. *Pediatr Int* **54**, 829-37 (2012).
210. Wascher, T.C. *et al.* Associations of a human G protein beta3 subunit dimorphism with insulin resistance and carotid atherosclerosis. *Stroke* **34**, 605-9 (2003).
211. D'Angelo, C.S. *et al.* Chromosomal microarray analysis in the genetic evaluation of 279 patients with syndromic obesity. *Mol Cytogenet* **11**, 14 (2018).
212. Soong, B.W. *et al.* Exome sequencing identifies GNB4 mutations as a cause of dominant intermediate Charcot-Marie-Tooth disease. *Am J Hum Genet* **92**, 422-30 (2013).
213. Miura, S. *et al.* A novel missense variant (Gln220Arg) of GNB4 encoding guanine nucleotide-binding protein, subunit beta-4 in a Japanese family with autosomal dominant motor and sensory neuropathy. *Eur J Med Genet* **60**, 474-478 (2017).
214. Wall, M.A., Posner, B.A. & Sprang, S.R. Structural basis of activity and subunit recognition in G protein heterotrimers. *Structure* **6**, 1169-1183 (1998).
215. Gaudet, R., Bohm, A. & Sigler, P.B. Crystal structure at 2.4 angstrom resolution of the complex of transducin beta gamma and its regulator, phosducin. *Cell* **87**, 577-588 (1996).
216. Khan, S.M. *et al.* G beta(4)gamma(1) as a modulator of M3 muscarinic receptor signalling and novel roles of G beta(1) subunits in the modulation of cellular signalling. *Cellular Signalling* **27**, 1597-1608 (2015).
217. Chandler, N.J. *et al.* Molecular Architecture of the Human Sinus Node Insights Into the Function of the Cardiac Pacemaker. *Circulation* **119**, 1562-1575 (2009).
218. Fleischmann, B.K. *et al.* Differential subunit composition of the G protein-activated inward-rectifier potassium channel during cardiac development. *Journal of Clinical Investigation* **114**, 994-1001 (2004).
219. Rosskopf, D. *et al.* The human G protein beta 4 subunit: gene structure, expression, G gamma and effector interaction. *Febs Letters* **544**, 27-32 (2003).
220. Ruiz-Velasco, V., Ikeda, S.R. & Puhl, H.L. Cloning, tissue distribution, and functional expression of the human G protein beta 4-subunit. *Physiological Genomics* **8**, 41-50 (2002).
221. Smolock, E.M. *et al.* Genetic locus on mouse chromosome 7 controls elevated heart rate. *Physiological Genomics* **44**, 689-698 (2012).
222. Patil, D.N. *et al.* Structural organization of a major neuronal G protein regulator, the RGS7-Gbeta5-R7BP complex. *Elife* **7**(2018).
223. Nini, L., Zhang, J.H., Pandey, M., Panicker, L.M. & Simonds, W.F. Expression of the G beta(5)/R7-RGS protein complex in pituitary and pancreatic islet cells. *Endocrine* **42**, 214-217 (2012).
224. Sanchez-Blazquez, P., Rodriguez-Diaz, M., Lopez-Fando, A., Rodriguez-Munoz, M. & Garzon, J. The GBeta5 subunit that associates with the R7 subfamily of RGS proteins regulates mu-opioid effects. *Neuropharmacology* **45**, 82-95 (2003).

225. Sondek, J. & Siderovski, D.P. G gamma-like (CG-L) domains: new frontiers in G-protein signaling and beta-propeller scaffolding. *Biochemical Pharmacology* **61**, 1329-1337 (2001).
226. Witherow, D.S. & Slepak, V.Z. A novel kind of G protein heterodimer: The G beta 5-RGS complex. *Receptors & Channels* **9**, 205-212 (2003).
227. Xie, K.Q. *et al.* G beta 5 recruits R7 RGS proteins to GIRK channels to regulate the timing of neuronal inhibitory signaling. *Nature Neuroscience* **13**, 661-663 (2010).
228. Xie, K.Q., Masuho, I., Brand, C., Dessauer, C.W. & Martemyanov, K.A. The Complex of G Protein Regulator RGS9-2 and G beta(5) Controls Sensitization and Signaling Kinetics of Type 5 Adenylyl Cyclase in the Striatum. *Science Signaling* **5**(2012).
229. Shao, Z. *et al.* Unique retinal signaling defect in GNB5-related disease. *Documenta Ophthalmologica* (2019).
230. Veerman, C.C. *et al.* Genetic variation in GNB5 causes bradycardia by augmenting the cholinergic response via increased acetylcholine-activated potassium current (I-K,I-ACh). *Disease Models & Mechanisms* **12**(2019).
231. Krispel, C.M., Chen, C.K., Simon, M.I. & Burns, M.E. Prolonged photoresponses and defective adaptation in rods of Gbeta5-/- mice. *J Neurosci* **23**, 6965-71 (2003).
232. Rao, A., Dallman, R., Henderson, S. & Chen, C.K. G beta 5 is required for normal light responses and morphology of retinal ON-bipolar cells. *Journal of Neuroscience* **27**, 14199-14204 (2007).
233. Tian, M. *et al.* Light-Induced Translocation of RGS9-1 and G beta 5L in Mouse Rod Photoreceptors. *Plos One* **8**(2013).
234. Kulkarni, K. *et al.* The influences of the M2R-GIRK4-RGS6 dependent parasympathetic pathway on electrophysiological properties of the mouse heart (vol 13, e0193798, 2018). *Plos One* **13**(2018).
235. Maity, B. *et al.* Regulator of G Protein Signaling 6 (RGS6) Protein Ensures Coordination of Motor Movement by Modulating GABA(B) Receptor Signaling. *Journal of Biological Chemistry* **287**, 4972-4981 (2012).
236. Posokhova, E., Wydeven, N., Allen, K.L., Wickman, K. & Martemyanov, K.A. RGS6/G beta 5 Complex Accelerates I-KACh Gating Kinetics in Atrial Myocytes and Modulates Parasympathetic Regulation of Heart Rate. *Circulation Research* **107**, 1350-1354 (2010).

Aim of the PhD project

The goal of my PhD project was to identify the genetic and molecular cause of a complex phenotypic spectrum. The affected patients showed intellectual disability with early-onset sinus node dysfunction, hypotonia, seizures and vision abnormalities. The work principally aimed at giving a genetic diagnosis to the patients and their families - who were unaware of the nature of their genetic disorder for years – thus providing opportunities to improve their clinical care, family planning and follow-up. It also allowed to unravel a new ID gene, in the context of a syndrome presenting comorbidity with heart conduction and ophthalmic problems. Concurrently, it favored the description of a novel syndrome that helped the diagnosis of further patients presenting similar traits.

The discoveries we made also contributed to broaden the knowledge on the function of the causative gene (*GNB5*, MIM: 604447) and its biological mechanism.

Briefly, following the molecular diagnosis, we provided biochemical and animal model studies allowing us to confirm the involvement of *GNB5* in the disease manifestations. We aimed at exploring phenotypic and molecular signatures useful to delineate pathological mechanisms of the syndrome with the ultimate goal of driving future therapeutic approaches.

Summary of the Results

The projects I carried out during my doctorate gave me the possibility to reach a conclusive molecular diagnosis for a family I studied and whose affected individuals presented a unique combination of manifestations, not corresponding to any previously described syndrome.

The chapters that will follow represent the projects I led during my PhD; the first one regards the identification of the first affected individuals and exemplifies a great international and collaborative effort to gather subjects presenting overlapping clinical signs and carrying mutations in the same gene. I started this project studying an Italian family (Family A in[1]) with two siblings showing signs of global developmental delay and severe ID combined with absent speech, epileptic spasms, severe hypotonia, retinal disease and nystagmus, and gastric problems. Whole exome sequencing of the affected individuals and their unaffected parents, enabled the identification of compound heterozygous loss of function variants in the gene encoding the subunit β_5 of the Guanine Nucleotide-Binding protein, *GNB5*. I performed *in vitro* studies to demonstrate the pathogenicity of the detected variants, a splice-site mutation altering splicing accuracy and a nonsense substitution subjected to nonsense-mediated decay. Thanks to worldwide collaborations, I was then able to gather nine affected individuals from six different families sharing phenotypes and variants in *GNB5* gene. I observed a genotype-phenotype correlation among individuals carrying loss-of-function mutations and displaying a severe end of the disease spectrum, compared to carriers of missense alleles presenting a milder phenotype. Genome-editing using a zebrafish model finally provided functional evidence of *GNB5* involvement in disease manifestations. Findings related to this project were published in the American Journal of Human Genetics, in 2016 and the genetic disorder we described was subsequently named Intellectual Developmental Disorder with Cardiac Arrhythmia (IDDCA).

In the second study, we expanded further the number of IDDCA-affected individuals by reporting a new compound heterozygous IDDCA patient[2]. Since our description of the first cases, other researchers have detected and described more IDDCA patients to reach a total of 27 published cases[3-6] including the one above[2].

In the third chapter of my thesis project, I found and documented 6 more patients to increase the number of ascertained IDDCA patients to 33 individuals. This task was performed in collaboration with colleagues from France and United Kingdom. While, 4 out of 6 patients

presented with previously reported mutations, we also pinpointed two novel variants, whose pathogenicity was supported by *in silico* modeling studies, thus expanding the *GNB5* mutational spectrum. In this third work, we also investigated the involvement of the autonomic nervous system in heart rhythmicity, using the mouse as a model. We unraveled that the heart of *Gnb5*-null mice was smaller but showed increased contractile properties. We demonstrated that this is not due to anomalies in the sympathetic innervation of the heart that might influence the capacity of the heart to contract; rather it represents a compensatory mechanism to counteract the smaller volume of blood and to ensure proper body dynamics. Accordingly, transcriptome comparison of atria and ventricles of knock-out *vs.* control animals revealed dysregulation of genes involved in cardiac muscle contractility and pacemaker cell formation. While sympathetic response remained unchanged, we found an enhanced parasympathetic sensitivity causing a strong bradycardia in knock-out mice, reminiscent of the cardiac phenotype observed in human carriers. Additionally, and further corroborating human findings, *Gnb5* knock-out mice showed a high number of cardiac arrhythmias. These recent findings will soon be submitted for peer-review.

Finally, I was also involved as first co-author in the writing of a review focusing on the contribution of genes encoding the β subunits of the Guanine Nucleotide-Binding protein in the etiology of genetic disorders involving neurologic, cardiac and ophthalmic systems. This work was very recently published in *Cells*[7].

References:

1. Lodder, E.M. *et al.* GNB5 Mutations Cause an Autosomal-Recessive Multisystem Syndrome with Sinus Bradycardia and Cognitive Disability. *Am J Hum Genet* **99**, 786 (2016).
2. Vernon, H. *et al.* Intellectual developmental disorder with cardiac arrhythmia syndrome in a child with compound heterozygous GNB5 variants. *Clin Genet* **93**, 1254-1256 (2018).
3. Malerba, N. *et al.* A NGS-Targeted Autism/ID Panel Reveals Compound Heterozygous GNB5 Variants in a Novel Patient. *Front Genet* **9**, 626 (2018).
4. Poke, G. *et al.* The epileptology of GNB5 encephalopathy. *Epilepsia* **60**, e121-e127 (2019).
5. Shamseldin, H.E. *et al.* GNB5 mutation causes a novel neuropsychiatric disorder featuring attention deficit hyperactivity disorder, severely impaired language development and normal cognition. *Genome Biol* **17**, 195 (2016).

6. Turkdogan, D., Usluer, S., Akalin, F., Agyuz, U. & Aslan, E.S. Familial early infantile epileptic encephalopathy and cardiac conduction disorder: A rare cause of SUDEP in infancy. *Seizure* **50**, 171-172 (2017).
7. Malerba, N., De Nittis, P. & Merla, G. The Emerging Role of Gbeta Subunits in Human Genetic Diseases. *Cells* **8**(2019).

Chapter 1: *GNB5* Mutations Cause an Autosomal-Recessive Multisystem Syndrome with Sinus Bradycardia and Cognitive Disability

Summary of the contribution

This article was published in American Journal of Human Genetics (2016), doi: 10.1016/j.ajhg.2016.06.025

My contribution to this work concerned patients' recruitment, clinical information gathering, preparation of samples, downstream analysis of whole-exome sequence data, and mutational analysis. I contributed as well to the manuscript writing under the supervision of Alexandre Reymond, and together with Giuseppe Merla, Connie R. Bezzina and Jeroen Bakkers. I personally presented part of this work at the Italian Society of Human Genetics congress (i) in Rimini in 2015 and (ii) Turin in 2016, and (iii) at the American Society of Human Genetics congress in Vancouver, Canada in 2016. I was one of the semifinalists for the Charles J. Epstein Trainee Awards for Excellence in Human Genetics Research at the Vancouver conference and was awarded the "Leopoldo Zelante" price for an outstanding talk in the field of medical genetics research at 2016 meeting of the Italian Society of Human Genetics.

The results are presented in three main figures (named **Figure 1-3**), eight supplementary figures (**Figure S1-8**), one table included in the text and one supplementary table (named **Table S1**). Supplemental videos are available in the online version of the paper.

REPORT

GNB5 Mutations Cause an Autosomal-Recessive Multisystem Syndrome with Sinus Bradycardia and Cognitive Disability

Elisabeth M. Lodder,[1,22] Pasquelena De Nittis,[2,3,22] Charlotte D. Koopman,[4,5,22] Wojciech Wiszniewski,[6] Carolina Fischinger Moura de Souza,[7] Najim Lahrouchi,[1] Nicolas Guex,[2,8] Valerio Napolioni,[9] Federico Tessadori,[5] Leander Beekman,[1] Eline A. Nannenberg,[10] Lamiae Boualla,[11] Nico A. Blom,[12] Wim de Graaff,[13] Maarten Kamermans,[13,14] Dario Cocciadiferro,[3,15] Natascia Malerba,[3,15] Barbara Mandriani,[3,16] Zeynep Hande Coban Akdemir,[6] Richard J. Fish,[17] Mohammad K. Eldomery,[6] Ilham Ratbi,[11] Arthur A.M. Wilde,[1] Teun de Boer,[4] William F. Simonds,[18] Marguerite Neerman-Arbez,[17] V. Reid Sutton,[6,19] Fernando Kok,[20] James R. Lupski,[6,19,21] Alexandre Reymond,[2,23] Connie R. Bezzina,[1,23] Jeroen Bakkers,[4,5,23,*] and Giuseppe Merla[3,23,*]

GNB5 encodes the G protein β subunit 5 and is involved in inhibitory G protein signaling. Here, we report mutations in *GNB5* that are associated with heart-rate disturbance, eye disease, intellectual disability, gastric problems, hypotonia, and seizures in nine individuals from six families. We observed an association between the nature of the variants and clinical severity; individuals with loss-of-function alleles had more severe symptoms, including substantial developmental delay, speech defects, severe hypotonia, pathological gastro-esophageal reflux, retinal disease, and sinus-node dysfunction, whereas related heterozygotes harboring missense variants presented with a clinically milder phenotype. Zebrafish *gnb5* knockouts recapitulated the phenotypic spectrum of affected individuals, including cardiac, neurological, and ophthalmological abnormalities, supporting a direct role of GNB5 in the control of heart rate, hypotonia, and vision.

Heterotrimeric G proteins trigger a signal transduction cascade composed of α, β, and γ subunits. They are associated with G protein-coupled receptors (GPCRs) in modulating an array of cellular functions, including release of a multitude of hormones and growth factors, regulation of cell contraction and migration, and cell growth and differentiation during development.[1–4] G protein-coupled signaling plays a crucial role in neuronal communication, including regulation of the antagonistic effects of the parasympathetic and sympathetic branches of the autonomic nervous system throughout the body. We report a genetic disorder caused by mutations affecting *GNB5* (MIM: 604447), encoding guanine nucleotide-binding protein subunit beta-5, and with disease manifestation in multiple systems.

We identified nine affected individuals (six females and three males) from six unrelated families presenting with a clinical overlap of neurological and cardiac conduction defects; all subjects were found to have variation in the same gene, *GNB5*, and share a similar rare phenotype. This work results from exome and phenotype data aggregation among independent groups engaged in studying the molecular basis of yet unsolved human genetic rare disease traits. Shared phenotypic features representing the cardinal characteristics of the syndrome include global developmental delay, seizures, generalized hypotonia, retinal disease, and the uncommon feature of early-onset sinus-node dysfunction (Table 1). Additional clinical investigations and diagnostic studies did not show any evidence of structural CNS, ocular, or cardiac anomalies. Affected individuals from four of the six families (families A–D) demonstrated the severe end of the disease spectrum, including substantial cognitive deficits, delayed motor development, severe

[1]Department of Clinical and Experimental Cardiology, Heart Center, Academic Medical Center, University of Amsterdam, 1105 AZ Amsterdam, the Netherlands; [2]Center for Integrative Genomics, University of Lausanne, 1015 Lausanne, Switzerland; [3]Medical Genetics Unit, IRCCS Casa Sollievo della Sofferenza, viale Cappuccini, 71013 San Giovanni Rotondo, Foggia, Italy; [4]Department of Medical Physiology, Division of Heart and Lungs, University Medical Center Utrecht, 3584 CT Utrecht, the Netherlands; [5]Hubrecht Institute– Royal Netherlands Academy of Arts and Sciences (KNAW), University Medical Centre Utrecht, 3584 CT Utrecht, the Netherlands; [6]Department of Molecular and Human Genetics, Baylor College of Medicine, Houston, TX 77030, USA; [7]Medical Genetics Service, Hospital de Clinicas de Porto Alegre, 2350 Porto Alegre, Brazil; [8]Swiss Institute of Bioinformatics, 1015 Lausanne, Switzerland; [9]Department of Neurology and Neurological Sciences, Stanford University School of Medicine, Palo Alto, CA 94304, USA; [10]Department of Clinical Genetics, Academic Medical Center, University of Amsterdam, 1105 AZ Amsterdam, the Netherlands; [11]Centre de Génomique Humaine, Faculté de Médecine et Pharmacie, Mohammed V University of Rabat, 8007, Rabat, Morocco; [12]Department of Pediatric Cardiology, Emma Children's Hospital, Academic Medical Centre, 1105 AZ Amsterdam, the Netherlands; [13]Retinal Signal Processing Lab, Netherlands Institute for Neuroscience, 1105 BA Amsterdam, the Netherlands; [14]Department of Genome Analysis, Academic Medical Center, University of Amsterdam, 1105 AZ Amsterdam, the Netherlands; [15]PhD Program in Experimental and Regenerative Medicine, Faculty of Medicine, University of Foggia, 71121 Foggia, Italy; [16]PhD Program in Molecular Genetics Applied to Medical Sciences, Department of Molecular and Translational Medicine, University of Brescia, 25121 Brescia, Italy; [17]Department of Genetic Medicine and Development, University Medical Centre (CMU), 1211 Geneva, Switzerland; [18]Metabolic Diseases Branch, National Institute of Diabetes and Digestive and Kidney Diseases, NIH, Bethesda, MD 20892-2560, USA; [19]Texas Children's Hospital, Houston, TX 77030, USA; [20]Child Neurology Division, Department of Neurology, School of Medicine, University of Sao Paulo, 01246903 Sao Paulo, Brazil; [21]Department of Pediatrics, Baylor College of Medicine, Houston, TX 77030, USA
[22]These authors contributed equally to this work
[23]These authors contributed equally to this work
*Correspondence: j.bakkers@hubrecht.eu (J.B.), g.merla@operapadrepio.it (G.M.)
http://dx.doi.org/10.1016/j.ajhg.2016.06.025.

Table 1. Overlapping Clinical Features of Individuals with *GNB5* Mutations

	Family A		Family B	Family C		Family D	Family E		Family F
	II.1	II.2	II.1	II.2	II.3	II.2	II.1	II.2	II.1
Gender, age (years)	F, 22	F, 20	F, 6	F, 11	M, 9	F, 12	F, 13	M, 8	M, 23
Birth weight	3,580 g (50^{th} percentile)	NA	2,980 g (15^{th} percentile)	2,751 g (15^{th} percentile)	NA	2,845 g (15^{th} percentile)	NA	NA	NA
Ethnicity	Italy	Italy	Jordan	Puerto Rico	Puerto Rico	India	Morocco	Morocco	Brazil
Consanguinity	–	–	+	+	+	–	–	–	+
Altered speech development	+	+	+	+	+	+	+	+	NA
Verbal understanding	NA	NA	nonverbal	unremarkable	unremarkable	NA	NA	NA	NA
Lexical production	NA	NA	nonverbal	delayed	delayed	nonverbal	delayed	delayed	NA
Intellectual disability	+	+	+	+	+	+	mild	mild	mild
Epilepsy	+	+	+	–	–	+	–	–	–
Sinus sick syndrome	+	+	+	+	+	increased PR interval (intermittent Weckenbach)	+	+	+
Minimum heart rate (bpm)	24	39	NA	paced	paced	NA	20	16	
Maximum heart rate (bpm)	163	192	NA	paced (27% heartbeats on Holter)	paced (20% heartbeats on Holter)	NA	176	180	NA
Chronotropic response	NA	NA	NA	+	+	NA	unremarkable	unremarkable	NA
Escape beats	+	+	NA	paced	paced	NA	+	+	NA
Pacemaker implantation	–	–	–	+	+	–	–	+	NA
Heart structural abnormalities	–	PFO	NA	–	–	–	–	–	NA
Hypotonia	+	+	+	+	+	+	–	impaired fine motor skills	–
Pathological gastric reflux	+	+	–	+	+	+	–	–	NA
Nystagmus	+	+	+	+	+	+	NA	–	NA
Plasma amino acids chromatography	938 μm/L (restored)	+ (restored)	unremarkable	unremarkable	unremarkable	unremarkable	444 μm/L	unremarkable	NA
Urine organic acids	unremarkable	unremarkable	increased excretion of 3-methyl-glutaconic acid	unremarkable	unremarkable	unremarkable	NA	NA	NA

Affected individual numbers refer to those in the pedigree in Figure 1. Complete pedigree charts, consanguinity status, variants, and related homozygous and/or compound heterozygous alleles are reported in Figure 1 and Table S1. Abbreviations are as follows: M, male; f, female; NA, not available; +, clinical trait present; –, clinical trait not present; PFO, patent foramen ovale; bpm, beats per minute.

hypotonia, retinal disease, pathological gastro-esophageal reflux, and sinus-node dysfunction. Affected individuals in families E and F presented with a milder phenotype, including mild intellectual impairment, language delay, and bradycardia (Figure 1, Table 1, Supplemental Note).

Given that no potentially pathogenic genomic structural abnormalities were identified by array comparative genomic hybridization and karyotyping of the affected subjects, we applied whole-exome sequencing to all the affected individuals and their healthy parents. Families were recruited in Italy (family A), Brazil (B and F), the United States (C and D), and the Netherlands (E). The institutional review boards of the IRCCS Casa Sollievo Della Sofferenza Hospital, the Hospital das Clínicas da Universidade de São Paulo, the

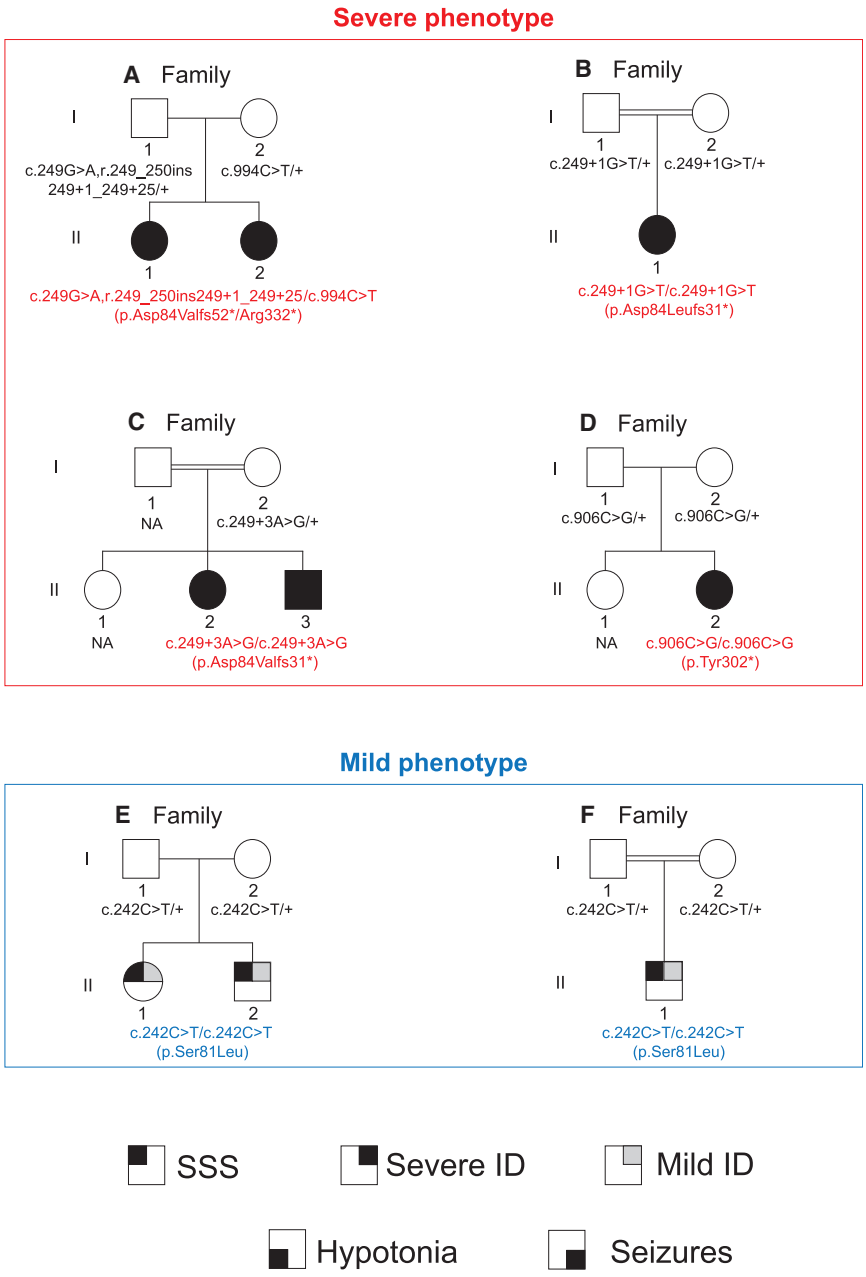

Figure 1. Pedigrees from the Six Families Investigated in this Study

Affected members of families A to D (upper red-lined panel) and E to F (lower blue-lined panel) show severe and mild manifestation of the core symptoms of the syndrome defined in this study. Filled symbols represent individuals with severe sinus sick syndrome (SSS; top left quarter), intellectual disability (ID; top right quarter), hypotonia (bottom left quarter), and seizures (bottom right quarter), whereas a light-gray top left quarter indicates the presence of mild ID. Genotypes are specified according to GenBank: NM_006578.3.

Baylor College of Medicine, the Amsterdam Academic Medical Center, and the University of Lausanne approved this study. Participants were enrolled after written informed consent was obtained from parents or legal guardians. The clinical evaluation included medical history interviews, a physical examination, and review of medical records. To uncover genetic variants associated with the complex phenotype shown by the nine affected subjects, we sequenced their exomes and those of their parents. DNA libraries were prepared from blood-derived genomic DNAs according to standard procedures. Exomes were captured and sequenced with different platforms to reach 50- to 120-fold coverage on average. Variants were called as previously described.[5–7] Variants were filtered on the basis of inheritance patterns, including autosomal recessive, X-linked, and de novo and/or autosomal dominant. Variants with MAF < 0.05% in control cohorts (dbSNP, the 1000 Genome Project, NHLBI GO Exome Sequencing Project, the Exome Aggregation Consortium database, and our in-house databases) and predicted to be deleterious by SIFT,[8] PolyPhen-2,[9] and/or UMD-Predictor[10] were prioritized.

Given a potential history of consanguinity reported in some families (families B, C, and F [Figure 1, Table 1]), we filtered variants by using Mendelian expectations for the assumption of a rare autosomal-recessive trait. We found *GNB5* to be compliant with Mendelian expectations and bearing bi-allelic putative deleterious variants in all affected individuals (Figure 1, Table S1). Sanger sequencing in each family confirmed the anticipated segregation of the *GNB5* variants. Strikingly, the variants found in the severely affected individuals (families A–D) were predicted to be loss-of-function (LoF) alleles, whereas the more mildly affected individuals from families E and F were homozygous for the same missense variant, c.242C>T (p.Ser81Leu [GenBank: NM_006578.3]) (Figures 1 and S1A). In families B, C, and D the affected individuals were homozygous for splice variants (c.249+1G>T [p.Asp84Leufs31*] and c.249G+3A>G [p.Asp84Valfs31*]) and a nonsense variant (c.906C>G [p.Tyr302*]), respectively (Figures 1 and S1A, Table S1). In family A, the affected siblings were compound heterozygous for a maternally inherited nonsense variant (c.994C>T [p.Arg332*]) and a paternally inherited splice-site change (c.249G>A [p.(=)]), which gives rise to an aberrantly spliced isoform containing an additional 25 nucleotides of the intervening intron 2 (Figure S2A). We experimentally show that the transcripts from both alleles are targeted by nonsense-mediated mRNA-decay (Figure S2B).

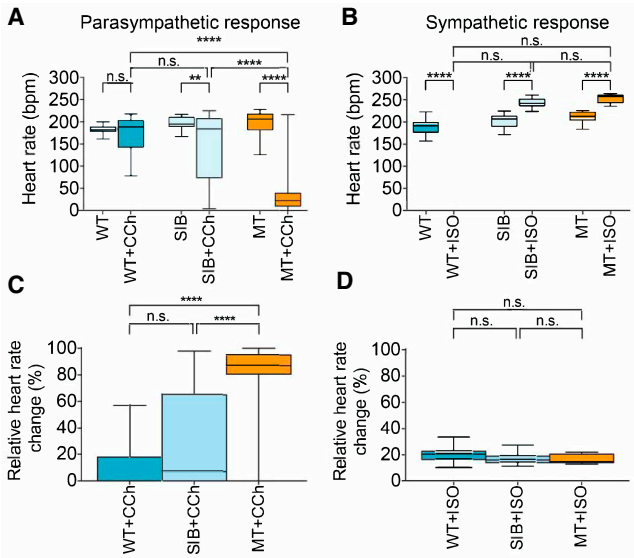

Figure 2. Cardiac Function in *gnb5* Mutant Zebrafish
(A–D) Box-whisker plots demonstrate the heart rate response and the relative heart rate change of 5 dpf wild-type (WT), sibling (SIB), and *gnb5* mutant (MT) larvae. Embryos at 5 dpf were embedded in 0.3% agarose prepared in E3 medium containing 16 mg/ml Tricaine. Basal heart rates were recorded first. Then, (A and C) 400 μM of the parasympathetic agonist carbachol (CCh; Sigma-Aldrich C4382) (WT n = 10, SIB n = 39, MT n = 14) or (B and D) 100 μM of the sympathetic agonist isoproterenol hydrochloride (ISO; Sigma-Aldrich 1351005) (WT n = 12, SIB n = 22, MT n = 9) was added and incubated for 30 min and heart rates were measured. Recordings were performed at 150 frames per second and were analyzed with ImageJ. The relative heart rate change is the percentage change between the basal heart rate measured and the heart rate after addition of CCh or ISO.
n denotes the number of fish used per dataset. Differences between two groups were analyzed via the Student's t test. Differences between more than two groups were analyzed via one-way ANOVA with Tukey's post-hoc test. Data are shown as mean ± SEM, and $p < 0.05$ was considered significant. *$p < 0.05$, **$p \leq 0.01$, ***$p \leq 0.001$, ****$p \leq 0.0001$. $p > 0.05$ was considered not significant (n.s.). bpm, beats per minute.

The five *GNB5* LoF variants identified in families A–D are either not present or present with MAF $\leq 8.25 \times 10^{-6}$ in ExAC (Exome Aggregation Consortium, v.0.3.1) (Table S1). Correspondingly, LoF variants in *GNB5* are underrepresented in comparison to expectation in this database; specifically, ExAC reports 8 LoF variants whereas 19 were expected. The c.242C>T (p.Ser81Leu) missense variant identified in family E, of Moroccan ancestry, and family F, of Brazilian ancestry, has a MAF $< 5 \times 10^{-5}$ (6/121,000) in the human population and 4.3×10^{-4} in Latinos (5/11,574). A sample of individuals from Morocco identified a prevalence of 1 out of 1,260 (7.94×10^{-4}) for this allele. We estimated the prevalence of the c.242C>T (p.Ser81Leu) variant in the Moroccan population by genotyping a total of 630 Moroccan individuals, including 394 Moroccans and 235 Dutch citizens of Moroccan descent by real-time PCR. Pathogenicity of this variant is further supported by three-dimensional representation of the encoded protein complexed with RGS9, a member of the R7 subfamily of regulators of G-protein signaling (RGS) proteins and common binding partner of GNB5. GNB5 is folded into essentially identical seven-bladed β-propellers (WD40 repeated domains) with equivalent N-terminal helical extensions.[11] Replacement of the evolutionarily conserved serine 81 (Figure S1B) by leucine will induce localized structural changes in the immediate vicinity of this residue, which could impair both the central pore of the β-propeller and the binding kinetics of RGS proteins (Figures S3– S5).

In line with the clinical presentation of affected individuals, *Gnb5* ablation in mice resulted in marked neurobehavioral abnormalities, including learning deficiencies, hyperactivity, impaired gross motor coordination, abnormal gait,[12] defective visual adaptation,[13] and perturbed development and functioning of retinal bipolar cells.[14] Correspondingly, mice lacking *Rgs6*, the *GNB5*-dependent RGS protein enriched in heart tissue, exhibit bradycardia and hypersensitivity to parasympathomimetics.[15,16] To independently investigate the functional effects of variation of *GNB5* in the full phenotypic spectrum of subjects reported herein, we engineered a zebrafish model knocked out for *gnb5*.

CRISPR/Cas9 genome editing was used to generate zebrafish with LoF mutations in *gnb5a* and *gnb5b*. This teleost has two *GNB5* paralogs as a result of an ancient genome duplication event[17] (Figure S6). We identified stable lines with a 7 bp insertion in *gnb5a* and a 8 bp deletion and 15 bp insertion in *gnb5b*, causing a frameshift and premature truncation of the encoded proteins, respectively (Figure S7). It was anticipated that *gnb5a* and *gnb5b* might have redundant functions, which was confirmed by the absence of overt phenotypes in embryos homozygous for either LoF mutations. As a consequence, a double knockout was generated to ensure complete loss of functional Gnb5. In-crosses of *gnb5a* and *gnb5b* double heterozygotes resulted in clutches of embryos containing the expected 6.25% of $gnb5a^{-/-}/gnb5b^{-/-}$ double mutants (henceforth referred to as *gnb5* mutants). Consistent with syndrome manifestations of affected individuals, zebrafish mutant embryos had no striking dysmorphologic features (Figure S7D). However, the larvae showed impaired swimming activity, remained small, and generally died 7–14 days post fertilization (dpf), most likely as a result of their inability to feed.

To assess the putative involvement of *GNB5* in autonomic nervous system functions, we investigated the GNB5-RGS-GIRK channel pathway. As GNB5 recruits RGS proteins to G protein-coupled inward rectifier potassium (GIRK) channels involved in the hyperpolarization of cell membranes,[16,18] we investigated whether LoF of *GNB5* could delay GIRK channel deactivation kinetics, increase hyperpolarization time of cell membranes, and impair cell responsiveness to new stimuli. Carbachol (PubChem CID: 5831) is a parasympathomimetic compound that activates acetylcholine receptors of the heart and the GNB5-RGS-GIRK channel pathway. Treatment of *gnb5* mutant larvae with carbachol resulted in a strong decrease of the heart rate, whereas it had little effect on wild-type and sibling larvae (Figure 2), consistent with loss of negative regulation of

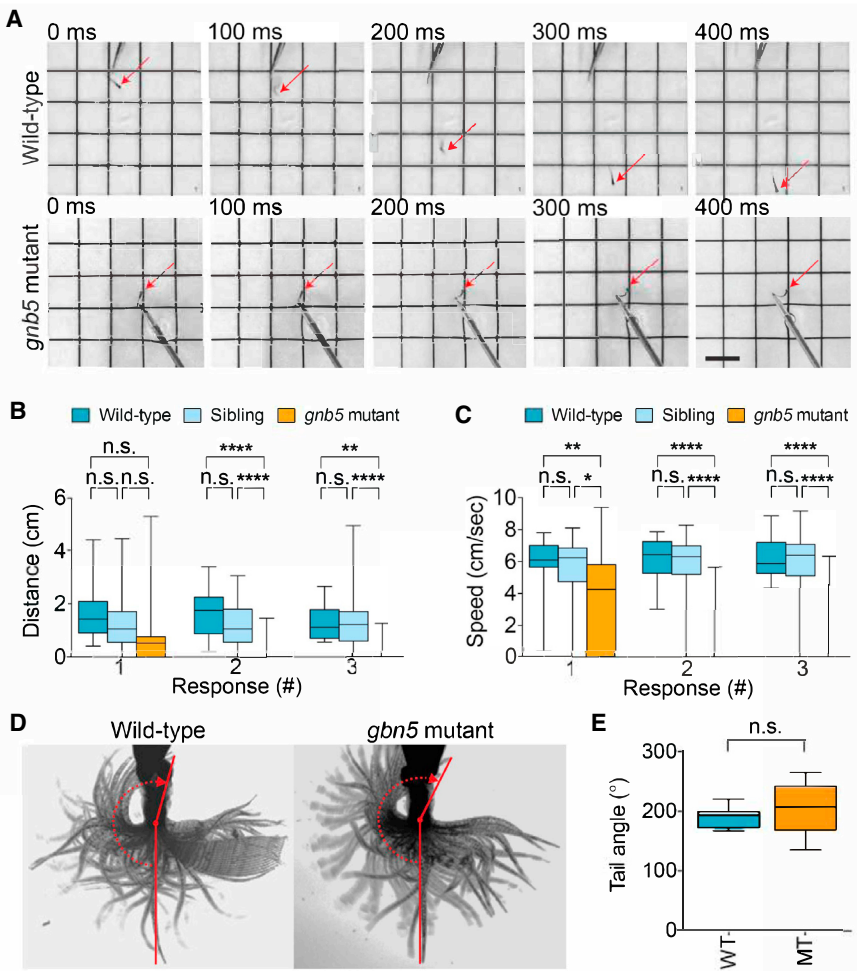

Figure 3. Neurologic Function in *gnb5* Mutant Zebrafish

(A–C) Touch-evoked escape response assay in which three consecutive tactile stimuli were applied. Embryos at 3 dpf were placed in the middle of a standard 88 mm petri dish containing E3 medium. Three consecutive tactile stimuli were applied by touching the tail of the embryo with an insect pin. Stimuli were only applied when the embryo was still. Behavior was recorded with a standard camera (30 fps) and analyzed with ImageJ (NIH) and the plugin MTrackJ.[19] (A) shows representative responses of 3 dpf wild-type and *gnb5* mutant embryos to a touch stimulus. Scale bar, 0.5 cm. Box-whisker plots show quantification of the (B) swimming distance and (C) swimming speed in TL wild-types (n = 19), siblings (n = 46), and *gnb5* mutants (n = 27).

(D and E) Analysis of maximum tail movement at 5 dpf. Larvae at 5 dpf were sedated in E3 containing 16 mg/ml Tricaine and embedded in 0.5% UltraPureTM agarose (Invitrogen 16500-500) in a 35 mm glass bottom dish. After setting, the agarose was cut away caudal to the swimming bladder, leaving the tail free to move. The dish was filled with E3 medium and embryos were left to recover from the sedation for 10 min at 28°C. Next, a maximal escape response was elicited by repeatedly touching the head of the embryo with an insect pin. Recordings were performed at 280 fps, for 30 s, with a high-speed CCD camera (Hamamatsu Photonics K.K., C9300-221) and analyzed with ImageJ (angle tool). (D) shows representative minimum projection images of tail movement in wild-type and *gnb5* mutant embryos, including tail angle analysis. The tail angle represents the angle between the head-tail midline axis in resting state and a line that was drawn from just caudal of the swimbladder to the tip of the tail at maximal tail movement. (E) Tail angle quantification is displayed in box-whisker plots (wild-type n = 10, *gnb5* mutants n = 10). fps, frames per second.

n denotes the number of fish used per dataset. Differences between two groups were analyzed via the Student's t test. Differences between more than two groups were analyzed via one-way ANOVA with Tukey's post-hoc test. Data are shown as mean ± SEM, and $p < 0.05$ was considered significant. *$p < 0.05$, **$p \leq 0.01$, ***$p \leq 0.001$, ****$p \leq 0.0001$. $p > 0.05$ was considered not significant (n.s.).

the cardiac GIRK channel by GNB5-RGS. In contrast, treatment with the sympathetic agonist isoproterenol resulted in an increased heart rate that was similar in wild-type, sibling, and *gnb5* mutant larvae (Figure 2). These results indicate that *GNB5* is crucial for parasympathetic control of heart rate, but not for sympathetic control, suggesting that lack of *GNB5* is associated with extreme bradycardia at rest. Correspondingly, affected individuals present with severe bradycardia at rest (minimal observed heart rates of <25 bpm [beats per minute]) combined with a normal chronotropic response (maximum heart rates >150 bpm).

The severe muscle hypotonia reported in affected individuals could result from GIRK-mediated hyperpolarization of neurons controlling skeletal muscle tone. *gnb5* mutant embryos hatched normally from their chorion, a process that requires muscle contraction, but their swimming behavior appeared abnormal at 3 dpf. To investigate whether this abnormal behavior was linked to neurologic dysfunction and hypotonia, we examined the touch-evoked escape response. We anticipated that neurons would only become fully hyperpolarized after an initial stimulus and thus presented the embryos with three consecutive tactile stimuli. Whereas wild-type larvae rapidly swam away in response to repeated tactile stimuli, *gnb5* mutants showed a significant decrease in swimming distance and swimming speed at stimuli two ($p \leq 0.0001$) and three ($p \leq 0.01$), but not after the first stimulus (Figures 3A–3C). Accordingly, *gnb5* mutant larvae were predominantly unresponsive to repeated tactile stimuli (Movies S1 and S2). To test whether this abnormal escape response is the consequence of neurologic dysfunction rather than reduced muscle function, we performed a tail movement assay. 5 dpf larvae were given a strong tactile stimulus while we recorded the movement of the tail (Figures 3D and 3E). No significant difference in the maximum tail angle was detected between wild-type and *gnb5* mutant larvae (Figure 3E). These results indicate that the tail muscles of *gnb5* mutants are fully functional

and that the abnormal escape response is associated with neurological dysfunction and possibly muscle hypotonia.

Given that affected individuals have visual problems, including nystagmus, we investigated the visual system by measuring the optokinetic response (OKR) of *gnb5* mutant larvae. When wild-type larvae were placed in a drum with a rotating light stimulus (Figure S8A), the OKR consisted of smooth pursuit eye movements followed by rapid rest saccades in the opposite direction (Figure S8B, Movie S3). In contrast, OKR was completely absent in *gnb5* mutant larvae although their eyes showed no morphological abnormalities and could make eye movements (Figure S8C, Movie S4). This indicates that the eye muscles are functional in *gnb5* mutants but that proper eye-movement control depends on *GNB5*. Overall these data show that *gnb5* mutants faithfully recapitulate the phenotypic spectrum of affected individuals, including cardiac, neurologic, and ophthalmologic abnormalities.

These results provide evidence for a direct role of *GNB5* in the control of heart rate, motor capacity, and vision. Whereas *GNB1* (MIM: 139380), *GNB2* (MIM: 139390), *GNB3* (MIM: 139130), and *GNB4* (MIM: 610863) are widely expressed and encode highly homologous proteins,[20] *GNB5* is preferentially expressed in the brain and nervous system and encodes a peptide with less homology with its four paralogs.[21,22]

Germline de novo *GNB1* variants cause severe neurodevelopmental disability,[23] hypotonia, and seizures. *GNB3* bi-allelic LoF has been linked to congenital stationary night blindness (MIM: 610445, 163500, 610444, 613830, 616389, 310500, 257270, 613216, 614565, 615058, 300071, and 610427) and recessive retinopathy in humans,[24,25] retinal degeneration in chickens,[26] and reduced cone sensitivity and mild bradycardia in mice.[27,28] A SNP in *GNB3* was associated with postural tachycardia syndrome[29] and incidence of cardiovascular disease and stroke.[30] Similarly, *GNB2* and *GNB4* map to loci governing heart rate on chromosomes 7 and 3, respectively.[31,32] We hereby demonstrate that bi-allelic LoF and missense variants in *GNB5* cause a multisystem syndrome with features that include global developmental delay, sinus-node dysfunction, seizures, eye abnormalities, gastric problems, and generalized hypotonia. We highlight the importance of *GNB5* for neuronal signaling, including the regulation of the antagonistic effects of the parasympathetic and sympathetic nervous system.

Supplemental Data

Supplemental Data includes Supplemental Acknowledgments, a Supplemental Note, eight figures, one table, and four movies and can be found with this article online at http://dx.doi.org/10.1016/j.ajhg.2016.06.025.

Conflicts of Interest

J.R.L. has stock ownership in 23andMe, is a paid consultant for Regeneron Pharmaceuticals, has stock options in Lasergen, is a member of the Scientific Advisory Board of Baylor Miraca Genetics Laboratories, and is a co-inventor on multiple United States and European patents related to molecular diagnostics for inherited neuropathies, eye diseases, and bacterial genomic fingerprinting. Baylor College of Medicine (BCM) and Miraca Holdings have formed a joint venture with shared ownership and governance of the Baylor Miraca Genetics Laboratories (BMGL), which performs clinical exome sequencing. The Department of Molecular and Human Genetics at BCM derives revenue from the chromosomal microarray analysis and clinical exome sequencing offered in the BMGL (http://www.bmgl.com/BMGL/Default.aspx/website). G.M. is a paid consultant for Takeda Pharmaceutical Company.

Received: May 18, 2016
Accepted: June 24, 2016
Published: August 11, 2016; corrected online: September 1, 2016

Web Resources

1000 Genomes, http://www.1000genomes.org
Berkeley Drosophila Genome Project NNSplice 0.9, http://www.fruitfly.org/seq_tools/splice.html
Burrows-Wheeler Aligner, http://bio-bwa.sourceforge.net/
dbSNP, http://www.ncbi.nlm.nih.gov/projects/SNP/
Ensembl Genome Browser, human genome, GRCh37, http://grch37.ensembl.org/Homo_sapiens/Info/Index
ExAC Browser, http://exac.broadinstitute.org/
ExomeDepth, https://cran.r-project.org/web/packages/ExomeDepth/index.html
GATK, https://www.broadinstitute.org/gatk/
GenBank, http://www.ncbi.nlm.nih.gov/genbank/
GraphPad, http://graphpad.com/
NetGene2, http://www.cbs.dtu.dk/services/NetGene2
NHLBI Exome Sequencing Project (ESP) Exome Variant Server, http://evs.gs.washington.edu/EVS/
OMIM, http://www.omim.org/
PolyPhen-2, http://genetics.bwh.harvard.edu/pph2/
PubChem, http://www.ncbi.nlm.nih.gov/pccompound
SIFT, http://sift.jcvi.org/
SnpEff, http://snpeff.sourceforge.net/
SOAPsnp, http://soap.genomics.org.cn/soapsnp.html
Swiss PDB Viewer, http://www.expasy.org/spdbv/
UMD-Predictor, http://umd-predictor.eu/

References

1. Daly, A.F., Lysy, P.A., Desfilles, C., Rostomyan, L., Mohamed, A., Caberg, J.H., Raverot, V., Castermans, E., Marbaix, E., Maiter, D., et al. (2016). GHRH excess and blockade in X-LAG syndrome. Endocr. Relat. Cancer *23*, 161–170.
2. Daly, A.F., Yuan, B., Fina, F., Caberg, J.H., Trivellin, G., Rostomyan, L., de Herder, W.W., Naves, L.A., Metzger, D., Cuny, T., et al. (2016). Somatic mosaicism underlies X-linked acrogigantism syndrome in sporadic male subjects. Endocr. Relat. Cancer *23*, 221–233.
3. Trivellin, G., Daly, A.F., Faucz, F.R., Yuan, B., Rostomyan, L., Larco, D.O., Schernthaner-Reiter, M.H., Szarek, E., Leal, L.F., Caberg, J.H., et al. (2014). Gigantism and acromegaly due to Xq26 microduplications and GPR101 mutation. N. Engl. J. Med. *371*, 2363–2374.

4. Krishnan, A., Mustafa, A., Almén, M.S., Fredriksson, R., Williams, M.J., and Schiöth, H.B. (2015). Evolutionary hierarchy of vertebrate-like heterotrimeric G protein families. Mol. Phylogenet. Evol. *91*, 27–40.
5. Alfaiz, A.A., Micale, L., Mandriani, B., Augello, B., Pellico, M.T., Chrast, J., Xenarios, I., Zelante, L., Merla, G., and Reymond, A. (2014). TBC1D7 mutations are associated with intellectual disability, macrocrania, patellar dislocation, and celiac disease. Hum. Mutat. *35*, 447–451.
6. Borck, G., Hög, F., Dentici, M.L., Tan, P.L., Sowada, N., Medeira, A., Gueneau, L., Holger, T., Kousi, M., Lepri, F., et al. (2015). BRF1 mutations alter RNA polymerase III-dependent transcription and cause neurodevelopmental anomalies. Genome Res. *25*, 609.
7. Yuan, B., Pehlivan, D., Karaca, E., Patel, N., Charng, W.L., Gambin, T., Gonzaga-Jauregui, C., Sutton, V.R., Yesil, G., Bozdogan, S.T., et al. (2015). Global transcriptional disturbances underlie Cornelia de Lange syndrome and related phenotypes. J. Clin. Invest. *125*, 636–651.
8. Ng, P.C., and Henikoff, S. (2001). Predicting deleterious amino acid substitutions. Genome Res. *11*, 863–874.
9. Adzhubei, I.A., Schmidt, S., Peshkin, L., Ramensky, V.E., Gerasimova, A., Bork, P., Kondrashov, A.S., and Sunyaev, S.R. (2010). A method and server for predicting damaging missense mutations. Nat. Methods *7*, 248–249.
10. Salgado, D., Desvignes, J.P., Rai, G., Blanchard, A., Miltgen, M., Pinard, A., Lévy, N., Collod-Béroud, G., and Béroud, C. (2016). UMD-Predictor: A High-Throughput Sequencing Compliant System for Pathogenicity Prediction of any Human cDNA Substitution. Hum. Mutat. *37*, 439–446.
11. Cheever, M.L., Snyder, J.T., Gershburg, S., Siderovski, D.P., Harden, T.K., and Sondek, J. (2008). Crystal structure of the multifunctional Gbeta5-RGS9 complex. Nat. Struct. Mol. Biol. *15*, 155–162.
12. Zhang, J.H., Pandey, M., Seigneur, E.M., Panicker, L.M., Koo, L., Schwartz, O.M., Chen, W., Chen, C.K., and Simonds, W.F. (2011). Knockout of G protein β5 impairs brain development and causes multiple neurologic abnormalities in mice. J. Neurochem. *119*, 544–554.
13. Krispel, C.M., Chen, C.K., Simon, M.I., and Burns, M.E. (2003). Novel form of adaptation in mouse retinal rods speeds recovery of phototransduction. J. Gen. Physiol. *122*, 703–712.
14. Rao, A., Dallman, R., Henderson, S., and Chen, C.K. (2007). Gbeta5 is required for normal light responses and morphology of retinal ON-bipolar cells. J. Neurosci. *27*, 14199–14204.
15. Yang, J., Huang, J., Maity, B., Gao, Z., Lorca, R.A., Gudmundsson, H., Li, J., Stewart, A., Swaminathan, P.D., Ibeawuchi, S.R., et al. (2010). RGS6, a modulator of parasympathetic activation in heart. Circ. Res. *107*, 1345–1349.
16. Posokhova, E., Wydeven, N., Allen, K.L., Wickman, K., and Martemyanov, K.A. (2010). RGS6/Gβ5 complex accelerates IKACh gating kinetics in atrial myocytes and modulates parasympathetic regulation of heart rate. Circ. Res. *107*, 1350–1354.
17. Meyer, A., and Schartl, M. (1999). Gene and genome duplications in vertebrates: the one-to-four (-to-eight in fish) rule and the evolution of novel gene functions. Curr. Opin. Cell Biol. *11*, 699–704.
18. Xie, K., Allen, K.L., Kourrich, S., Colón-Saez, J., Thomas, M.J., Wickman, K., and Martemyanov, K.A. (2010). Gbeta5 recruits R7 RGS proteins to GIRK channels to regulate the timing of neuronal inhibitory signaling. Nat. Neurosci. *13*, 661–663.
19. Meijering, E., Dzyubachyk, O., and Smal, I. (2012). Methods for cell and particle tracking. Methods Enzymol. *504*, 183–200.
20. Gautam, N., Downes, G.B., Yan, K., and Kisselev, O. (1998). The G-protein betagamma complex. Cell. Signal. *10*, 447–455.
21. Watson, A.J., Katz, A., and Simon, M.I. (1994). A fifth member of the mammalian G-protein beta-subunit family. Expression in brain and activation of the beta 2 isotype of phospholipase C. J. Biol. Chem. *269*, 22150–22156.
22. Witherow, D.S., and Slepak, V.Z. (2003). A novel kind of G protein heterodimer: the G beta5-RGS complex. Receptors Channels *9*, 205–212.
23. Petrovski, S., Kury, S., Myers, C.T., Anyane-Yeboa, K., Cogne, B., Bialer, M., Xia, F., Hemati, P., Riviello, J., Mehaffey, M., et al. (2016). Germline De Novo Mutations in GNB1 Cause Severe Neurodevelopmental Disability, Hypotonia, and Seizures. American journal of human genetics.
24. Vincent, A., Audo, I., Tavares, E., Maynes, J.T., Tumber, A., Wright, T., Li, S., Michiels, C., Consortium, G.N.B., Condroyer, C., et al. (2016). Biallelic Mutations in GNB3 Cause a Unique Form of Autosomal-Recessive Congenital Stationary Night Blindness. American journal of human genetics.
25. Arno, G., Holder, G.E., Chakarova, C., Kohl, S., Pontikos, N., Fiorentino, A., Plagnol, V., Cheetham, M.E., Hardcastle, A.J., Webster, A.R., et al. (2016). Recessive Retinopathy Consequent on Mutant G-Protein beta Subunit 3 (GNB3). J. Am. Med. Assoc. Ophthalmol.
26. Tummala, H., Ali, M., Getty, P., Hocking, P.M., Burt, D.W., Inglehearn, C.F., and Lester, D.H. (2006). Mutation in the guanine nucleotide-binding protein beta-3 causes retinal degeneration and embryonic mortality in chickens. Invest. Ophthalmol. Vis. Sci. *47*, 4714–4718.
27. Nikonov, S.S., Lyubarsky, A., Fina, M.E., Nikonova, E.S., Sengupta, A., Chinniah, C., Ding, X.Q., Smith, R.G., Pugh, E.N., Jr., Vardi, N., and Dhingra, A. (2013). Cones respond to light in the absence of transducin β subunit. J. Neurosci. *33*, 5182–5194.
28. Ye, Y., Sun, Z., Guo, A., Song, L.S., Grobe, J.L., and Chen, S. (2014). Ablation of the GNB3 gene in mice does not affect body weight, metabolism or blood pressure, but causes bradycardia. Cell. Signal. *26*, 2514–2520.
29. Nakao, R., Tanaka, H., Takitani, K., Kajiura, M., Okamoto, N., Kanbara, Y., and Tamai, H. (2012). GNB3 C825T polymorphism is associated with postural tachycardia syndrome in children. Pediatrics international: official journal of the Japan Pediatric Society *54*, 829–837.
30. Zhang, L., Zhang, H., Sun, K., Song, Y., Hui, R., and Huang, X. (2005). The 825C/T polymorphism of G-protein beta3 subunit gene and risk of ischaemic stroke. J. Hum. Hypertens. *19*, 709–714.
31. den Hoed, M., Eijgelsheim, M., Esko, T., Brundel, B.J., Peal, D.S., Evans, D.M., Nolte, I.M., Segrè, A.V., Holm, H., Handsaker, R.E., et al.; Global BPgen Consortium; CARDIoGRAM Consortium; PR GWAS Consortium; QRS GWAS Consortium; QT-IGC Consortium; CHARGE-AF Consortium (2013). Identification of heart rate-associated loci and their effects on cardiac conduction and rhythm disorders. Nat. Genet. *45*, 621–631.
32. Smolock, E.M., Ilyushkina, I.A., Ghazalpour, A., Gerloff, J., Murashev, A.N., Lusis, A.J., and Korshunov, V.A. (2012). Genetic locus on mouse chromosome 7 controls elevated heart rate. Physiol. Genomics *44*, 689–698.

The American Journal of Human Genetics, Volume *99*

Supplemental Data

GNB5 Mutations Cause an Autosomal-Recessive Multisystem Syndrome with Sinus Bradycardia and Cognitive Disability

Elisabeth M. Lodder, Pasquelena De Nittis, Charlotte D. Koopman, Wojciech Wiszniewski, Carolina Fischinger Moura de Souza, Najim Lahrouchi, Nicolas Guex, Valerio Napolioni, Federico Tessadori, Leander Beekman, Eline A. Nannenberg, Lamiae Boualla, Nico A. Blom, Wim de Graaff, Maarten Kamermans, Dario Cocciadiferro, Natascia Malerba, Barbara Mandriani, Zeynep Hande Coban Akdemir, Richard J. Fish, Mohammad K. Eldomery, Ilham Ratbi, Arthur A.M. Wilde, Teun de Boer, William F. Simonds, Marguerite Neerman-Arbez, V. Reid Sutton, Fernando Kok, James R. Lupski, Alexandre Reymond, Connie R. Bezzina, Jeroen Bakkers, and Giuseppe Merla

Case Reports

Family A: The proband (A.II.2, **Figure 1**) is a 20-year-old woman born from healthy non-consanguineous parents of Italian ancestry. Clinical synopsis includes severe ID and speech disorder, nystagmus, bradyarrhythmia, postural defects, epilepsy, hypotonia, and pathological gastric reflux. Brain magnetic resonance imaging (MRI) at 2 years of age was normal. Electroencephalography (EEG) reported signs of disordered electrogenesis and changes in vigil-state brain bioelectric activity. Episodes of sudden sinus pauses followed by junction escape beats were observed. Cardiac echocardiogram (ECHO) revealed Patent Foramen Ovale (PFO).

Ophthalmology records reported retinal degeneration; ISCEV standard Electroretinogram (ERG) was electronegative. Amniotic fluid chromosome analysis was normal.

The proband's 22-year-old sister (A.II.1, **Figure 1**) presented with severe ID hypotonia, nystagmus, epilepsy, and pathological gastric reflux.

Brain MRIs, at 14 months and 9 years of age, revealed no clinically substantial alterations. Electroretinography and Visually Evoked Potentials (PEV) recording sessions revealed electronegative ERG and retinal degeneration with rods' involvement, respectively. Fundus photography documented thinned retinal vessels, oblique implantation of the optic nerve head, and no macular abnormalities or pigment accumulation. Electrocardiography (ECG) and Holter monitoring identified bradycardic sinus rhythm. Genomic array using the Affymetrix CytoScan HD (Affymetrix, Santa Clara, CA, USA) revealed no pathological CNVs.

Family B: The 6-year-old proband is the only child born to Jordanian first-cousin parents **(Figure 1)**. She was born in Brazil by caesarean section after an uneventful pregnancy. At 2 months of age, she presented with infantile spasms with EEG demonstrating hypsarrhythmia. Treatments with vigabatrin and valproic acid were unsuccessful in controlling the seizures. When evaluated at 6 months of age, she had a profound developmental delay and, because of apneic spells and desaturation episodes, she was admitted in the Intensive Care Unit. She was not dysmorphic and internal organs were normal. A brain MRI performed at 1 year of age showed T2 hyperintensities in

thalamus, globus pallidus and brainstem tegmentum (likely related to vigabatrin use). A second brain MRI performed two years later failed to show remarkable abnormalities. Acylcarnitine and plasma amino acids analyses were normal, whereas urine organic acid analysis showed an increase in 3-methyl-glutaconic acid. At 5 years of age, she was unable to support her head and had no eye contact.

Family C: The proband is an 11-year-old female (**Figure 1**). She presented with absent speech, severe ID, hyporeflexia and nystagmus. She is hypotonic with no head control and has never sat independently. ECG detected prolonged cardiac pauses and symptomatic chronotropic incompetence that were treated with a pacemaker. EEG was normal. Brain MRI showed supratentorial volume loss anterior>posterior in a watershed distribution, attributed to episodes of hypotension. Skeletal muscle biopsy histopathology revealed focal z-band streaming and type 1 fiber predominance, with enlarged and abnormally shaped mitochondria, and increased glycogen as free particles. Severely decreased levels of ubiquinol cytochrome c-oxidoreductase (complex III) were reported, whereas PAA, UOA, and ACP were normal. Oligonucleotide/SNP array detected no pathogenic CNVs. Parents are consanguineous and of Puerto Rican Roma ancestry. There is a 9-year-old affected brother who was born at term by normal vaginal delivery after an uneventful pregnancy. He showed global developmental delay, nystagmus, sinus-node dysfunction and gastric reflux. EEG investigation showed no disturbance of brain function. No structural abnormalities were identified by echocardiography (ECHO). A progressive cardiac arrhythmia with prolonged cardiac pauses resulted in the implantation of a pacemaker. Metabolic work-up (plasma amino acids (PAA), urine organic acids (UOA), and plasma acylcarnitine profile (ACP) was normal. Oligonucleotide and SNP arrays did not identify CNVs.

Family D: The proband is a female currently 12-years-old (Figure 1). She was born after a pregnancy characterized by decreased fetal movements. Her healthy parents are non-consanguineous individuals of Indian descent. She presented with severe cognitive and psychomotor delay, epilepsy and

hypotonia. When awake, she has normal rhythm and PR intervals (i.e. time from the onset of the atrial depolarization to the start of the ventricular depolarization). In contrast when asleep she starts to increase her PR interval, suggestive of intermittent Wenckebach (i.e. progressive atrio-ventricular block resulting in irregular cardiac rhythm). No structural heart abnormalities were demonstrated on conventional ECHO. She has nystagmus and ophthalmological evaluation demonstrated abnormal ERG studies (both photopic and scotopic) and grossly normal funduscopic examination. She has a history of gastric reflux. The laboratory workup included metabolic studies, chromosome analysis and aCGH studies – all normal.

Family E: The proband was born to non-consanguineous, healthy parents of Moroccan ancestry after an uneventful pregnancy **(Figure 1)**. He presented at the age of 1 year with an episode of prolonged syncope, which prompted his father to start cardiopulmonary resuscitation. Electrocardiographic monitoring showed severe sinus-node dysfunction with sinus bradycardia, marked sinus arrhythmia, and multiple sinus pauses up to 4.4 seconds, requiring pacemaker implantation (AAI). The patient also presents with mild learning delay mainly characterized by late speech development, as well as impaired fine motor skills. No brain MRI or EEG were performed. No cardiac structural abnormality was seen on echocardiography. His older sister was similarly affected with sinus-node dysfunction including multiple sinus pauses up to 3.2 seconds, mild mental retardation and late speech development. Echocardiography of her heart did not show any substantial abnormality. None of the siblings suffers from epilepsy and no abnormality was observed in the sister on either brain MRI and EEG. Both siblings had normal eyesight, no hearing problems and no involvement of the gastro-intestinal tract. ECG and Holter monitoring of the parents did not reveal any signs of sinus node dysfunction.

Family F: The proband is a 23-year-old male born from consanguineous parents **(Figure 1)**. His phenotypic manifestations range from borderline/mild ID, to keratoconus, and sinus arrhythmia.

Acknowledgments

We thank the families of affected individuals for their contribution. We are grateful to R. Tadros, K.Y. van Spaendonck-Zwarts for helpful discussion. We thank the members of the Lausanne Genomic Technologies Facility for exome sequencing support and B. Augello B and M.T. Pellico for technical support. We dedicate this study to Dr. Leopoldo Zelante who headed for 40 years the Medical Genetics Unit, Casa Sollievo della Sofferenza, San Giovanni Rotondo and recently passed away. Leopoldo's devotion to the families who nurture affected children and passion for medical genetics was, is and will remain exemplar for all of us. We are grateful to the Genomic Disorder Biobank and

Telethon Network of Genetic Biobanks (Telethon Italy grant GTB12001G) for banking of biospecimens. This work was supported by grants from the Swiss National Science Foundation (31003A_160203) to AR; the US National Human Genome Research Institute (NHGRI)/National Heart Lung and Blood Institute (NHLBI) grant number HG006542 to the Baylor-Hopkins Center for Mendelian Genomics and the National Institute of Neurological Disorders and Stroke (NINDS) NS058529 to JRL; Career Development Award

K23NS078056 from NINDS to WW; the Italian Ministry of Health (Ricerca Corrente) to GM; the Dutch Heart Foundation (CVON 2012-10 Predict project and CVON 2014-18 CONCOR-genes project) to CRB, AAMW and JB and JB and CRB, respectively. The Intramural Research Program of NIDDK (WFS), as well as the Genomic Disorder Biobank and Telethon Network of Genetic Biobanks (grant GTB12001G) also supported this research. The funders had no role in study design, data collection and analysis, decision to publish, or preparation of the manuscript. The authors declare no conflicts of interest with the exception of JRL and GM whose competing interests are detailed in the Conflicts of interest statement.

Supplemental References

1. Dombrovski L, D.A., Wasney GA, Tempel W, Senisterra G, Bolshan Y, Smil D, Nguyen KT, Hajian T, Poda G, Al-Awar R, Bountra C, Weigelt

J, Edwards AM, Brown PJ, Schapira M, Arrowsmith CH, Vedadi M, Wu H. Crystal structure of human wd repeat domain 5 with compound.
2. Thomas, L.R., Wang, Q., Grieb, B.C., Phan, J., Foshage, A.M., Sun, Q., Olejniczak, E.T., Clark, T., Dey, S., Lorey, S., et al. (2015). Interaction with WDR5 promotes target gene recognition and tumorigenesis by MYC. Molecular cell 58, 440-452.
3. Cavaliere, P., Levi-Acobas, F., Mayer, C., Saul, F.A., England, P., Weber, P., Raynal, B., Monteil, V., Bellalou, J., Haouz, A., et al. (2014). Structural and functional features of Crl proteins and identification of conserved surface residues required for interaction with the RpoS/sigmaS subunit of RNA polymerase. The Biochemical journal 463, 215-224.
4. Cheever, M.L., Snyder, J.T., Gershburg, S., Siderovski, D.P., Harden, T.K., and Sondek, J. (2008). Crystal structure of the multifunctional Gbeta5-RGS9 complex. Nature structural & molecular biology 15, 155-162.
5. Lovell, S.C., Word, J.M., Richardson, J.S., and Richardson, D.C. (2000). The penultimate rotamer library. Proteins 40, 389-408.
6. Guex, N., and Peitsch, M.C. (1997). SWISS-MODEL and the Swiss-PdbViewer: an environment for comparative protein modeling. Electrophoresis 18, 2714-2723.

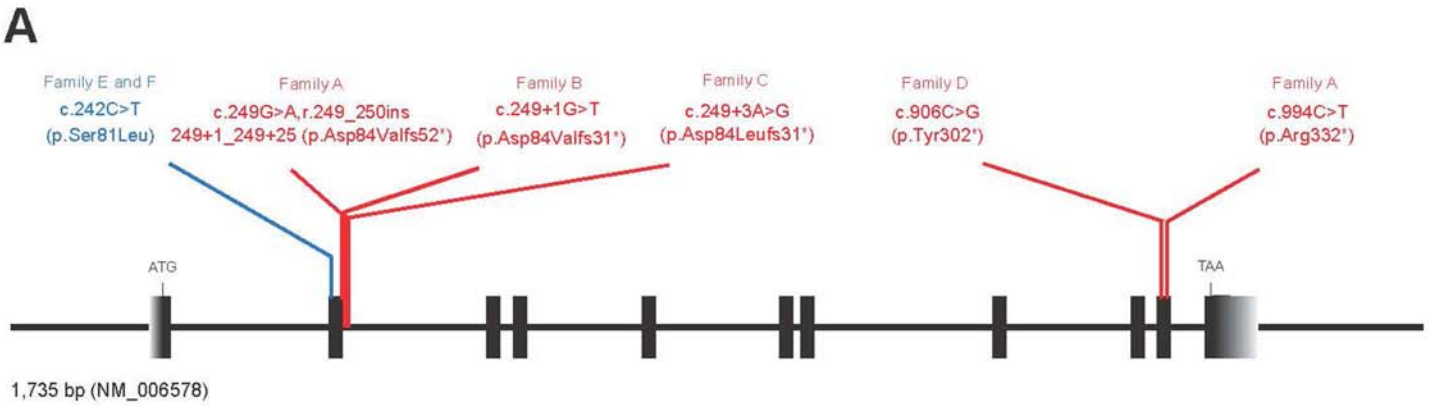

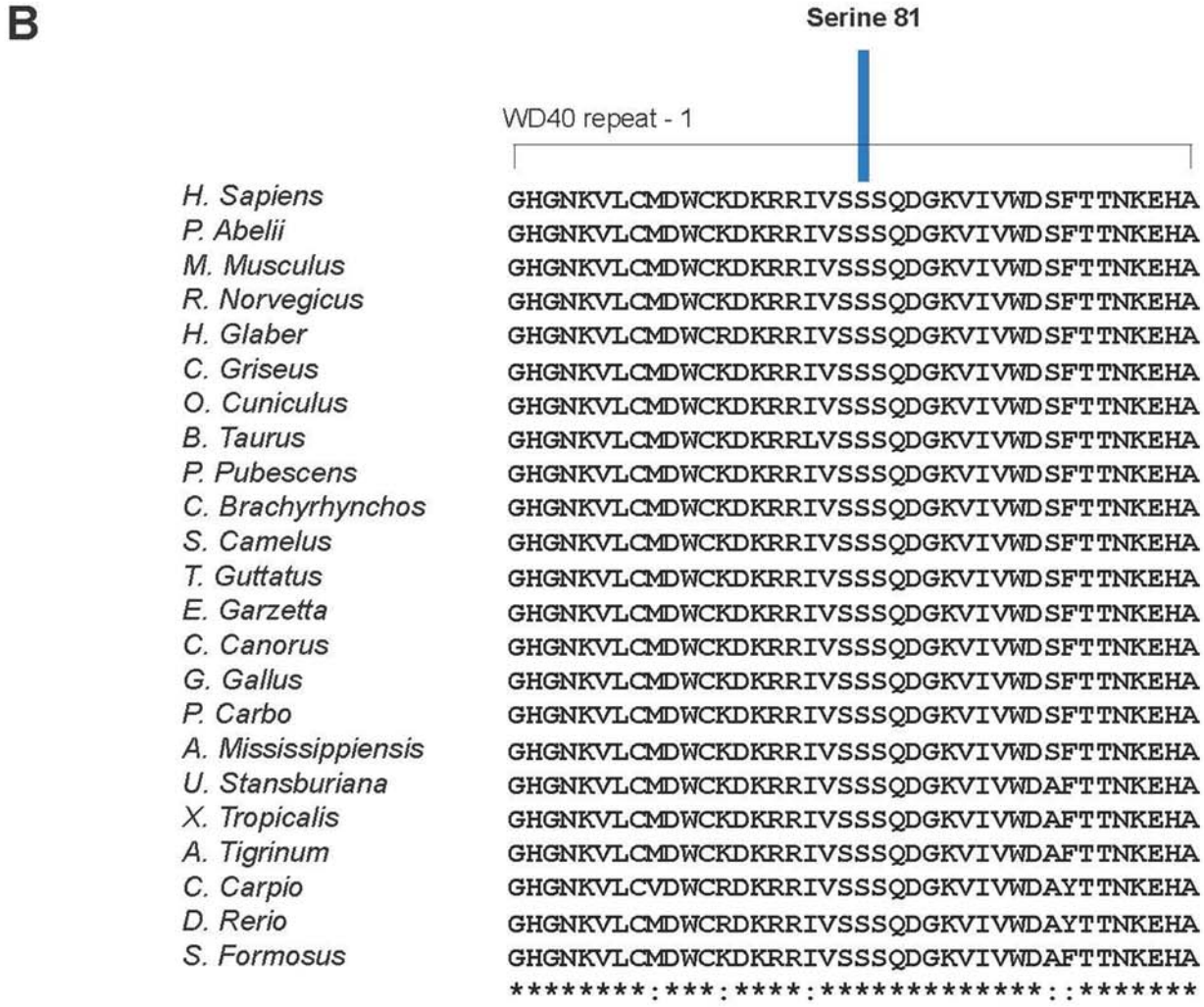

Figure S1. *GNB5* mutational landscape

(**A**) Schematic representation of the exon-intron structure of human *GNB5* gene (NM_006578). Loss-of-function (red) and missense (blue) variants detected in the six studied families. Their respective positions are indicated on the corresponding exons. The predicted protein changes are shown in brackets. (**B**) Conservation across vertebrates of the first WD40 domain of GNB5 and Serine 81 residue that is altered by a missense substitution (p.(Ser81Leu)) in families E and F.

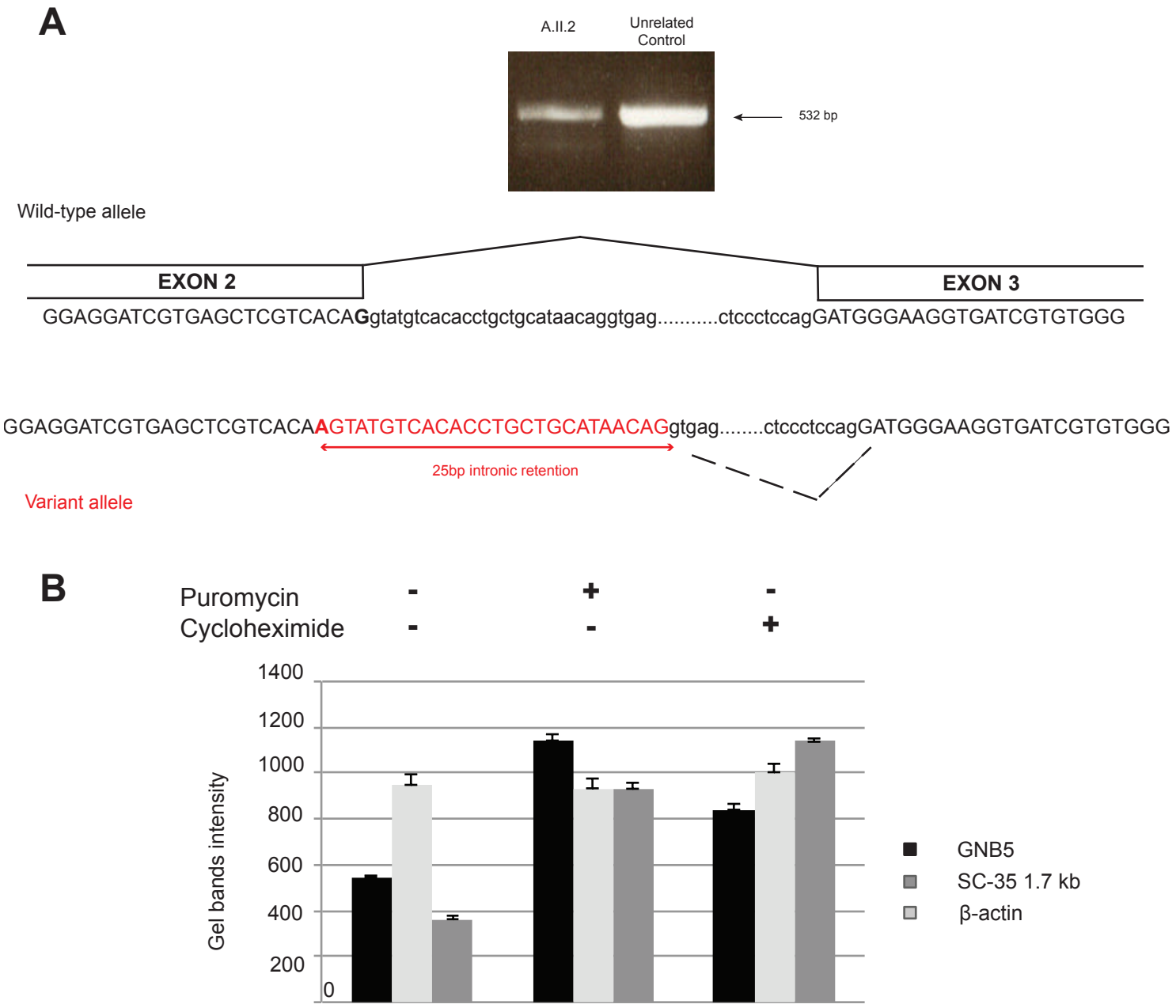

Figure S2. Molecular characterization of Family A variants

(**A**) The synonymous substitution c.249G>A (p.(=)), affecting the last nucleotide of the second exon of *GNB5*, is predicted to alter splicing accuracy by both NetGene2 and NNSPLICE (**Table S1**). To clarify the nature of this variant we RT-PCR amplified and sequenced the allele carrying the splice-site change from total RNA from primary fibroblasts of individual A.II.2. *GNB5* exon 1 to 6 amplification (top) and sequencing (bottom) from RNA of the II.2 affected individual of family A who carries the c.249G>A splice-site variant are shown. The variant transcript contains an additional 25 bp (red), corresponding to the intervening intron 2. (**B**) The r.249_250ins249+1_249+25 allele is predicted to encode a truncated polypeptide containing a stretch of 52 incorrect amino acids starting with an Asp to Val substitution at position 84 (p.(Asp84Valfs52X)). Cloning and sequencing of amplicons from individual A.II.1 and A.II.2 further revealed that all transcripts containing the paternal allele were aberrantly spliced. Using the same approach, we examined the relative abundance of the c.249G>A and c.994C>T alleles. Both altered transcripts are less frequent than their unchanged counterpart in parents' cells of father (A.I.1) and mother (A.I.2) (5 out of 14 amplicons (35.7%) for the paternal allele and 2 out of 15 (13.3%) for the maternal one). These results prompted us to hypothesize that both mutant alleles of family A might be targeted by nonsense-mediated mRNA-decay (NMD) pathway. We measured by RT-PCR the levels of *GNB5* mRNA in proband's fibroblasts after treatment with Puromycin or Cycloheximide. The mRNA level of *GNB5* was restored after treatment with both of these known indirect NMD inhibitors suggesting that the c.249G>A and c.994C>T variants trigger NMD of the corresponding transcripts and thus represent LoF alleles. The physiological NMD substrate SC-35 1.7 Kb was included as positive control (dark grey bars). β-actin (light grey bars) was used as internal control.

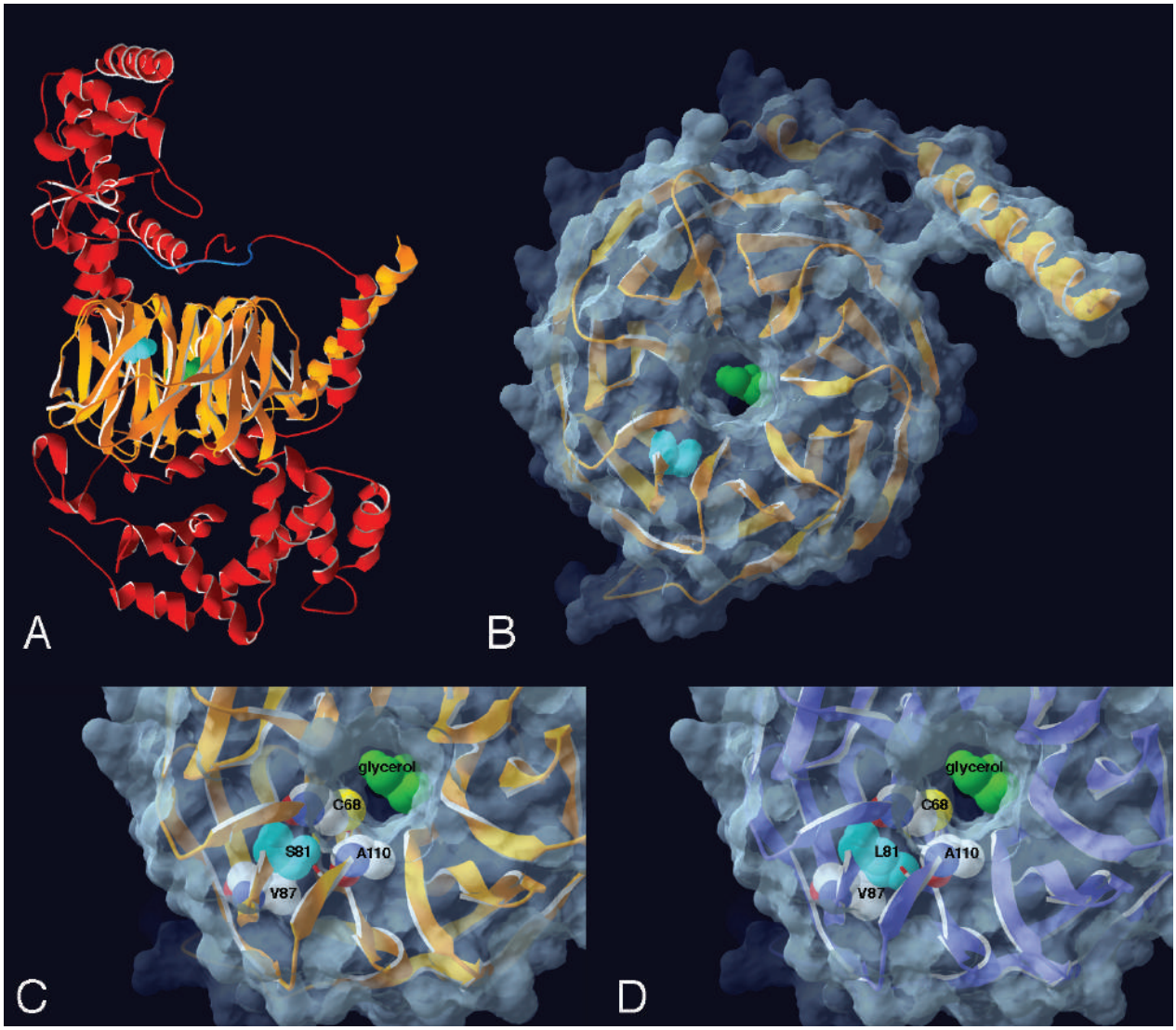

Figure S3. 3D model of the GNB5-RGS complex

(**A**) To gain independent support for the pathogenicity of the GNB5 Ser81Leu missense substitution, we used a three-dimensional representation of the GNB5 encoded protein (orange) complexed with RGS9 (red, MIM: 604067), a member of the R7-subfamily of Regulators of G-protein Signaling (RGS) proteins. The evolutionarily conserved Serine 81 (cyan) is located in a β-strand very close to the central pore, where a glycerol molecule (green) is displayed in 2pbi and various molecules have been shown to bind in related structures (pdb entries 3smr, 4y7r, 4q11)[1,2,3]. A loop of RGS9 (blue) blocks the access to the central pore of GNB5. (**B**) Top view of the GNB5 molecular surface. The evolutionary conserved Ser81 (cyan) is located in a β-strand, very close to the central pore of the β-propeller, but not directly solvent accessible. The glycerol molecule is shown in green (RGS9 and Cys111 have been removed for clarity). (**C**) Detailed views of the Ser81 aminoacidic context. The replacement of Serine 81 by a Leucine will induce localized structural changes in the immediate vicinity of this residue. The positioning of Cys68 could also be altered potentially permitting the formation of a disulphide bridge with Cys111. Additionally, the rearrangements occurring between Leu81 and Ala110, Met109 and Try107 could impair the binding kinetics of RGS proteins, given that both these residues contribute to the contact surface between GNB5 and RGS9. (**D**) These Leu81-induced structural changes can be accommodated after a few cycles of energy minimization (see **Figure S5** for rotamer modeling).

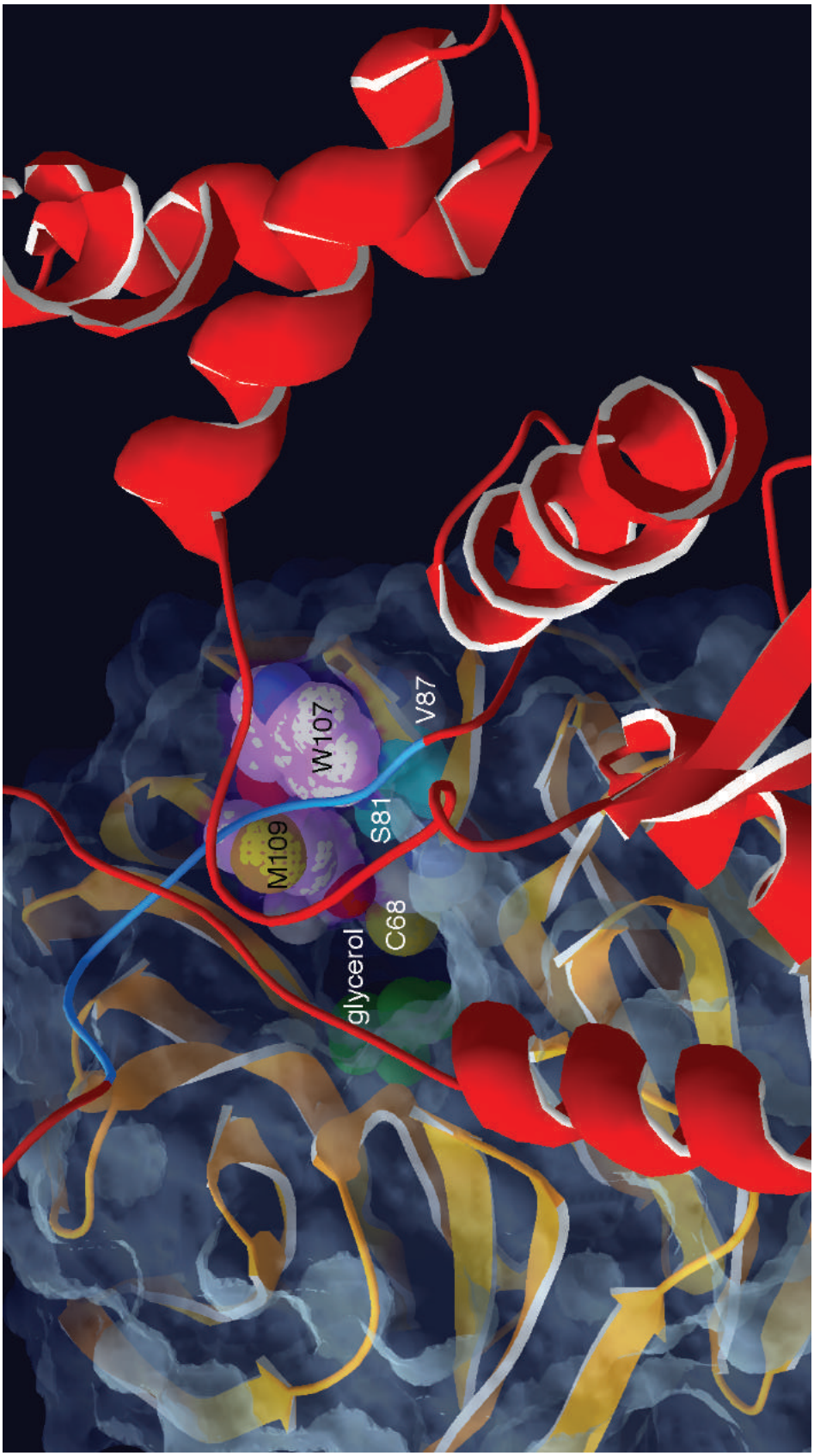

Figure S4. Ser81Leu protein modeling

GNB5 (red) complexed to RGS9 (orange) 3D model showing the proximity of residue Ser81 (cyan) with Cys68 (yellow), Met109, Trp107 and Val87 (white), as well as with the glycerol molecule (green) included in the PDB entry 2pbi[4]. The RGS9 loop (blue) blocks the access to the central pore of GNB5. Highlighted in purple are the side-chains of Trp107 and Met109 that directly contribute to the contact surface between GNB5 and RGS9.

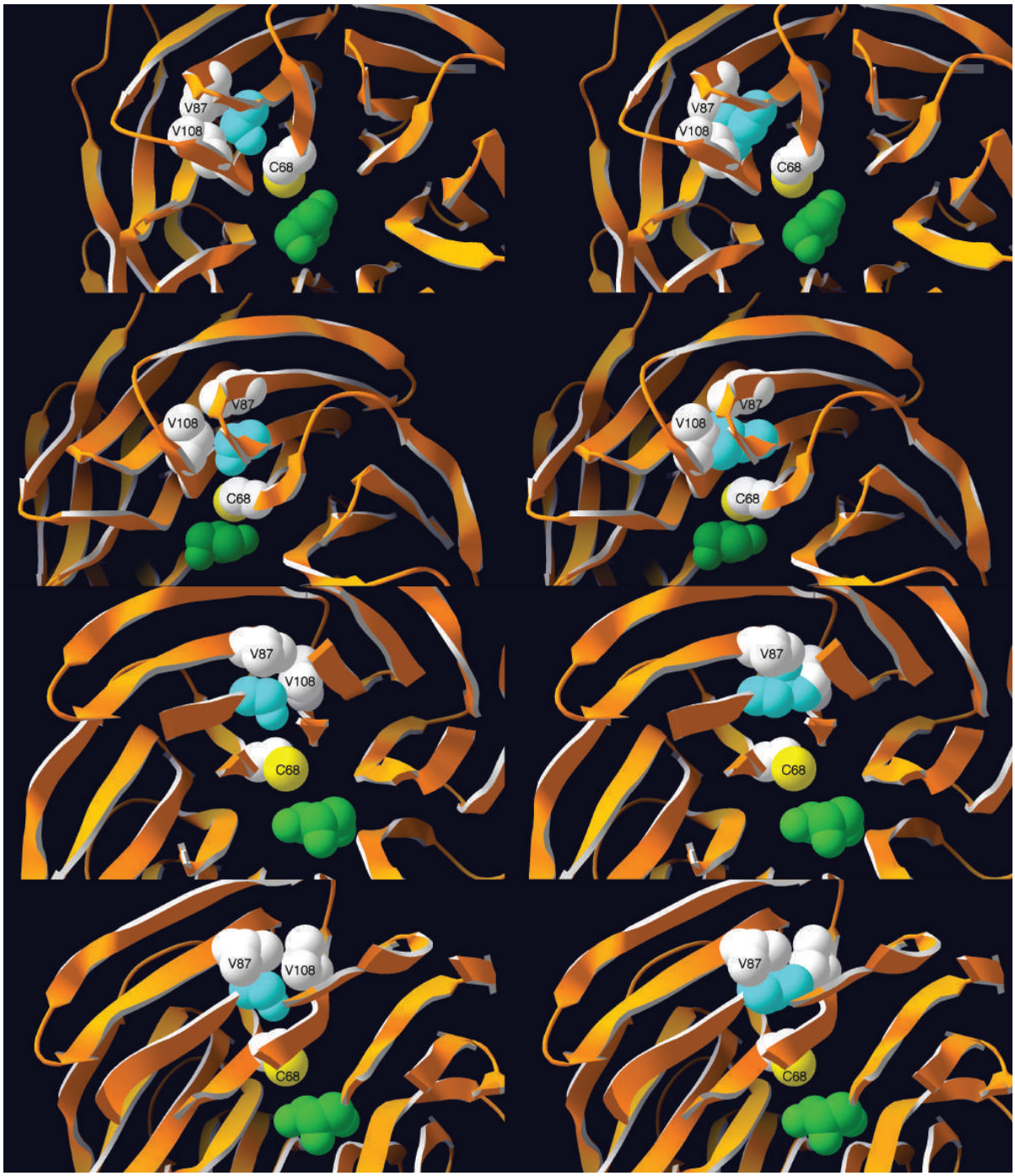

Figure S5. Ser81Leu protein rotamers modeling

Diverse views of the GNB5 3D model showing the Ser81 residue (cyan) compared to the glycerol molecule in the pore (green) and nearby residues (left column). Related rotamers emphasizing the steric hindrances-induced local rearrangements associated with the Leucine replacement identified in families E and F are shown for comparison on the right. Perturbations of the rotamers were evaluated using the backbone dependent rotamer library[5] implemented in the Swiss-PdbViewer[6].

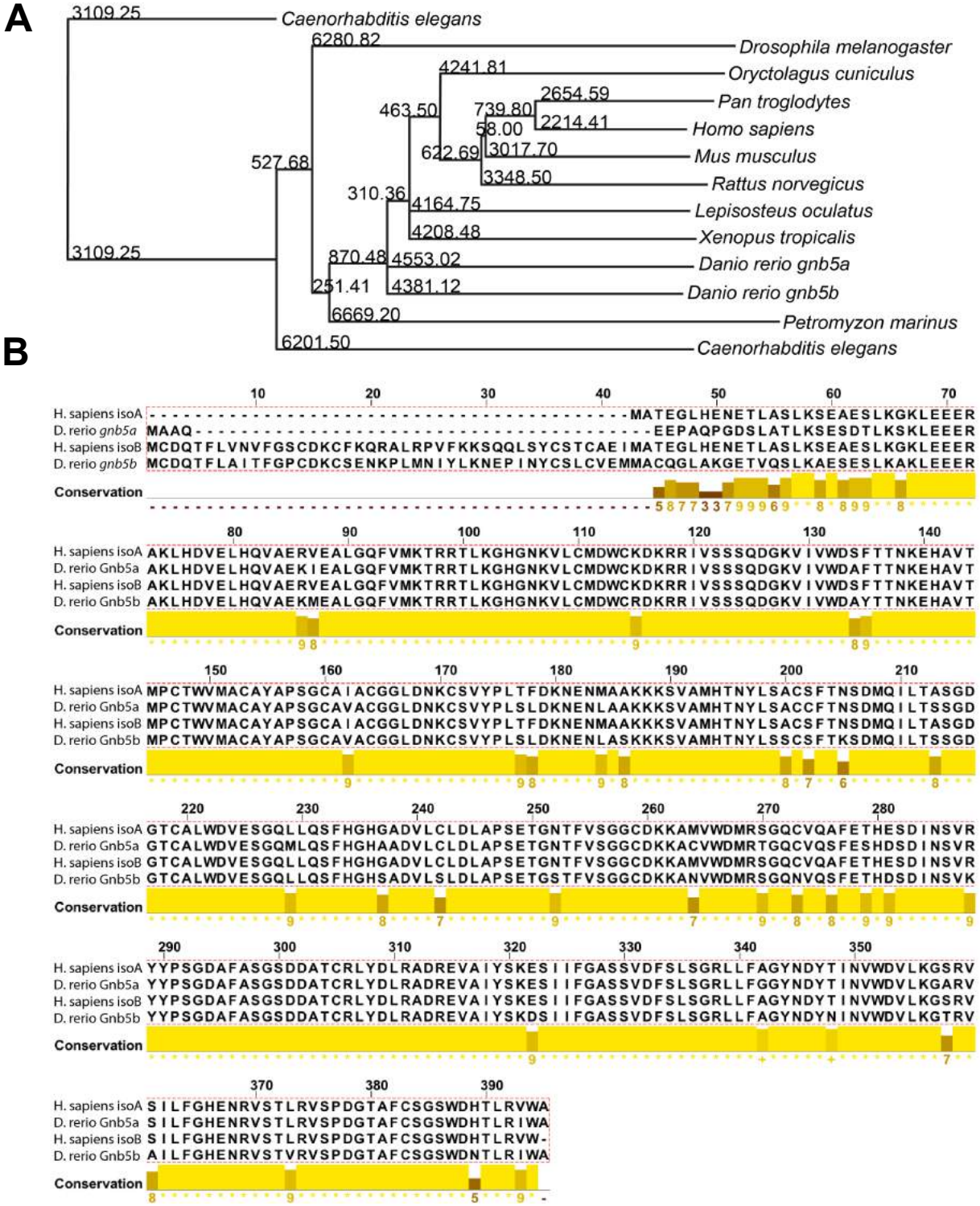

Figure S6. Evolutionary conservation of *GNB5* genomic sequences across species

(**A**) Phylogenetic tree based on the genomic sequences of 13 different species. For each species the longest or most validated coding transcript was selected. Linkage is based on neighbor joining. Values represent the branch lengths. (**B**) Conservation of zebrafish gnb5a and gnb5b compared to the human GNB5 proteins. Human *GNB5* is translated into two protein isoforms; isoform A is the shorter variant (353 aa), while isoform B is the longer variant (395 aa). gnb5a aligns with GNB5 isoform A, gnb5b with GNB5 isoform B. Yellow indicates full conservation between the four proteins. H. sapiens, Homo sapiens; D. rerio, Danio rerio.

A

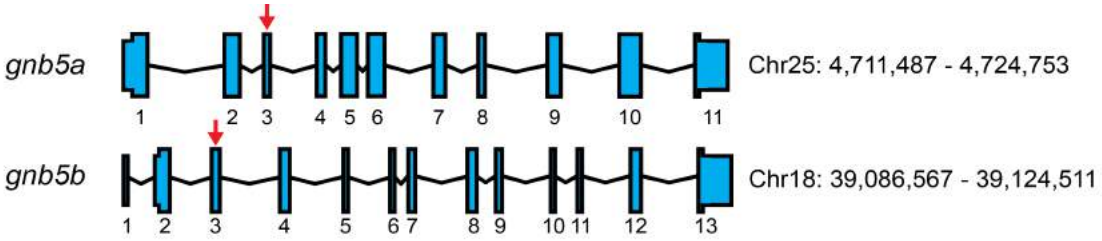

B

gnb5a +7bp insertion mutation

WT T T T A C C A C A A - - - - - - - A T A A G G T A A A T

MT T T T A C C A C A A G G T A A A C A T A A G G T A A A T

gnb5b -8bp +15bp deletion/insertion mutation

WT A A A A G C C A A A C T G G A G - - - - - - - G A G G A

MT A A A A G C C A G G A G G A G A G A G G A G A G A G G A

C

Gnb5a wild-type protein sequence (355 aa)

MAAQEEPAQPGDSLATLKSESDTLKSKLEEERAKLHDVELHQVAEKIEALGQFVMKTRRTLKGHGNKVLCMDWCKDKRRIVSSSQ
DGKVIVWDAFTTNKEHAVTMPCTWVMACAYAPSGCAVACGGLDNKCSVYPLSLDKNENLAAKKKSVAMHTNYLSACCFTNSDMQI
LTSSGDGTCALWDVESGQMLQSFHGHAADVLCLDLAPSETGNTFVSGGCDKKACVWDMRTGQCVQSFESHDSDINSVRYYPSGDA
FASGSDDATCRLYDLRADREVAIYSKESIIFGASSVDFSLSGRLLFGGYNDYTINVWDVLKGARVSILFGHENRVSTLRVSPDGT
AFCSGSWDHTLRIWA

Gnb5a mutant protein sequence (98 aa)

MAAQEEPAQPGDSLATLKSESDTLKSKLEEERAKLHDVELHQVAEKIEALGQFVMKTRRTLKGHGNKVLCMDWCKDKRRIVSSSQ
DGKVIVWDAFTTR

Gnb5b wild-type protein sequence (395 aa)

MCDQTFLAITFGPCDKCSENKPLMNIYLKNEPINYCSLCVEMMACQGLAKGETVQSLKAESESLKAKLEEERAKLHDVELHQVAE
KMEALGQFVMKTRRTLKGHGNKVLCMDWCRDKRRIVSSSQDGKVIVWDAYTTNKEHAVTMPCTWVMACAYAPSGCAVACGGLDNK
CSVYPLSLDKNENLASKKKSVAMHTNYLSSCSFTKSDMQILTSSGDGTCALWDVESGQLLQSFHGHSADVLSLDLAPSETGSTFV
SGGCDKKANVWDMRSGQNVQSFETHDSDINSVKYYPSGDAFASGSDDATCRLYDLRADREVAIYSKDSIIFGASSVDFSLSGRL
LFAGYNDYNINVWDVLKGTRVAILFGHENRVSTVRVSPDGTAFCSGSWDNTLRIWA

Gnb5b mutant protein sequence (108 aa)

MCDQTFLAITFGPCDKCSENKPLMNIYLKNEPINYCSLCVEMMACQGLAKGETVQSLKAESESLKARRREERGESQTTRRRAAS
GGRKDGSSGSVCHEDPSNVKRAWK

D

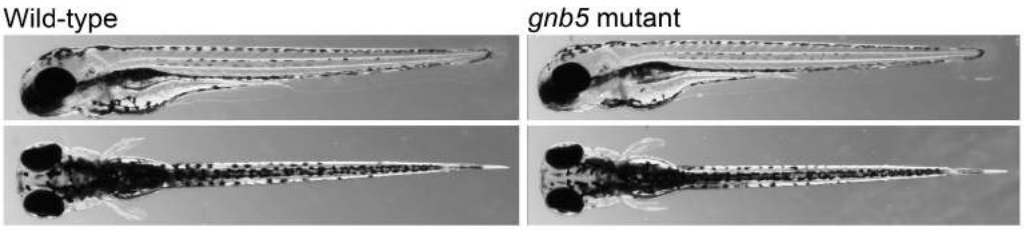

Figure S7. Genomic editing of zebrafish *gnb5a* and *gnb5b*

(**A**) *gnb5a* and *gnb5b* exons, introns and chromosomal location. Red arrows indicate the sites of CRISPR/Cas9-induced mutations. (**B**) Partial sequences of *gnb5a* and *gnb5b* demonstrating the specific mutations that were generated; *gnb5a* +7bp insertion of GGTAAAC; *gnb5b* -8bp deletion of AACTGGAG and +15bp insertion of GGAGGAGAGAGGAGA. WT, wild-type *gnb5* sequence; MT, *gnb5* mutant sequence. (**C**) Gnb5 wild-type and mutant protein sequences. Both mutations result in an early stop codon and truncation of the protein. (**D**) Representative images illustrating the morphology of 3 dpf wild-type and *gnb5* mutants as seen from a left lateral view (top) and dorsal view (bottom).

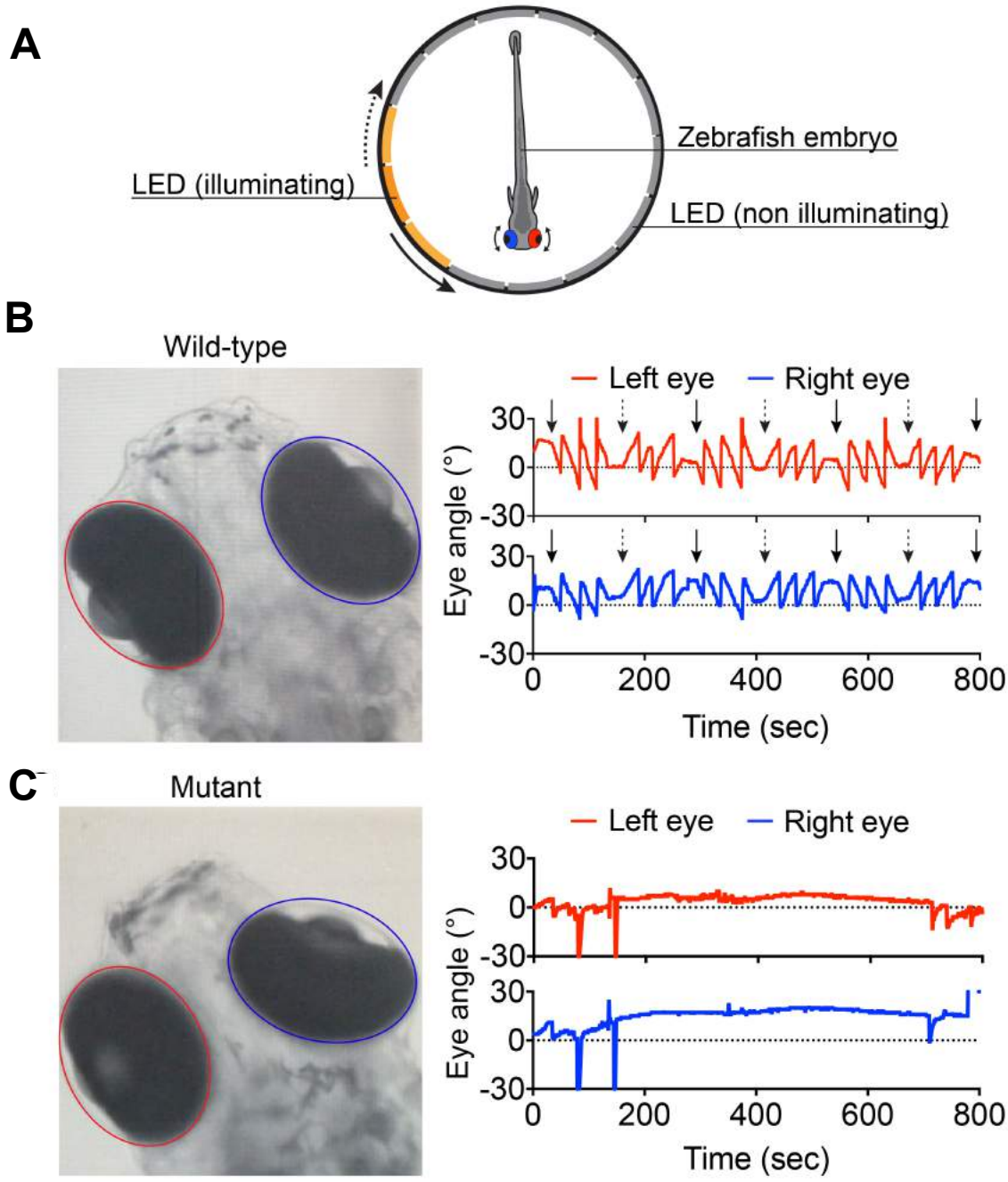

Figure S8. Optokinetic response in *gnb5* double mutant zebrafish larvae (**A**) Schematic of the optokinetic response set-up. Larvae at 7 dpf were embedded dorsal side up in a petri dish and placed in the center of an optokinetic drum containing circularly-placed plexiglass slides, each illuminated by 5 LEDs at the top and 5 LEDs at the bottom. 2 LEDs were red (630 nm), 4 LEDs were green (526 nm), and 4 LEDs were blue (458 nm). A light stimulus was rotated around the embryo, and changed direction periodically. The intensities of the LEDs were adjusted such that each stimulus wavelength delivered an equal amount of quanta, thus generating a white stimulus. Sinusoids with 100% contrast, a spatial frequency of 0.014 cycles/deg were rotated around the fish with an angular velocity of 18 deg/sec. This resulted in a temporal frequency of 0.25 cycles/sec. The average intensity was 16 lux. To avoid habituation of the optokinetic response, the stimulus changed direction periodically. It first moved counterclockwise for 12 sec, then held still for 3 sec before it moved clockwise for another 12 sec. Eye position and angle were automatically tracked over time and translated into graphs. Dashed arrow, rightward rotation; solid arrow, leftward rotation. (**B, C**) Representative optokinetic images and graphs of a wild-type and *gnb5* mutant embryo (total recordings wild-type N=6, mutants N=6). Red, left eye; blue, right eye.

Table S1: *In silico* pathogenic prediction of all detected variants in *GNB5* gene

***GNB5* Variations**	**Mode of inheritance**	**dbSNP138**	**ExAC AF**	**SIFT/Provean prediction**	**PolyPhen-2**	**MutationTaster**	**NNSPLICE**	**NetGene2**	**UMD-Predictor**
Splice site change									
c.249G>A - r.[249G>A;249-250ins25] p.(D84Vfs52X)	Compound heterozygous	-	-	Tolerated/Neutral	NR	Disease causing	reduced splicing efficiency in donor site (score = 0.78)	reduced splicing efficiency in donor site (score = 0.70)	Pathogenic
c.249+1G>T p.(D84Lfs31X)	Recessive	-	-	NR	NR	Disease causing	loss of the canonical splice site	loss of the canonical splice site	NS
c.249+3A>G p.(D84Vfs31X)	Recessive	-	-	NR	NR	Disease causing	slight reduced splicing efficiency in donor site (score = 0.97)	no change	NS
Nonsense									
c.994C>T p.(R332X)	Compound heterozygous	-	8,24E-06	NS	NS	Disease causing	NR	NR	Pathogenic
c.906C>G p.(Y302X)	Recessive	-	8,26E-06	NS	NS	Disease causing	NR	NR	Pathogenic
Missense									
c.242C>T p.(S81L)	Recessive	-	4,96E-05	Damaging (score = 0)	Possibly damaging (score = 0.867)	Disease causing	NR	NR	Pathogenic

NS = Not Scored
NR = Not Relevant

Chapter 2: Intellectual developmental disorder with cardiac arrhythmia syndrome in a child with compound heterozygous *GNB5* variants

Summary of the contribution

The present chapter was accepted for publication in Clinical Genetics (2017), https://doi.org/10.1111/cge.13194.

My contribution to this work regarded mutational analysis, interpretation of 3D modeling, as well as writing of the manuscript.

The results are presented as a case report with 1 Figure.

Received: 9 November 2017 | Revised: 30 November 2017 | Accepted: 4 December 2017

DOI: 10.1111/cge.13194

WILEY CLINICAL GENETICS

LETTER TO THE EDITOR

Intellectual developmental disorder with cardiac arrhythmia syndrome in a child with compound heterozygous *GNB5* variants

KEYWORDS: cardiac arrhythmia, GNB5, ID, IDDCA, LADCI

To the Editor:

GNB5 has key roles in parasympathetic regulation of heart rate, neuronal development, vision and motor function.[1] Biallelic variants in *GNB5* are associated with clinical presentations ranging from a severe multisystem disorder including intellectual disability, seizures, retinal abnormalities and cardiac arrhythmias, known as intellectual developmental disorder with cardiac arrhythmia (IDDCA, MIM#617173)[1,2] to a milder disorder of language delay, attention-deficit/hyperactivity disorder, cognitive impairment with or without cardiac arrhythmia (LADCI; MIM#617182).[3] Individuals at the milder and severe end of the *GNB5*-associated pathologies carry homozygous S81L and biallelic loss-of-function variants, respectively.[1–3]

We describe a 2-year-old male proband compound heterozygote for *GNB5* (NM_006578.3) p.(D74EfsX52) c.222_226delTAAGA, and p.(R246Q) c.737G>A, maternally and paternally inherited, respectively (Figure 1A). These variants, unreported in ExAC, were identified by WES and confirmed by Sanger. The missense variant, predicted to be deleterious by PolyPhen (http://genetics.bwh.harvard.edu/pph2/) and MutationTaster (http://www.mutationtaster.org/), impacts a conserved residue positioned on the binding surface of the central pore. Its alteration could influence binding affinities (Figure 1B,C). It may act, alternatively, on splicing, as this substitution affects the last nucleotide of exon 7, as predicted by NetGene2 (http://www.cbs.dtu.dk/services/NetGene2/) and Splicing Finder (http://www.umd.be/HSF3/).

The child was the product of an uncomplicated pregnancy and non-consanguineous Caucasian parents (Figure 1A). Family history was negative for epilepsy, DD/ID, vision problems or known genetic conditions. Clinical and genetic investigations were conducted in accordance with institutional IRB regulations, and conducted in accordance with the Helsinki Declaration. Informed consent was obtained from parents. He was admitted to the NICU for respiratory distress, periodic breathing, and bradycardia. Laryngomalacia hypertonia and clenched hands were noted. He showed upbeat nystagmus at 3 months. Electroretinography at 6 months showed severe reduction in cone and rod function. Auditory brainstem response at 6 months showed left-sided hearing loss. Brain MRI, performed at 4 days, 4 and 8 months showed a thin corpus callosum. Spine MRI was within normal limits. EEG at 17 months showed high-voltage cortical activity, with sharp waves occurring in a multifocal fashion over the right and left posterior parietal areas, independently over the temporal regions, and occasionally over the right occipital region during sleep. No frank seizures were documented.

Sleep electrocardiogram at 4 months showed sinus arrhythmia with sinus pauses of up to 3 seconds. Heart rate ranged from 71 to 183 beats per minute, with sinus pauses as long as 3.1 seconds according to Holter monitoring at 17 months. Atrial, junctional and ventricular escape beats followed the sinus pauses. No evidence of AV block was observed. He had a pacemaker placed at 22 months due to intermittent bradycardia and sinus arrhythmia. The pacemaker set to pace at 70 bpm has been estimated to pace approximately 15% of the time. The proband has never required a blood transfusion, and does not have a history of malabsorption or pancreatic insufficiency.

At 17 months, the proband was at the 66th percentile for weight, 18th for height, 56th for head circumference, and 91st for BMI. He was a non-dysmorphic, non-verbal child unable to sit independently, and with minimal voluntary movements. He had central hypotonia and intermittent extremity hypertonia, intermittent upper extremity jerking motions, sometimes in conjunction with a stimulus.

The severity of the proband's features and their resemblance with those harboring biallelic truncating variants, corroborated by 3D modeling and in silico predictions, suggest that the GNB5 variants are causal (Figure 1C). By extending the number of affected individuals, this report emphasizes the phenotypic consequences of *GNB5* deficiency.

Abbreviations: AV, atrioventricular; BMI, body mass index; DD/ID, developmental disability/intellectual disability; EEG, electroencephalogram; ExAC, Exome Aggregation Consortium; IRB, institutional review board; MRI, magnetic resonance imaging; NICU, neonatal intensive care unit; WES, whole exome-sequencing

ACKNOWLEDGEMENTS

This work was supported by the Italian Ministry of Health, Daunia Plast and Stuppiello's Family to G.M. and the SNSF (31003A_160203) to A.R.

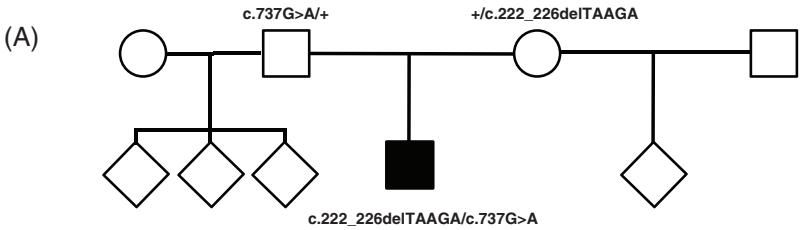

(B)

p.R246Q

```
H. sapiens              LCLDLAPSETGNTFVSGGCDKKAMVWDMRSGQCVQAFETHESDINSVRYYPSGDAFASGS
P. abelii               LCLDLAPSETGNTFVSGGCDKKAMVWDMRSGQCVQAFETHESDINSVRYYPSGDAFASGS
M. musculus             LCLDLAPSETGNTFVSGGCDKKAMVWDMRSGQCVQAFETHESDVNSVRYYPSGDAFASGS
R. norvegicus           LCLDLAPSETGNTFVSGGCDKKAMVWDMRSGQCVQAFETHESDVNSVRYYPSGDAFASGS
H. glaber               LCLDLAPSETGNTFVSGGCDKKAMVWDMRSGQCVQAFETHESDINSVRYYPSGDAFASGS
C. griseus              LCLDLAPSETGNTFVSGGCDKKAMVWDMRSGQCVQAFETHESDVNSVRYYPSGDAFASGS
O. cuniculus            LCLDLAPSETGNTFVSGGCDKKAMVWDMRSGQCVQAFETHESDINSVRYYPSGDAFASGS
B. taurus               LCLDLAPSETGNTFVSGGCDKKAMVWDMRSGQCVQAFETHESDINSVRYYPSGDAFASGS
P. pubescensis          LCLDLAPSETGNTFVSGGCDKKAMVWDMRSGQCIQSFETHDSDINSVRYYPSGDAFASGS
C. brachyrhynchos       LCLDLAPSETGNTFVSGGCDKKAMVWDMRSGQCVQSFETHDSDINSVRYYPSGDAFASGS
S. camelus              LCLDLAPSETGNTFVSGGCDKKAMVWDMRSGQCIQSFETHDSDINSVRYYPSGDAFASGS
T. guttatus             LCLDLAPSETGNTFVSGGCDKKAMVWDMRSGQCIQSFETHDSDINSVRYYPSGDAFASGS
E. garzetta             LCLDLAPSETGNTFVSGGCDKKAMVWDMRSGQCIQSFETHDSDINSVRYYPSGDAFASGS
C. canorus              LCLDLAPSETGNTFVSGGCDKKAMVWDMRSGQCIQSFETHDSDINSVRYYPSGDAFASGS
G. gallus               LCLDLAPSETGNTFVSGGCDKKAMVWDMRSGQCIQSFETHDSDINSVRYYPSGDAFASGS
P. carbo                LCLDLAPSETGNTFVSGGCDKKAMVWDMRSGQCIQSFETHDSDINSVRYYPSGDAFASGS
A. mississippiensis     LCLDLAPSETGNTFVSGGCDKKAMVWDMRSGQCIQSFETHESDINSVRYYPSGDAFASGS
U. stansburiana         LCLDLAPSETGNTFVSGGCDKKAMVWDMRTGQCIQSFETHESDINSVRYYPSGDAFASGS
X. tropicalis           LCLDLAPSETGNTFVSGGCDKKAMVWDMRTGQCIQSFETHESDINSVRYYPSGDAFASGS
A. tigrinum             LCLDLAPSETGNTFVSGGCDKKAMVWDMRSGQCIQSFETHESDINSVRYYPSGDAFASGS
C. carpio               LSLNLAPSETGNTFVSGGCDKKANVWDMRSGQNVQSFETHESDINSVKYYPSGDAFATGS
D. rerio                LSLDLAPSETGSTFVSGGCDKKANVWDMRSGQNVQSFETHDSDINSVKYYPSGDAFASGS
S. formosus             LCLDLAPSETGNTFVSGGCDKKANVWDMRSGQCIQSFETHESDINSVRYYPSGDAFASGS
                        *.*:*******.********** *****:** :*:****:**:***:*********:**
                        199                                                      258
```

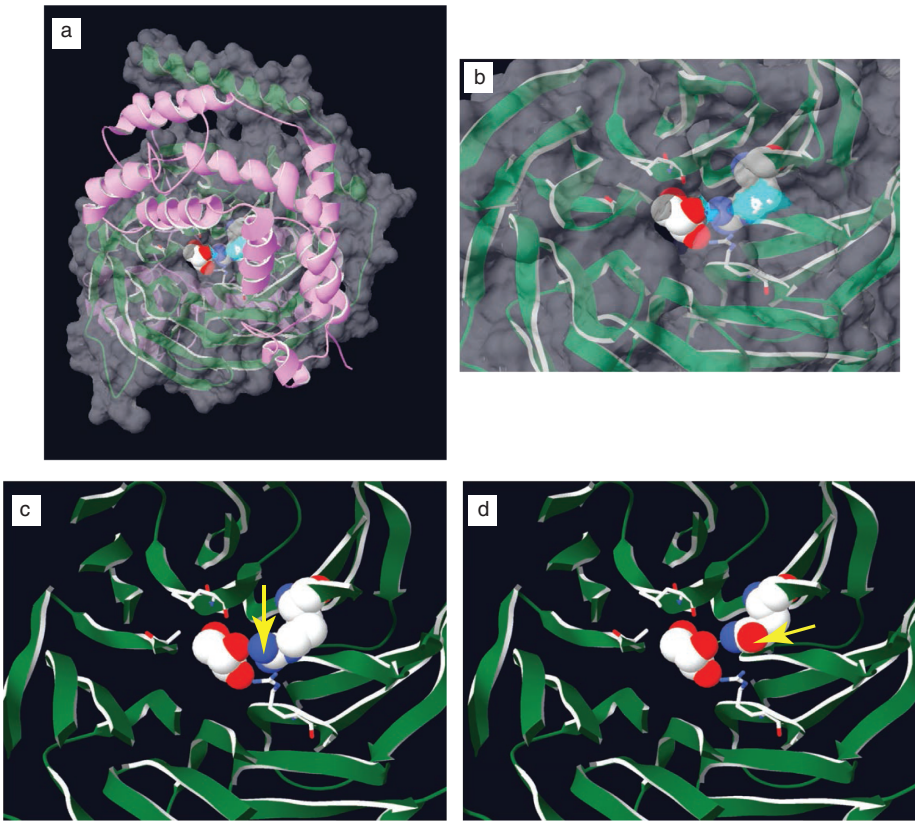

FIGURE 1 A, Family pedigree. B, Evolutionary conservation of portions of WD4 and WD5 domains of GNB5 across vertebrates. Asterisks indicate full conservation. C, (a) Top view of GNB5 (green with the blur of its molecular surface shown in gray) complexed with RGS9 (purple). In the central pore a glycerol molecule (white/red) is displayed (b) Zoom view of the evolutionary conserved Arginine 246 (cyan), located at the binding surface of the propeller. (c, d) Comparison of the 3D GNB5 propeller structure (green) without the blur of the molecular surface of the pore with an Arginine (c) and a Glutamine (d) residue at position 246. Both residues (yellow arrow) face the internal section and binding surface of the pore

ORCID

G. Merla http://orcid.org/0000-0001-5078-928X

H. Vernon,[1] J. Cohen,[1] P. De Nittis,[2] A. Fatemi,[1] R. McClellan,[1] A. Goldstein,[3] N. Malerba,[4] N. Guex,[2,5] A. Reymond,[2] G. Merla,[4]

[1]*Department of Neurogenetics, Kennedy Krieger Institute, Baltimore, Maryland*

[2]*Center for Integrative Genomics, University of Lausanne, Lausanne, Switzerland*

[3]*Division of Human Genetics, Children's Hospital of Philadelphia, Philadelphia, Pennsylvania*

[4]*Division of Medical Genetics, IRCCS Casa Sollievo della Sofferenza, San Giovanni Rotondo, Foggia, Italy*

[5]*Swiss Institute of Bioinformatics, Lausanne, Switzerland*

Correspondence

Giuseppe Merla, Division of Medical Genetics, IRCCS Casa Sollievo della Sofferenza, San Giovanni, Rotondo, Foggia, Italy.

Email: g.merla@operapadrepio.it

DOI 10.1111/cge.13194

REFERENCES

1. Lodder EM, De Nittis P, Koopman CD, et al. GNB5 mutations cause an autosomal-recessive multisystem syndrome with sinus bradycardia and cognitive disability. *Am J Hum Genet*. 2016;99:704-710.
2. Turkdogan D, Usluer S, Akalin F, Agyuz U, Aslan ES. Familial early infantile epileptic encephalopathy and cardiac conduction disorder: a rare cause of SUDEP in infancy. *Seizure*. 2017;50:171-172.
3. Shamseldin HE, Masuho I, Alenizi A, et al. GNB5 mutation causes a novel neuropsychiatric disorder featuring attention deficit hyperactivity disorder, severely impaired language development and normal cognition. *Genome Biol*. 2016;17:195.

Chapter 3: Inhibition of G-protein signaling in cardiac dysfunction of Intellectual Developmental Disorder with Cardiac Arrhythmia (IDDCA) syndrome

Summary of the contribution

This chapter represents the natural continuation of the previous gene discovery papers. As first author of this paper, I was in charge of the writing, literature mining and figures assembly, under the supervision of Alexandre Reymond. I participated to the experimental design of the mouse study, obtained veterinary authorization to perform experiments, created mouse cohorts, and performed transcriptome analysis. The cardiac evaluation was performed in collaboration with the Cardiovascular Assessment facility (CAF, at CHUV Hospital) with the help of Alexandre Sarre and Thierry Pedrazzini, who contributed to results interpretation. I coordinated data sharing between researchers and clinicians involved. I personally presented this work (i) at the European Society of Human Genetics 2019 congress in Gothenburg, Sweden, (ii) at the Swiss Society of Medical Genetics 2019 in Lausanne, Switzerland, (iii) at the MedLem 2019 meeting in Lausanne, Switzerland, and (iv) was invited as an external speaker at the NIDDK Branch at NIH Institutes, Bethesda, MD, USA by William F. Simonds.

The results are summarized in six main figures (named **Figure 1-6**) and four supplementary figures (named **Figure S1-4**), two tables embedded in the text, and 7 supplementary Tables (named **Table S1-S7**).

Inhibition of G-protein signaling in cardiac dysfunction of Intellectual Developmental Disorder with Cardiac Arrhythmia (IDDCA) syndrome

Pasquelena De Nittis[1], Alexandre Sarre[2], Stephanie Efthymiou[3], Audrey Putoux[4], Nicolas Guex[5], Jacqueline Chrast[1], Reza Maroofian[3], SYNAPS Study Group, Gaetan Lesca[6,7], Nicolas Chatron[1,6,7], Tipu Sultan[8a], Javeria Raza Alvi[8], Zia ur Rahman[8], Faisal Zafar[9], Nuzhat Rana[9], Fatima Rahman[10], Najwa Anwar[10], Shazia Maqbool[10], Vincenzo Salpietro[3], Marilena Christoforou[3], Henry Houlden[3], William F. Simonds[11], Thierry Pedrazzini[12], Alexandre Reymond[1]

[1]Center for Integrative Genomics, University of Lausanne, Switzerland

[2]Cardiovascular Assessment Facility, University of Lausanne, Switzerland

[3]Department of Neuromuscular Disorders, Queen Square Institute of Neurology, University College London, WC1N 3BG, London, UK

[4]Department of Genetics, Hospital Femme Mère Enfant, Lyon, Bron, France

[5]BioInformatics Competence Center, University of Lausanne, Switzerland

[6]Service de Génétique, Hospices Civils de Lyon, Lyon, France

[7]Université Claude Bernard Lyon 1, CNRS UMR 5310, INSERM U1217, Institut NeuroMyoGène, Lyon, France

[8]Department of Pediatric Neurology,

[9]Department of Paediatric Neurology, Children's Hospital and Institute of Child Health, Multan, 60000, Pakistan

[10]Department of Developmental-Behavioural Paediatrics, The Children's Hospital and Institute of Child Health 54600 Lahore, Pakistan

[11]Metabolic Diseases Branch/NIDDK, National Institutes of Health, Bethesda, MD, USA

[12]Experimental Cardiology Unit, Department of Cardiovascular Medicine, University of Lausanne, Switzerland

Correspondence should be addressed to:

Alexandre Reymond, alexandre.reymond@unil.ch

Abstract

Background

Pathogenic variants of *GNB5* encoding the β_5 subunit of the guanine nucleotide-binding protein cause IDDCA syndrome, an autosomal recessive neurodevelopmental disorder associated with cognitive disability and cardiac arrhythmia, particularly severe bradycardia.

Methods

To investigate the consequences of *Gnb5* loss in the heart, we monitored heart electrophysiology through *in vivo* electrocardiography telemetry and cardiac function by echocardiography in *Gnb5*$^{+/-}$, *Gnb5*$^{-/-}$ and wild-type littermates.

Results

We delineated the role of the mouse orthologous *Gnb5* in heart sinus conduction and showed that *Gnb5*-inhibitory signaling is essential for parasympathetic control of the heart rate. *Gnb5*$^{-/-}$ mice were smaller and had a smaller heart than *Gnb5*$^{+/+}$ and *Gnb5*$^{+/-}$ mice, but exhibited better cardiac function. Their increased fractional shortening and ejection fraction allowed to maintain the cardiac output unchanged. *Gnb5*$^{-/-}$ mice also exhibited profound bradycardia upon treatment with the parasympathomimetic drug, Carbachol (CCh). In contrast, sympathetic modulation of the cardiac stimulation was not altered. Concordantly, transcriptome study pinpointed altered expression of genes involved in cardiac muscle contractility in atria and ventricles of knocked-out mice. We observed increased *Gnb3* gene expression possibly suggesting that loss of *Gnb5* is partially compensated in the heart. Homozygous loss of *Gnb5* resulted in significantly higher frequencies of sinus arrhythmias such as atrial escape beat and atrioventricular block. Moreover, we identified six affected individuals, increasing the IDDCA cohort to 33 patients.

Conclusions

Our data demonstrate that loss of negative regulation of the inhibitory G-protein signaling causes heart rate perturbations in *Gnb5*$^{-/-}$ mice, an effect mainly driven by impaired parasympathetic activity. We anticipate that unraveling the mechanism of *Gnb5*-signaling in the autonomic control of the heart will pave the way for future drug screening.

Keywords: *GNB5* variants, *Gnb5*-null mouse models, IDDCA, cardiac conduction anomalies

Background

Intellectual Developmental Disorder with Cardiac Arrhythmia (IDDCA, OMIM: #617173) is an autosomal recessive neurodevelopmental disorder with onset in early childhood. Inactivating and hypomorphic mutations in the β_5 subunit of guanine nucleotide-binding protein (*GNB5*), respectively cause severe and mild forms of the disorder(1). The former is associated with cognitive disability, poor or absent speech and/or severe cardiac arrhythmias. The moderate manifestation of the syndrome also named LADCI syndrome (OMIM: #617182; Language delay and ADHD/cognitive impairment with or without cardiac arrhythmia) consists of mild intellectual impairment, language delay, attention deficit hyperactivity disorder (ADHD) and, in about half the cases, severe cardiac arrhythmia(1, 2). Some IDDCA patients also showed retinal dysfunction and nystagmus, epilepsy, hypotonia and gastric reflux(1-8). The *GNB5* retinopathy is a unique combination of dual retinal signaling defects reminiscent of features of both bradyopsia and rod ON-bipolar dysfunction(5), while the IDDCA epilepsy is characterized by early seizure onset (~ 3 months of age) with focal seizures rapidly evolving into epileptic spasms and consequent generalized multifocal discharges(4).

The sympathetic and parasympathetic branches of the autonomic nervous system control cardiac electrophysiology. Parasympathetic modulation of cardiac output is primarily mediated by acetylcholine release, which activates M_2-muscarinic receptors (M_2R) present on cells innervated by parasympathetic postganglionic neurons. The activation of M_2R triggers $G_{i/o}$ subfamily G-proteins, which turn on G-protein-gated inwardly rectifying K^+ channels (GIRK) resulting in membrane hyperpolarization. Regulator of G-protein Signaling (RGS) proteins negatively regulate the timing of this M_2R-GIRK signaling. GNB5, a divergent member of the Gβ family, has the unique property of forming complexes with R7-RGS proteins(9-14). In particular, the GNB5-RGS6 complex is involved in cardiac GIRK deactivation kinetics. *Rgs6*-null mice manifested heart conduction anomalies and hypersensitivity to parasympathomimetics(15). Zebrafish model defective for *gnb5* gene correspondingly showed reduced heartbeat upon reinforced parasympathetic stimulation, eye movement defects and altered swimming behavior(1) and cardiomyocytes differentiated from human iPSCs (induced Pluripotent Stem Cells) edited to engineer the

GNB5-Ser81Leu missense variant associated with LADCI showed a decrease in spontaneous activity upon stimulation with Carbachol compared to normal cells(7).

Whereas homozygous *Gnb5*-null mice recapitulated many of the corresponding human disease phenotypes such as learning deficiencies, hyperactivity, impaired motor coordination and perturbed vision(16-20), a systematic cardiac evaluation has never been performed in a mammalian model. Here, we assessed heart electrophysiology of *Gnb5* mice models. We detected an increased frequency of sinus arrhythmias in $Gnb5^{-/-}$ animals, which have a smaller heart than wild-type and $Gnb5^{+/-}$ mice, but exhibited better cardiac function. $Gnb5^{-/-}$ mice also displayed enhanced parasympathetic sensitivity upon stimulation with a cholinergic agonist. Consistently, transcriptome profiling of atria and ventricles revealed overexpression of genes involved in cardiac muscle contractility along with reduced ventricular expression of genes required for development of pacemaker cells in $Gnb5^{-/-}$ mice. Finally, we expanded the number of ascertained IDDCA individuals and the *GNB5* mutational spectrum.

Methods

Enrollment

All affected individuals and their family members were recruited in Pakistan (Families O-S) and France (Family T) after signing a written informed consent according to ethical review boards policies. Clinical ascertainment included physical examinations, medical history interviews and specialized consultations by a certified neurologist and cardiologist as appropriate. Venous blood was collected in EDTA for DNA extraction according to standard procedures.

Exome sequencing

Whole Exome Sequencing of families O-S was performed by Macrogen, Korea as described in reference (21). Briefly, target enrichment was performed with 2 µg genomic DNA using the SureSelectXT Human All Exon Kit version 6 (Agilent Technologies, Santa Clara, CA, USA) to generate barcoded whole-exome sequencing libraries. Libraries were sequenced on the HiSeqX platform (Illumina, San Diego, CA, USA) with 50x coverage. Quality assessment of the sequence reads was performed by generating QC statistics with FastQC(22). The filtering strategy included screening for only exonic and donor/acceptor splicing variants. In

accordance with the pedigree and phenotype, priority was given to variants rare or absent in public databases (1,000 Genomes project, NHLBI Exome Variant Server, Complete Genomics 69 and Exome Aggregation Consortium [ExAC v0.2]).

Trio exome sequencing was performed in proband T and her parents using SeqCap EZ Medexome library preparation kit following manufacturer's recommendations (Roche, Indiana, IN, USA). Libraries were sequenced on a NextSeq500 (Illumina, San Diego, CA, USA) at mean depth coverage of 73x with 93.3% of the target bases above 30x. Genomic alignment against the hg19/GRCh37 assembly and variant calling were, respectively, done with BWAMEM v.0.7.12 and GATK HaplotypeCaller v.3.4 (Broad Institute, Boston, MA, USA). Only highly confident variants were kept for analysis (total depth >9; alternative allele depth >4; no strand bias; mosaicism >10%). Rare variants were considered as having a frequency <1% in GnomAD v2 dataset.

Sanger sequencing in each family confirmed the segregation of *GNB5* variants with the phenotype.

Mouse husbandry

The *Gnb5* mouse line was recovered from cryopreserved sperm using *in vitro* fertilization**.** The knockout allele was engineered in a C57BL/6J inbred genetic background by heterozygous deletion of exon 3 in the germline, as previously described(16, 20). Genetically modified animals were born and housed in the Animal Facility of the Center for Integrative Genomics, under controlled temperature conditions and a 12-h light-dark cycle with free access to water, normal chow and nest building material. Mouse genomic DNA was extracted from ear biopsies using the Hot Shot protocol(23) and used for genotyping as described(20). To prevent the previously documented high mortality of *Gnb5*$^{-/-}$ pups at weaning(16), heterozygous breeding couples used to obtain knockout pups were given breeding food pellet enriched for proteins and vitamins (Kliba 3336, extrudate). Additionally, litters including *Gnb5*$^{-/-}$ pups were fed from 14 to 28 days of age, i.e. starting one week before weaning, with powdered wet maintenance food (Kliba 3436) in a Petri dish placed directly onto the floor of the cages, an expedient that should provide easier access to the food for the pups. Maintenance and mouse experimental procedures were approved by institutional and Swiss Federal Veterinary Office (experimental protocol VD3289.c).

In vivo transthoracic ultrasound imaging protocol

Transthoracic echocardiography was performed using a 30 MHz probe and the Vevo 2100 Ultrasound machine (VisualSonics, Toronto, ON, Canada). A light anesthesia was achieved with 1-1.5% isoflurane, maintaining heart rate (HR) at 400-500 beats per minute (bpm). The mice were placed in decubitus dorsal on a heated 37ºC platform to maintain body temperature. The heart was imaged in the 2D mode in the parasternal long-axis view. From this view, an M-mode cursor was positioned perpendicular to the interventricular septum and the posterior wall of the left ventricle, at the level of the papillary muscles. Diastolic and systolic inter-ventricular septum, left ventricular posterior wall thickness, and left ventricular internal end-diastolic and end-systolic chamber dimensions were measured. Three separate M-mode images were measured and averaged. Left ventricular fractional shortening and ejection fraction were also calculated. Fractional shortening and ejection fraction were assessed from M-mode based on the percentage changes of left ventricular end-diastolic and end-systolic diameters and volumes, respectively.

In vivo electrocardiography measurements

For *in vivo* electrocardiography (ECG) monitoring we have subcutaneously implanted biopotential telemetric transponders (ETA-F10, Data Sciences International) allowing continuous monitoring in conscious freely moving animals. Baseline ECG was recorded ten days after device implantation, over a period of 86 hours. After 30 minutes of basal measurements, we injected mice with 0.9% saline solution (i.p. NaCl, 10ml/kg) as a vehicle control; next the following compounds were administered one at a time: Atropine (PubChem CID: 174174, i.p., 1mg/kg), Carbachol (PubChem CID: 5831, i.p. 0.1mg/kg), and in a subset of mice Isoprenaline (PubChem CID: 3779, i.p. 4mg/kg) and Atenolol (PubChem CID: 2249, i.p. 2mg/kg) as well, with a one night interval between each injection. The amount of Isoprenaline and Atenolol were chosen after testing 10 doses ranging from 4μg/kg to 4mg/kg and 2μg/kg to 2mg/kg, respectively. While Atropine and Carbachol inhibits and activates the parasympathetic system respectively, Atenolol and Isoprenaline respectively blocks and promotes the sympathetic response.

At the end of the experiment, mice were sacrificed by CO_2 inhalation; the heart was digitally imaged both within its thoracic position and after excision. Heart weight was recorded and tibia length was measured to normalize the heart weight to body size.

Baseline ECG lines were analyzed as follows: 10 minutes of recording were analyzed using ECG-Auto software in shape recognition mode (EMKA Technology, France) every 30 minutes, during night and day phases. Mean was reported for each analyzed parameter. During pharmacological challenges, ECG recording was analyzed continuously, with 10 minutes' steps, thus one mean of each parameter was calculated every 10 minutes. On ECG line we analyzed: i) RR interval (measured at R peak), and expressed in milliseconds (ms)), ii) Heart rate (HR): heart beating rate, calculated as 60/(RR/1000), expressed in bpm; iii) PR interval (interval between beginning of P wave and R peak, expressed in ms); iv) QT duration: duration of the QT complex, v) QTc (corrected QT, calculated from QT/√(RR/100)(24) (all expressed in ms), that allows correction of QT from HR variations).
Temperature and activity were also recorded. Activity was estimated by displacement of the telemetric device from the antennas of the recording plate. This measurement was only used as a qualitative index of mouse activity/movement. Temperature and activity values are mean values of one-hour interval.

Arrhythmias assessment

Arrhythmias were identified based on ECG line (RR interval) and counted. Observed arrhythmias were defined as follows: i) escape atrial beat, with a P wave morphology different from that of the sinus P wave, classified as "long" and "short" according to the location of the P wave on the ECG line; ii) atrio-ventricular block defined on ECG by more than one P wave for one QRS complex; iii) premature beats; and iv) episodes of tachycardia followed by bradycardia, with HR oscillation between high and low values within a few seconds, independently of other type of arrhythmias.

Statistical tests

Each parameter measured was reported as mean ± standard deviation (SD). Standard t-test was used to assess differences between two groups. ANOVA tests, followed by Tukey post-hoc tests were also calculated and are displayed. $p < 0.05$ was considered significant and stars on the plot(s) represent the level of significance (*$p \leq 0.05$, **$p \leq 0.01$, *** $p \leq 0.001$, ****$p \leq 0.0001$; $p > 0.05$ was considered not significant (ns)).

Transcriptome profiling, data processing and differential expression analysis

A total of 72 RNA sequencing libraries were generated from two heart tissues, atria and ventricles, and three brain regions, cerebellum, hippocampus and cerebral cortex. For this

experiment we created a cohort of adult (18 weeks) male mice including 6 *Gnb5*$^{-/-}$, 6 *Gnb5*$^{+/-}$ and 6 *Gnb5*$^{+/+}$ animals. Brain transcriptome was only assessed in *Gnb5*$^{-/-}$ and *Gnb5*$^{+/+}$ animals. Tissue collection and processing procedures were designed to minimize biological and technical variation. Specifically, tissues were dissociated in QIAzol Lysis Reagent (Qiagen) using the gentleMACS™ Dissociator (Miltenyi Biotec). Cell suspension was used to obtain total RNA. Genomic DNA contamination was removed by digestion with RNase-free Deoxyribonuclease I (DNase I) (Qiagen). RNA concentration and purity were measured by ND-1000 spectrophotometer (Thermo Scientific, Wilmington, NC, USA) and RNA integrity was verified by fragment analyzer automated CE system (Advanced Analytical Technologies, Inc) according to manufacturer's instructions. Libraries were then prepared with TruSeq Stranded RNA Library Prep Kit (Illumina) and sequenced on multiple lanes of an Illumina HiSeq4000 platform, generating an average of 50M single-end 125-cycle reads for each sample. Quality of sequence was assessed by FastQC (version v0.11.4)(22). Purity-filtered reads were adapters- and quality- trimmed with Cutadapt (v1.8)(25). Reads matching to ribosomal RNA sequences were removed with fastq_screen (v. 0.11.1). Remaining reads were further filtered for low complexity with reaper (v. 15-065)(26). Reads were then aligned against *Mus Musculus.GRCm38.92* genome using STAR (v.2.5.3a)(27). The number of read counts per gene locus was summarized with htseq-count (v0.9.1)(28) using *Mus Musculus.GRCm38.92* gene annotations. Quality of the RNA-seq data alignment was assessed using RSeQC (v. 2.3.7)(29). Reads were also aligned to the *Mus Musculus.GRCm38.92* transcriptome using STAR (v. 2.5.3a)(27) and the estimation of the isoforms abundance was computed using RSEM (v. 1.2.31)(30). To assess differential expression between genotypes within each tissue, we compared *Gnb5*$^{-/-}$ and *Gnb5*$^{+/-}$ samples to wild-type specimens. Data analysis was performed with the R Bioconductor package DESeq2 (version 1.14.1)(31). Differentially Expressed Genes (DEGs) were identified at the Benjamini-Hochberg (BH) adjusted $p < 0.05$ level, using Wald test under design ~ genotype. For gene set enrichment analysis no direction criterion on fold change was applied. Enriched Gene Ontology (GO) categories were identified using the enrichment analysis package in R/Bioconductor, clusterProfiler(32), considering only categories with at least ten and maximum 500 annotated genes. Nominally significant enriched terms were retained for results interpretation.

Results

Clinical and molecular features of six novel IDDCA patients

We identified six additional IDDCA cases (**Figure 1**, **Table 1**) through exome sequencing of six consanguineous families and data aggregation of multiple laboratories and clinical centers via GeneMatcher(33, 34) or direct contacts. Consistent with previous reports(1-8), the carrier of a homozygous *GNB5* missense variant on Ser81 presented with LADCI, the mild form of IDDCA (Family T), while the four individuals with bi-allelic loss-of-function (LoF) alleles due to truncating mutations displayed phenotypes corresponding to the severe end of the disease spectrum (Families O-P and R-S). A sixth individual (Family Q) carrying a novel homozygous missense variant on Gly215 similarly presented with the severe IDDCA phenotypic spectrum. Clinical features of affected individuals are presented in **Table 1** and detailed in the **Supplemental Note**. The two missense variants (c.644G>A, p.(Gly215Glu), Family Q, and c. 242C>G, p.(Ser81Trp), Family T; transcript NM_006578.3) were not reported before (**Figure 1**). They are predicted by a majority of prediction tools to be likely damaging to protein function (**Supplementary Table S1**) and are absent from GnomAD (v3)(35). To assess possible impact, we modeled these two substitutions using the crystal structure of the GNB5-RGS9 complex(36) and found that both variants might impact the potential binding properties of the GNB5 central pore (**Figure 1B**). Specifically, Serine 81 is buried inside a β strand of the first WD40 repeat close to the central pore of the β propeller structure(1, 2) where a glycerol molecule is observed in pbi structure 2pbi (**Figure 1B**, left panel). Reminiscent to the Ser81Leu variant previously documented(1), a Tryptophan at position 81 cannot be accommodated without disrupting the structure and potential binding properties of the pore. Our model suggests that the rearrangements necessary to settle such a bulky sidechain will change the channel characteristics. We have investigated the related rotamers, emphasizing the steric hindrances-induced local rearrangements associated with the Tryptophan replacement, whose perturbations were evaluated using the backbone dependent rotamer library implemented in the Swiss-PdbViewer(37). Depending on the rotamer, Tryptophan 81 will severely encroach with Leucine 67 (grey), Cysteine 68, Valine 87, Cysteine 111, Valine 108, and/or Alanine 110 (**Figure 1B**).

The Glycine 215 (**Figure 1B**, right panel) lies in a beta-sheet, between Alanine 221 and Cysteine 200. It faces a beta-strand harboring Valine 242 and Valine 245. There is not enough space to accommodate the Glutamic acid sidechain as it would encroach into one or

more sidechains of the above-enumerated residues. All rotamers would also probably force the sidechain of Cysteine 200 to reorient itself toward the interior of the channel to accommodate the Glutamic Acid 215 sidechain. This will infringe on the glycerol molecule space(36) changing the channel characteristics. Additionally, the c.644G>A, p.(Gly215Glu) variant that affects the second to last nucleotide of exon 6 might alter the activity of the donor splice site as well as create cryptic exonic splicing enhancers (ESE) or silencers (ESS) according to the NNSplice, NetGene2 and Splicing Finder prediction tools (**Supplementary Table S1**).

To date a total of 14 pathogenic *GNB5* variants have been identified in 33 IDDCA individuals (**Figure 1C**, **Table 1**). Suggestive of a founder effect the eight affected individuals from three families (Families E-G) carrying the Ser81Leu variant all originate from Arab countries (Morocco, Algeria and Saudi Arabia). Of note, the Greater Middle East Variome Project(38) (http://igm.ucsd.edu/gme/) did not identify this variant within 2497 individuals. Similarly, the patients from five families (Families D, L, O, P and S) harboring the amber nonsense c.906C>G (Tyr302*) variant are from the Indian subcontinent (one from India and four from Pakistan). Another variant modifying the Tyr302 codon in an ochre codon (c.906C>A) was found in two additional Pakistani families (Families N and R) suggesting again a possible founder effect. The 23 IDDCA individuals present with the severe end of the disease spectrum which is characterized by severe ID (21 out of 23) with poor or absent speech (17/23), early onset sinus node dysfunction (15/23) with 3/15 who had a pacemaker implanted, variable visual abnormalities (17/23), seizures (15/23), hypotonia (19/23) and gastric problems (8/23). Additionally, 6/23 individuals showed different types of dysmorphic features (**Table 1**) and MRI evaluation revealed altered brain structure in 3/23 children, with two having thinner corpus callosum, and one cerebral atrophy. A single individual (individual 16, Family H) showed autistic features. All severely affected individuals carry either bi-allelic truncation mutations or bi-allelic missense variants that probably result in LoF. Nine patients displayed the milder LADCI syndrome and bi-allelic missense variants at position 81: 4/9 presented mild ID with 6/9 showing language deficits, 4/9 were noted to have sinus node dysfunction (one of which with pacemaker implantation) and 3/9 were reported with impaired fine motor skills. Behaviorally, 3/9 patients exhibited Attention Deficit Hyperactivity Disorder (ADHD). The remaining patient (Family J) is compound heterozygous for the LoF p.Asp74Glufs52* and the Ser81Leu variants(3). She presented with an

intermediate manifestation of the symptoms with mild ID accompanied by speech delay, hypotonia and sinus bradycardia. Like patient 21 from Family I who carries the same LoF p.Asp74Glufs52* combined with a different missense, p.(Arg246Gln)(8), she is affected by hearing loss (**Table 1**).

***Gnb5* knock-out mouse cohort**

To model the cardiac manifestations occurring in IDDCA syndrome, we used the mouse model knock-out for *Gnb5* (*Gnb5*$^{-/-}$), thus mimicking a complete LoF. Whereas ~66% of the pups carrying the homozygous null allele were previously reported to die prior to or at weaning(16), pre-weaning mortality was very low in our husbandry setting (Methods). We experienced only 5%, 11% and 6% of losses in the three cohorts we generated by mating heterozygous parents (**Figure 2A**). We recorded 2-8 breeding events during three generations of husbandry with an average litter size of 4-10 pups. The vast majority of pre-weaning lethality appears to be associated with *Gnb5*$^{-/-}$ as shown by the quasi Mendelian distribution of genotypes (**Figure 2A**). We longitudinally monitored the body weight of *Gnb5*$^{+/+}$ (wild-type), *Gnb5*$^{+/-}$, and *Gnb5*$^{-/-}$ male and female mice from 3 to 46 weeks of age (**Figure 2C-D**). We confirmed previous reports(16, 20) that showed that females and males knock-out animals are smaller (**Figure 2B-C-D**) and that heterozygote males are heavier (**Figure 2C-D**). Importantly, knock-out mice had a smaller heart (**Figure 2E**), even smaller than expected when the heart weight was normalized to the tibia length, a proxy for animal size (**Figure 2F**). During animal handling, no obvious gender differences were observed regarding development, behavior or other gross phenotypes.

Ultrasound scans pinpointed increased cardiac function in *Gnb5* knock-out mice

To characterize the *Gnb5* knockout mouse line at cardiac level, we first performed ultrasound scans in baseline conditions. We used 16 *Gnb5*$^{+/+}$, 8 *Gnb5*$^{+/-}$ and 16 *Gnb5*$^{-/-}$ male mice (9 wo (weeks of age)) and analyzed heart morphology and function (Methods). Echocardiography confirmed that *Gnb5*$^{-/-}$ animals had smaller hearts, as demonstrated by reduced ventricular chambers both in diastole and systole (**Figure 3A**). Consequently, ventricular volume was also smaller (**Figure 3B**). Estimated left ventricular weight was significantly lower in *Gnb5*$^{-/-}$ compared to *Gnb5*$^{+/-}$ and wild-type (**Figure 3C**). Left posterior ventricular wall and interventricular septum thickness were not substantially modified (**Figure S1A-B**). Interestingly, *Gnb5*$^{-/-}$ mice demonstrated improved cardiac function, as judged by increased fractional shortening (**Figure 3D**) and ejection fraction (**Figure 3E**).

However, stroke volume (**Figure 3F**) and cardiac output (**Figure 3G**) were similar to those measured in wild-type mice. Notably, and unexpectedly, *Gnb5*$^{+/-}$ have a bigger heart (**Figure 3A-C**) compared to wild-type, while their cardiac function remains unchanged (**Figure 3D-E**). Therefore, the increased stroke volume (**Figure 3F**) and cardiac output (**Figure 3G**) reflected an increased volume of blood pumped by the ventricle.

Taken together, these results indicated that *Gnb5*$^{-/-}$ mouse hearts were smaller than that of the other two genotypes, but compensated their smaller size by increased cardiac efficiency.

Loss of functional *Gnb5* determines the onset of sinus arrhythmias

As cardiac arrhythmia in the form of bradycardia and ectopic beats is one of the core symptoms in IDDCA, we examined HR variations in *Gnb5* mouse models with *in vivo* ECG monitoring. ECG was performed at 12-weeks on the same male mice used for echocardiography. Baseline ECG parameters were not different among *Gnb5*$^{+/+}$, *Gnb5*$^{+/-}$ and *Gnb5*$^{-/-}$ animals, except for HR in knocked-out animals that showed a trend toward higher values (**Figure S1C**, significance varying between p = 1.28E-04 and p = 0.9971, over 36 daylight time points).

Close inspection of baseline ECG over a 24 hours' window allowed the quantification and characterization of small changes in the intervals between successive heartbeats (RR interval) corresponding to cardiac arrhythmias (Methods). The 24h-ECGs unearthed a significant increase in arrhythmic events in *Gnb5*$^{-/-}$ mice compared to heterozygous and wild-type littermates. We counted on average 53 short atrial escape beats in *Gnb5*$^{+/+}$ and 204 in *Gnb5*$^{-/-}$ animals over 24 hours (**Figure 4B-E**; p=4.936e-06). Long atrial escape beats (**Figure 4C-F,** 1 *vs.* 117 events; p=7.792e-06) and atrioventricular blocks (**Figure 4D-G,** 0.6 *vs.* 30 events; p=0.04078) were similarly observed significantly more frequently in knockout animals. Few episodes of tachycardia followed by bradycardia and premature beats were also observed in homozygous knock-outs.

These results demonstrated that *Gnb5*$^{-/-}$ mice have a defect at the level of sinus node as well as of cardiac conduction.

***Gnb5* deficient mice exhibit higher cholinergic sensitivity and normal sympathetic activity**

Human homozygote carriers of *GNB5* pathogenic variants show severe bradycardia at rest with a maximal HR unchanged during exercise. Zebrafish and human cell-modeling supported the participation of the parasympathetic modulation in the etiology of HR

disturbances in IDDCA individuals(1, 7). To better assess the possible involvement of the autonomic innervation we used an *in vivo* mammalian model system whose physiology is closer to humans. We used ECG telemetry to monitor heart's rate and observed higher HR in baseline conditions (**Figure S1C**) possibly reflecting a higher rate of activity of the *Gnb5*$^{-/-}$ mice, as measured qualitatively here and reported previously(20) (**Figure S1D-E**), or alternatively differences in the HR regulation.

Parasympathetic blockade with Atropine (1mg/kg) had a positive chronotropic effect, i.e. HR increased (HR *Gnb5*$^{+/+}$ = 690 bpm ± 68, HR *Gnb5*$^{+/-}$ = 700 bpm ± 34, HR *Gnb5*$^{-/-}$ = 758 bpm ± 28 ($p_{+/+ \text{ vs. } +/-}$ = 0.63, $p_{+/+ \text{ vs. } -/-}$ = 2.62E-03, $p_{+/- \text{ vs. } -/-}$ = 2.38E-03)) (**Figure S2A**). In contrast, Carbachol administration (0.1 mg/kg) triggered a rapid decrease of the HR in the three groups, with a significant effect in *Gnb5*$^{-/-}$ mice, whose HR dropped until 335 bpm (HR *Gnb5*$^{+/+}$ = 448 bpm ± 147, HR *Gnb5*$^{+/-}$ = 415 bpm ± 157, HR *Gnb5*$^{-/-}$ = 335 bpm ± 141 ($p_{+/+ \text{ vs. } -/-}$ = 3E-02, **Figure S2B**). HR quickly recovered in all genotypes. The duration of the bradycardia was similar in the three groups (~ 1 hour). Moreover, since the baseline HR of knockout animals was higher, when expressed in relation to the basal values, the effect of Atropine was not different in the three groups of mice ($p_{+/+ \text{ vs. } +/-}$ = 0.22, $p_{+/+ \text{ vs. } -/-}$ = 0.07, $p_{+/- \text{ vs. } -/-}$ = 0.77**,** **Figure 5A**), while the Carbachol-induced bradycardia was more severe in *Gnb5*$^{-/-}$ (p = 1.79E-03, **Figure 5B**).

To mimic the sympathetic response, and investigate a possible role of the β–adrenergic response in the heart rhythm perturbations of IDDCA syndrome, we challenged *Gnb5*$^{+/+}$ and *Gnb5*$^{-/-}$ animals with either Atenolol or Isoprenaline. The sympathetic antagonist Atenolol (2mg/kg) induced a similar decrease of HR in both groups (p = 0.73, p = 0.22 when compared to baseline (**Figure S2C, Figure 5C**). Injection of the sympathetic agonist Isoprenaline (4mg/kg) resulted in a prolonged (~ 1 hour) increase of HR, with values comparable in both genotypes (p = 0.41, **Figure S2D**). HR slowly decreased to baseline; this reduction reached lower than baseline values in *Gnb5*$^{-/-}$ mice (**Figure S2D**). However, when expressed in percentage of the baseline, the tachycardia seemed stronger in wild-type (p = 0.09, **Figure 5D).**

These results indicate that the *Gnb5*$^{-/-}$ mice bradycardia results from enhanced parasympathetic (cholinergic) stimulation/reflex. Our data also suggest an increased parasympathetic activation when animals are under stress.

The higher HR of *Gnb5*$^{-/-}$ mice in baseline conditions, prompted us to analyze its fluctuations after drugs administration, and assess a possible relationship between the vagal (parasympathetic) and sympathetic tones. Atropine-mediated parasympathetic inhibition induced an increase in HR with a delta lower in knockout animals than in wild types (**Figure 5E**) pinpointing that the parasympathetic tone is lower in *Gnb5*$^{-/-}$ mice. Conversely, the sympathetic blockade by atenolol induced a greater reduction of the HR in *Gnb5*$^{-/-}$ than control littermates (**Figure 5E**) evocative of the greater sympathetic tone observed in basal conditions. Our results suggest that higher basal HR in *Gnb5*$^{-/-}$ mice could be due to lower parasympathetic tone and higher sympathetic tone.

Transcriptome analysis of *Gnb5* mice

To explore the transcriptional consequences of *Gnb5* loss in the heart, we profiled the transcriptomes of atria and ventricles of *Gnb5*$^{-/-}$, *Gnb5*$^{+/-}$ and wild-type male mice at 18 weeks of age using RNA-sequencing (RNA-seq) (**Supplementary Table S2**). RNA-seq libraries were sequenced to a median depth of ~50,000,000 single-end reads per samples. Samples clustering (using Poisson model(39)) to define the global relationship among all samples, showed a very clear separation of atria and ventricles (**Figure S3A**) as well as of hippocampus, cerebellum and cerebral cortex (**Figure S3B**). Transcripts quantification confirmed that *Gnb5,* the orthologue of *GNB5*, is expressed in brain (**Figure S4**) and cardiac tissues (atria and ventricles) of adult mice and that its expression levels correlated with gene dosage (**Figure 6A-B**, top). We identified 98 significantly differentially expressed genes (DEGs) in atria (**Supplementary Table S3**) and 63 in ventricles (**Supplementary Table S4**) applying a false discovery rate method for multiple testing with a 5% threshold. Consistent with the phenotype described in *Gnb5*$^{-/-}$ mice, we found altered expression of genes involved in cardiac muscle contractility, HR regulation and cardiac conduction. Among the upregulated genes falling into these categories in atria were *Npr3* (p = 9.71E-04), *Comp* (p = 3.7E-05), and *Scn10a* (p = 2.88E-02); while downregulated transcripts were *Myh7* (p = 1.31E-02), *Lmod2* (p = 1.04E-04), and *Agt* (p = 7.97E-03) (**Figure 6A**, top). Profiling of the ventricles demonstrated significant upregulation of *Lrrc10* (p = 3.91E-02), *Tnnt2* (cardiac troponin, p = 2.88E-02), *Scn10a* (p = 1.84E-02), and *Drd2* (p = 8.28E-04) (**Figure 6B**, top) and reduced expression of *Tbx18* (p = 1.32E-04). Notably, the expression level of *TNNT2* gene was not modified in GNB5-Ser81Leu hiPSC(7). Correspondingly, nominally enriched gene sets were associated with development of the cardiac conduction system (GO:0003161,

Supplementary Table S5, S6), regulation of HR (GO:0002027, **Supplementary Table S5, S6**), and cardiac muscle contraction (GO:0060047, GO:0060048, **Supplementary Table S5, S6**).

Scn10a encodes for the voltage-gated sodium channel $Na_V1.8$. Its human ortholog was associated with HR regulation and genome-wide association studies suggested it as a modulator of PR interval duration, i.e. atrial conduction time(40). *Lrrc10* and *Lmod2* are associated with dilated cardiomyopathy in both human and mice(41-44); while *Lrrc10* functions in the sarcomeric Z-disc and the T-tubule components, involved in muscle contraction(41), loss of functional *Lmod2* has been linked to short thin filaments and reduction in maximum calcium-activated force production(42). Rodent ventricular cardiomyocytes are converted into spontaneous firing cells (e.g. sinoatrial-node pacemaker cells) by expression of the transcription factor *Tbx18*(45), whereas a polymorphism in *DRD2* has been associated with motor learning and HR(46). Common variants in *RYR1* are associated with left ventricular hypertrophy(47).

Given that i) *Gnb5* has four paralogous genes, with ~50% sequence identity(48, 49), ii) the respective encoded proteins may have redundant function iii) the propagation of the Gnb5-mediated signal is controlled by Regulator of G-protein Signaling (RGS)(13, 14, 50) and iv) Gnb5 and Rgs (i.e. Rgs6, and Rgs7) are co-expressed both at RNA (**Figure S5**) and protein levels(15), we investigated the expression patterns of these two families of genes in our transcriptome profiles to investigate possible compensatory mechanisms. We found significant upregulation of *Gnb3* in ventricles (**Figure 6B**, bottom, p = 5.21E-03) and a trend toward increased expression level in atria (**Figure 6A**, bottom, p = 0.24). The genes encoding the other Gβ subunits, named *Gnb1*, *Gnb2* and *Gnb4* did not change expression (**Figure 6A-B**, bottom). In ventricles, the three R7-Rgs expressed in heart, *Rgs6*, *Rgs7* and *Rgs11*, showed a trend towards increased expression when *Gnb5* was knocked-out (**Figure 6B**, bottom). Only *Rgs6* showed a similar trend in atria (**Figure 6A**, bottom). $Gnb5^{+/-}$ mice showed no or very subtle changes of their transcriptome compared to controls; we unraveled only 6 differentially expressed genes in atria (**Supplementary Table S7**) and 1 in ventricles (**Supplementary Table S8**) beside the engineered *Gnb5*.

We further investigated transcriptome signatures in three brain regions relevant for the IDDCA pathology: the cortex because of its role in higher cognitive function, the hippocampus as it participates to the formation of long-term and spatial memories, and the cerebellum for its motor control and language processing. Cerebellar and hippocampal

anomalies were documented in *Gnb5* knock-out pups(20). Overall, we observed 206 DEGs in cerebellum, 105 in hippocampus and 48 in cerebral cortex (at FDR 5%) (**Supplementary Table S9-S11**). These genes resulted in overrepresentation of GO terms involved in regulation of excitatory postsynaptic membrane potential (GO:0060079), regulation of neurotransmitters secretion (GO:0046928), learning (GO:0007612) and synapse organization (GO:0050808), regulation of inositol 3-phosphate (GO:0014065), regulation of cAMP-mediated signaling (GO:0043951) (in cerebellum, **Supplementary Table S12**); visual perception (GO:0007601), phototransduction (GO:007602), guanylate cyclase activity (GO:0031282), and regulator of signaling receptors (GO:2000272) (in hippocampus, **Supplementary Table S13**); and sensory perception of light stimuli (GO:0050953) and lens development (GO:0002088) (in cortex, **Supplementary Table S14**).

Quantitative RT-PCR and microarray data previously indicated altered expression levels of genes implicated in neuronal development and function, such as *Grid2* (glutamate ionotropic receptor, delta 2) and *Synpo* (Synaptopodin)(20), as well as *Guca1a* and *Guca1b,* calcium-binding protein activating photoreceptor guanylate cyclases*. Guca1a* ($p_{hippocampus}$ = 1.81E-03) and *Guca1b* ($p_{cerebellum}$ = 1.56E-302, $p_{hippocampus}$ = 1.9589E-196, p_{cortex} = 2.209E-178) were DEGs in the brain of *Gnb5* knock-out mice (**Figure S4**). *Synpo* showed a trend of increased expression in the hippocampus (**Figure S4B**, p = 0.55).

A subset of additional differentially expressed genes included *Grin2a* (p = 1.044E-06), *Snca* (p = 7.96E-03), *Gnai2* (p = 7.79E-03), and *Kcnj2* (p = 0.04), in cerebellum (**Figure S4A)**, *Hes5* (p = 0.04) and *Sox6* (p = 0.02) in hippocampus (**Figure S4B**) and *Ntrk3* (p = 9.69E-04) and *Cacna2d4* (p = 0.03) in cortex (**Figure S4C**). The glutamate-gated ion channel Grin2a protein plays important roles in long-term potentiation, and in efficient synaptic transmission. Disruption of this gene is associated with focal epilepsy and speech disorder with or without cognitive disability(51). *Hes5* and *Sox6* genes are respectively a transcriptional repressor and activator, required for the regulation of transition timing of neurogenesis and gliogenesis in mammalian neocortical development(52) and in the normal development of the central nervous system(53). *Cacna2d4* encodes for a calcium channel whose mutations are associated with retinal dysfunction in human(54). The expression of transcripts encoding for different Gβ subunits and R7-RGS genes remained unchanged (**Figure S4 A-B-C,** bottom) suggesting that the brain could be less proficient than the heart in compensating dysregulated pathways.

Discussion

The advent of high-throughput sequencing allowed identifying the cause of hundreds of Mendelian diseases(55) in particular those involving intellectual disability(56). For example data aggregation of exome sequencing uncovered a link between variants in genes encoding the Gβ subunits of the heterotrimeric G-proteins with a group of neuropsychiatric conditions with cardiac manifestations and ophthalmic pathologies(1-4, 6, 8, 57-72). Mutations in *GNB5,* encoding the divergent $G\beta_5$ subunit of the guanine-nucleotide binding protein family, were recently shown to be causative of the autosomal recessive IDDCA syndrome. Differently from $G\beta_{1–4}$, $G\beta_5$ forms irreversible dimer with the G-protein γ-like (GGL) domain(73) present in the R7 regulator group of G-protein signaling proteins (R7 RGS). Dimerization with $G\beta_5$ is absolutely required for the stability of the R7 RGS proteins[16].

Genotype-phenotype correlation showed that carriers of truncating *GNB5* variants present the severe form of this syndrome, while missense alleles are associated with milder phenotypic manifestations. In this work we expanded the number of IDDCA affected individuals and associated variants through identification of two novel causative variants and six novel families. The core symptoms of IDDCA include cognitive disability, epilepsy, retinopathy and cardiac arrhythmia(1-8). These are life-long and life-threatening conditions with five of the six deceased IDDCA individuals suspected to have died from sudden cardiac death. Although the genetic of the syndrome is delineated, the overall molecular mechanism by which perturbations of *GNB5* translates into IDDCA phenotypic manifestations remains unclear. Modeling in zebrafish and cardiomyocytes differentiated from human iPSCs provided initial answers(1, 7), however we thought that the mouse would be a more appropriate tool to investigate consequences of this human syndromic neurodevelopmental condition. As little was known about possible cardiac conduction anomalies in mice, we characterized both the cardiac phenotype and molecular outcome of knocking-out *Gnb5*. *Gnb5*$^{-/-}$ animals were smaller and had smaller ventricles with consequent less volume of blood, but exhibited an increase in fractional shortening and ejection fraction, a sign of compensatory cardiac function: the quantity of blood ejected by the ventricles, as defined by the cardiac output and stroke volume, remained unchanged between *Gnb5*$^{-/-}$ and *Gnb5*$^{+/+}$ mice indicating that *Gnb5*$^{-/-}$ heart has adapted to ensure that it efficiently meets the body's demands for perfusion.

ECG measurements showed that, conversely to IDDCA affected individuals presenting with severe bradycardia at rest, *Gnb5*$^{-/-}$ mice have higher HRs in basal condition, especially during the day, the mice sleeping phase. Zebrafish knocked-out for all *gnb5a* and *gnb5b* copies present in the fish genome, showed a similar trend of increased basal HR(1). It is plausible that these differences are linked to a lower parasympathetic tone in fish and rodents compared to humans. Of note, we showed that the parasympathetic and sympathetic tones of *Gnb5*$^{-/-}$ mice were, respectively, lower and higher than that of controls (**Figure 5E**), thus possibly influencing the basal HR. Whereas we cannot conclude that this higher basal HR is exclusively due to changes in HR regulation as we and others observed an increase in activity of *Gnb5*$^{-/-}$ mice(19, 20) (**Figure S1D**), the zebrafish model showed no sign of hyperactivity(1).

ECG recordings additionally revealed a high number of arrhythmias in knock-out animals, including escape beats, tachycardia/bradycardia episodes and atrioventricular block. These sinus arrhythmias and conduction problems, reminiscent of arrhythmias observed in IDDCA subjects, further corroborate the involvement of *Gnb5* gene in altered cardiac function and irregular heartbeat. Finally, our mice study showed that *Gnb5*-inhibitory signaling is essential for the parasympathetic control of the HR as suggested by previous studies in other models(1, 7). Knockout mice treated with a parasympathomimetic presented with bradycardia, while injection of an anti-parasympathetic drug atropine had the same effect as in wild-type. The β-adrenergic activity of *Gnb5*$^{-/-}$ mice was unaltered, suggesting a normal sympathetic modulation of the cardiac stimulation, and further confirming that the more efficient cardiac function is an adaptation to counteract the reduced size of the *Gnb5*$^{-/-}$ heart.

Consistent with this observation, transcriptome profiling provided insights into modifications of cardiac contraction properties, along with reduced ventricular expression of genes required for development of pacemaker cells. These data further challenge our study, since we cannot unravel whether the transcriptome modifications are cause or consequence of the augmented contractility. We argue, in line with the abovementioned results, that we are possibly investigating a compensatory mechanism. Interestingly, mice lacking *Gnb5* overexpress *Gnb3,* a gene encoding a different Gβ subunit and involved in the activation of GIRK channels(74). Differently from *Gnb1* and *Gnb4* that have a well-documented role in the nervous system(69, 75), *Gnb3*-null mice presented with cardiac

manifestations including slower HRs. However, their isolated hearts responded equivalently to muscarinic receptor- and β-adrenergic receptor-stimulations, thus suggesting that *Gnb3* is unlikely to be involved directly in the G-protein signaling controlling heart pacemaker activity(76). Nonetheless, its higher expression may play a role in coping with the loss of *Gnb5*; further studies are warranted to elucidate such compensatory mechanisms. The expression of *Gnb2* is unchanged in the cardiac tissue of *Gnb5* knock-outs, however it was also linked to heart functions in mouse and human(59, 62) with *Gnb2* knock-out mice having increased HR, and ECG line revealing shortened RR and PQ intervals and ST segment (https://www.mousephenotype.org/data/genes/MGI:95784)(77).

The transcriptome data provided molecular data supporting an increased cardiac function of *Gnb5*$^{-/-}$ mice. It probably results from both a compensatory mechanism as shown by misexpression of genes involved in cardiac muscle contractility, as well as alteration of the expression of genes involved in regulation of the HR. We also documented transcriptional changes in three brain regions of knock-out mice coherent with the IDDCA neuropsychiatric disease spectrum.

HR regulation by the parasympathetic and sympathetic branches of the autonomic nervous system takes place in the pacemaker cells of the sinoatrial node. While sympathetic modulation increases pacemaker cell firing rate, the vagal parasympathetic activity decreases the HR. Both activities are mediated by G-protein coupled signaling on β-adrenergic (sympathetic) and cholinergic M_2 muscarinic (parasympathetic) receptors, respectively. Autonomic innervation is regulated *in vivo* by Regulator of G-protein signaling (RGS) proteins. In particular, in the heart the M_2 receptor signaling is mediated by the Rgs6-Gnb5 complex(15). As *Gnb5* and *Rgs* genes are co-expressed and as the physical association of the encoded proteins is critical for complex stability, we expected to observe reduced *Rgs* expression levels. In a previous report(15), no Rgs6 was detected in the atria and in the brain of *Gnb5* knock-out mice. Surprisingly, we detected a trend of increased expression of *Rgs* subunits, in particular *Rgs6*, contrary to findings in reference (7) where expression of *RGS6* was not different between GNB5-Ser81Leu and wild-type hiPSCs. These discrepancies may stem from the fact that we are investigating different model systems, i.e. mouse tissues *vs.* human cells, as well as by the use of different technologies to detect mRNA abundance, i.e. RNA-sequencing *vs.* qRT-PCR and that in case of hiPSCs data were generated from one clone per genotype.

Altogether our results unveil that potentially compensatory changes occur at transcriptional level in *Gnb5*$^{-/-}$ mice through higher expression of *Gnb3* and *Rgs* genes in heart tissues. Additional evidence at protein level is warranted to corroborate our findings. The above-cited link between *GNB5* and the R7-RGS *RGS6* and *RGS11* suggest that they are part of the same pathway. Consistent with this hypothesis, the members of a Tunisian family presenting with cataract, mental retardation and microcephaly were carriers of bi-allelic mutations in *RGS6(78)*. Another unpublished case harboring mutation in *RGS11* presented with overlapping neuropsychiatric phenotype (Sarah Montgomery, *in litt*). As cardiac symptoms were never investigated in these individuals, this should be recommended. Co-occurrence of neuropsychiatric symptoms with visual and cardiac manifestations could represent a unique combination associated with Gβ and the R7-RGS related proteins. We hypothesize that the disease mechanism responsible for HR perturbations is the reduction or the loss of negative regulation by Rgs6 on the inhibitory $G\beta_5$-signaling, resulting in enhanced parasympathetic activity.

Conclusions

Overall, our work highlights that *Gnb5*$^{-/-}$ mice not only recapitulate IDDCA's neurologic manifestations, but also mimic its cardiac perturbations, allowing for future screening of drugs modulating the parasympathetic branch of the autonomic nervous system, in view of the development of patients' therapy.

Supplementary information

Supplemental data include: 5 figures, 10 tables, Supplemental Note and Appendix.

Figure S1: Unchanged morphological parameters measured by echocardiography.

Figure S2: Pharmacological challenges expressed in raw values.

Figure S3: Samples distance of RNA samples.

Figure S4: Expression profile of relevant genes in cerebellum hippocampus, and cerebral cortex of *Gnb5*$^{-/-}$ vs. *Gnb5*$^{+/+}$ mice.

Figure S5: Co-expression of *Gnb5* and *Rgs* genes in human and mouse.

Table S1: Pathogenicity prediction of the two novel *GNB5* variants

Table S2: Description of the mouse samples used for transcriptome

Table S3: List of Differentially Expressed genes at FDR 5% in *Gnb5*$^{-/-}$ - atria

Table S4: List of Differentially Expressed genes at FDR 5% in *Gnb5*$^{-/-}$ - ventricle

Table S5: List of Biological Processes (BP) at FDR 5% - atria

Table S6: List of Biological Processes (BP) at FDR 5% - ventricle

Table S7: List of Differentially Expressed genes at FDR 5% in *Gnb5*$^{+/-}$ - atria

Table S8: List of Differentially Expressed genes at FDR 5% in *Gnb5*$^{+/-}$ - ventricle

Table S9: List of Differentially Expressed genes at FDR 5% in *Gnb5*$^{-/-}$ - cerebellum

Table S10: List of Differentially Expressed genes at FDR 5% in *Gnb5*$^{-/-}$ - hippocampus

Table S11: List of Differentially Expressed genes at FDR 5% in *Gnb5*$^{-/-}$ - cerebral cortex

Table S12: List of Biological Processes (BP) at FDR 5% - cerebellum

Table S13: List of Biological Processes (BP) at FDR 5% - hippocampus

Table S14: List of Biological Processes (BP) at FDR 5% - cerebral cortex

Supplemental Note: Case Reports

SYNAPS Appendix: Consortia and networks involved in this study

Ethics approval and consent to participate

Maintenance and mouse experimental procedures were approved by institutional and Swiss Federal Veterinary Office (experimental protocol VD3289.c). All affected individuals and their family members were enrolled after signing a written informed consent according to ethical review boards policies.

Consent for publication

All affected individuals and their family members signed a written informed consent to publish.

Availability of data and materials

The RNA-seq data have been deposited in the Gene Expression Omnibus database under accession number XXXXXX.

Competing interests

We declare no competing or financial interests.

Funding

This work was supported by grants from the Swiss National Science Foundation (31003A_182632) and the Jérôme Lejeune Foundation to AR, the MRC (MR/S01165X/1, MR/S005021/1, G0601943), Rosetree Trust, Ataxia UK, MSA Trust, Brain Research UK, Sparks GOSH Charity, Muscular Dystrophy UK (MDUK) and Muscular Dystrophy Association (MDA USA) to HH. The families (O-S) were collected as part of the SYNaPS Study Group collaboration funded by The Wellcome Trust and strategic award (Synaptopathies) funding (WT093205 MA and WT104033AIA). Their assessment was conducted as part of the Queen Square Genomics group at University College London with support from the National Institute for Health Research University College London Hospitals Biomedical Research Centre.

Authors' contributions

P.D.N. and A.R. conceived and directed the study. S.E., A.P., R.M., G.L., N.C., T.S., J.R.A., Z.u.R., F.Z., N.R., F.R., N.A., S.M., V.S., M.C., and H.H. recruited patients, gathered clinical information, prepared samples, performed whole-exome and mutational analysis. P.D.N., A.S. and J.C. carried out the other experiments. N.G. performed structural modeling of GNB5 variants. A.S., T.P., P.D.N. and A.R. designed the mouse experiments. A.S. with the help of P.D.N. conducted the mouse experiments. P.D.N. and A.S. performed statistical analysis and analyzed the data. W.F.S. provided Gnb5 knock-out mouse model. P.D.N. and A.R. wrote the manuscript. All authors reviewed and approved the manuscript.

Acknowledgments

We thank the probands and their families for their participation in this study and Jacques S. Beckmann for comments. We are grateful to the Genomics Technologies Facility of the University of Lausanne and the Transgenic Core Facility of the EPFL.

Appendix

SYNAPS Study Group

Full details are available in the Supplementary information.

Stanislav Groppa, Blagovesta Marinova Karashova, Wolfgang Nachbauer, Sylvia Boesch, Larissa Arning, Dagmar Timmann, Bru Cormand, Belen Pérez-Dueñas, Jatinder S. Goraya,, Tipu Sultan, Jun Mine, Daniela Avdjieva, Hadil Kathom, Radka Tincheva, Selina Banu, Mercedes Pineda-Marfa, Pierangelo Veggiotti, Michel D. Ferrari, Arn M. J. M. van den Maagdenberg, Alberto Verrotti, Giangluigi Marseglia, Salvatore Savasta, Mayte García-Silva, Alfons Macaya Ruiz, Barbara Garavaglia, Eugenia Borgione, Simona Portaro, Benigno Monteagudo Sanchez, Richard Boles, Savvas Papacostas, Michail Vikelis, Eleni Zamba Papanicolaou, Efthymios Dardiotis, Shazia Maqbool, Shahnaz Ibrahim, Salman Kirmani, Nuzhat Noureen Rana, Osama Atawneh, George Koutsis, Salvatore Mangano, Carmela Scuderi, Eugenia Borgione, Giovanna Morello, Tanya Stojkovic, Massimo Zollo, Gali Heimer, Yves A. Dauvilliers, Pasquale Striano, Issam Al-Khawaja, Fuad Al-Mutairi, Hamed Sherifa.

References

1. Lodder EM, De Nittis P, Koopman CD, Wiszniewski W, Moura de Souza CF, Lahrouchi N, et al. GNB5 Mutations Cause an Autosomal-Recessive Multisystem Syndrome with Sinus Bradycardia and Cognitive Disability. Am J Hum Genet. 2016;99(3):786.
2. Shamseldin HE, Masuho I, Alenizi A, Alyamani S, Patil DN, Ibrahim N, et al. GNB5 mutation causes a novel neuropsychiatric disorder featuring attention deficit hyperactivity disorder, severely impaired language development and normal cognition. Genome Biol. 2016;17(1):195.

3. Malerba N, Towner S, Keating K, Squeo GM, Wilson W, Merla G. A NGS-Targeted Autism/ID Panel Reveals Compound Heterozygous GNB5 Variants in a Novel Patient. Front Genet. 2018;9:626.
4. Poke G, King C, Muir A, de Valles-Ibanez G, Germano M, Moura de Souza CF, et al. The epileptology of GNB5 encephalopathy. Epilepsia. 2019;60(11):e121-e7.
5. Shao Z, Tumber A, Maynes J, Tavares E, Kannu P, Heon E, et al. Unique retinal signaling defect in GNB5-related disease. Doc Ophthalmol. 2019.
6. Turkdogan D, Usluer S, Akalin F, Agyuz U, Aslan ES. Familial early infantile epileptic encephalopathy and cardiac conduction disorder: A rare cause of SUDEP in infancy. Seizure. 2017;50:171-2.
7. Veerman CC, Mengarelli I, Koopman CD, Wilders R, van Amersfoorth SC, Bakker D, et al. Genetic variation in GNB5 causes bradycardia by augmenting the cholinergic response via increased acetylcholine-activated potassium current (I-K,I-ACh). Dis Model Mech. 2019;12(7).
8. Vernon H, Cohen J, De Nittis P, Fatemi A, McClellan R, Goldstein A, et al. Intellectual developmental disorder with cardiac arrhythmia syndrome in a child with compound heterozygous GNB5 variants. Clin Genet. 2018;93(6):1254-6.
9. Nini L, Zhang JH, Pandey M, Panicker LM, Simonds WF. Expression of the G beta(5)/R7-RGS protein complex in pituitary and pancreatic islet cells. Endocrine. 2012;42(1):214-7.
10. Sanchez-Blazquez P, Rodriguez-Diaz M, Lopez-Fando A, Rodriguez-Munoz M, Garzon J. The GBeta5 subunit that associates with the R7 subfamily of RGS proteins regulates mu-opioid effects. Neuropharmacology. 2003;45(1):82-95.
11. Sondek J, Siderovski DP. G gamma-like (CG-L) domains: new frontiers in G-protein signaling and beta-propeller scaffolding. Biochem Pharmacol. 2001;61(11):1329-37.
12. Witherow DS, Slepak VZ. A novel kind of G protein heterodimer: The G beta 5-RGS complex. Receptor Channel. 2003;9(3):205-12.
13. Xie KQ, Allen KL, Kourrich S, Colon-Saez J, Thomas MJ, Wickman K, et al. G beta 5 recruits R7 RGS proteins to GIRK channels to regulate the timing of neuronal inhibitory signaling. Nature Neuroscience. 2010;13(6):661-3.
14. Xie KQ, Ge SC, Collins VE, Haynes CL, Renner KJ, Meisel RL, et al. G beta 5-RGS complexes are gatekeepers of hyperactivity involved in control of multiple neurotransmitter systems. Psychopharmacology. 2012;219(3):823-34.

15. Posokhova E, Wydeven N, Allen KL, Wickman K, Martemyanov KA. RGS6/G beta 5 Complex Accelerates I-KACh Gating Kinetics in Atrial Myocytes and Modulates Parasympathetic Regulation of Heart Rate. Circulation Research. 2010;107(11):1350-4.
16. Chen CK, Eversole-Cire P, Zhang H, Mancino V, Chen YJ, He W, et al. Instability of GGL domain-containing RGS proteins in mice lacking the G protein beta-subunit Gbeta5. Proc Natl Acad Sci U S A. 2003;100(11):6604-9.
17. Krispel CM, Chen CK, Simon MI, Burns ME. Prolonged photoresponses and defective adaptation in rods of Gbeta5-/- mice. J Neurosci. 2003;23(18):6965-71.
18. Rao A, Dallman R, Henderson S, Chen CK. G beta 5 is required for normal light responses and morphology of retinal ON-bipolar cells. Journal of Neuroscience. 2007;27(51):14199-204.
19. Wang Q, Levay K, Chanturiya T, Dvoriantchikova G, Anderson KL, Bianco SDC, et al. Targeted deletion of one or two copies of the G protein beta subunit G beta 5 gene has distinct effects on body weight and behavior in mice. Faseb J. 2011;25(11):3949-57.
20. Zhang JH, Pandey M, Seigneur EM, Panicker LM, Koo L, Schwartz OM, et al. Knockout of G protein beta5 impairs brain development and causes multiple neurologic abnormalities in mice. J Neurochem. 2011;119(3):544-54.
21. Mencacci NE, Kamsteeg EJ, Nakashima K, R'Bibo L, Lynch DS, Balint B, et al. De Novo Mutations in PDE10A Cause Childhood-Onset Chorea with Bilateral Striatal Lesions. Am J Hum Genet. 2016;98(4):763-71.
22. Andrews S. FastQC: a quality control tool for high throughput sequence data. . 2010.
23. Truett GE, Heeger P, Mynatt RL, Truett AA, Walker JA, Warman ML. Preparation of PCR-quality mouse genomic DNA with hot sodium hydroxide and tris (HotSHOT). Biotechniques. 2000;29(1):52, 4.
24. Mitchell GF, Jeron A, Koren G. Measurement of heart rate and Q-T interval in the conscious mouse. Am J Physiol. 1998;274(3):H747-51.
25. Martin M. Cutadapt removes adapter sequences from high-throughput sequencing reads. EMBnet Journal. 2011;17(1).
26. Davis MP, van Dongen S, Abreu-Goodger C, Bartonicek N, Enright AJ. Kraken: a set of tools for quality control and analysis of high-throughput sequence data. Methods. 2013;63(1):41-9.
27. Dobin A, Davis CA, Schlesinger F, Drenkow J, Zaleski C, Jha S, et al. STAR: ultrafast universal RNA-seq aligner. Bioinformatics. 2013;29(1):15-21.

28. Anders S, Pyl PT, Huber W. HTSeq--a Python framework to work with high-throughput sequencing data. Bioinformatics. 2015;31(2):166-9.
29. Wang L, Wang S, Li W. RSeQC: quality control of RNA-seq experiments. Bioinformatics. 2012;28(16):2184-5.
30. Li B, Dewey CN. RSEM: accurate transcript quantification from RNA-Seq data with or without a reference genome. BMC Bioinformatics. 2011;12:323.
31. Love MI, Huber W, Anders S. Moderated estimation of fold change and dispersion for RNA-seq data with DESeq2. Genome Biol. 2014;15(12):550.
32. Yu G, Wang LG, Han Y, He QY. clusterProfiler: an R package for comparing biological themes among gene clusters. OMICS. 2012;16(5):284-7.
33. Sobreira N, Schiettecatte F, Boehm C, Valle D, Hamosh A. New tools for Mendelian disease gene identification: PhenoDB variant analysis module; and GeneMatcher, a web-based tool for linking investigators with an interest in the same gene. Hum Mutat. 2015;36(4):425-31.
34. Sobreira N, Schiettecatte F, Valle D, Hamosh A. GeneMatcher: a matching tool for connecting investigators with an interest in the same gene. Hum Mutat. 2015;36(10):928-30.
35. Karczewski KJ, Francioli, L.C., Tiao, G., Cummings, B.B., Alföldi, J., Wang, Q., Collins, R.L., Laricchia, K.M., Ganna, A., Birnbaum, D.P., et al. Variation across 141,456 human exomes and genomes reveals the spectrum of loss-of-function intolerance across human protein-coding genes. bioRxiv. 2019;531210.
36. Cheever ML, Snyder JT, Gershburg S, Siderovski DP, Harden TK, Sondek J. Crystal structure of the multifunctional Gbeta5-RGS9 complex. Nat Struct Mol Biol. 2008;15(2):155-62.
37. Guex N, Peitsch MC. SWISS-MODEL and the Swiss-PdbViewer: An environment for comparative protein modeling. Electrophoresis. 1997;18(15):2714-23.
38. Scott EM, Halees A, Itan Y, Spencer EG, He Y, Azab MA, et al. Characterization of Greater Middle Eastern genetic variation for enhanced disease gene discovery. Nat Genet. 2016;48(9):1071-6.
39. Witten DM. Classification and Clustering of Sequencing Data Using a Poisson Model. Ann Appl Stat. 2011;5(4):2493-518.
40. Chambers JC, Zhao J, Terracciano CMN, Bezzina CR, Zhang WH, Kaba R, et al. Genetic variation in SCN10A influences cardiac conduction. Nature Genetics. 2010;42(2):149-U80.

41. Brody MJ, Lee Y. The Role of Leucine-Rich Repeat Containing Protein 10 (LRRC10) in Dilated Cardiomyopathy. Front Physiol. 2016;7:337.
42. Pappas CT, Mayfield RM, Henderson C, Jamilpour N, Cover C, Hernandez Z, et al. Knockout of Lmod2 results in shorter thin filaments followed by dilated cardiomyopathy and juvenile lethality. Proc Natl Acad Sci U S A. 2015;112(44):13573-8.
43. Brody MJ, Hacker TA, Patel JR, Feng L, Sadoshima J, Tevosian SG, et al. Ablation of the cardiac-specific gene leucine-rich repeat containing 10 (Lrrc10) results in dilated cardiomyopathy. PLoS One. 2012;7(12):e51621.
44. Ahrens-Nicklas RC, Pappas CT, Farman GP, Mayfield RM, Larrinaga TM, Medne L, et al. Disruption of cardiac thin filament assembly arising from a mutation in LMOD2: A novel mechanism of neonatal dilated cardiomyopathy. Sci Adv. 2019;5(9):eaax2066.
45. Kapoor N, Liang W, Marban E, Cho HC. Direct conversion of quiescent cardiomyocytes to pacemaker cells by expression of Tbx18. Nat Biotechnol. 2013;31(1):54-62.
46. Huertas E, Buhler KM, Echeverry-Alzate V, Gimenez T, Lopez-Moreno JA. C957T polymorphism of the dopamine D2 receptor gene is associated with motor learning and heart rate. Genes Brain Behav. 2012;11(6):677-83.
47. Hong KW, Shin DJ, Lee SH, Son NH, Go MJ, Lim JE, et al. Common variants in RYR1 are associated with left ventricular hypertrophy assessed by electrocardiogram. Eur Heart J. 2012;33(10):1250-6.
48. Watson AJ, Aragay AM, Slepak VZ, Simon MI. A novel form of the G protein beta subunit Gbeta5 is specifically expressed in the vertebrate retina. J Biol Chem. 1996;271(45):28154-60.
49. Watson AJ, Katz A, Simon MI. A fifth member of the mammalian G-protein beta-subunit family. Expression in brain and activation of the beta 2 isotype of phospholipase C. J Biol Chem. 1994;269(35):22150-6.
50. Xie KQ, Masuho I, Brand C, Dessauer CW, Martemyanov KA. The Complex of G Protein Regulator RGS9-2 and G beta(5) Controls Sensitization and Signaling Kinetics of Type 5 Adenylyl Cyclase in the Striatum. Sci Signal. 2012;5(239).
51. Strehlow V, Heyne HO, Vlaskamp DRM, Marwick KFM, Rudolf G, de Bellescize J, et al. GRIN2A-related disorders: genotype and functional consequence predict phenotype. Brain. 2019;142(1):80-92.

52. Bansod S, Kageyama R, Ohtsuka T. Hes5 regulates the transition timing of neurogenesis and gliogenesis in mammalian neocortical development. Development. 2017;144(17):3156-67.
53. Lee KE, Seo J, Shin J, Ji EH, Roh J, Kim JY, et al. Positive feedback loop between Sox2 and Sox6 inhibits neuronal differentiation in the developing central nervous system. Proc Natl Acad Sci U S A. 2014;111(7):2794-9.
54. Wycisk KA, Zeitz C, Feil S, Wittmer M, Forster U, Neidhardt J, et al. Mutation in the auxiliary calcium-channel subunit CACNA2D4 causes autosomal recessive cone dystrophy. Am J Hum Genet. 2006;79(5):973-7.
55. Bamshad MJ, Nickerson DA, Chong JX. Mendelian Gene Discovery: Fast and Furious with No End in Sight. Am J Hum Genet. 2019;105(3):448-55.
56. Vissers LE, Gilissen C, Veltman JA. Genetic studies in intellectual disability and related disorders. Nat Rev Genet. 2016;17(1):9-18.
57. Arno G, Holder GE, Chakarova C, Kohl S, Pontikos N, Fiorentino A, et al. Recessive Retinopathy Consequent on Mutant G-Protein beta Subunit 3 (GNB3). JAMA Ophthalmol. 2016;134(8):924-7.
58. Endo W, Ikemoto S, Togashi N, Miyabayashi T, Nakajima E, Hamano SI, et al. Phenotype-genotype correlations in patients with GNB1 gene variants, including the first three reported Japanese patients to exhibit spastic diplegia, dyskinetic quadriplegia, and infantile spasms. Brain Dev. 2019.
59. Fukuda T, Hiraide T, Yamoto K, Nakashima M, Kawai T, Yanagi K, et al. Exome reports A de novo GNB2 variant associated with global developmental delay, intellectual disability, and dysmorphic features. Eur J Med Genet. 2019:103804.
60. Hemati P, Revah-Politi A, Bassan H, Petrovski S, Bilancia CG, Ramsey K, et al. Refining the phenotype associated with GNB1 mutations: Clinical data on 18 newly identified patients and review of the literature. Am J Med Genet A. 2018;176(11):2259-75.
61. Jones HF, Morales-Briceno H, Barwick K, Lewis J, Sanchis-Juan A, Raymond FL, et al. Myoclonus-dystonia caused by GNB1 mutation responsive to deep brain stimulation. Mov Disord. 2019;34(7):1079-80.
62. Kuss J, Stallmeyer B, Goldstein M, Rinne S, Pees C, Zumhagen S, et al. Familial Sinus Node Disease Caused by a Gain of GIRK (G-Protein Activated Inwardly Rectifying K(+) Channel) Channel Function. Circ Genom Precis Med. 2019;12(1):e002238.

63. Lassuthova P, Safka Brozkova D, Neupauerova J, Krutova M, Mazanec R, Seeman P. Confirmation of the GNB4 gene as causal for Charcot-Marie-Tooth disease by a novel de novo mutation in a Czech patient. Neuromuscul Disord. 2017;27(1):57-60.
64. Lohmann K, Masuho I, Patil DN, Baumann H, Hebert E, Steinrucke S, et al. Novel GNB1 mutations disrupt assembly and function of G protein heterotrimers and cause global developmental delay in humans. Hum Mol Genet. 2017;26(6):1078-86.
65. Malerba N, De Nittis P, Merla G. The Emerging Role of Gbeta Subunits in Human Genetic Diseases. Cells. 2019;8(12).
66. Miura S, Morikawa T, Fujioka R, Noda K, Kosaka K, Taniwaki T, et al. A novel missense variant (Gln220Arg) of GNB4 encoding guanine nucleotide-binding protein, subunit beta-4 in a Japanese family with autosomal dominant motor and sensory neuropathy. Eur J Med Genet. 2017;60(9):474-8.
67. Peng J, Wang Y, He F, Chen C, Wu LW, Yang LF, et al. Novel West syndrome candidate genes in a Chinese cohort. CNS Neurosci Ther. 2018;24(12):1196-206.
68. Petrovski S, Kury S, Myers CT, Anyane-Yeboa K, Cogne B, Bialer M, et al. Germline De Novo Mutations in GNB1 Cause Severe Neurodevelopmental Disability, Hypotonia, and Seizures. Am J Hum Genet. 2016;98(5):1001-10.
69. Soong BW, Huang YH, Tsai PC, Huang CC, Pan HC, Lu YC, et al. Exome sequencing identifies GNB4 mutations as a cause of dominant intermediate Charcot-Marie-Tooth disease. Am J Hum Genet. 2013;92(3):422-30.
70. Steinrucke S, Lohmann K, Domingo A, Rolfs A, Baumer T, Spiegler J, et al. Novel GNB1 missense mutation in a patient with generalized dystonia, hypotonia, and intellectual disability. Neurol Genet. 2016;2(5):e106.
71. Szczaluba K, Biernacka A, Szymanska K, Gasperowicz P, Kosinska J, Rydzanicz M, et al. Novel GNB1 de novo mutation in a patient with neurodevelopmental disorder and cutaneous mastocytosis: Clinical report and literature review. Eur J Med Genet. 2018;61(3):157-60.
72. Vincent A, Audo I, Tavares E, Maynes JT, Tumber A, Wright T, et al. Biallelic Mutations in GNB3 Cause a Unique Form of Autosomal-Recessive Congenital Stationary Night Blindness. Am J Hum Genet. 2016;98(5):1011-9.
73. Patil DN, Rangarajan ES, Novick SJ, Pascal BD, Kojetin DJ, Griffin PR, et al. Structural organization of a major neuronal G protein regulator, the RGS7-Gbeta5-R7BP complex. Elife. 2018;7.

74. Lei Q, Jones MB, Talley EM, Garrison JC, Bayliss DA. Molecular mechanisms mediating inhibition of G protein-coupled inwardly-rectifying K+ channels. Mol Cells. 2003;15(1):1-9.
75. Okae H, Iwakura Y. Neural tube defects and impaired neural progenitor cell proliferation in Gbeta1-deficient mice. Dev Dyn. 2010;239(4):1089-101.
76. Ye YC, Sun ZZ, Guo A, Song LS, Grobe JL, Chen SH. Ablation of the GNB3 gene in mice does not affect body weight, metabolism or blood pressure, but causes bradycardia. Cellular Signalling. 2014;26(11):2514-20.
77. Dickinson ME, Flenniken AM, Ji X, Teboul L, Wong MD, White JK, et al. High-throughput discovery of novel developmental phenotypes. Nature. 2016;537(7621):508-+.
78. Chograni M, Alkuraya FS, Maazoul F, Lariani I, Chaabouni-Bouhamed H. RGS6: a novel gene associated with congenital cataract, mental retardation, and microcephaly in a Tunisian family. Invest Ophthalmol Vis Sci. 2014;56(2):1261-6.

Web links and URLs

GnomAD: https://gnomad.broadinstitute.org/about

IMPC: http://www.mousephenotype.org/MutationTaster2: http://www.mutationtaster.org/

PolyPhen-2:http://genetics.bwh.harvard.edu/pph2/index.shtml

PROVEAN: http://provean.jcvi.org/index.phpSIFT: http://sift.jcvi.org/

UMD Predictor: http://umd-predictor.eu/

Functional Analysis through Hidden Markov Models (v2.3):

http://fathmm.biocompute.org.uk/

Splice Site Prediction by Neural Network (NNSplice):

https://www.fruitfly.org/seq_tools/splice.html

NetGene2 server**:** http://www.cbs.dtu.dk/services/NetGene2/

Human Splicing Finder: http://www.umd.be/HSF/

CADD: https://cadd.gs.washington.edu/

Greater Middle East Variome Project: http://igm.ucsd.edu/gme/

Figure legends

Figure 1. IDDCA pedigrees and mutational spectrum. (**A**) Pedigrees of the six consanguineous families described in this study; affected individuals carry homozygous

GNB5 variants inherited from heterozygous parents. Filled symbols represent individuals with severe sinus node dysfunction (top left quarter), intellectual disability (ID, top right quarter), seizures (bottom right quarter) and hypotonia (bottom left quarter). The light grey top quarter indicates the occurrence of mild ID. The affected individuals of families Q and T harbor novel variants which are modeled in panel B. The variants of IDDCA affected individuals are displayed in red (LoF), whereas missense LADCI variants are in blue. (**B, left**) Top view of the GNB5 (orange, pdb entry 2pbi) 3D protein model, showing the mutated Trp81 (yellow) and the glycerol molecule (green) in the center of the pore. The rearrangements necessary to accommodate a Tryptophan residue at position 81 will change the channel characteristics. The rotamer displayed here highlights clashes of Trp81 with Cys68 (white) and Cys111 (magenta). In additional rotamers, the bulky Tryptophan sidechain will severely bump into Leu67 (grey), Val87 (pink), Val108 (cyan), and Ala110 (brown). (**B, right**) As shown in this view of the beta propeller from above, the "wild-type" Gly215 (not shown) lays in a beta-sheet, with on top Ala221 (pink), at the bottom Cys200 (magenta), and in front a beta-strand harboring Val242 (grey) and Val245 (cyan). The presence of Glu215 cannot be tolerated, as it will encroach into one of the residues previously enumerated. Another rotamer shows clashes into Val245 (cyan). Overall, all rotamers may also force the sidechain of Cys200 (magenta) to reorient itself toward the internal part of the channel to provide space to accommodate Glutamine at position 215 (yellow). In this position the Cys200 sidechain will occupy the space dedicated to the glycerol (green), thus changing the properties of the channel. (**C**) Distribution of the IDDCA published and novel variants along the schematically represented 11 exons of the human *GNB5* gene (transcript NM_006578.3; Ensembl (release 98, September 2019). The variants are color coded like in panel A. The yellow star marks the variant of Middle-Eastern descent, while green stars indicate the amber and ochre variants from the Indian subcontinent (dark green) and of Pakistani descent (light green), respectively.

Figure 2. *Gnb5* mouse line features. **(A)** Mouse mating strategy and gender and genotype distribution over 3 successive generations. Pre- and post-weaning mortality is reported for each colony. (**B**) Size of $Gnb5^{+/+}$ and $Gnb5^{-/-}$ mice. (**C-D**) Body weights profile monitored from 3 to 46 weeks of age. All mice were weaned on week 3. Data are shown as mean ± SD. C and D panels separate body weights according to sex. $Gnb5^{+/+}$ are depicted in grey, $Gnb5^{+/-}$ in

blue and *Gnb5*$^{-/-}$ in red. (**E**) At sacrifice, neither significant morphology difference nor thoracic position of the heart were observed among groups. (**F**) Bar plot showing that *Gnb5*$^{-/-}$ hearts (red, n = 16) are smaller compared to the other genotypes (*Gnb5*$^{+/-}$, blue (n = 8) and *Gnb5*$^{+/+}$, grey (n = 16)). Data are shown as mean of the ratio between heart weight and tibia length (used to normalize for animal size) ± SEM.

Figure 3. **Morphological and functional parameters measured by ultrasound scan in *Gnb5*$^{+/+}$, *Gnb5*$^{+/-}$, and *Gnb5*$^{-/-}$ mice**. (**A**) Left Ventricular Internal Diameter at diastole (left) and systole (right). (**B**) Left ventricular volume in diastole (left) and systole (right). (**C**) Mass of the left ventricle. (**D-G**) Cardiac function expressed as fractional shortening (D), ejection fraction (E), cardiac output (F) and stroke volume (G). Parameters unchanged between the three genotypes are shown in **Figure S1A-B**.

Figure 4. **Cardiac arrhythmias recorded in *Gnb5* mouse line**. (**A**) Normal ECG line recorded in wild-type mice with the main spikes specified as used in the text. (**B-C**) ECG line showing escape atrial beats classified as short (B) and long (C) and characterized by the occurrence of a late P-wave (red arrow). (**D**) ECG line demonstrating atrioventricular blocks, with more than one P-wave per QRS complex (consecutive red arrows). (**E-G**) Respective box-plots indicating the number of arrhythmias, i.e. number of short (E) and long (F) escape atrial beats and atrioventricular blocks (G) per 24 hours.

Figure 5. **Pharmacological administration of compounds mimicking parasympathetic and sympathetic stimulation**. (**A**) Heart rate monitoring after injection of Atropin (i.p. 1mg/kg). (**B**) Bradycardia measured in response to Carbachol (i.p. 0.1m/kg). (**C**) Heart rate variation in response to Atenolol (i.p. 2mg/kg). (**D**) Increased heart rate after Isoprenaline administration (i.p. 4mg/kg). Data points are expressed as percentage of the baseline values. (**E**) Smaller parasympathetic and bigger sympathetic blockade in *Gnb5*$^{-/-}$ mice (red), compared to wild-type littermates (black), indicative of a lower parasympathetic and a higher sympathetic tone in basal conditions.

Figure 6. **Comparison of transcriptome profiles of Atria and ventricles in *Gnb5*$^{+/+}$, *Gnb5*$^{+/-}$, and *Gnb5*$^{-/-}$ mice**. (**A**) Atrial expression profiles of *Gnb5* (top, left) and other differentially

expressed genes (top lane); *Gnb* and *Rgs* transcripts quantification in atria (bottom lane). (**B**) Ventricular expression profiles of *Gnb5* gene (top, left) and other differentially expressed genes (top lane); *Gnb* and *Rgs* transcripts quantification in ventricles (bottom).

Supplemental note: Case Reports

Family O

Family O (**Figure 1A, Table 1**) is a Pakistani trio from Lahore. The proband is an 8-month-old boy born from healthy consanguineous parents and with a healthy female sibling. He presented with global developmental delay characterized by intellectual disability (ID), severe hypotonia, and altered speech development. Physical examination of this child revealed stridor, dysmorphism and failure to thrive. The child has passed away in the last months. Cardiologic assessment was not performed prior.

Family P

Family P (**Figure 1A, Table 1**) is a consanguineous Pakistani family from the Multan region with one affected 15-year-old boy who showed global developmental delay and flexor spasm seizures, kept under control with the administration of Valproic Acid. He was non-verbal and presented impaired verbal understanding too. He was hypotonic with no head control. He was thin, and showed nystagmus and gastric reflux.

EEG demonstrated modified hypsarrhythmia. MRI revealed hypogenesis of the corpus callosum. He experienced episodes of breath holding spell.

Family Q

Family Q (**Figure 1A, Table 1**) is a consanguineous Pakistani family from Lahore with two affected daughters. The older sister likely died of cardiac arrest. The younger sister is the proband. At 1.2-year of age, she showed global developmental delay, ID, nystagmus and no neck holding. She did not reach developmental milestones regarding lexical production and verbal understanding. Holter monitoring revealed signs of sick sinus syndrome, with severe bradycardia at rest and prolonged sinus pauses.

Family R

Family R (**Figure 1A, Table 1**) is a consanguineous Pakistani trio family from Lahore with an affected 1 year-old female child. Of the main IDDCA characteristics, the proband displayed ID, inability to hold her neck, and lack of eye contact. She also presented with Fatty Acid Oxidation disorder. MRI showed cerebral atrophy. Dysmorphic features of this individual

included prominent philtral ridges, micrognathia, prominent ears and craniofacial disproportion.

Family S

Family S (**Figure 1A, Table 1**) is a consanguineous Pakistani trio family from Lahore with an affected male child showing severe ID, developmental delay, hypotonia and seizures, kept under control with the administration of Epictam. He had no eye contact, no social smile and did not respond to his name. He presented with nystagmus and some dysmoprhic features (blond hair, frontal bossing, epicanthic folds, small palpebral fissure, depressed nasal bridge, high arched palate). Urinary organic acid and plasma amino acids were normal. Holter monitoring revealed a sinus rhythm with insignificant (<3 sec) sinus pauses.

Family T

Family T (**Figure 1A, Table 1**) is a Tunisian family with one non-dysmorphic affected child and two healthy siblings born to consanguineous parents who are first cousins. The affected 7-year old girl was born at term and weighed 2.9 kg (with a body height of 49 cm, and head circumference of 35 cm). She was delayed in her early developmental milestones and first walked at 31 months; she remains nonverbal with mild intellectual disability (a formal neuropsychological assessment was not performed). Growth parameters at evaluation (5 yo) include height and weight at 2 SD and head circumference at 3 SD. Neurologically, she demonstrated impaired fine motor skills. Both MRI and EEG failed to show anything abnormal. Electrocardiographic monitoring showed sinus-node dysfunction with sinus bradycardia, and prolonged sinus pauses.

At 21 months, she experienced an unexplained coma after a septic shock subsequent to a digestive tract infection. She also had an episode of pyelonephritis, concluded without complications. She had shorter thumbs, but no history of eye disease, nor gastric problems. Metabolic screening reported plasma amino acids imbalances with higher phenylalanine concentrations. Currently, her fine movements progressed with re-education, and she developed sign language; she is enrolled in a special education class.

Family history revealed a non-verbal paternal uncle with severe cognitive impairment with no diagnosis. Additionally, a maternal aunt, a maternal uncle and the son of another

maternal aunt presented with severe neurodevelopmental problems, including speech impairment.

Consortia and networks involved in this study

The Synaptopathies and Paroxysmal Syndromes (SYNaPS) Study Group (http://neurogenetics.co.uk/synaptopathies-synaps/)

Study Group Members:

Prof Stanislav Groppa

Affiliation: Department of Neurology and Neurosurgery, Institute of Emergency Medicine, Chisinau, Republic of Moldova.

Email: sgroppa@gmail.com

Dr. Blagovesta Marinova Karashova

Affiliation: Department of Paediatrics, Medical University of Sofia, Sofia 1431, Bulgaria

Email: blagovestakarashova@gmail.com

Dr. Wolfgang Nachbauer

Affiliation: Department of Neurology, Medical University Innsbruck, Anichstrasse 35, Innsbruck 6020, Austria

Email: Wolfgang.Nachbauer@i-med.ac.at

Prof. Sylvia Boesch

Affiliation: Department of Neurology, Medical University Innsbruck, Anichstrasse 35, Innsbruck 6020, Austria

Email: sylvia.boesch@i-med.ac.at

Dr. Larissa Arning

Affiliation: Department of Human Genetics, Ruhr-University Bochum, Bochum 44801, Germany

Email: Larissa.Arning@ruhr-uni-bochum.de

Prof. Dagmar Timmann

Affiliation: Braun Neurologische Universitätsklinik Universität Essen, Hufelandstr 55, Essen D-45122, Germany

Email: Dagmar.Timmann-Braun@uni-duisburg-essen.de

Prof. Bru Cormand

Affiliation: Department of Genetics, Universitat de Barcelona, Barcelona 08007, Spain

Email: bcormand@ub.edu

Dr. Belen Pérez-Dueñas

Affiliation: Hospital Sant Joan de Deu, Esplugues de Llobregat 08950, Barcelona, Spain

Email: bperez@sjdhospitalbarcelona.org

Dr Gabriella Di Rosa, MD, PhD

Affiliation: Department of Pediatrics, University of Messina, Messina 98123, Italy

Email: gdirosa@unime.it

Prof. Jatinder S. Goraya, MD, FRCP

Affiliation: Division of Paediatric Neurology, Dayanand Medical College & Hospital, Ludhiana, Punjab 141001, India

Email: gorayajs@gmail.com

Prof. Tipu Sultan

Affiliation: Division of Paediatric Neurology, Children's Hospital of Lahore, Lahore 381-D/2, Pakistan

Email: tipusultanmalik@hotmail.com

Prof Jun Mine

Affiliation: Department of Paediatrics, Shimane University, Faculty of Medicine, Izumo, 693-8501, Japan

Email: jmine@med.shimane-u.ac.jp

Prof. Daniela Avdjieva,
Affiliation: Department of Paediatrics, Medical University of Sofia, Sofia 1431, Bulgaria
Email: davdjieva@yahoo.com

Dr. Hadil Kathom,
Affiliation: Department of Pediatrics, Medical University of Sofia, Sofia 1431, Bulgaria
Email: hadilmk@gmail.com

Prof.Dr Radka Tincheva
Affiliation: Head of Department of Clinical Genetics, University Pediatric Hospital, Sofia 1431, Bulgaria
Email: radka.tincheva@gmail.com

Prof. Selina Banu
Affiliation: Neurosciences Unit, Institute of Child Health and Shishu Shastho Foundation Hospital, Mirpur, Dhaka 1216, Bangladesh
Email: selinabanu17@gmail.com

Prof. Mercedes Pineda-Marfa
Affiliation Servei de Neurologia Pediàtrica, l'Hospital Universitari Vall d'Hebron, Barcelona 08035, Spain
Email: pineda@hsjdbcn.org

Prof. Pierangelo Veggiotti
Affiliation: Unit of Infantile Neuropsychiatry Fondazione
Istituto Neurologico "C. Mondino" IRCCS, Via Mondino 2, Pavia 27100, Italy
Email: pierangelo.veggiotti@unipv.it

Prof. Michel D. Ferrari
Affiliation: Leiden University Medical Center, Albinusdreef 2, Leiden 2333, Netherlands
Email: M.D.Ferrari@lumc.nl

Prof. Alberto Verrotti
Affiliation: University of L'Aquila, L'Aquila, Italy
Email: verrottidipianella@univaq.it

Prof Giangluigi Marseglia
Affiliation: Department of Pediatrics, University of Pavia, IRCCS Policlinico "San Matteo", Pavia 27100, Italy
Email: gl.marseglia@smatteo.pv.it

Dr. Salvatore Savasta
Affiliation: Division of Pediatric Neurology, Department of Pediatrics, University of Pavia, IRCCS Policlinico "San Matteo", Pavia 27100, Italy
Email: S.Savasta@smatteo.pv.it

Dr. Mayte García-Silva
Affiliation: Hospital Universitario 12 de Octubre, Madrid 28041, Spain
Email: mgarciasilva@salud.madrid.org

Dr. Alfons Macaya Ruiz
Affiliation: University Hospital Vall d'Hebron, Barcelona 08035, Spain
Email: amacaya@vhebron.net

Prof. Barbara Garavaglia
Affiliation: IRCCS Foundation, Neurological Institute "Carlo Besta", Molecular Neurogenetics, 20126 Milan, Italy
Email: segr.neurogenetica@istituto-besta.it

Dr. Eugenia Borgione
Affiliation: Laboratorio di Neuropatologia Clinica, U.O.S. Malattie, Neuromuscolari Associazione OASI Maria SS. ONLUS – IRCCS, Via Conte Ruggero 73, 94018 Troina, Italy
Email: eborgione@oasi.en.it

Dr. Simona Portaro

Affiliation: IRCCS Centro Neurolesi "Bonino Pulejo", SS113, c.da Casazza, 98124 Messina, Italy

Email: simonaportaro@hotmail.it

Dr. Benigno Monteagudo Sanchez

Affiliation: Hospital Arquitecto Marcide, Avenida de la Residencia S/N, Ferrol (A Coruña), 15401 Spain

Email: benims@hotmail.com

Dr. Richard Boles

Affiliation: Courtagen Life Sciences, 12 Gill Street Suite 3700, Woburn, MA 01801 USA

Email: Richard.Boles@courtagen.com

Prof. Savvas Papacostas

Affiliation: Neurology Clinic B, The Cyprus Institute of Neurology and Genetics, 6 International Airport Road, 1683 Nicosia, Cyprus

Email: savvas@cing.ac.cy

Dr. Michail Vikelis

Affiliation: Iatreio Kefalalgias Glyfadas, 8 Lazaraki str, 3rd floor, 16675, Athens, Greece

Email: mvikelis@headaches.gr

Prof Eleni Zamba Papanicolaou

Affiliation: The Cyprus Institute of Neurology & Genetics, Nicosia, Cyprus

Email: ezamba@cing.ac.cy

Dr Efthymios Dardiotis

Affiliation: UNIVERSITY HOSPITAL OF LARISSA, NEUROLOGY Department, Greece

Email: edar@med.uth.gr

Prof Shazia Maqbool

Affiliation: Department of Developmental and Behavioral Pediatrics, CH&ICH, Lahore, Pakistan
Email: drshazimaq@yahoo.com

Prof Shahnaz Ibrahim
Affiliation: Department of Pediatrics and child health, Aga Khan University, Karachi, Pakistan
Email: shahnaz.ibrahim@aku.edu

Prof Salman Kirmani
Affiliation: Department of Paediatrics & Child Health, The Aga Khan University, Karachi , Pakistan
Email: salman.kirmani@aku.edu

Dr. Nuzhat Noureen Rana
Affiliation: Department of Paediatric Neurology, Children Hospital Complex and ICH, Multan, Pakistan
Email: drnuzhatrana@gmail.com

Dr. Osama Atawneh
Affiliation: Hilal Pediatric Hospital Hebron, Hebron West Bank, Palestine
Email: osamaat@gmail.com

Prof George Koutsis
Dr Marianthi Breza
Affiliation: Neurogenetics Unit, Neurology Department, Eginition Hospital, National and Kapodistrian University, Athens, Greece
Email: marianthibr@med.uoa.gr

Prof Salvatore Mangano
Affiliation: Unità di Neuropsichiatria Infantile, AOUP "P.Giaccone" Palermo, Italy
Email: salvatore.mangano@unipa.it

Dr Carmela Scuderi

Affiliation: Associazione Oasi Maria SS, 94018 Troina, Italy

Email: cscuderi@oasi.en.it

Dr Eugenia Borgione

Affiliation: Associazione Oasi Maria SS, 94018 Troina, Italy

Email: eborgione@oasi.en.it

Dr Giovanna Morello

Affiliation: Institute of Neurological Sciences, National Research Council, Mangone, Italy

Email: g.morello@isn.cnr.it

Dr Tanya Stojkovic

Affiliation: Institute of Myology, Hôpital La Pitié Salpêtrière, Paris, France

Email: stojkovic.tanya@aphp.fr

Prof Massimi Zollo

Affiliation: CEINGE, Biotecnologie Avanzate S.c.a.rl., Naples, Italy

Email: massimo.zollo@unina.it

Dr Gali Heimer

Affiliation: University Hospital of Tel Aviv, Tel Aviv, Israel

Email: galih.md@gmail.com

Prof Yves A. Dauvilliers

Affiliation: University Hospital Montpellier, Montpellier, France

Email: ydauvilliers@yahoo.fr

Prof Pasquale Striano

Affiliation: Institute “Giannina Gaslini”, Genova, Italy

Email: strianop@gmail.com

Dr Issam Al-Khawaja

Affiliation: Albashir University Hospital, Amman, Jordan

Email: isamkhawaja61@gmail.com

Dr Fuad Al-Mutairi

Affiliation: King Saud University, Riyadh, Saudi Arabia

Email: almutairifu@NGHA.MED.SA

Prof Hamed Sherifa

Affiliation: Assiut University Hospital, Assiut, Egypt

Email: hamed_sherifa@yahoo.com

Figure 1

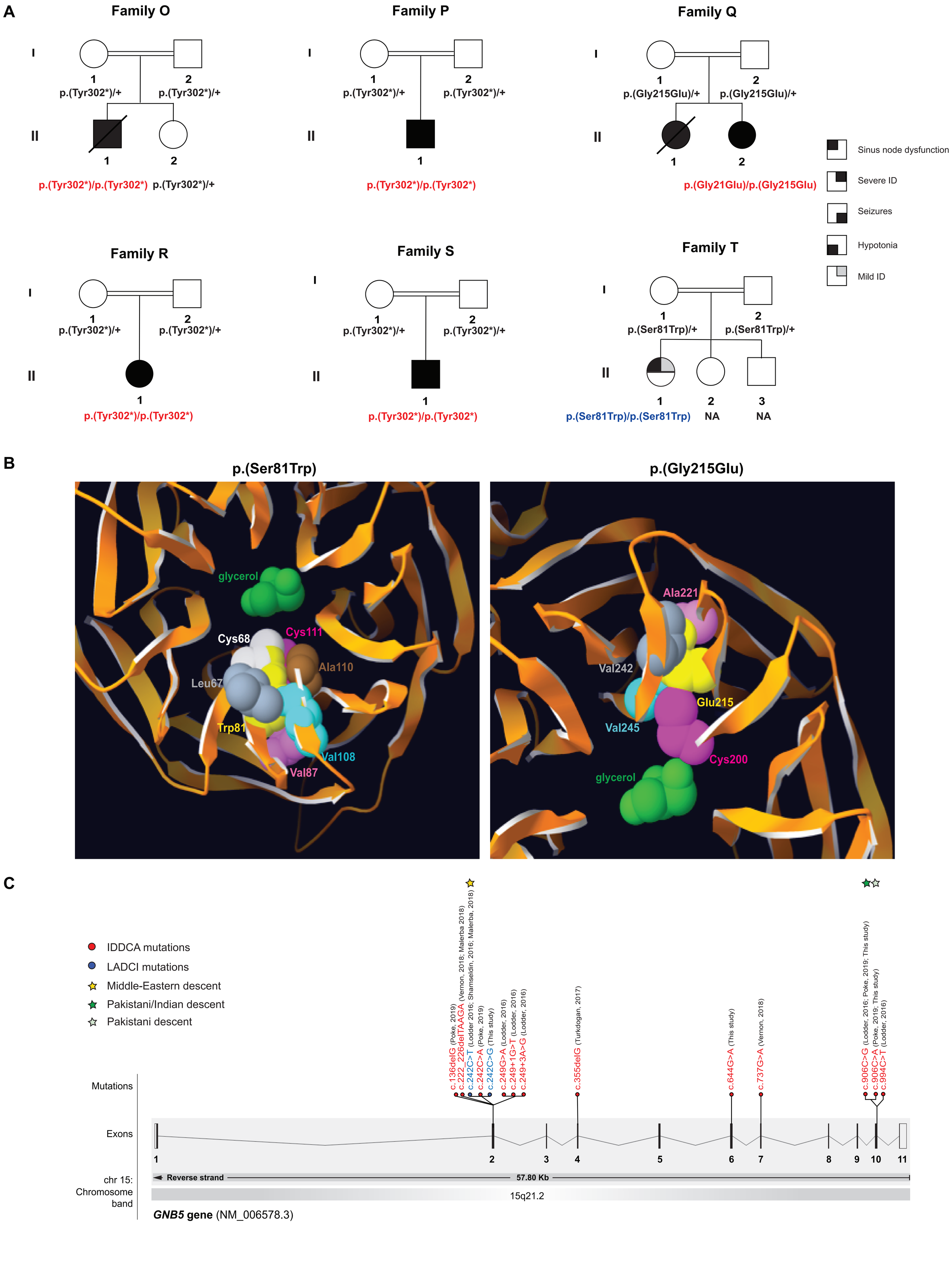
A
Family O
I
1
p.(Tyr302*)/+
2
p.(Tyr302*)/+
II
1
2
p.(Tyr302*)/p.(Tyr302*)
p.(Tyr302*)/+
Family P
I
1
p.(Tyr302*)/+
2
p.(Tyr302*)/+
II
1
p.(Tyr302*)/p.(Tyr302*)
Family Q
I
1
p.(Gly215Glu)/+
2
p.(Gly215Glu)/+
II
1
2
p.(Gly21Glu)/p.(Gly215Glu)
Sinus node dysfunction
Severe ID
Seizures
Hypotonia
Mild ID
Family R
I
1
p.(Tyr302*)/+
2
p.(Tyr302*)/+
II
1
p.(Tyr302*)/p.(Tyr302*)
Family S
I
1
p.(Tyr302*)/+
2
p.(Tyr302*)/+
II
1
p.(Tyr302*)/p.(Tyr302*)
Family T
I
1
p.(Ser81Trp)/+
2
p.(Ser81Trp)/+
II
1
2
3
p.(Ser81Trp)/p.(Ser81Trp)
NA
NA
B
p.(Ser81Trp)
glycerol
Cys68
Cys111
Ala110
Leu67
Trp81
Val108
Val87
p.(Gly215Glu)
Ala221
Val242
Glu215
Val245
Cys200
glycerol
C
IDDCA mutations
LADCI mutations
Middle-Eastern descent
Pakistani/Indian descent
Pakistani descent
c.136delG (Poke, 2019)
c.222_226delTAAGA (Vernon, 2018; Ma
c.242C>T (Lodder 2016; Shamseldin, 2016
c.242C>A (Poke, 2019)
c.242C>G (This study)
c.249G>A (Lodder, 2016)
c.249+1G>T (Lodder, 2016)
c.249+3A>G (Lodder, 2016)
c.355delG (Turkdogan, 2017)
c.644G>A (This study)
c.737G>A (Vernon, 2018)
c.906C>G (Lodder, 2016; Poke, 2019; This
c.906C>A (Poke, 2019; This study)
c.994C>T (Lodder, 2016)
Mutations
Exons
1
2
3
4
5
6
7
8
9
10
11
chr 15:
Reverse strand
57.80 Kb
Chromosome band
15q21.2
GNB5 gene (NM_006578.3)

Figure 2

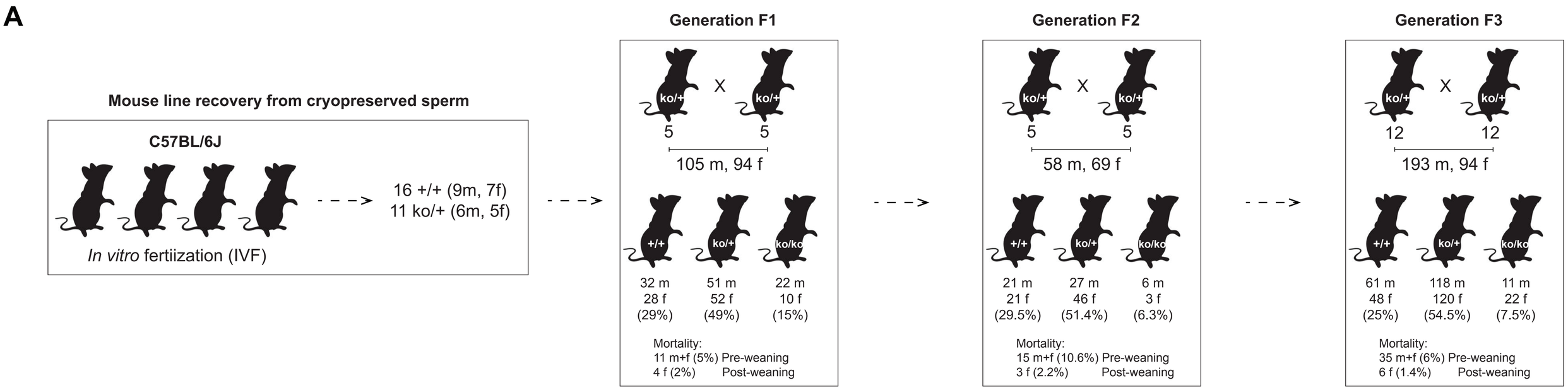
A
Mouse line recovery from cryopreserved sperm
C57BL/6J
16 +/+ (9m, 7f)
11 ko/+ (6m, 5f)
In vitro fertiization (IVF)
Generation F1
ko/+ X ko/+
5 5
105 m, 94 f
+/+ ko/+ ko/ko
32 m 51 m 22 m
28 f 52 f 10 f
(29%) (49%) (15%)
Mortality:
11 m+f (5%) Pre-weaning
4 f (2%) Post-weaning
Generation F2
ko/+ X ko/+
5 5
58 m, 69 f
+/+ ko/+ ko/ko
21 m 27 m 6 m
21 f 46 f 3 f
(29.5%) (51.4%) (6.3%)
Mortality:
15 m+f (10.6%) Pre-weaning
3 f (2.2%) Post-weaning
Generation F3
ko/+ X ko/+
12 12
193 m, 94 f
+/+ ko/+ ko/ko
61 m 118 m 11 m
48 f 120 f 22 f
(25%) (54.5%) (7.5%)
Mortality:
35 m+f (6%) Pre-weaning
6 f (1.4%) Post-weaning


B
ko/ko
+/+

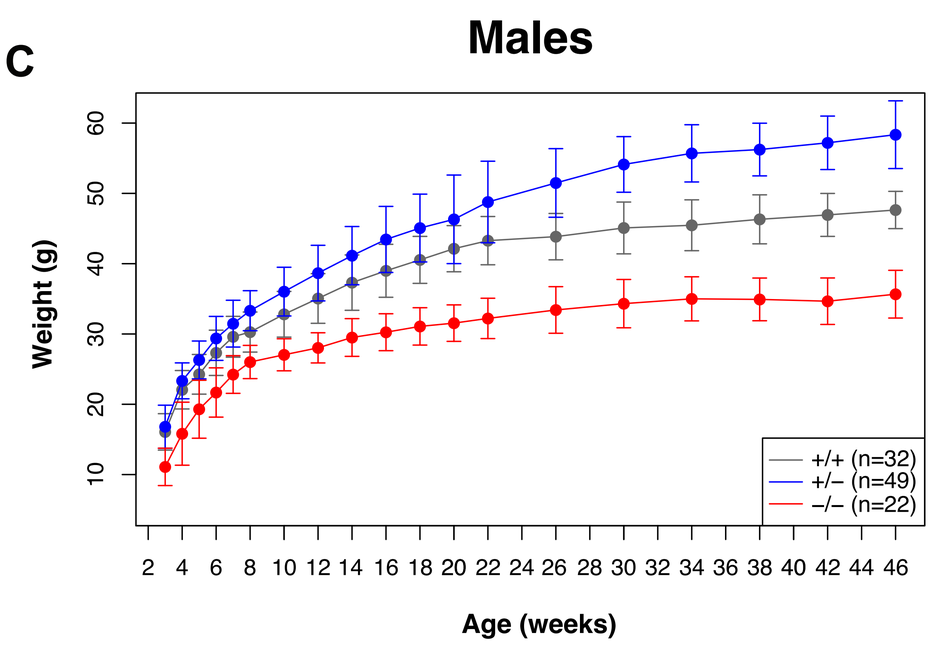
C
Males
Weight (g)
Age (weeks)
+/+ (n=32)
+/– (n=49)
–/– (n=22)

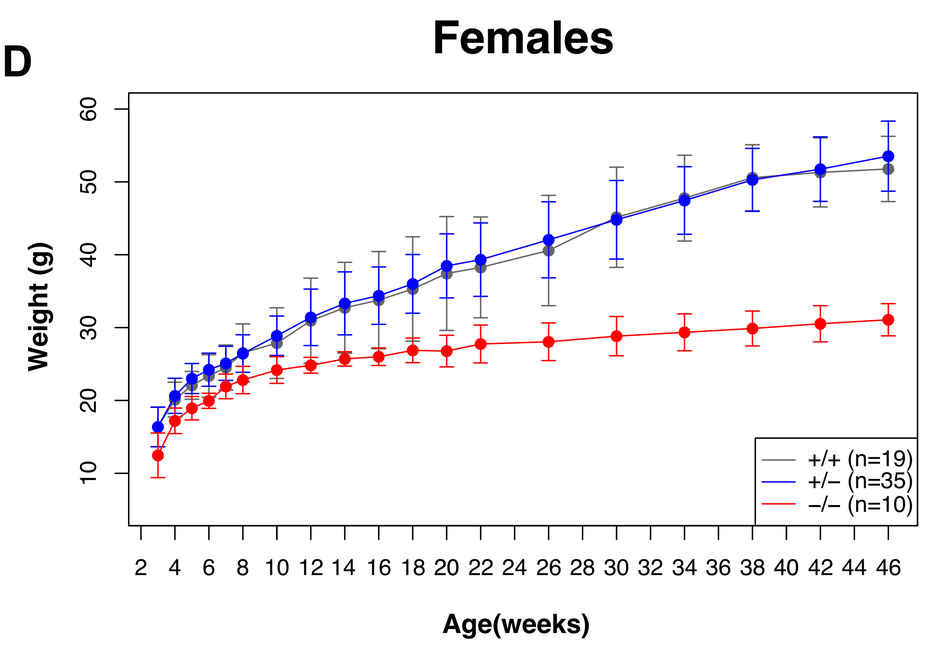
D
Females
Weight (g)
Age(weeks)
+/+ (n=19)
+/– (n=35)
–/– (n=10)

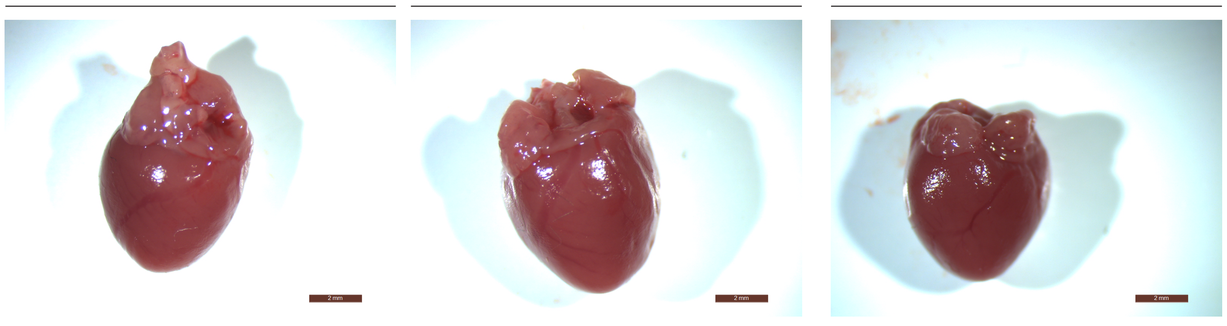
E
Gnb5+/+
Gnb5+/-
Gnb5-/-

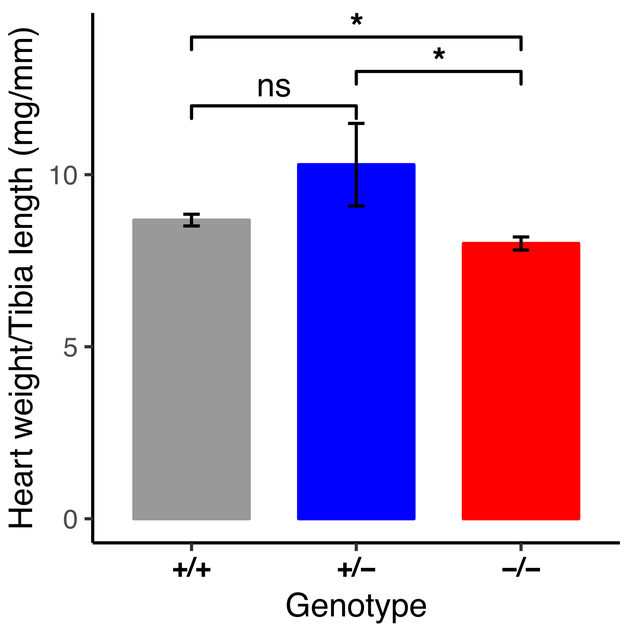
F
Heart weight/Tibia length (mg/mm)
ns
*
*
Genotype
+/+
+/–
–/–

Figure 3

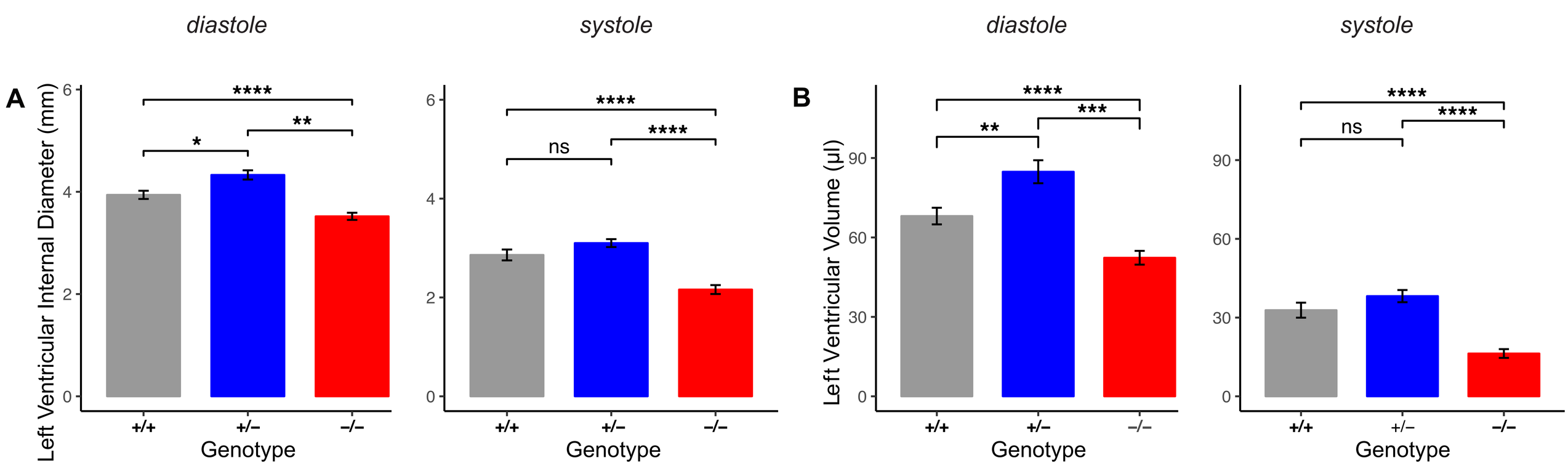
A
diastole
systole
Left Ventricular Internal Diameter (mm)
0
2
4
6
****
*
**
ns
****
****
+/+
+/–
–/–
Genotype
B
diastole
systole
Left Ventricular Volume (µl)
0
30
60
90
****
**
***
ns
****
****
+/+
+/–
–/–
Genotype
C
Left Ventricular mass (mg)
0
50
100
150
***
**
*
+/+
+/–
–/–
Genotype
D
Fractional Shortening (%)
0
10
20
30
40
50
***
ns
****
+/+
+/–
–/–
Genotype
E
Ejection Fraction (%)
0
25
50
75
***
ns
****
+/+
+/–
–/–
Genotype
F
Stroke volume (µl)
0
20
40
60
ns
**
**
+/+
+/–
–/–
Genotype
G
Cardiac output (ml/min)
0
10
20
30
ns
ns
**
+/+
+/–
–/–
Genotype
Gnb5
Genotype
+/+
+/-
-/-

Figure 4

A

Normal QRS complex

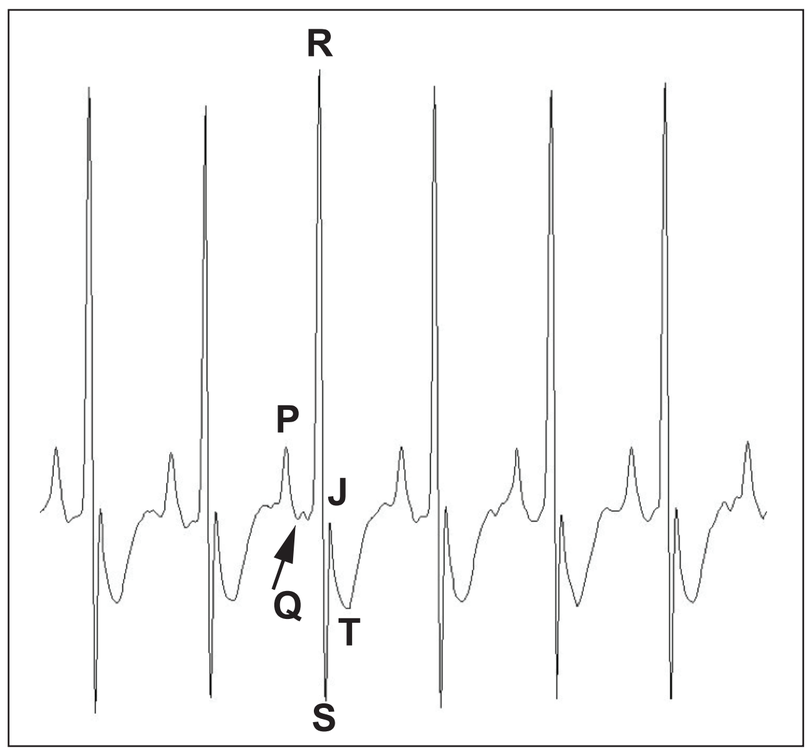

Gnb5 Genotype

+/+

+/-

-/-

B

Short Escape Atrial Beat

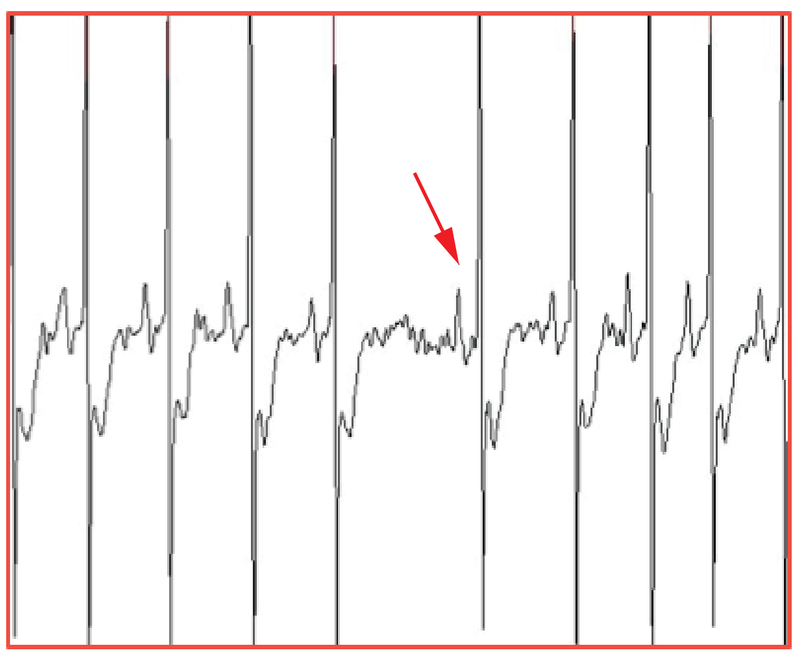

C

Long Escape Atrial Beat

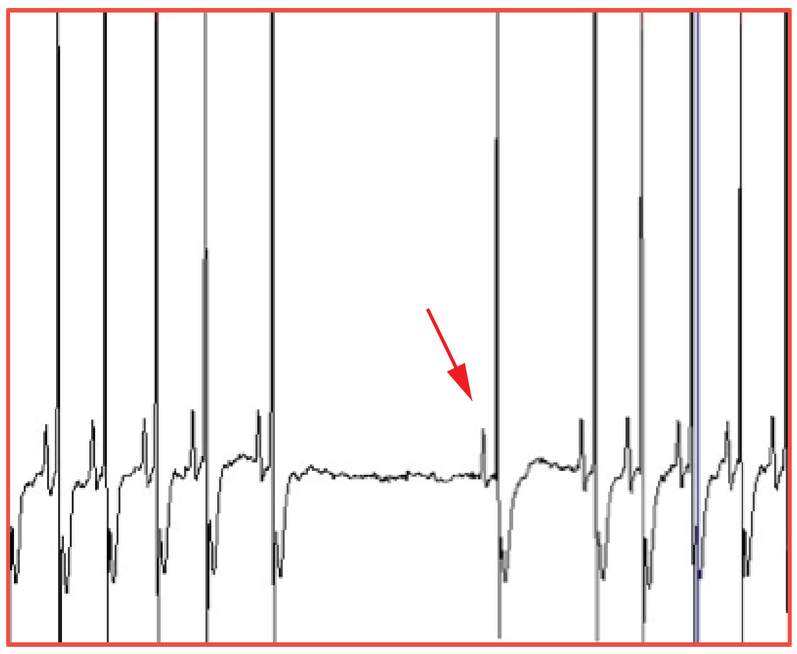

D

Atrioventricular Block

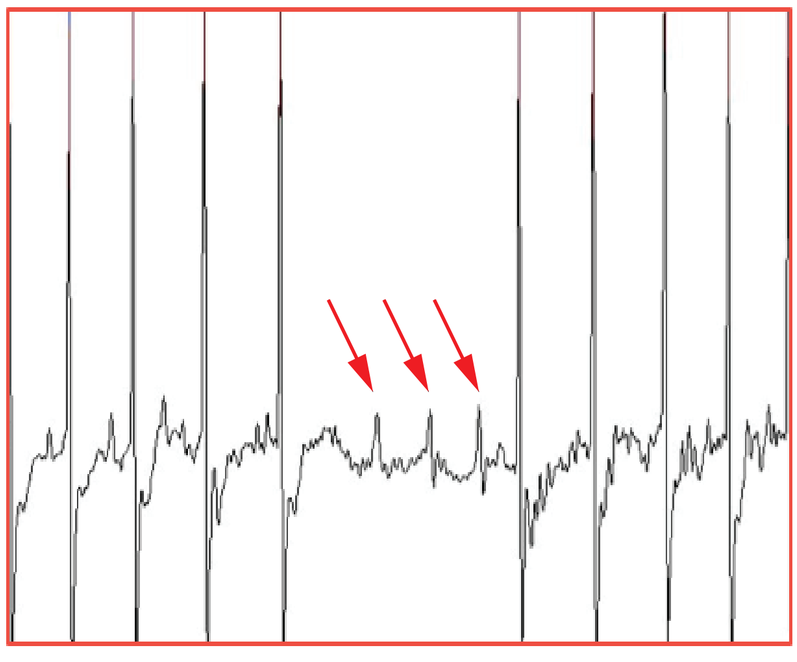

E

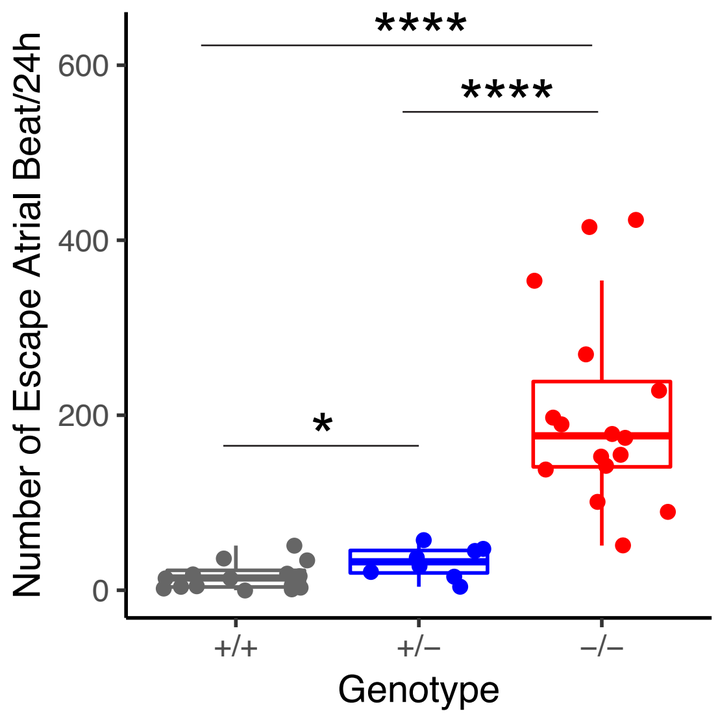

F

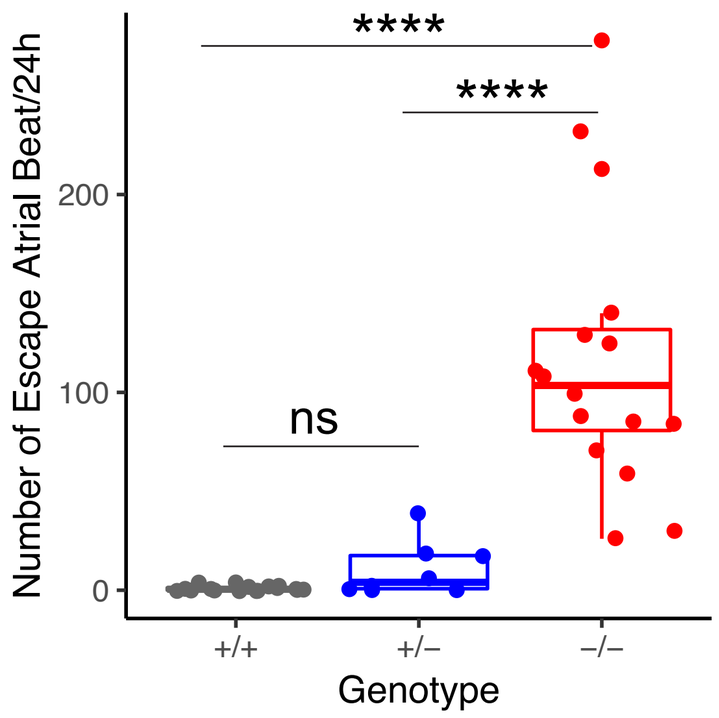

G

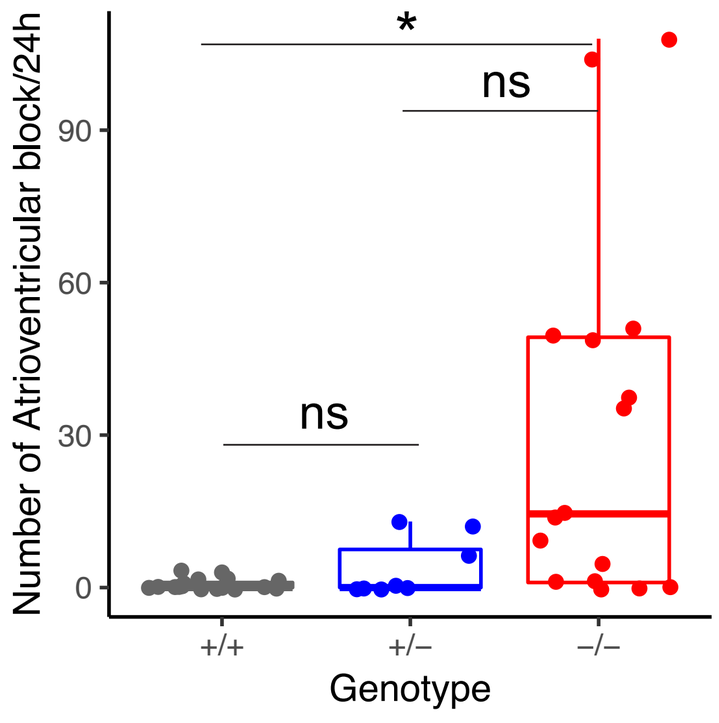

Figure 5

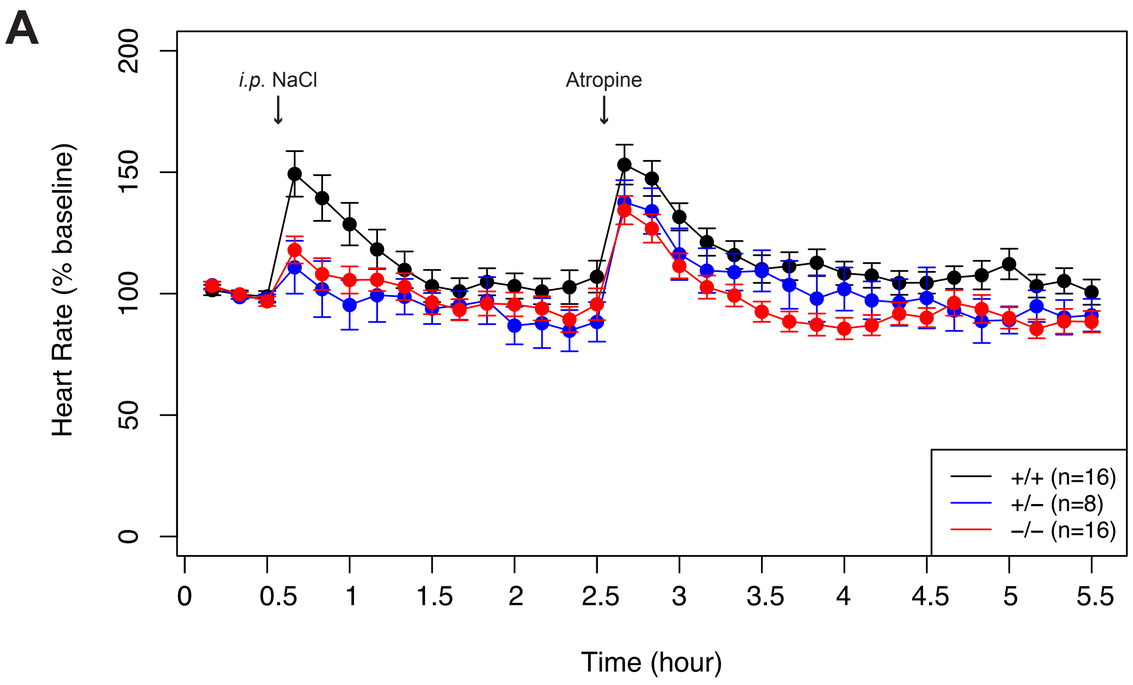
A
i.p. NaCl
Atropine
Heart Rate (% baseline)
Time (hour)
+/+ (n=16)
+/– (n=8)
–/– (n=16)

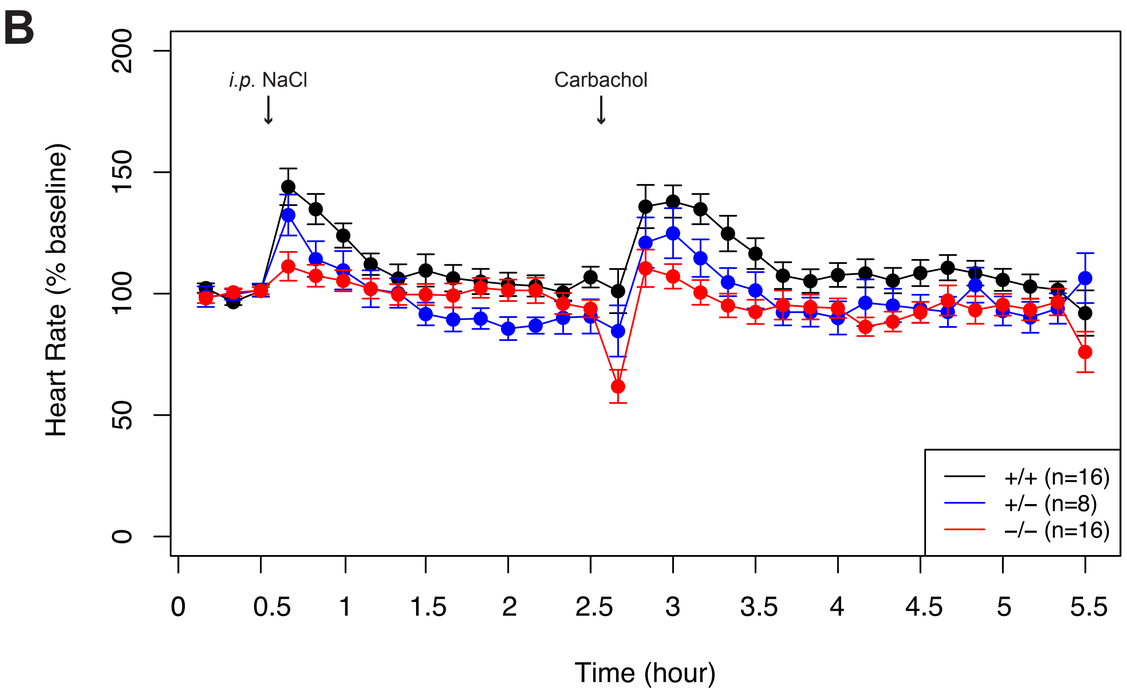
B
i.p. NaCl
Carbachol
Heart Rate (% baseline)
Time (hour)
+/+ (n=16)
+/– (n=8)
–/– (n=16)

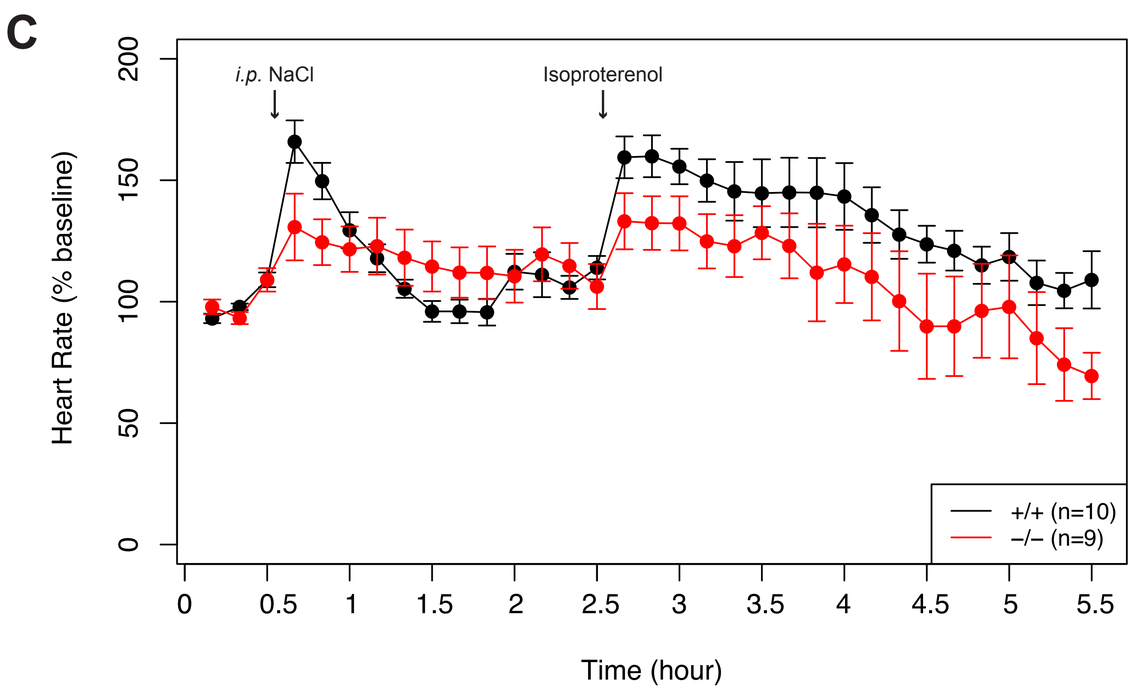
C
i.p. NaCl
Isoproterenol
Heart Rate (% baseline)
Time (hour)
+/+ (n=10)
–/– (n=9)

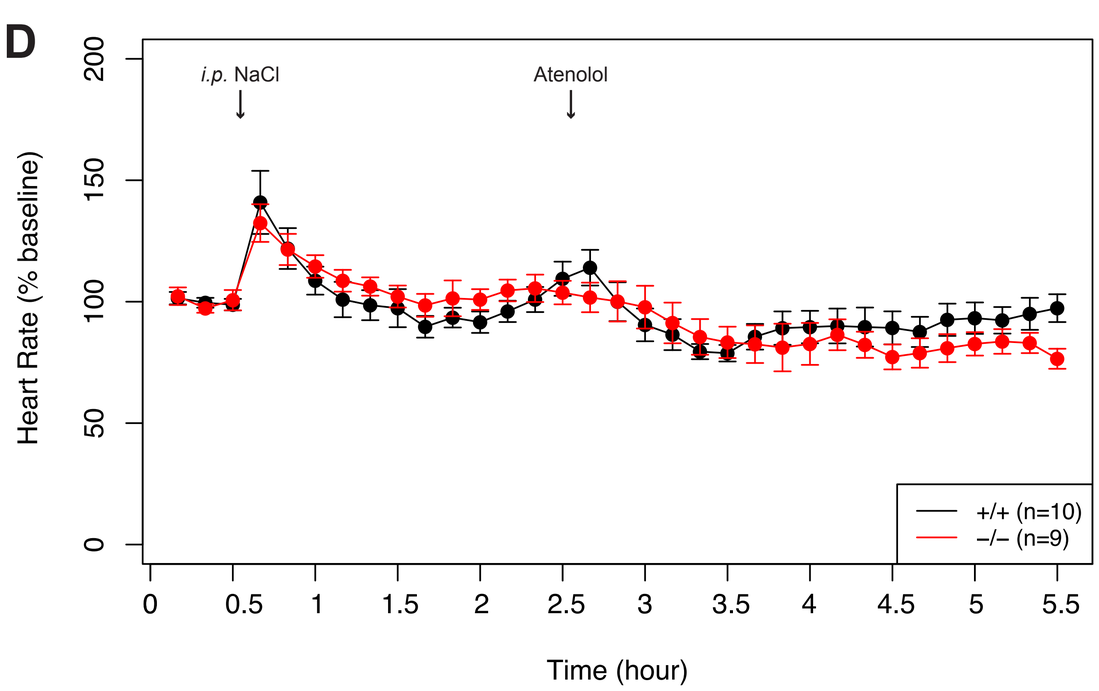
D
i.p. NaCl
Atenolol
Heart Rate (% baseline)
Time (hour)
+/+ (n=10)
–/– (n=9)

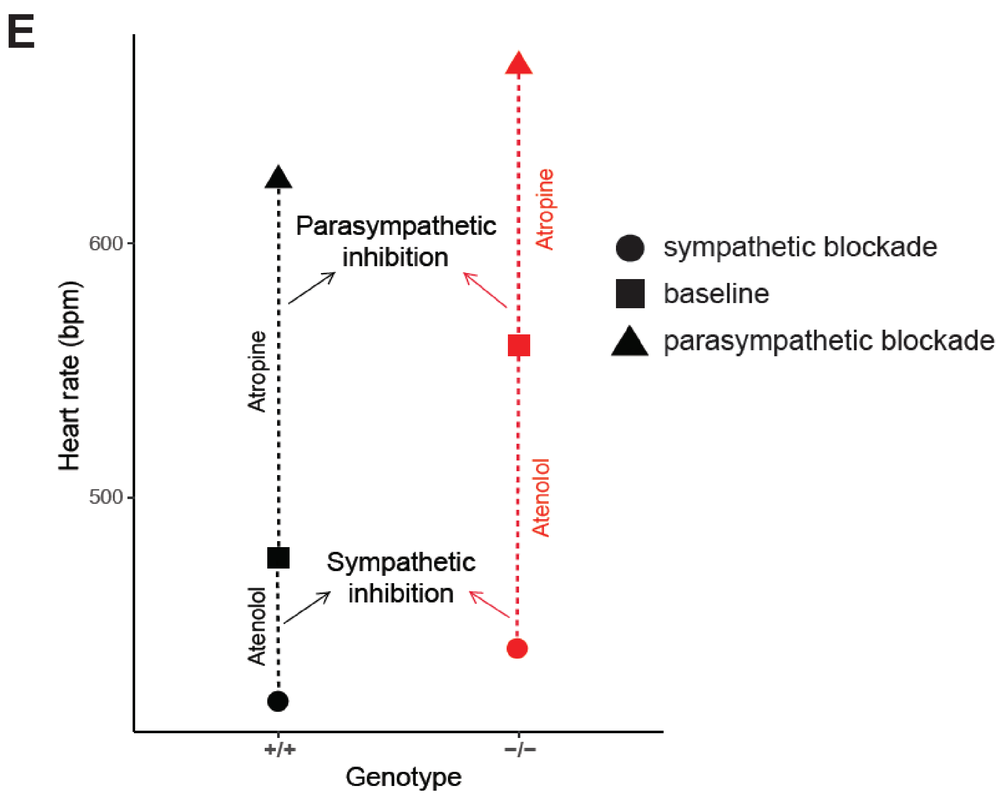
E
Heart rate (bpm)
600
500
Parasympathetic inhibition
Sympathetic inhibition
Atropine
Atenolol
Atropine
Atenolol
sympathetic blockade
baseline
parasympathetic blockade
+/+
–/–
Genotype

Figure 6

Atria

A

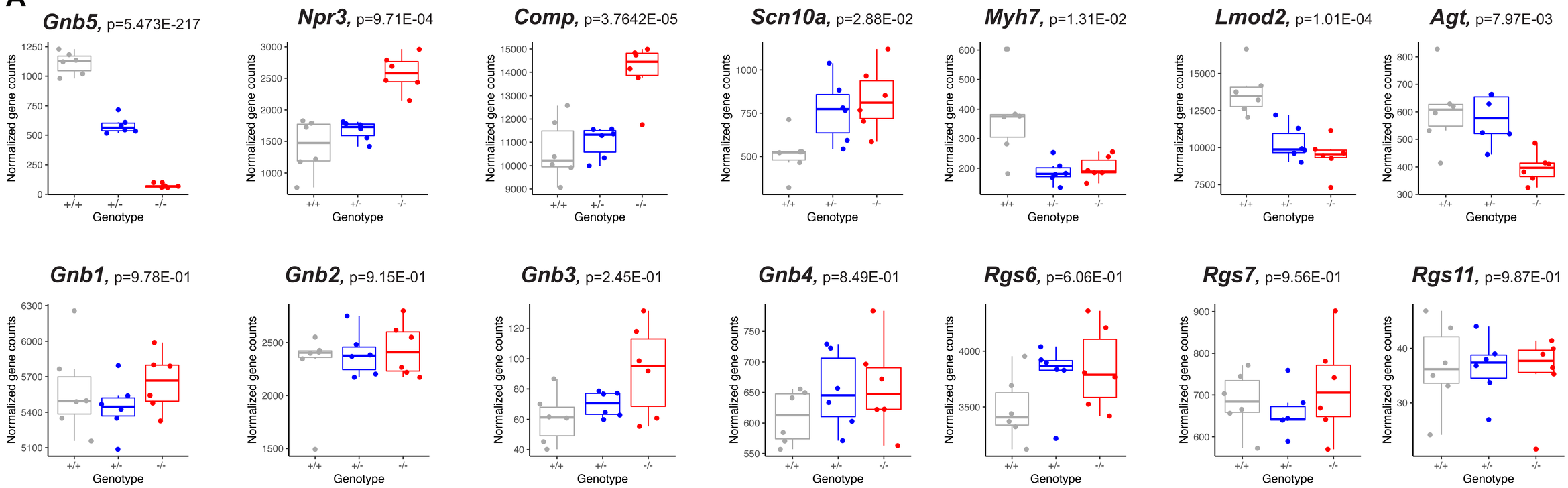

Ventricles

B

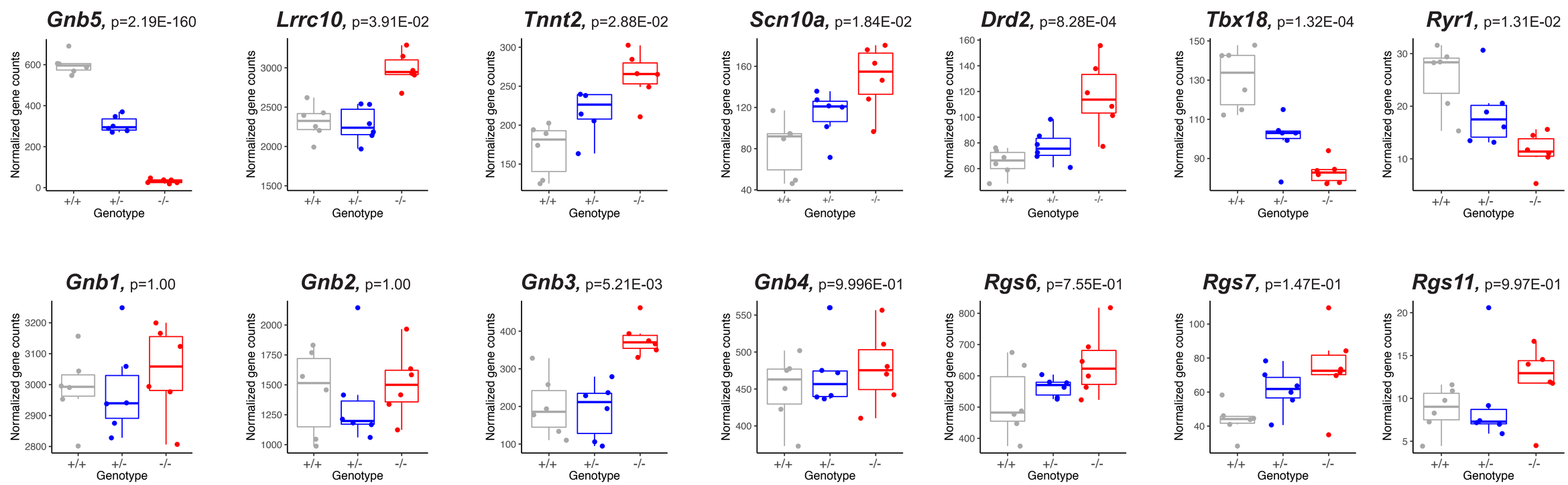

Figure S1

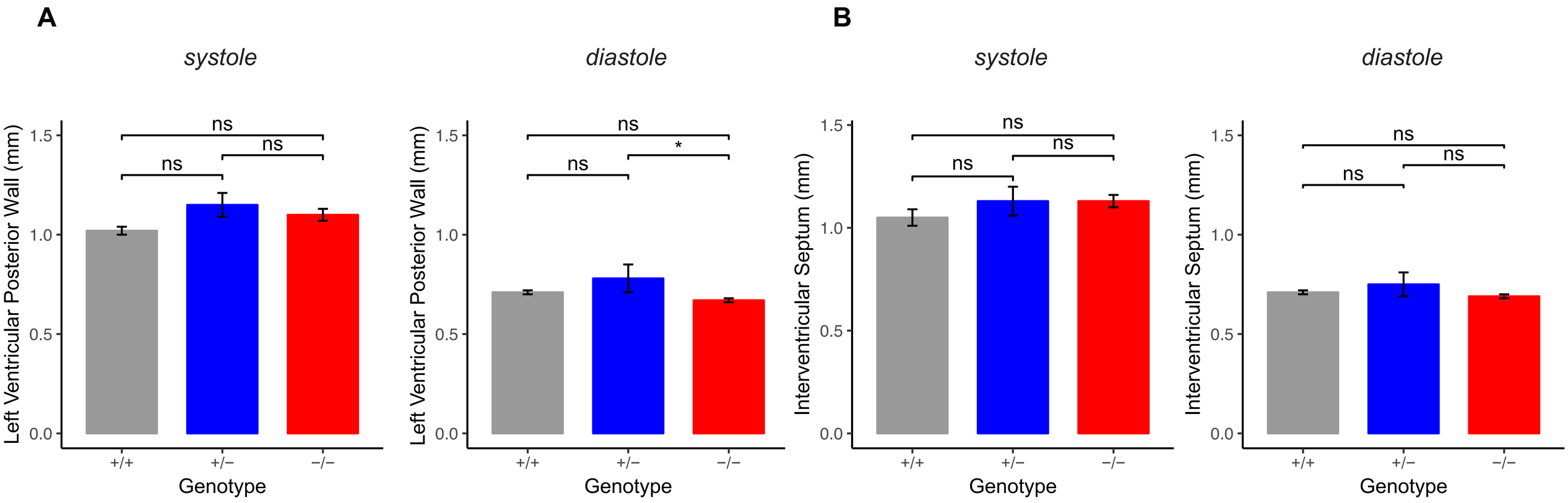

Figure S1: **Unchanged morphological parameters measured by echocardiography.** (**A**) Cardiac wall tickness in systole (right) and diasto-le (left). (**B**) Interventricular septum (at systole and diastole). (**C**) Heart rate measured in baseline condition through *in vivo* ECG. Values of knock-out (red) mice show a trend toward increased heart rate both during day and night (grey windows). (**D**) Qualitative mesaure of the mouse activity, consisting in displacement of the telemetric device. *Gnb5*$^{-/-}$ animals seem to be more active during the day, usually representing the sleeping phase for a mouse. (**E**) Measurements of the body temperature showing a similar trend to the activity.

Figure S2

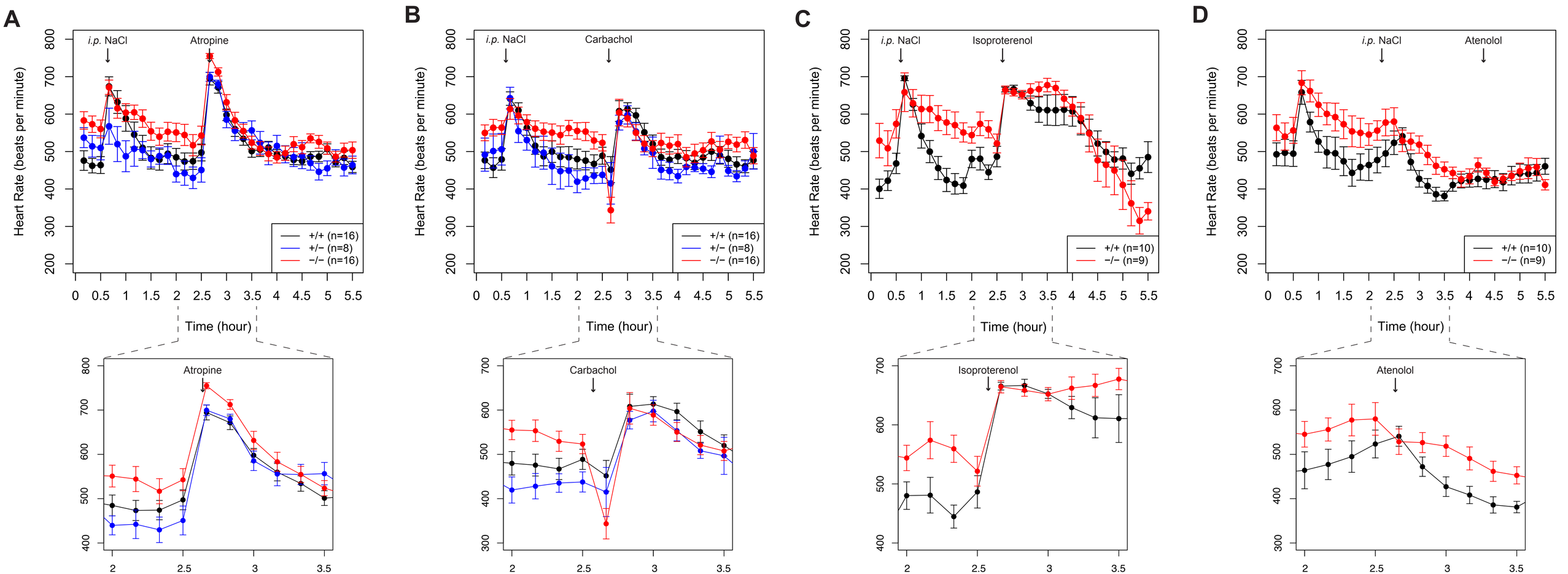

Figure S2: **Pharmacological challenges expressed in raw values.** Parasympathetyc (**A-B**) and sympathetyc (**C-D**) stimulation expressed in raw values (top). Zoom in on times ~ 2 to 3.5 hours illustrating peak and nadir heart rate differ-ences among the genotypes (bottom).

Figure S3

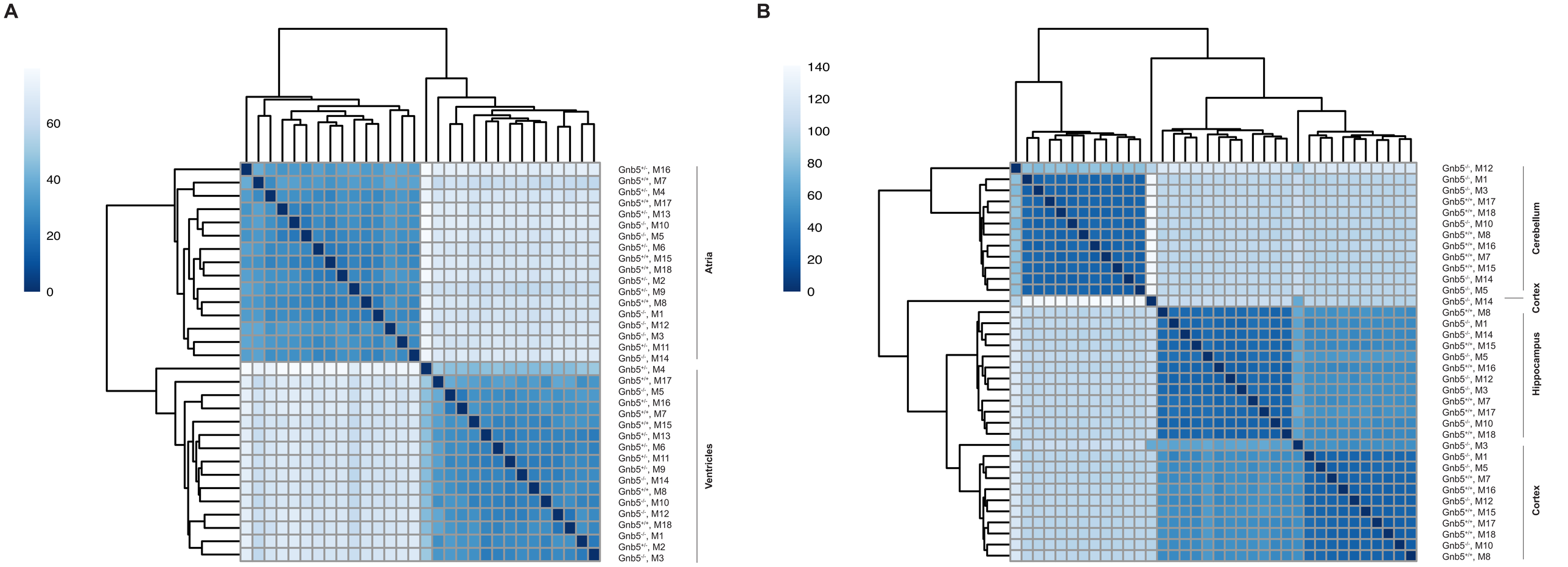

Figure S3: Samples distance of RNA samples. Heat map depicting hierarchical clustering of sample-to-sample distances for heart tissues (**A**) and brain regions (**B**) using normalized RNA-seq gene read counts. Blue color represents the nearest distance and light grey color indicates long sample-sample distance. Samples are clustered by tissue: (**A**) atria (top), and ventricles (bottom); (**B**) cerebellum (top), hippocampus (middle), and cortex (bottom). Samples M12-cerebellum, M14-cortex and M3-cortex were excluded from the analysis due to pronounced 3' mRNA degradation observed at the quality control step.

Figure S4

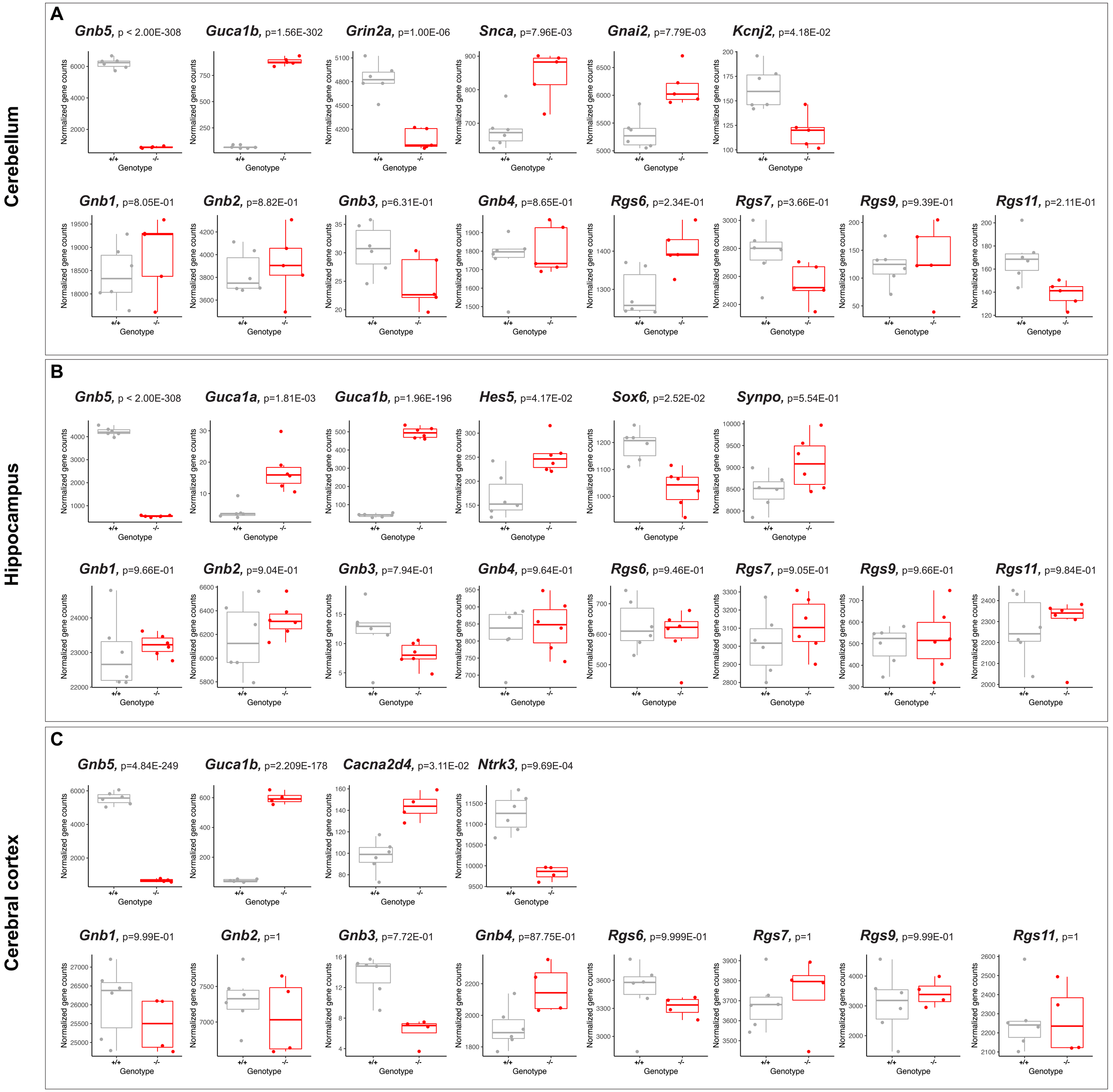

Figure S4: Expression profile of relevant genes in cerebellum, hippocampus and cerebral cortex of *Gnb5*$^{-/-}$, *vs*. *Gnb5*$^{+/+}$ mice. Expression levels of *Gnb5* (top left in each panel) and other differentially expressed genes in cerebellum (**A**, top), hippocampus (**B**, top) and cerebral cortex (**C**, top); *Gnb* and *Rgs* transcripts quantification in cerebellum (**A**, bottom), hippocampus (**B**, bottom) and cerebral cortex (**C**, bottom).

Figure S5

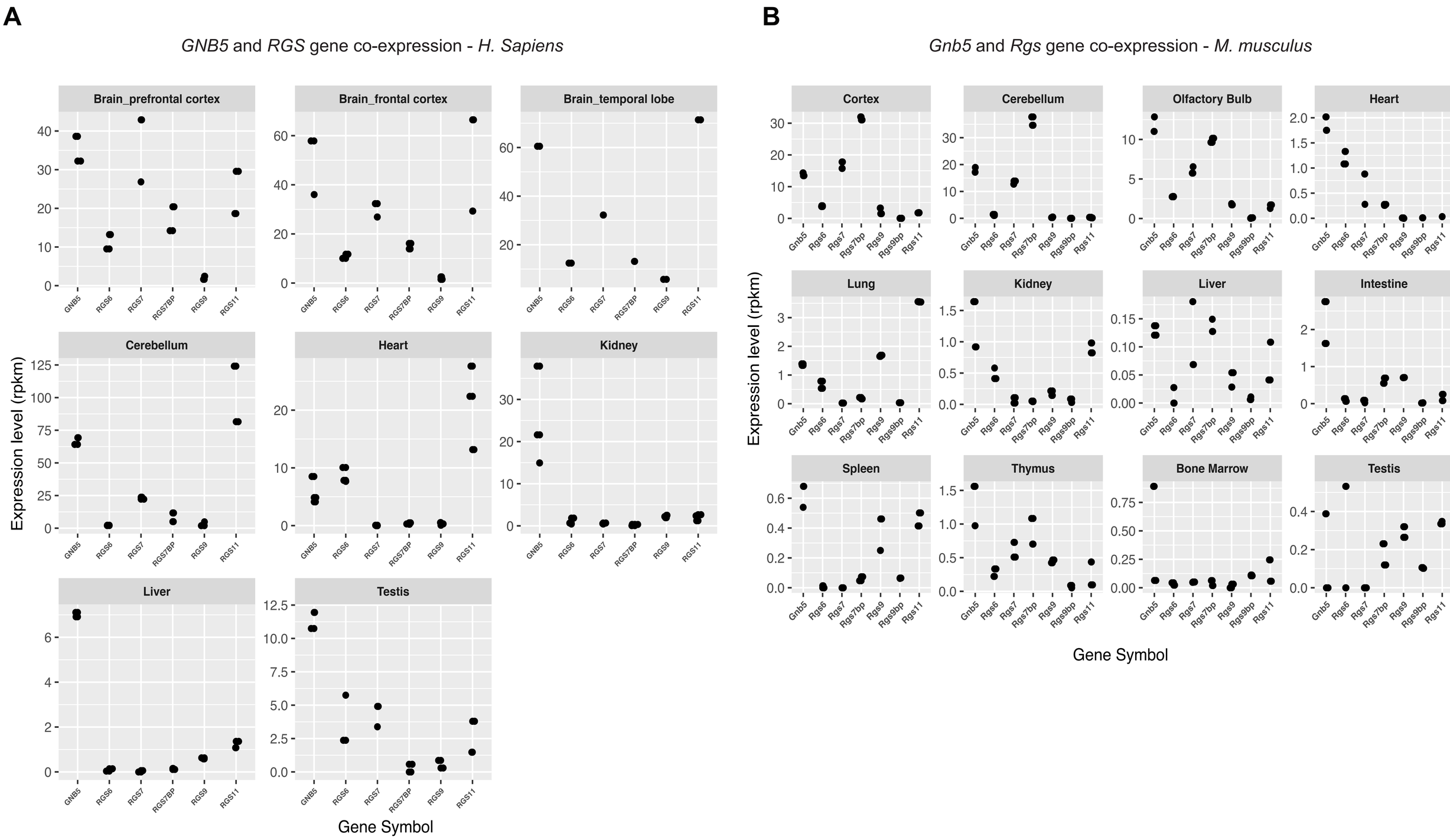

Figure S5: **Co-expression of *Gnb5* and *Rgs* genes in human and mouse.** *Gnb5* and *Rgs* genes expression was evaluated using publicly available transcritpome datasets in human (**A**) and mouse (**B**). Human data were re-trieved from (Brawand D. Nature. 2012); gene expression files for mouse tissues were obtained through the ENCODE website. Each point in the plots represents a replicate. Genes ecnoding for the R7 family of RGS proteins, known partners of GNB5, were inspected. In human, *GNB5* shows co-expression with *RGS7* and *RGS11* in the brain regions, while in heart co-epxression occurs between *GNB5* and *RGS6* and *RGS11*. A similar itrend is observed in mouse, with *Gnb5* being co-expressed with *Rgs7* in brain, and with *Rgs6* in heart. Accordingly, *RGS9* is only expressed in eye, therefore we do not capture any co-expression profile with this subunit.

Table1. Overlapping clinical features of individuals with IDDCA syndrome

	Lodder E., De Nittis P., Koopman C. *et al*., 2016								
	Family A		**Family B**	**Family C**		**Family D**	**Family E**		**Family F**
Individual	**1**	**2**	**3**	**4**	**5**	**6**	**7**	**8**	**9**
Gender, Age (years)	F, 22	F, 20	F, 6	F, 11	M, 9	F, 12	F, 13	M, 8	M, 23
Nucleotide change (NM_006578.3)	c.249G>A,r.249_250ins249+1_249+25/ c.994C>T	c.249G>A,r.249_250ins249+1_249+25/ c.994C>T	c.249+1G>T/ c.249+1G>T	c.249+3G>T/ c.249+3G>T	c.249+3G>T/ c.249+3G>T	c.906C>G / c.906C>G	c.242C>T/ c.242C>T	c.242C>T/ c.242C>T	c.242C>T/ c.242C>T
Amino acid change (NP_006569.1)	p.Asp84Valfs52*/ p.(Arg332*)	p.Asp84Valfs52*/ p.(Arg332*)	p.Asp84Leufs31*/p.Asp84Leufs31*	p.Asp84Valfs31*/p.Asp84Valfs31*	p.Asp84Valfs31*/p.Asp84Valfs31*	p.Tyr302*/p.Tyr302*	p.(Ser81Leu)/p.(Ser81Leu)	p.(Ser81Leu)/p.(Ser81Leu)	p.(Ser81Leu)/p.(Ser81Leu)
Birth weight	3580 g (50th percentile)	NA	NA	2751 g (15 th percentile)	NA	2845 g (15th percentile)	NA	NA	NA
Ethnicity	Italy	Italy	Jordan	Puerto Rico	Puerto Rico	India	Morocco	Morocco	Brazil
Consanguinity	−	−	+	+	+	−	−	−	+
Altered speech development	+	+	NR	+	+	+	+	+	NA
- Verbal understanding	NA	NA	nonverbal	unremarkable	unremarkable	NA	NA	NA	NA

- Lexical production	NA	NA	nonverbal	delayed	delayed	nonverbal	delayed	delayed	NA
Intellectual disability (ID)	+	+	+	+	+	+	mild	mild	mild
Epilepsy	+	+	+	-	-	+	-	-	-
Sinus Sick Syndrome (SSS)	+	+	+	+	+	increased PR interval (intermittent Weckenbach)	+	+	+
- Minimum heart rate	24	39	NA	paced	paced	NA	20	16	NA
- Maximum heart rate	163	192	NA	paced (27% heartbeats on Holter)	paced (20% heartbeats on Holter)	NA	176	180	NA
- Chronotropic response	NA	NA	NA	+	+	NA	unremarkable	unremarkable	NA
- Escape beats	+	+	NA	paced	paced	NA	+	+	NA
- Pacemaker implantation	-	-	-	+	+	-	-	+	NA
- Heart structural abnormalities	-	PFO	NA	-	-	-	-	-	NA
Hypotonia	+	+	+	+	+	+	-	impaired fine motor skills	-
Pathological gastric reflux	+	+	NA	+	+	+	-	-	NA

Nystagmus	+	+	+	+	+	+	NA	-	NA
Retinal Disease	+	NA	NA	NA	NA	+	NA	NA	NA
Metabolic work-up									
- Plasma amino acids chromatography	938 µm/l (restored)	+ (restored)	NA	unremarkable	unremarkable	unremarkable	444 µm/l	unremarkable	NA
- Urine organic acids	unremarkable	unremarkable	increased excretion of 3-methyl-glutaconic acid	unremarkable	unremarkable	unremarkable	NA	NA	NA
Others	-	-	-	-	-	-	-	-	-
Dysmorphic feature(s)	-	-	-	-	-	-	-	-	-

Family history	-	-	-	-	-	-	-	-	-

Shamseldin *et al*., 2016					Turkdogan D. *et al.*, 2016					
Family G					**Family H**					
10	**11**	**12**	**13**	**14**	**15**	**16**	**17**	**18**	**19**	**20**
F, 10	F, 9	F, 3	F, 5	F, 9	M, 2 (second degree cousin of pt 16)	F, 10 - pair of a monozygotic twin	F (deceased 5.5months)	M (deceased 7months)	F - pair of a monozygotic twin (deceased 8months)	M (deceased 7yo)
c.242C>T/ c.242C>T	c.242C>T/ c.242C>T	c.242C>T/ c.242C>T	c.242C>T/ c.242C>T	c.242C>T/ c.242C>T	c.355delG/ c.355delG	c.355delG/ c.355delG	c.355delG/ c.355delG	c.355delG/ c.355delG	c.355delG/ c.355delG	c.355delG/ c.355delG
p.(Ser81Leu)/p.(Ser81Leu)	p.(Ser81Leu)/p.(Ser81Leu)	p.(Ser81Leu)/p.(Ser81Leu)	p.(Ser81Leu)/p.(Ser81Leu)	p.(Ser81Leu)/p.(Ser81Leu)	p.Ala119Profs16*/p.Ala119Profs16*	p.Ala119Profs16*/p.Ala119Profs16*	p.Ala119Profs16*/p.Ala119Profs16*	p.Ala119Profs16*/p.Ala119Profs16*	p.Ala119Profs16*/p.Ala119Profs16*	p.Ala119Profs16*/p.Ala119Profs16*
50th centile	50th centile	NA	50th centile	NA	NA	1800 g (<1st)	NA	NA	NA	NA
Saudi	Saudi	Saudi	Saudi	Saudi	Turkish	Turkish	Turkish	Turkish	Turkish	Turkish

+	+	+	-	-	+	+	+	+	+	+
+	+	+	-	-	+	+	NA	NA	NA	NA
+	+	+	+	+	no developmental milestones	no developmental milestones	NA	NA	NA	NA
delayed	delayed	delayed	delayed	delayed	no developmental milestones	no developmental milestones	NA	NA	NA	NA
Normal IQ, but school performance issues	normal cognitive development	NA	normal IQ	NA	+	+	+	+	+	+
NA	NA	NA	NA	NA	+	+	NA	+	+	NA
NA	NA	NA	NA	NA	+	+	NA	NA	NA	+
NA	NA	NA	NA	NA	NA	NA	NA	NA	NA	NA
NA	NA	NA	NA	NA	NA	NA	NA	NA	NA	NA
NA	NA	NA	NA	NA	NA	NA	NA	NA	NA	NA
NA	NA	NA	NA	NA	NA	NA	NA	NA	NA	NA
NA	NA	NA	NA	NA	− (suggested, but refused by parents)	− (suggested, but refused by parents)	NA	NA	NA	NA
NA	NA	NA	NA	NA	−	−	NA	NA	NA	NA
-	-	NA	+	NA	+	+	NA	NA	NA	NA

NA	NA	NA	NA	NA	NA	normal (abdominal US examination)	NA	NA	NA	NA
NA	NA	NA	NA	NA	+	+ (horizontal)	NA	NA	NA	NA
NA	NA	NA	NA	NA	+	+	NA	NA	NA	NA
						unremarkable	NA	NA	NA	NA
NA	NA	NA	NA	NA	NA	unremarkable	NA	NA	NA	NA
NA	NA	NA	NA	NA	NA	unremarkable	NA	NA	NA	NA
ADHD, Marked hyperactivity	Inattentive type ADHD	-	motor delay	ADHD, mild motor delay	-	autistic (midline hand automatisms, lack of eye contact)	NA	NA	NA	NA

-	-	-	-	-	-	prominent forhead, acquired micro-brachycephaly	NA	NA	NA	NA
-	-	-	-	-	-	-	NA	NA	NA	NA

Vernon H. *et al.*, 2017	Malerba N. *et al.*, 2018	Poke G. *et al.*, 2019				
Family I	**Family J**	**Family K**	**Family L**	**Family M**		**Family N**
21	**22**	**23**	**24**	**25**	**26**	**27**
M, 2	F, 2.5	M, 10	M, 3	F (deceased 13yo)	F, 2	F, 3
c.222_226delTAAGA/ c.737G>A	c.222_226delTAAGA/ c.242C>T	c.136delG/c.136delG	c.906C>G/ c.906C>G	c.242C>A/c.242C >A	c.242C>A/c.242C >A	c.906C>A/c.906C >A

p.Asp74Glufs52*/p.(Arg246Gln)	p.Asp74Glufs52*/p.(Ser81Leu)	p.Glu46fs68*/p.Glu46fs68*	p.Tyr302*/p.Tyr302*	p.Ser81*/p.Ser81*	p.Ser81*/p.Ser81*	p.Tyr302*/p.Tyr302*
3,311 g (50th)	1698 g (< 1st percentile)	NA	NA	NA	NA	NA
European/Caucasian	European/Caucasian	Cambodia	Pakistan	Algeria	Algeria	Pakistan
−	-	+ (second cousins)	+ (first cousin once removed)	+ (first cousins)	+ (first cousins)	-
+	+	+	+	+	+	+
nonverbal	+	nonverbal	nonverbal	nonverbal	nonverbal	nonverbal
nonverbal	expressive speech delay (spoken vocabulary of ~ 12 words)	nonverbal	nonverbal	nonverbal	nonverbal	nonverbal
+	mild	+	+	+	+	+
−	-	+	+	+	+	+
+	+	+	+	normal ECG	+	+
71	36	NA	NA	NA	NA	NA
183	176	NA	NA	NA	NA	NA
NA	NA	NA	NA	NA	NA	NA
+ (prior to pacing)	+	+	+	NA	NA	NA
+	+	NA	NA	NA	NA	NA

–	-	NA	NA	NA	NA	NA
+	+	+ (contractures, nonambulatory, no head control)	+ (nonambulatory)	+ (nonambulatory)	+ (nonambulatory)	+ (nonambulatory)
+	-	+	NA	NA	NA	NA
+	strabismus (surgically corrected at 16 mo)	NA	+	+	+	+
+	-	+	NA	NA	+	+
NA	NA	NA	NA	NA	NA	NA
NA	NA	NA	NA	NA	NA	NA
NA	NA	NA	NA	NA	NA	NA
left-sided hearing loss, intermittent extremity hypertonia, intermittent upper extremity jerking motions - sometimes in conjuction with a stimulus, laryngomalacia hypertonia, clenched hands, high-voltage cortical activity (EEG), pain of unknown etiology	bilateral tympanostomy tubes; high activity level and short attentions span compared to peers	pyloric stenosis, G-tube. Scoliosis	NA	NA	NA	NA

thin corpus callosum (brain MRI)	plagiocephaly associated with torticollis at 8 mo (solved with molding helmet therapy)	NA	microcephaly	NA	NA	NA
-	maternal uncle and paternal first-cousin suspected to have ASD	NA	NA	NA	NA	NA

This study					
Family O	**Family P**	**Family Q**	**Family R**	**Family S**	**Family T**
28	**29**	**30**	**31**	**32**	**33**
M, 8 months (deceased)	M, 15	F, 1.2	F, 4	2, M	F, 7
c.906C>G/c.906C>G	c.906C>G/c.906C>G	c.644G>A/c.644G>A	c.906C>A/c.906C>A	c.906C>G/c.906C>G	c.242C>G/c.242C>G

p.Tyr302*/p.Tyr302*	p.Tyr302*/p.Tyr302*	p.(Gly215Glu)/p.(Gly215Glu)	p.Tyr302*/p.Tyr302*	p.Tyr302*/p.Tyr302*	p.(Ser81Trp)/p.(Ser81Trp)
NA	NA	NA	NA	NA	2900g
Pakistan	Pakistan	Pakistan	Pakistan	Pakistan	Tunisia
+	+	+	+	+	+ (first cousins)
+	+	+	-	+ (vocalization at 1.10yo)	+
+	+	no developmental milestones	unremarkable	NA	low
+	+	no developmental milestones	unremarkable	NA	nonverbal
+	+	-	+	NA	+ (no neuropsychological assessment)
-	+	-	-	+	normal EEG
NA (inconsistent heart rate noted at Echo)	NA	+	NA	NA	+
NA	NA	18	32	29	30
NA	154	142	152	158	160
NA	NA	NA	NA	NA	NA
NA	-	+	NA	NA	+
NA	-	-		-	-

-	-	NA	NA	-	-
+	+ (no head control)	+ (no neck holding)	+ (no neck holding)	+ (along with hyporeflexia)	+ (impaired fine motor skills)
NA	+	-	NA	-	-
_	+	+	no eye contact	no eye contact, convergent squint (strabismus) right eye	-
NA	NA	-	NA	myopia (-1.5)	-
NA	NA	NA	NA	unremarkable	unremarkable
NA	non specific	unremarkable	unremarkable	unremarkable	global hypoAA, High Phe (146, N: 39-77)
NA	unremarkable	NA	Fatty Acid Oxidation Disorder	unremarkable	normal
-	thining, hypogenesis of corpus callosum, modified hypsarythmia, breath holding spell, taking EPIVAL (VAP) and fits are controlled	-	Cerebral Atrophy on MRI	-	unexplained coma secondary to sepsis in the context of digestive infection; one episode of pyelonephritis without complications

dysmorphism stridor	-	-	deep philtrum, micrognathia, prominent ears, disproportion of skull to face	blond hair, frontal bossing, epicanthic folds, small palpebral fissure, depressed nasal bridge, high arched palate	shorter tumbs
-	-	one sibling with similar phenotype died, likely due to cardiac arrest	-	-	paternal uncle with severe cognitive impairment and no language; maternal aunt and uncle are severely handicapped and no language, similar to the son of another maternal aunt

Patient numbers refer to those of the publshed pedigrees

NA = Not Available

"+" present clinical trait

"-" not present clinical trait

"PFO" Patent Foramen Ovale
ADHD = Attention Deficit Hyperactivity Disorder

ASD = Autism Spectrum Disorder

ECG = Electrocardiogram

EEG = Electroencephalogram

Supp. Table S1. Pathogenic prediction of the two novel *GNB5* variants

	GNB5 variants	
Prediction tool	p.(S81W)	p.(G215E)
Mutation Taster	Disease causing (0.99)	Disease causing (0.99)
PolyPhen-2	Probably Damaging (1)	Probably Damaging (1)
SIFT	Deleterious (0.00)	Deleterious (0.00)
Provean	Deleterious (-5.274)	Deleterious (-7.426)
UMD-predictor	Pathogenic (100)	Pathogenic (99)
FATHMM	Damaging (-6.79)	Damaging (-6.92)
NNSplice	-	Donor increased
NetGene2	-	Activation of donor splice site
Splicing Finder	Activation of an exonic cryptic donor site, creation of an exonic ESS site	Creation of an exonic ESS site, alteration of an exonic ESE site
CADD	31	29.1

Supp. Table S2. Description of the mouse samples used for transcriptome

Sample name	Gnb5 genotype	Tissue
KO_At_M1	-/-	Atria
HET_At_M2	+/-	Atria
KO_At_M3	-/-	Atria
HET_At_M4	+/-	Atria
KO_At_M5	-/-	Atria
HET_At_M6	+/-	Atria
WT_At_M7	+/+	Atria
WT_At_M8	+/+	Atria
HET_At_M9	+/-	Atria
KO_At_M10	-/-	Atria
HET_At_M11	+/-	Atria
KO_At_M12	+/-	Atria
HET_At_M13	+/-	Atria
KO_At_M14	-/-	Atria
WT_At_M15	+/+	Atria
WT_At_M16	+/+	Atria
WT_At_M17	+/+	Atria
WT_At_M18	+/+	Atria
KO_At_M1	-/-	Ventricles
HET_At_M2	+/-	Ventricles
KO_At_M3	-/-	Ventricles
HET_At_M4	+/-	Ventricles
KO_At_M5	-/-	Ventricles
HET_At_M6	+/-	Ventricles
WT_At_M7	+/+	Ventricles
WT_At_M8	+/+	Ventricles
HET_At_M9	+/-	Ventricles
KO_At_M10	-/-	Ventricles
HET_At_M11	+/-	Ventricles
KO_At_M12	+/-	Ventricles
HET_At_M13	+/-	Ventricles
KO_At_M14	-/-	Ventricles
WT_At_M15	+/+	Ventricles
WT_At_M16	+/+	Ventricles
WT_At_M17	+/+	Ventricles
WT_At_M18	+/+	Ventricles
KO_At_M1	-/-	Cerebellum
KO_At_M3	-/-	Cerebellum
KO_At_M5	-/-	Cerebellum

WT_At_M7	+/+	Cerebellum
WT_At_M8	+/+	Cerebellum
KO_At_M10	-/-	Cerebellum
KO_At_M12	+/-	Cerebellum
KO_At_M14	-/-	Cerebellum
WT_At_M15	+/+	Cerebellum
WT_At_M16	+/+	Cerebellum
WT_At_M17	+/+	Cerebellum
WT_At_M18	+/+	Cerebellum
KO_At_M1	-/-	Hippocampus
KO_At_M3	-/-	Hippocampus
KO_At_M5	-/-	Hippocampus
WT_At_M7	+/+	Hippocampus
WT_At_M8	+/+	Hippocampus
KO_At_M10	-/-	Hippocampus
KO_At_M12	+/-	Hippocampus
KO_At_M14	-/-	Hippocampus
WT_At_M15	+/+	Hippocampus
WT_At_M16	+/+	Hippocampus
WT_At_M17	+/+	Hippocampus
WT_At_M18	+/+	Hippocampus
KO_At_M1	-/-	Cerebral cortex
KO_At_M3	-/-	Cerebral cortex
KO_At_M5	-/-	Cerebral cortex
WT_At_M7	+/+	Cerebral cortex
WT_At_M8	+/+	Cerebral cortex
KO_At_M10	-/-	Cerebral cortex
KO_At_M12	+/-	Cerebral cortex
KO_At_M14	-/-	Cerebral cortex
WT_At_M15	+/+	Cerebral cortex
WT_At_M16	+/+	Cerebral cortex
WT_At_M17	+/+	Cerebral cortex
WT_At_M18	+/+	Cerebral cortex

Supp Table S3. List of Differentially Expressed genes at FDR 5% in *Gnb5-/-* mice - atria

Ensembl ID	Gene Symbol	Gene name	baseMean	log2FoldChange	lfcSE	stat	pvalue	padj
ENSMUSG00000032192	Gnb5	guanine nucleotide binding protein (G protein), beta 5	588.3942165	-3.98100257	0.125384112	-31.7504546	3.13E-221	5.47E-217
ENSMUSG00000033419	Snap91	synaptosomal-associated protein 91	593.4008865	-2.204605213	0.126013386	-17.49500813	1.56E-68	1.37E-64
ENSMUSG00000048758	Rpl29	ribosomal protein L29	199.1838179	-3.250034673	0.22769114	-14.2738741	3.18E-46	1.39E-42
ENSMUSG00000032224	Fam81a	family with sequence similarity 81, member A	292.8574685	2.572498612	0.253223883	10.15898889	3.02E-24	1.06E-20
ENSMUSG00000032179	Bmp5	bone morphogenetic protein 5	205.0671832	1.328934231	0.136737848	9.718847054	2.51E-22	7.30E-19
ENSMUSG00000033590	Myo5c	myosin VC	163.7773657	-1.49164629	0.195137706	-7.644070025	2.10E-14	5.26E-11
ENSMUSG00000023979	Guca1b	guanylate cyclase activator 1B	58.67765502	1.533209378	0.212719605	7.207654307	5.69E-13	1.24E-09
ENSMUSG00000039716	Dock3	dedicator of cyto-kinesis 3	188.3304401	-1.168897128	0.168267704	-6.94665168	3.74E-12	7.27E-09
ENSMUSG00000032184	Lysmd2	LysM, putative peptidoglycan-binding, domain containing 2	586.6508467	0.667351463	0.097089163	6.873593728	6.26E-12	1.09E-08
ENSMUSG00000023249	Parp3	poly (ADP-ribose) polymerase family, member 3	1837.440683	-0.66820649	0.10214733	-6.541595295	6.09E-11	9.68E-08
ENSMUSG00000032556	Bfsp2	beaded filament structural protein 2, phakinin	57.65614782	-2.234680029	0.347888403	-6.423554248	1.33E-10	1.94E-07
ENSMUSG00000042073	Abhd14b	abhydrolase domain containing 14b	580.8699606	-0.801977921	0.127326525	-6.298592679	3.00E-10	4.04E-07
ENSMUSG00000032579	Hemk1	HemK methyltransferase family member 1	597.5715156	0.879217891	0.141144598	6.229199738	4.69E-10	5.56E-07
ENSMUSG00000032872	Cyb5r4	cytochrome b5 reductase 4	1656.745906	-0.509974877	0.081905477	-6.226383107	4.77E-10	5.56E-07
ENSMUSG00000066456	Hmgn3	high mobility group nucleosomal binding domain 3	282.7147136	-0.762798777	0.13316698	-5.728137557	1.02E-08	1.11E-05
ENSMUSG00000031849	Comp	cartilage oligomeric matrix protein	1890.434541	0.863942512	0.156893591	5.506550687	3.66E-08	3.76E-05
ENSMUSG00000043587	Pxylp1	2-phosphoxylose phosphatase 1	553.184341	-1.06209914	0.195018224	-5.446153283	5.15E-08	5.00E-05
ENSMUSG00000032563	Mrpl3	mitochondrial ribosomal protein L3	1799.161022	-0.582173662	0.107712274	-5.404896214	6.48E-08	5.97E-05

ENSMUSG00000010057	Nprl2	NPR2 like, GATOR1 complex subunit	671.0578114	0.433311959	0.080955871	5.352446372	8.68E-08	7.23E-05
ENSMUSG00000044938	Klhl31	kelch-like 31	2434.146223	-0.686725512	0.129907316	-5.286272829	1.25E-07	9.92E-05
ENSMUSG00000029683	Lmod2	leiomodin 2 (cardiac)	11173.11087	-0.54016025	0.102389096	-5.275564196	1.32E-07	1.01E-04
ENSMUSG00000015354	Pcolce2	procollagen C-endopeptidase enhancer 2	1381.444784	0.377432306	0.072416176	5.21198893	1.87E-07	1.36E-04
ENSMUSG00000113637	Gm7049	predicted gene 7049	15.78647891	2.22274028	0.431035014	5.156751094	2.51E-07	1.76E-04
ENSMUSG00000039313	Minar1	membrane integral NOTCH2 associated receptor 1	31.93558633	1.962031653	0.383199078	5.120136678	3.05E-07	2.05E-04
ENSMUSG00000078137	Ankrd63	ankyrin repeat domain 63	231.3397505	0.742695994	0.148629054	4.99697718	5.82E-07	3.77E-04
ENSMUSG00000063564	Col23a1	collagen, type XXIII, alpha 1	520.8704226	0.624586575	0.126165837	4.950520603	7.40E-07	4.62E-04
ENSMUSG00000038156	Spon1	spondin 1, (f-spondin) extracellular matrix protein	3543.885101	0.371254886	0.075961149	4.887431184	1.02E-06	6.16E-04
ENSMUSG00000032058	Ppp2r1b	protein phosphatase 2, regulatory subunit A, beta	374.2643884	0.599231525	0.123151982	4.86578874	1.14E-06	6.65E-04
ENSMUSG00000041112	Elmo1	engulfment and cell motility 1	700.2407007	0.415448791	0.085517427	4.858059972	1.19E-06	6.69E-04
ENSMUSG00000091537	Tma7	translational machinery associated 7	483.7361455	-0.685576063	0.143465638	-4.77867782	1.76E-06	9.64E-04
ENSMUSG00000022206	Npr3	natriuretic peptide receptor 3	11899.26299	0.399734149	0.083783676	4.771026642	1.83E-06	9.71E-04
ENSMUSG00000032370	Lactb	lactamase, beta	346.157966	-0.422281978	0.09066889	-4.65740759	3.20E-06	1.65E-03
ENSMUSG00000043719	Col6a6	collagen, type VI, alpha 6	1411.565721	0.828808973	0.179039549	4.629194943	3.67E-06	1.83E-03
ENSMUSG00000026638	Irf6	interferon regulatory factor 6	354.4281902	0.612952619	0.132744643	4.61753185	3.88E-06	1.89E-03
ENSMUSG00000033453	Adamts15	a disintegrin-like and metallopeptidase (reprolysin type) with thrombospondin type 1 motif, 15	1535.603828	0.567295151	0.123255032	4.60261251	4.17E-06	1.97E-03
ENSMUSG00000032498	Mlh1	mutL homolog 1	433.7803123	-0.38578188	0.084367758	-4.572622185	4.82E-06	2.22E-03
ENSMUSG00000028476	Reck	reversion-inducing-cysteine-rich protein with kazal motifs	744.0022468	0.325339922	0.071357088	4.559321694	5.13E-06	2.30E-03

ENSMUSG00000021596	Mctp1	multiple C2 domains, transmembrane 1	179.9515026	0.502011368	0.111477268	4.5032622	6.69E-06	2.93E-03
ENSMUSG00000090626	Tex9	testis expressed gene 9	278.1642117	-0.734429387	0.163584055	-4.489614741	7.14E-06	3.04E-03
ENSMUSG00000032567	Aste1	asteroid homolog 1	192.4949534	-0.666334448	0.14938301	-4.460577198	8.17E-06	3.40E-03
ENSMUSG00000032431	Crtap	cartilage associated protein	1361.165212	0.364784746	0.082147038	4.440631755	8.97E-06	3.65E-03
ENSMUSG00000049624	Slc17a5	solute carrier family 17 (anion/sugar transporter), member 5	349.6898644	0.434839012	0.09846974	4.415965889	1.01E-05	4.00E-03
ENSMUSG00000053040	Aph1c	aph1 homolog C, gamma secretase subunit	68.79153406	-0.82659287	0.187704162	-4.403700279	1.06E-05	4.14E-03
ENSMUSG00000024806	Mlana	melan-A	1627.583495	0.52838317	0.122891802	4.299580298	1.71E-05	6.51E-03
ENSMUSG00000028132	Tmem56	transmembrane protein 56	245.5306833	-0.815298268	0.191265107	-4.262660763	2.02E-05	7.52E-03
ENSMUSG00000090215	Trim34b	tripartite motif-containing 34B	11.6973086	-2.582632252	0.607008212	-4.254690792	2.09E-05	7.63E-03
ENSMUSG00000028396	2310002L09Rik	RIKEN cDNA 2310002L09 gene	344.3905263	-0.626139305	0.147377011	-4.248554772	2.15E-05	7.68E-03
ENSMUSG00000037736	Limch1	LIM and calponin homology domains 1	5228.144385	-0.312723246	0.073777902	-4.238711583	2.25E-05	7.86E-03
ENSMUSG00000031980	Agt	angiotensinogen (serpin peptidase inhibitor, clade A, member 8)	524.2715869	-0.609713334	0.144159559	-4.229433963	2.34E-05	7.97E-03
ENSMUSG00000040848	Sft2d2	SFT2 domain containing 2	2529.424876	0.234751352	0.055536798	4.226951515	2.37E-05	7.97E-03
ENSMUSG00000068227	Il2rb	interleukin 2 receptor, beta chain	82.42680251	0.659994674	0.156469105	4.218051048	2.46E-05	8.13E-03
ENSMUSG00000074059	Fbxw18	F-box and WD-40 domain protein 18	62.68513319	3.258911738	0.774283545	4.208938393	2.57E-05	8.31E-03
ENSMUSG00000078307	AI593442	expressed sequence AI593442	39.35947148	-1.838584277	0.438071347	-4.196997335	2.70E-05	8.60E-03
ENSMUSG00000019102	Aldh3a1	aldehyde dehydrogenase family 3, subfamily A1	66.67934433	1.063561484	0.253673991	4.192631185	2.76E-05	8.61E-03
ENSMUSG00000100782	Gm28231	predicted gene 28231	22.5434237	1.248506266	0.301217727	4.144863178	3.40E-05	1.04E-02
ENSMUSG00000051855	Mest	mesoderm specific transcript	455.3390815	0.528823455	0.129171073	4.093977412	4.24E-05	1.28E-02
ENSMUSG00000045594	Glb1	galactosidase, beta 1	946.3638084	-0.476991352	0.11686762	-4.081467171	4.48E-05	1.31E-02

ENSMUSG00000053093	Myh7	myosin, heavy polypeptide 7, cardiac muscle, beta	251.3134444	-0.866946809	0.212498462	-4.079779212	4.51E-05	1.31E-02
ENSMUSG00000006941	Eif1b	eukaryotic translation initiation factor 1B	1363.496793	-0.405756831	0.100156813	-4.051215455	5.10E-05	1.40E-02
ENSMUSG00000032342	Mto1	mitochondrial tRNA translation optimization 1	741.1169021	-0.255310451	0.063047704	-4.04948058	5.13E-05	1.40E-02
ENSMUSG00000111278	Gm32743	predicted gene 32743	25.8092539	-1.363865868	0.336722402	-4.050416183	5.11E-05	1.40E-02
ENSMUSG00000050640	Tmem150c	transmembrane protein 150C	40.08771757	-1.128379631	0.279418769	-4.038310072	5.38E-05	1.45E-02
ENSMUSG00000056880	Gadl1	glutamate decarboxylase-like 1	41.12226685	-1.172852268	0.291809453	-4.019240144	5.84E-05	1.55E-02
ENSMUSG00000006587	Snai3	snail family zinc finger 3	38.46789747	-1.556170083	0.3914073	-3.975833063	7.01E-05	1.83E-02
ENSMUSG00000032860	P2ry2	purinergic receptor P2Y, G-protein coupled 2	427.8475396	-0.417060355	0.105028679	-3.970918781	7.16E-05	1.84E-02
ENSMUSG00000021622	Ckmt2	creatine kinase, mitochondrial 2	30570.15221	-0.358321877	0.09037697	-3.964747643	7.35E-05	1.86E-02
ENSMUSG00000104344	Gm38077	predicted gene 38077	110.0410307	-0.694683493	0.17726808	-3.918830127	8.90E-05	2.22E-02
ENSMUSG00000032181	Scg3	secretogranin III	41.68914485	1.290206572	0.330188439	3.907485597	9.33E-05	2.30E-02
ENSMUSG00000020253	Ppm1m	protein phosphatase 1M	612.6332904	0.364501693	0.094443251	3.859478465	1.14E-04	2.76E-02
ENSMUSG00000097088	Gm26615	predicted gene 26615	43.50706638	0.836267574	0.216957467	3.854523129	1.16E-04	2.78E-02
ENSMUSG00000010064	Slc38a3	solute carrier family 38, member 3	1610.204165	-0.651101006	0.169436841	-3.842735747	1.22E-04	2.80E-02
ENSMUSG00000031709	Tbc1d9	TBC1 domain family, member 9	542.8723027	0.411804108	0.107166775	3.842647212	1.22E-04	2.80E-02
ENSMUSG00000034533	Scn10a	sodium channel, voltage-gated, type X, alpha	703.8602467	0.70040763	0.183064182	3.826022233	1.30E-04	2.88E-02
ENSMUSG00000040875	Osbpl10	oxysterol binding protein-like 10	79.84746132	-0.766643335	0.200280981	-3.82783892	1.29E-04	2.88E-02
ENSMUSG00000101257	2310015K22Rik	RIKEN cDNA 2310015K22 gene	12.05415905	-1.633324502	0.426600907	-3.828694395	1.29E-04	2.88E-02
ENSMUSG00000019817	Plagl1	pleiomorphic adenoma gene-like 1	2018.952602	0.453482958	0.119673938	3.789320943	1.51E-04	3.29E-02
ENSMUSG00000019890	Nts	neurotensin	85.16574876	-0.855082132	0.225793704	-3.787006094	1.52E-04	3.29E-02
ENSMUSG00000030515	Tarsl2	threonyl-tRNA synthetase-like 2	1170.685678	-0.243655404	0.064511345	-3.776938834	1.59E-04	3.39E-02
ENSMUSG00000006611	Hfe	hemochromatosis	890.846647	0.435320115	0.11562911	3.764796886	1.67E-04	3.51E-02

ENSMUSG00000045967	Gpr158	G protein-coupled receptor 158	373.298715	-0.686733554	0.18272265	-3.75833841	1.71E-04	3.52E-02
ENSMUSG00000047686	Rtl3	retrotransposon Gag like 3	266.2423324	0.760639578	0.20238611	3.758358611	1.71E-04	3.52E-02
ENSMUSG00000035606	Ky	kyphoscoliosis peptidase	125.6420813	-0.986271443	0.263125553	-3.748292139	1.78E-04	3.61E-02
ENSMUSG00000074207	Adh1	alcohol dehydrogenase 1 (class I)	1168.841709	0.378713887	0.101093013	3.746192504	1.80E-04	3.61E-02
ENSMUSG00000000184	Ccnd2	cyclin D2	7244.566123	0.321075122	0.085868752	3.739138085	1.85E-04	3.67E-02
ENSMUSG00000021557	Agtpbp1	ATP/GTP binding protein 1	3779.137522	-0.28831125	0.077403559	-3.724780271	1.95E-04	3.84E-02
ENSMUSG00000021557	A230056J06Rik	RIKEN cDNA A230056J06 gene	3779.137522	-0.28831125	0.077403559	-3.724780271	1.95E-04	3.84E-02
ENSMUSG00000043795	Prr33	proline rich 33	112.7136835	-0.776040696	0.208764671	-3.717298975	2.01E-04	3.91E-02
ENSMUSG00000026604	Ptpn14	protein tyrosine phosphatase, non-receptor type 14	3680.35312	0.257384789	0.069385735	3.70947703	2.08E-04	3.99E-02
ENSMUSG00000029359	Tesc	tescalcin	181.5637758	-0.947384507	0.256043393	-3.700093552	2.16E-04	4.05E-02
ENSMUSG00000031637	Lrp2bp	Lrp2 binding protein	140.0742862	-0.59046599	0.159527357	-3.701346278	2.14E-04	4.05E-02
ENSMUSG00000021957	Tkt	transketolase	1797.82233	0.732078661	0.198124968	3.695034851	2.20E-04	4.06E-02
ENSMUSG00000061780	Cfd	complement factor D (adipsin)	904.2314372	2.994362377	0.810510725	3.694414255	2.20E-04	4.06E-02
ENSMUSG00000037887	Dusp8	dual specificity phosphatase 8	774.5163123	-0.572804466	0.155345266	-3.68729915	2.27E-04	4.13E-02
ENSMUSG00000091345	Col6a5	collagen, type VI, alpha 5	326.9932512	2.283384011	0.622617345	3.667395437	2.45E-04	4.42E-02
ENSMUSG00000060639	Hist1h4i	histone cluster 1, H4i	144.8255591	-0.691858999	0.188964427	-3.661318753	2.51E-04	4.48E-02
ENSMUSG00000064371	mt-Tt	mitochondrially encoded tRNA threonine	67.46562005	-0.989792385	0.27087529	-3.654051962	2.58E-04	4.56E-02
ENSMUSG00000034485	Uaca	uveal autoantigen with coiled-coil domains and ankyrin repeats	1707.508249	-0.254012029	0.069644209	-3.647281416	2.65E-04	4.63E-02
ENSMUSG00000059742	Kcnh7	potassium voltage-gated channel, subfamily H (eag-related), member 7	286.2843348	0.587508859	0.161412283	3.639802667	2.73E-04	4.72E-02

Supp Table S4. List of Differentially Expressed genes at FDR 5% in *Gnb5-/-* mice - ventricle

Ensembl ID	Gene Symbol	Gene name	baseMean	log2FoldChange	lfcSE	stat	pvalue	padj
ENSMUSG00000032192	Gnb5	guanine nucleotide binding protein (G protein), beta 5	313.5699776	-4.21550606	0.154170849	-27.34308137	1.31E-164	2.19E-160
ENSMUSG00000033419	Snap91	synaptosomal-associated protein 91	130.8116563	-2.993668387	0.230324744	-12.9975978	1.26E-38	1.06E-34
ENSMUSG00000048758	Rpl29	ribosomal protein L29	148.0555782	-2.768271599	0.258451771	-10.71097942	9.04E-27	5.05E-23
ENSMUSG00000032224	Fam81a	family with sequence similarity 81, member A	535.3572241	1.400193385	0.158370442	8.841254493	9.46E-19	3.96E-15
ENSMUSG00000032579	Hemk1	HemK methyltransferase family member 1	699.5483486	1.255117802	0.16788463	7.476073332	7.66E-14	2.57E-10
ENSMUSG00000113637	Gm7049	predicted gene 7049	16.81236237	2.249097307	0.306354635	7.341482876	2.11E-13	5.90E-10
ENSMUSG00000111765	Gm10635	predicted gene 10635	108.9820339	-1.98648208	0.288335345	-6.889485152	5.60E-12	1.34E-08
ENSMUSG00000066456	Hmgn3	high mobility group nucleosomal binding domain 3	80.22459437	-1.098602846	0.160705843	-6.836110138	8.14E-12	1.70E-08
ENSMUSG00000023249	Parp3	poly (ADP-ribose) polymerase family, member 3	1606.053611	-0.717032187	0.109004266	-6.578019501	4.77E-11	8.88E-08
ENSMUSG00000010057	Nprl2	NPR2 like, GATOR1 complex subunit	491.5575602	0.487515133	0.082544171	5.906112138	3.50E-09	5.34E-06
ENSMUSG00000100782	Gm28231	predicted gene 28231	48.63773997	1.405293992	0.238858846	5.883365906	4.02E-09	5.61E-06
ENSMUSG00000020902	Ntn1	netrin 1	2523.450781	0.593131025	0.102551465	5.783740167	7.31E-09	9.42E-06
ENSMUSG00000019817	Plagl1	pleiomorphic adenoma gene-like 1	76.29245071	0.819492865	0.146652951	5.587973925	2.30E-08	2.57E-05
ENSMUSG00000042073	Abhd14b	abhydrolase domain containing 14b	312.5043269	-0.742734019	0.132845695	-5.590952862	2.26E-08	2.57E-05
ENSMUSG00000038801	Scgb1c1	secretoglobin, family 1C, member 1	193.8961	1.137948154	0.205183249	5.546009029	2.92E-08	2.88E-05
ENSMUSG00000097099	Gm9917	predicted gene 9917	111.2305592	-0.971774724	0.179085224	-5.426325529	5.75E-08	5.35E-05
ENSMUSG00000107653	Gm31520	sterol-C5-desaturase pseudogene	38.9097343	1.461818509	0.276075681	5.294991955	1.19E-07	1.05E-04
ENSMUSG00000032419	Tbx18	T-box18	104.4903783	-0.654370039	0.125020141	-5.234116949	1.66E-07	1.32E-04
ENSMUSG00000020253	Ppm1m	protein phosphatase 1M	224.4754793	0.629411893	0.120929771	5.204772037	1.94E-07	1.48E-04
ENSMUSG00000032563	Mrpl3	mitochondrial ribosomal protein L3	1783.956096	-0.436886258	0.085393676	-5.116143011	3.12E-07	2.27E-04

ENSMUSG00000032261	Sh3bgrl2	SH3 domain binding glutamic acid-rich protein like 2	105.6921769	-0.653725	0.128760505	-5.077061488	3.83E-07	2.68E-04
ENSMUSG00000023979	Guca1b	guanylate cyclase activator 1B	25.91071064	1.315395153	0.259962618	5.059939622	4.19E-07	2.81E-04
ENSMUSG00000091345	Col6a5	collagen, type VI, alpha 5	29.84898234	1.907639946	0.3775694	5.052422015	4.36E-07	2.81E-04
ENSMUSG00000032359	Ctsh	cathepsin H	710.7231171	-0.623022117	0.125532066	-4.963051582	6.94E-07	4.15E-04
ENSMUSG00000022219	Cideb	cell death-inducing DNA fragmentation factor, alpha subunit-like effector B	74.13239706	0.858582759	0.175534791	4.891239831	1.00E-06	5.79E-04
ENSMUSG00000010064	Slc38a3	solute carrier family 38, member 3	2341.478262	-0.809203125	0.167037335	-4.844444656	1.27E-06	7.09E-04
ENSMUSG00000032259	Drd2	dopamine receptor D2	85.88598789	0.839883098	0.174723741	4.8069203	1.53E-06	8.28E-04
ENSMUSG00000032537	Ephb1	Eph receptor B1	585.1805641	2.398021253	0.521600636	4.597427777	4.28E-06	2.24E-03
ENSMUSG00000104344	Gm38077	predicted gene 38077	168.5348807	-0.988910029	0.216709138	-4.563305623	5.04E-06	2.56E-03
ENSMUSG00000030990	Pgap2	post-GPI attachment to proteins 2	688.9552575	0.468413015	0.104101368	4.499585592	6.81E-06	3.36E-03
ENSMUSG00000062270	Morf4l1	mortality factor 4 like 1	1196.914037	-0.415696122	0.093949616	-4.424670816	9.66E-06	4.62E-03
ENSMUSG00000062270	Morf4l1b	mortality factor 4 like 1B	1196.914037	-0.415696122	0.093949616	-4.424670816	9.66E-06	4.62E-03
ENSMUSG00000032872	Cyb5r4	cytochrome b5 reductase 4	1012.878713	-0.551302186	0.125317439	-4.399245566	1.09E-05	4.92E-03
ENSMUSG00000079355	Ackr4	atypical chemokine receptor 4	94.67720248	-0.760983138	0.172765696	-4.404712012	1.06E-05	4.92E-03
ENSMUSG00000020431	Adcy1	adenylate cyclase 1	97.1204426	0.866213531	0.197445358	4.38710508	1.15E-05	4.93E-03
ENSMUSG00000023439	Gnb3	guanine nucleotide binding protein (G protein), beta 3	256.1773659	0.925120884	0.249262978	3.711425138	2.06E-04	5.21E-03
ENSMUSG00000043587	Pxylp1	2-phosphoxylose phosphatase 1	148.4011593	-0.941500636	0.215647645	-4.365921245	1.27E-05	5.21E-03
ENSMUSG00000100410	2310020H05Rik	RIKEN cDNA 2310020H05 gene	82.70867895	-0.95306705	0.218380045	-4.364258874	1.28E-05	5.21E-03
ENSMUSG00000023262	Acy1	aminoacylase 1	275.312161	0.52627658	0.12086618	4.354208773	1.34E-05	5.28E-03
ENSMUSG00000032420	Nt5e	5' nucleotidase, ecto	531.2462273	0.575371191	0.132243883	4.35083406	1.36E-05	5.28E-03
ENSMUSG00000032342	Mto1	mitochondrial tRNA translation optimization 1	628.7435289	-0.35212118	0.081316245	-4.330268576	1.49E-05	5.54E-03

ENSMUSG00000036006	Ripor2	RHO family interacting cell polarization regulator 2	280.1521625	0.766998221	0.178845813	4.288600385	1.80E-05	6.55E-03
ENSMUSG00000032567	Aste1	asteroid homolog 1	136.4175984	-0.546329802	0.129600006	-4.215507543	2.49E-05	8.88E-03
ENSMUSG00000007033	Hspa1l	heat shock protein 1-like	313.1401892	-0.868331662	0.207647674	-4.181754823	2.89E-05	1.01E-02
ENSMUSG00000062991	Nrg1	neuregulin 1	36.63309961	1.167251298	0.281216976	4.150714202	3.31E-05	1.13E-02
ENSMUSG00000057802	Gm10030	predicted gene 10030	23.54320155	1.146733244	0.277719383	4.129107706	3.64E-05	1.22E-02
ENSMUSG00000032500	Dclk3	doublecortin-like kinase 3	16.62670461	1.320424335	0.32048356	4.120100055	3.79E-05	1.24E-02
ENSMUSG00000030592	Ryr1	ryanodine receptor 1, skeletal muscle	18.10439933	-1.213191335	0.295663089	-4.103289788	4.07E-05	1.31E-02
ENSMUSG00000034533	Scn10a	sodium channel, voltage-gated, type X, alpha	113.9830881	0.858252285	0.213468675	4.020506927	5.81E-05	1.84E-02
ENSMUSG00000031066	Usp11	ubiquitin specific peptidase 11	212.3557436	0.528925104	0.131795322	4.013231248	5.99E-05	1.86E-02
ENSMUSG00000071708	Sms	spermine synthase	825.2887178	-0.362951165	0.090642781	-4.004192737	6.22E-05	1.86E-02
ENSMUSG00000113321	Gm8775	predicted gene 8775	29.48173879	1.076447965	0.268553676	4.008315883	6.12E-05	1.86E-02
ENSMUSG00000073485	H3f3aos	H3 histone, family 3A	31.32162143	-0.946720716	0.236742268	-3.998950945	6.36E-05	1.87E-02
ENSMUSG00000026414	Tnnt2	troponin T2, cardiac	217.8533484	0.619746386	0.156123287	3.969596064	7.20E-05	2.08E-02
ENSMUSG00000031637	Lrp2bp	Lrp2 binding protein	63.26457812	-1.031672567	0.264188857	-3.90505709	9.42E-05	2.68E-02
ENSMUSG00000045594	Glb1	galactosidase, beta 1	384.1377132	-0.474925266	0.123283793	-3.852292773	1.17E-04	3.27E-02
ENSMUSG00000010051	Hyal1	hyaluronoglucosaminidase 1	122.0241169	0.64246724	0.167341124	3.839266904	1.23E-04	3.39E-02
ENSMUSG00000020534	Shmt1	serine hydroxymethyltransferase 1 (soluble)	289.1479786	0.655279666	0.171422662	3.822596498	1.32E-04	3.57E-02
ENSMUSG00000060187	Lrrc10	leucine rich repeat containing 10	2494.259676	0.407948338	0.111196436	3.668717757	2.44E-04	3.91E-02
ENSMUSG00000027313	Chac1	ChaC, cation transport regulator 1	44.4569393	-1.241707583	0.328017443	-3.785492538	1.53E-04	4.08E-02
ENSMUSG00000024145	Pigf	phosphatidylinositol glycan anchor biosynthesis, class F	53.55766273	0.70037248	0.186231311	3.760766521	1.69E-04	4.37E-02
ENSMUSG00000052485	Tmem171	transmembrane protein 171	169.2165357	0.76792289	0.204074434	3.762954896	1.68E-04	4.37E-02
ENSMUSG00000031461	Myom2	myomesin 2	39422.33605	0.551200865	0.150744712	3.65651875	2.56E-04	4.71E-02

Supp. Table S5. List of Biological Processes (BP) at FDR 5% - atria

GO ID	Description	BgRatio	pvalue	p.adjust	qvalue	geneID	Count
GO:0046184	aldehyde biosynthetic process	18/21092	5.11E-05	7.82E-02	0.075133254	Bmp5/Adh1/Tkt	3
GO:0006081	cellular aldehyde metabolic process	68/21092	1.72E-04	1.32E-01	0.126431472	Bmp5/Aldh3a1/Adh1/Tkt	4
GO:0032892	positive regulation of organic acid transport	47/21092	9.32E-04	4.20E-01	0.403462799	Agt/P2ry2/Slc38a3	3
GO:0015802	basic amino acid transport	14/21092	1.45E-03	4.20E-01	0.403462799	Agt/Slc38a3	2
GO:1903793	positive regulation of anion transport	63/21092	2.18E-03	4.20E-01	0.403462799	Agt/P2ry2/Slc38a3	3
GO:0006883	cellular sodium ion homeostasis	19/21092	2.69E-03	4.20E-01	0.403462799	Agt/Tesc	2
GO:0008015	blood circulation	466/21092	2.94E-03	4.20E-01	0.403462799	Comp/Npr3/Agt/Myh7/P2ry2/Scn10a/Nts	7
GO:0003013	circulatory system process	475/21092	3.27E-03	4.20E-01	0.403462799	Comp/Npr3/Agt/Myh7/P2ry2/Scn10a/Nts	7
GO:0032890	regulation of organic acid transport	77/21092	3.85E-03	4.20E-01	0.403462799	Agt/P2ry2/Slc38a3	3
GO:0043687	post-translational protein modification	23/21092	3.93E-03	4.20E-01	0.403462799	Crtap/Agtpbp1	2
GO:0014829	vascular smooth muscle contraction	25/21092	4.64E-03	4.20E-01	0.403462799	Comp/Agt	2
GO:0050880	regulation of blood vessel size	168/21092	4.97E-03	4.20E-01	0.403462799	Comp/Agt/P2ry2/Nts	4
GO:0035150	regulation of tube size	169/21092	5.07E-03	4.20E-01	0.403462799	Comp/Agt/P2ry2/Nts	4
GO:0032526	response to retinoic acid	86/21092	5.25E-03	4.20E-01	0.403462799	Mest/Adh1/Tesc	3
GO:0051957	positive regulation of amino acid transport	28/21092	5.80E-03	4.20E-01	0.403462799	Agt/Slc38a3	2
GO:0006936	muscle contraction	281/21092	5.87E-03	4.20E-01	0.403462799	Comp/Lmod2/Agt/Myh7/Scn10a	5
GO:0002027	regulation of heart rate	91/21092	6.14E-03	4.20E-01	0.403462799	Agt/Myh7/Scn10a	3
GO:0045652	regulation of megakaryocyte differentiation	30/21092	6.64E-03	4.20E-01	0.403462799	Tesc/Hist1h4i	2
GO:1900274	regulation of phospholipase C activity	30/21092	6.64E-03	4.20E-01	0.403462799	Snap91/Agt	2

GO:0003018	vascular process in circulatory system	193/21092	8.05E-03	4.20E-01	0.403462799	Comp/Agt/P2ry2/Nts	4
GO:0006739	NADP metabolic process	36/21092	9.46E-03	4.20E-01	0.403462799	Cyb5r4/Tkt	2
GO:0042445	hormone metabolic process	207/21092	1.02E-02	4.20E-01	0.403462799	Bmp5/Agt/Hfe/Adh1	4
GO:0031279	regulation of cyclase activity	41/21092	1.22E-02	4.20E-01	0.403462799	Guca1b/Npr3	2
GO:0044070	regulation of anion transport	117/21092	1.22E-02	4.20E-01	0.403462799	Agt/P2ry2/Slc38a3	3
GO:0051339	regulation of lyase activity	43/21092	1.33E-02	4.20E-01	0.403462799	Guca1b/Npr3	2
GO:0032007	negative regulation of TOR signaling	45/21092	1.45E-02	4.20E-01	0.403462799	Nprl2/Minar1	2
GO:0010862	positive regulation of pathway-restricted SMAD protein phosphorylation	49/21092	1.71E-02	4.20E-01	0.403462799	Bmp5/Hfe	2
GO:0050905	neuromuscular process	133/21092	1.72E-02	4.20E-01	0.403462799	Comp/Tmem150c/Agtpbp1	3
GO:0032941	secretion by tissue	50/21092	1.77E-02	4.20E-01	0.403462799	Npr3/P2ry2	2
GO:0051955	regulation of amino acid transport	50/21092	1.77E-02	4.20E-01	0.403462799	Agt/Slc38a3	2
GO:0055078	sodium ion homeostasis	50/21092	1.77E-02	4.20E-01	0.403462799	Agt/Tesc	2
GO:0002064	epithelial cell development	245/21092	1.80E-02	4.20E-01	0.403462799	Bmp5/Bfsp2/Col23a1/Agt	4
GO:0030219	megakaryocyte differentiation	51/21092	1.84E-02	4.20E-01	0.403462799	Tesc/Hist1h4i	2
GO:0051954	positive regulation of amine transport	51/21092	1.84E-02	4.20E-01	0.403462799	Agt/Slc38a3	2
GO:0001505	regulation of neurotransmitter levels	376/21092	1.88E-02	4.20E-01	0.403462799	Snap91/Mctp1/Agt/P2ry2/Agtpbp1	5
GO:0030198	extracellular matrix organization	249/21092	1.89E-02	4.20E-01	0.403462799	Comp/Col23a1/Reck/Agt	4
GO:0034308	primary alcohol metabolic process	52/21092	1.91E-02	4.20E-01	0.403462799	Bmp5/Adh1	2
GO:0003012	muscle system process	383/21092	2.02E-02	4.20E-01	0.403462799	Comp/Lmod2/Agt/Myh7/Scn10a	5
GO:0010517	regulation of phospholipase activity	54/21092	2.05E-02	4.20E-01	0.403462799	Snap91/Agt	2
GO:0050879	multicellular organismal movement	54/21092	2.05E-02	4.20E-01	0.403462799	Comp/Myh7	2
GO:0050881	musculoskeletal movement	54/21092	2.05E-02	4.20E-01	0.403462799	Comp/Myh7	2
GO:1905952	regulation of lipid localization	143/21092	2.07E-02	4.20E-01	0.403462799	Agt/Mest/P2ry2	3

GO:0006865	amino acid transport	145/21092	2.15E-02	4.20E-01	0.403462799	Slc17a5/Agt/Slc38a3	3
GO:0061337	cardiac conduction	58/21092	2.34E-02	4.20E-01	0.403462799	Agt/Scn10a	2
GO:0015807	L-amino acid transport	59/21092	2.42E-02	4.20E-01	0.403462799	Agt/Slc38a3	2
GO:0014911	positive regulation of smooth muscle cell migration	60/21092	2.50E-02	4.20E-01	0.403462799	Agt/P2ry2	2
GO:0035296	regulation of tube diameter	156/21092	2.60E-02	4.20E-01	0.403462799	Comp/Agt/P2ry2	3
GO:0097746	regulation of blood vessel diameter	156/21092	2.60E-02	4.20E-01	0.403462799	Comp/Agt/P2ry2	3
GO:2001238	positive regulation of extrinsic apoptotic signaling pathway	62/21092	2.65E-02	4.20E-01	0.403462799	Ppp2r1b/Agt	2
GO:0006801	superoxide metabolic process	63/21092	2.73E-02	4.20E-01	0.403462799	Cyb5r4/Agt	2
GO:0060393	regulation of pathway-restricted SMAD protein phosphorylation	63/21092	2.73E-02	4.20E-01	0.403462799	Bmp5/Hfe	2
GO:1901264	carbohydrate derivative transport	64/21092	2.81E-02	4.20E-01	0.403462799	Slc17a5/P2ry2	2
GO:0060389	pathway-restricted SMAD protein phosphorylation	66/21092	2.98E-02	4.20E-01	0.403462799	Bmp5/Hfe	2
GO:0030509	BMP signaling pathway	165/21092	3.00E-02	4.20E-01	0.403462799	Bmp5/Comp/Hfe	3
GO:0001885	endothelial cell development	67/21092	3.06E-02	4.20E-01	0.403462799	Col23a1/Agt	2
GO:0051604	protein maturation	291/21092	3.12E-02	4.20E-01	0.403462799	Comp/Spon1/Aph1c/Tesc	4
GO:0043062	extracellular structure organization	293/21092	3.19E-02	4.20E-01	0.403462799	Comp/Col23a1/Reck/Agt	4
GO:0046942	carboxylic acid transport	297/21092	3.33E-02	4.20E-01	0.403462799	Slc17a5/Agt/P2ry2/Slc38a3	4
GO:0008016	regulation of heart contraction	172/21092	3.33E-02	4.20E-01	0.403462799	Agt/Myh7/Scn10a	3
GO:0015849	organic acid transport	298/21092	3.36E-02	4.20E-01	0.403462799	Slc17a5/Agt/P2ry2/Slc38a3	4
GO:0042446	hormone biosynthetic process	72/21092	3.49E-02	4.20E-01	0.403462799	Bmp5/Hfe	2
GO:0071772	response to BMP	176/21092	3.53E-02	4.20E-01	0.403462799	Bmp5/Comp/Hfe	3
GO:0071773	cellular response to BMP stimulus	176/21092	3.53E-02	4.20E-01	0.403462799	Bmp5/Comp/Hfe	3
GO:0051145	smooth muscle cell differentiation	73/21092	3.58E-02	4.20E-01	0.403462799	Comp/Agt	2
GO:0060191	regulation of lipase activity	73/21092	3.58E-02	4.20E-01	0.403462799	Snap91/Agt	2
GO:0003333	amino acid transmembrane transport	74/21092	3.67E-02	4.20E-01	0.403462799	Agt/Slc38a3	2

GO:0007219	Notch signaling pathway	181/21092	3.79E-02	4.20E-01	0.403462799	Reck/Aph1c/Cfd	3
GO:0055002	striated muscle cell development	181/21092	3.79E-02	4.20E-01	0.403462799	Comp/Lmod2/Agt	3
GO:0043270	positive regulation of ion transport	310/21092	3.80E-02	4.20E-01	0.403462799	Agt/P2ry2/Slc38a3/Tesc	4
GO:0002181	cytoplasmic translation	76/21092	3.86E-02	4.20E-01	0.403462799	Rpl29/Tma7	2
GO:0034765	regulation of ion transmembrane transport	459/21092	3.96E-02	4.20E-01	0.403462799	Gnb5/Agt/Scn10a/Tesc/Kcnh7	5
GO:0030534	adult behavior	185/21092	4.00E-02	4.20E-01	0.403462799	Adh1/Ccnd2/Agtpbp1	3
GO:0006995	cellular response to nitrogen starvation	10/21092	4.00E-02	4.20E-01	0.403462799	Nprl2	1
GO:0007220	Notch receptor processing	10/21092	4.00E-02	4.20E-01	0.403462799	Aph1c	1
GO:0014883	transition between fast and slow fiber	10/21092	4.00E-02	4.20E-01	0.403462799	Myh7	1
GO:0016264	gap junction assembly	10/21092	4.00E-02	4.20E-01	0.403462799	Agt	1
GO:0030049	muscle filament sliding	10/21092	4.00E-02	4.20E-01	0.403462799	Myh7	1
GO:0030854	positive regulation of granulocyte differentiation	10/21092	4.00E-02	4.20E-01	0.403462799	Tesc	1
GO:0031282	regulation of guanylate cyclase activity	10/21092	4.00E-02	4.20E-01	0.403462799	Guca1b	1
GO:0031943	regulation of glucocorticoid metabolic process	10/21092	4.00E-02	4.20E-01	0.403462799	Bmp5	1
GO:0032342	aldosterone biosynthetic process	10/21092	4.00E-02	4.20E-01	0.403462799	Bmp5	1
GO:0043562	cellular response to nitrogen levels	10/21092	4.00E-02	4.20E-01	0.403462799	Nprl2	1
GO:0048149	behavioral response to ethanol	10/21092	4.00E-02	4.20E-01	0.403462799	Adh1	1
GO:0060710	chorio-allantoic fusion	10/21092	4.00E-02	4.20E-01	0.403462799	Bmp5	1
GO:0070142	synaptic vesicle budding	10/21092	4.00E-02	4.20E-01	0.403462799	Snap91	1
GO:0070257	positive regulation of mucus secretion	10/21092	4.00E-02	4.20E-01	0.403462799	P2ry2	1
GO:0070278	extracellular matrix constituent secretion	10/21092	4.00E-02	4.20E-01	0.403462799	Agt	1
GO:1902023	L-arginine transport	10/21092	4.00E-02	4.20E-01	0.403462799	Agt	1
GO:2000807	regulation of synaptic vesicle clustering	10/21092	4.00E-02	4.20E-01	0.403462799	Snap91	1
GO:0006942	regulation of striated muscle contraction	79/21092	4.14E-02	4.20E-01	0.403462799	Myh7/Scn10a	2
GO:0007269	neurotransmitter secretion	190/21092	4.27E-02	4.20E-01	0.403462799	Snap91/Mctp1/P2ry2	3

GO:0099643	signal release from synapse	190/21092	4.27E-02	4.20E-01	0.403462799	Snap91/Mctp 1/P2ry2	3
GO:1901888	regulation of cell junction assembly	81/21092	4.33E-02	4.20E-01	0.403462799	Limch1/Agt	2
GO:0006012	galactose metabolic process	11/21092	4.40E-02	4.20E-01	0.403462799	Glb1	1
GO:0006266	DNA ligation	11/21092	4.40E-02	4.20E-01	0.403462799	Parp3	1
GO:0006705	mineralocorticoid biosynthetic process	11/21092	4.40E-02	4.20E-01	0.403462799	Bmp5	1
GO:0006957	complement activation, alternative pathway	11/21092	4.40E-02	4.20E-01	0.403462799	Cfd	1
GO:0007128	meiotic prophase I	11/21092	4.40E-02	4.20E-01	0.403462799	Mlh1	1
GO:0010872	regulation of cholesterol esterification	11/21092	4.40E-02	4.20E-01	0.403462799	Agt	1
GO:0010958	regulation of amino acid import across plasma membrane	11/21092	4.40E-02	4.20E-01	0.403462799	Agt	1
GO:0014824	artery smooth muscle contraction	11/21092	4.40E-02	4.20E-01	0.403462799	Agt	1
GO:0019511	peptidyl-proline hydroxylation	11/21092	4.40E-02	4.20E-01	0.403462799	Crtap	1
GO:0032341	aldosterone metabolic process	11/21092	4.40E-02	4.20E-01	0.403462799	Bmp5	1
GO:0051324	prophase	11/21092	4.40E-02	4.20E-01	0.403462799	Mlh1	1
GO:0060405	regulation of penile erection	11/21092	4.40E-02	4.20E-01	0.403462799	P2ry2	1
GO:0060586	multicellular organismal iron ion homeostasis	11/21092	4.40E-02	4.20E-01	0.403462799	Hfe	1
GO:0086016	AV node cell action potential	11/21092	4.40E-02	4.20E-01	0.403462799	Scn10a	1
GO:0086027	AV node cell to bundle of His cell signaling	11/21092	4.40E-02	4.20E-01	0.403462799	Scn10a	1
GO:0097084	vascular smooth muscle cell development	11/21092	4.40E-02	4.20E-01	0.403462799	Comp	1
GO:1903867	extraembryonic membrane development	11/21092	4.40E-02	4.20E-01	0.403462799	Bmp5	1
GO:0055001	muscle cell development	195/21092	4.56E-02	4.20E-01	0.403462799	Comp/Lmod2/ Agt	3
GO:0014910	regulation of smooth muscle cell migration	85/21092	4.72E-02	4.20E-01	0.403462799	Agt/P2ry2	2
GO:0000279	M phase	12/21092	4.79E-02	4.20E-01	0.403462799	Mlh1	1
GO:0000963	mitochondrial RNA processing	12/21092	4.79E-02	4.20E-01	0.403462799	Mto1	1
GO:0001542	ovulation from ovarian follicle	12/21092	4.79E-02	4.20E-01	0.403462799	Agt	1
GO:0002016	regulation of blood volume by renin-angiotensin	12/21092	4.79E-02	4.20E-01	0.403462799	Agt	1
GO:0006098	pentose-phosphate shunt	12/21092	4.79E-02	4.20E-01	0.403462799	Tkt	1

GO:0008212	mineralocorticoid metabolic process	12/21092	4.79E-02	4.20E-01	0.403462799	Bmp5	1
GO:0015809	arginine transport	12/21092	4.79E-02	4.20E-01	0.403462799	Agt	1
GO:0030432	peristalsis	12/21092	4.79E-02	4.20E-01	0.403462799	Agt	1
GO:0032308	positive regulation of prostaglandin secretion	12/21092	4.79E-02	4.20E-01	0.403462799	P2ry2	1
GO:0032353	negative regulation of hormone biosynthetic process	12/21092	4.79E-02	4.20E-01	0.403462799	Bmp5	1
GO:0033275	actin-myosin filament sliding	12/21092	4.79E-02	4.20E-01	0.403462799	Myh7	1
GO:0034309	primary alcohol biosynthetic process	12/21092	4.79E-02	4.20E-01	0.403462799	Bmp5	1
GO:0042271	susceptibility to natural killer cell mediated cytotoxicity	12/21092	4.79E-02	4.20E-01	0.403462799	Hfe	1
GO:0048143	astrocyte activation	12/21092	4.79E-02	4.20E-01	0.403462799	Agt	1
GO:0070471	uterine smooth muscle contraction	12/21092	4.79E-02	4.20E-01	0.403462799	Agt	1
GO:0071281	cellular response to iron ion	12/21092	4.79E-02	4.20E-01	0.403462799	Hfe	1
GO:0071468	cellular response to acidic pH	12/21092	4.79E-02	4.20E-01	0.403462799	Slc38a3	1
GO:0098762	meiotic cell cycle phase	12/21092	4.79E-02	4.20E-01	0.403462799	Mlh1	1
GO:0098764	meiosis I cell cycle phase	12/21092	4.79E-02	4.20E-01	0.403462799	Mlh1	1
GO:1900244	positive regulation of synaptic vesicle endocytosis	12/21092	4.79E-02	4.20E-01	0.403462799	Snap91	1
GO:1902430	negative regulation of amyloid-beta formation	12/21092	4.79E-02	4.20E-01	0.403462799	Spon1	1
GO:1903961	positive regulation of anion transmembrane transport	12/21092	4.79E-02	4.20E-01	0.403462799	Agt	1

Supp. Table S6. List of Biological Processes (BP) at FDR 5% - ventricle

GO ID	Description	BgRatio	pvalue	p.adjust	qvalue	geneID	Count
GO:0021826	substrate-independent telencephalic tangential migration	10/21092	2.55E-04	1.52E-01	0.120425014	Drd2/Nrg1	2
GO:0021843	substrate-independent telencephalic tangential interneuron migration	10/21092	2.55E-04	1.52E-01	0.120425014	Drd2/Nrg1	2
GO:1901386	negative regulation of voltage-gated calcium channel activity	15/21092	5.90E-04	1.52E-01	0.120425014	Gnb5/Drd2	2
GO:0014706	striated muscle tissue development	441/21092	6.56E-04	1.52E-01	0.120425014	Plagl1/Tbx18/Ephb1/Ripor2/Nrg1/Ryr1	6

GO:0003161	cardiac conduction system development	16/21092	6.73E-04	1.52E-01	0.120425014	Tbx18/Nrg1	2
GO:0007409	axonogenesis	451/21092	7.38E-04	1.52E-01	0.120425014	Snap91/Ntn1/Drd2/Ephb1/Adcy1/Nrg1	6
GO:0060537	muscle tissue development	462/21092	8.36E-04	1.52E-01	0.120425014	Plagl1/Tbx18/Ephb1/Ripor2/Nrg1/Ryr1	6
GO:0061564	axon development	486/21092	1.09E-03	1.55E-01	0.122484614	Snap91/Ntn1/Drd2/Ephb1/Adcy1/Nrg1	6
GO:0007519	skeletal muscle tissue development	197/21092	1.31E-03	1.55E-01	0.122484614	Plagl1/Ephb1/Ripor2/Ryr1	4
GO:0071467	cellular response to pH	23/21092	1.40E-03	1.55E-01	0.122484614	Slc38a3/Hyal1	2
GO:0060538	skeletal muscle organ development	206/21092	1.54E-03	1.55E-01	0.122484614	Plagl1/Ephb1/Ripor2/Ryr1	4
GO:0050772	positive regulation of axonogenesis	98/21092	1.72E-03	1.55E-01	0.122484614	Snap91/Ntn1/Nrg1	3
GO:0043171	peptide catabolic process	26/21092	1.80E-03	1.55E-01	0.122484614	Ctsh/Chac1	2
GO:1901020	negative regulation of calcium ion transmembrane transporter activity	26/21092	1.80E-03	1.55E-01	0.122484614	Gnb5/Drd2	2
GO:0072522	purine-containing compound biosynthetic process	227/21092	2.20E-03	1.55E-01	0.122484614	Guca1b/Adcy1/Nt5e/Shmt1	4
GO:0042692	muscle cell differentiation	383/21092	2.28E-03	1.55E-01	0.122484614	Tbx18/Ripor2/Nrg1/Ryr1/Tnnt1	5
GO:0006506	GPI anchor biosynthetic process	31/21092	2.55E-03	1.55E-01	0.122484614	Pgap2/Pigf	2
GO:0042472	inner ear morphogenesis	113/21092	2.59E-03	1.55E-01	0.122484614	Ntn1/Tbx18/Ripor2	3
GO:0001964	startle response	32/21092	2.71E-03	1.55E-01	0.122484614	Drd2/Nrg1	2
GO:0006505	GPI anchor metabolic process	32/21092	2.71E-03	1.55E-01	0.122484614	Pgap2/Pigf	2
GO:1903170	negative regulation of calcium ion transmembrane transport	35/21092	3.24E-03	1.55E-01	0.122484614	Gnb5/Drd2	2
GO:0007517	muscle organ development	420/21092	3.38E-03	1.55E-01	0.122484614	Plagl1/Ephb1/Ripor2/Nrg1/Ryr1	5
GO:0050807	regulation of synapse organization	259/21092	3.53E-03	1.55E-01	0.122484614	Snap91/Ntn1/Drd2/Ephb1	4
GO:1901385	regulation of voltage-gated calcium channel activity	37/21092	3.62E-03	1.55E-01	0.122484614	Gnb5/Drd2	2
GO:0050808	synapse organization	427/21092	3.63E-03	1.55E-01	0.122484614	Snap91/Ntn1/Drd2/Ephb1/Nrg1	5
GO:0007616	long-term memory	38/21092	3.81E-03	1.55E-01	0.122484614	Drd2/Adcy1	2

GO:0048741	skeletal muscle fiber development	38/21092	3.81E-03	1.55E-01	0.122484614	Ripor2/Ryr1	2
GO:0060236	regulation of mitotic spindle organization	38/21092	3.81E-03	1.55E-01	0.122484614	Parp3/Ripor2	2
GO:0050803	regulation of synapse structure or activity	266/21092	3.88E-03	1.55E-01	0.122484614	Snap91/Ntn1/Drd2/Ephb1	4
GO:0009268	response to pH	40/21092	4.22E-03	1.55E-01	0.122484614	Slc38a3/Hyal1	2
GO:0042471	ear morphogenesis	135/21092	4.27E-03	1.55E-01	0.122484614	Ntn1/Tbx18/Ripor2	3
GO:0031279	regulation of cyclase activity	41/21092	4.43E-03	1.55E-01	0.122484614	Guca1b/Drd2	2
GO:2001258	negative regulation of cation channel activity	41/21092	4.43E-03	1.55E-01	0.122484614	Gnb5/Drd2	2
GO:0071496	cellular response to external stimulus	277/21092	4.48E-03	1.55E-01	0.122484614	Nprl2/Slc38a3/Ripor2/Ryr1	4
GO:0006024	glycosaminoglycan biosynthetic process	42/21092	4.64E-03	1.55E-01	0.122484614	Pxylp1/Hyal1	2
GO:0014904	myotube cell development	42/21092	4.64E-03	1.55E-01	0.122484614	Ripor2/Ryr1	2
GO:0090224	regulation of spindle organization	42/21092	4.64E-03	1.55E-01	0.122484614	Parp3/Ripor2	2
GO:0006936	muscle contraction	281/21092	4.71E-03	1.55E-01	0.122484614	Drd2/Ryr1/Scn10a/Tnnt1	4
GO:0007212	dopamine receptor signaling pathway	43/21092	4.86E-03	1.55E-01	0.122484614	Gnb5/Drd2	2
GO:0051339	regulation of lyase activity	43/21092	4.86E-03	1.55E-01	0.122484614	Guca1b/Drd2	2
GO:0098693	regulation of synaptic vesicle cycle	147/21092	5.41E-03	1.66E-01	0.131229692	Snap91/Drd2/Adcy1	3
GO:0006937	regulation of muscle contraction	148/21092	5.51E-03	1.66E-01	0.131229692	Ryr1/Scn10a/Tnnt1	3
GO:0090407	organophosphate biosynthetic process	474/21092	5.64E-03	1.66E-01	0.131229692	Guca1b/Pgap2/Adcy1/Shmt1/Pigf	5
GO:0090596	sensory organ morphogenesis	297/21092	5.73E-03	1.66E-01	0.131229692	Ntn1/Tbx18/Ephb1/Ripor2	4
GO:0051146	striated muscle cell differentiation	302/21092	6.07E-03	1.72E-01	0.136016787	Ripor2/Nrg1/Ryr1/Tnnt1	4
GO:0045927	positive regulation of growth	308/21092	6.50E-03	1.80E-01	0.141909734	Ntn1/Drd2/Nrg1/Hyal1	4
GO:0051954	positive regulation of amine transport	51/21092	6.78E-03	1.80E-01	0.141909734	Slc38a3/Drd2	2
GO:0048562	embryonic organ morphogenesis	315/21092	7.03E-03	1.80E-01	0.141909734	Ntn1/Tbx18/Ripor2/Hyal1	4
GO:0006023	aminoglycan biosynthetic process	52/21092	7.04E-03	1.80E-01	0.141909734	Pxylp1/Hyal1	2
GO:0045773	positive regulation of axon extension	52/21092	7.04E-03	1.80E-01	0.141909734	Ntn1/Nrg1	2

GO:0007416	synapse assembly	169/21092	7.94E-03	1.94E-01	0.153083885	Ntn1/Ephb1/Nrg1	3
GO:0009247	glycolipid biosynthetic process	56/21092	8.12E-03	1.94E-01	0.153083885	Pgap2/Pigf	2
GO:0006661	phosphatidylinositol biosynthetic process	59/21092	8.98E-03	1.94E-01	0.153083885	Pgap2/Pigf	2
GO:0010770	positive regulation of cell morphogenesis involved in differentiation	177/21092	9.01E-03	1.94E-01	0.153083885	Snap91/Ntn1/Nrg1	3
GO:0001764	neuron migration	181/21092	9.57E-03	1.94E-01	0.153083885	Ntn1/Drd2/Nrg1	3
GO:0048489	synaptic vesicle transport	181/21092	9.57E-03	1.94E-01	0.153083885	Snap91/Drd2/Adcy1	3
GO:0055002	striated muscle cell development	181/21092	9.57E-03	1.94E-01	0.153083885	Ripor2/Ryr1/Tnnt1	3
GO:0097480	establishment of synaptic vesicle localization	181/21092	9.57E-03	1.94E-01	0.153083885	Snap91/Drd2/Adcy1	3
GO:0051926	negative regulation of calcium ion transport	61/21092	9.58E-03	1.94E-01	0.153083885	Gnb5/Drd2	2
GO:0009988	cell-cell recognition	62/21092	9.88E-03	1.94E-01	0.153083885	Ephb1/Hspa1l	2
GO:0031669	cellular response to nutrient levels	185/21092	1.02E-02	1.94E-01	0.153083885	Nprl2/Slc38a3/Ryr1	3
GO:0042440	pigment metabolic process	63/21092	1.02E-02	1.94E-01	0.153083885	Cyb5r4/Shmt1	2
GO:0031638	zymogen activation	64/21092	1.05E-02	1.94E-01	0.153083885	Ctsh/Cideb	2
GO:0007269	neurotransmitter secretion	190/21092	1.09E-02	1.94E-01	0.153083885	Snap91/Drd2/Adcy1	3
GO:0099643	signal release from synapse	190/21092	1.09E-02	1.94E-01	0.153083885	Snap91/Drd2/Adcy1	3
GO:0032413	negative regulation of ion transmembrane transporter activity	66/21092	1.11E-02	1.94E-01	0.153083885	Gnb5/Drd2	2
GO:0097479	synaptic vesicle localization	192/21092	1.12E-02	1.94E-01	0.153083885	Snap91/Drd2/Adcy1	3
GO:0030307	positive regulation of cell growth	195/21092	1.17E-02	1.94E-01	0.153083885	Ntn1/Nrg1/Hyal1	3
GO:0055001	muscle cell development	195/21092	1.17E-02	1.94E-01	0.153083885	Ripor2/Ryr1/Tnnt1	3
GO:0022029	telencephalon cell migration	70/21092	1.25E-02	1.94E-01	0.153083885	Drd2/Nrg1	2
GO:0001505	regulation of neurotransmitter levels	376/21092	1.29E-02	1.94E-01	0.153083885	Snap91/Drd2/Adcy1/Shmt1	4
GO:0050770	regulation of axonogenesis	202/21092	1.29E-02	1.94E-01	0.153083885	Snap91/Ntn1/Nrg1	3
GO:0010822	positive regulation of mitochondrion organization	72/21092	1.32E-02	1.94E-01	0.153083885	Cideb/Hspa1l	2
GO:0021885	forebrain cell migration	73/21092	1.35E-02	1.94E-01	0.153083885	Drd2/Nrg1	2

GO:0048839	inner ear development	206/21092	1.36E-02	1.94E-01	0.153083885	Ntn1/Tbx18/Ripor2	3
GO:0003012	muscle system process	383/21092	1.37E-02	1.94E-01	0.153083885	Drd2/Ryr1/Scn10a/Tnnt1	4
GO:0060047	heart contraction	207/21092	1.37E-02	1.94E-01	0.153083885	Drd2/Scn10a/Tnnt1	3
GO:0051155	positive regulation of striated muscle cell differentiation	74/21092	1.39E-02	1.94E-01	0.153083885	Ripor2/Nrg1	2
GO:0007163	establishment or maintenance of cell polarity	208/21092	1.39E-02	1.94E-01	0.153083885	Snap91/Ephb1/Ripor2	3
GO:0032410	negative regulation of transporter activity	75/21092	1.42E-02	1.94E-01	0.153083885	Gnb5/Drd2	2
GO:0048639	positive regulation of developmental growth	210/21092	1.43E-02	1.94E-01	0.153083885	Ntn1/Drd2/Nrg1	3
GO:0048747	muscle fiber development	76/21092	1.46E-02	1.94E-01	0.153083885	Ripor2/Ryr1	2
GO:0006814	sodium ion transport	212/21092	1.46E-02	1.94E-01	0.153083885	Slc38a3/Drd2/Scn10a	3
GO:0031668	cellular response to extracellular stimulus	212/21092	1.46E-02	1.94E-01	0.153083885	Nprl2/Slc38a3/Ryr1	3
GO:0003015	heart process	215/21092	1.52E-02	1.94E-01	0.153083885	Drd2/Scn10a/Tnnt1	3
GO:0006664	glycolipid metabolic process	79/21092	1.57E-02	1.94E-01	0.153083885	Pgap2/Pigf	2
GO:0043279	response to alkaloid	79/21092	1.57E-02	1.94E-01	0.153083885	Drd2/Ryr1	2
GO:1901019	regulation of calcium ion transmembrane transporter activity	79/21092	1.57E-02	1.94E-01	0.153083885	Gnb5/Drd2	2
GO:0030073	insulin secretion	218/21092	1.58E-02	1.94E-01	0.153083885	Hmgn3/Drd2/Cyb5r4	3
GO:1903509	liposaccharide metabolic process	80/21092	1.61E-02	1.94E-01	0.153083885	Pgap2/Pigf	2
GO:0030203	glycosaminoglycan metabolic process	81/21092	1.64E-02	1.94E-01	0.153083885	Pxylp1/Hyal1	2
GO:1904063	negative regulation of cation transmembrane transport	82/21092	1.68E-02	1.94E-01	0.153083885	Gnb5/Drd2	2
GO:0099504	synaptic vesicle cycle	228/21092	1.77E-02	1.94E-01	0.153083885	Snap91/Drd2/Adcy1	3
GO:0016485	protein processing	229/21092	1.79E-02	1.94E-01	0.153083885	Ctsh/Cideb/Chac1	3
GO:0090257	regulation of muscle system process	232/21092	1.86E-02	1.94E-01	0.153083885	Ryr1/Scn10a/Tnnt1	3
GO:0021954	central nervous system neuron development	87/21092	1.88E-02	1.94E-01	0.153083885	Drd2/Ephb1	2
GO:0043583	ear development	236/21092	1.94E-02	1.94E-01	0.153083885	Ntn1/Tbx18/Ripor2	3
GO:0006497	protein lipidation	89/21092	1.96E-02	1.94E-01	0.153083885	Pgap2/Pigf	2

GO:0035914	skeletal muscle cell differentiation	89/21092	1.96E-02	1.94E-01	0.153083885	Plagl1/Ephb1	2
GO:0051149	positive regulation of muscle cell differentiation	89/21092	1.96E-02	1.94E-01	0.153083885	Ripor2/Nrg1	2
GO:0019932	second-messenger-mediated signaling	430/21092	2.00E-02	1.94E-01	0.153083885	Drd2/Ackr4/Adcy1/Nrg1	4
GO:0002027	regulation of heart rate	91/21092	2.05E-02	1.94E-01	0.153083885	Drd2/Scn10a	2
GO:0090068	positive regulation of cell cycle process	246/21092	2.16E-02	1.94E-01	0.153083885	Drd2/Ripor2/Hyal1	3
GO:0042158	lipoprotein biosynthetic process	94/21092	2.17E-02	1.94E-01	0.153083885	Pgap2/Pigf	2
GO:0099003	vesicle-mediated transport in synapse	249/21092	2.23E-02	1.94E-01	0.153083885	Snap91/Drd2/Adcy1	3
GO:0034766	negative regulation of ion transmembrane transport	98/21092	2.35E-02	1.94E-01	0.153083885	Gnb5/Drd2	2
GO:0006995	cellular response to nitrogen starvation	10/21092	2.39E-02	1.94E-01	0.153083885	Nprl2	1
GO:0007270	neuron-neuron synaptic transmission	10/21092	2.39E-02	1.94E-01	0.153083885	Drd2	1
GO:0009129	pyrimidine nucleoside monophosphate metabolic process	10/21092	2.39E-02	1.94E-01	0.153083885	Shmt1	1
GO:0009221	pyrimidine deoxyribonucleotide biosynthetic process	10/21092	2.39E-02	1.94E-01	0.153083885	Shmt1	1
GO:0014883	transition between fast and slow fiber	10/21092	2.39E-02	1.94E-01	0.153083885	Tnnt1	1
GO:0021554	optic nerve development	10/21092	2.39E-02	1.94E-01	0.153083885	Ephb1	1
GO:0031282	regulation of guanylate cyclase activity	10/21092	2.39E-02	1.94E-01	0.153083885	Guca1b	1
GO:0043562	cellular response to nitrogen levels	10/21092	2.39E-02	1.94E-01	0.153083885	Nprl2	1
GO:0046085	adenosine metabolic process	10/21092	2.39E-02	1.94E-01	0.153083885	Nt5e	1
GO:0048149	behavioral response to ethanol	10/21092	2.39E-02	1.94E-01	0.153083885	Drd2	1
GO:0051823	regulation of synapse structural plasticity	10/21092	2.39E-02	1.94E-01	0.153083885	Drd2	1
GO:0070142	synaptic vesicle budding	10/21092	2.39E-02	1.94E-01	0.153083885	Snap91	1
GO:1903749	positive regulation of establishment of protein localization to mitochondrion	10/21092	2.39E-02	1.94E-01	0.153083885	Hspa1l	1
GO:1905097	regulation of guanyl-nucleotide exchange factor activity	10/21092	2.39E-02	1.94E-01	0.153083885	Ripor2	1
GO:2000402	negative regulation of lymphocyte migration	10/21092	2.39E-02	1.94E-01	0.153083885	Ripor2	1
GO:2000807	regulation of synaptic vesicle clustering	10/21092	2.39E-02	1.94E-01	0.153083885	Snap91	1
GO:0006022	aminoglycan metabolic process	99/21092	2.40E-02	1.94E-01	0.153083885	Pxylp1/Hyal1	2
GO:0031346	positive regulation of cell projection organization	462/21092	2.53E-02	1.94E-01	0.153083885	Snap91/Ntn1/Ripor2/Nrg1	4

GO:0030336	negative regulation of cell migration	263/21092	2.57E-02	1.94E-01	0.153083885	Drd2/Ripor2/Nrg1	3
GO:0051650	establishment of vesicle localization	265/21092	2.62E-02	1.94E-01	0.153083885	Snap91/Drd2/Adcy1	3
GO:0048259	regulation of receptor-mediated endocytosis	104/21092	2.62E-02	1.94E-01	0.153083885	Snap91/Drd2	2
GO:2000300	regulation of synaptic vesicle exocytosis	104/21092	2.62E-02	1.94E-01	0.153083885	Drd2/Adcy1	2
GO:0006012	galactose metabolic process	11/21092	2.63E-02	1.94E-01	0.153083885	Glb1	1
GO:0006171	cAMP biosynthetic process	11/21092	2.63E-02	1.94E-01	0.153083885	Adcy1	1
GO:0006266	DNA ligation	11/21092	2.63E-02	1.94E-01	0.153083885	Parp3	1
GO:0009125	nucleoside monophosphate catabolic process	11/21092	2.63E-02	1.94E-01	0.153083885	Nt5e	1
GO:0021892	cerebral cortex GABAergic interneuron differentiation	11/21092	2.63E-02	1.94E-01	0.153083885	Drd2	1
GO:0034776	response to histamine	11/21092	2.63E-02	1.94E-01	0.153083885	Drd2	1
GO:0035999	tetrahydrofolate interconversion	11/21092	2.63E-02	1.94E-01	0.153083885	Shmt1	1
GO:0051967	negative regulation of synaptic transmission, glutamatergic	11/21092	2.63E-02	1.94E-01	0.153083885	Drd2	1
GO:0060159	regulation of dopamine receptor signaling pathway	11/21092	2.63E-02	1.94E-01	0.153083885	Drd2	1
GO:0060600	dichotomous subdivision of an epithelial terminal unit	11/21092	2.63E-02	1.94E-01	0.153083885	Ctsh	1
GO:0086016	AV node cell action potential	11/21092	2.63E-02	1.94E-01	0.153083885	Scn10a	1
GO:0086027	AV node cell to bundle of His cell signaling	11/21092	2.63E-02	1.94E-01	0.153083885	Scn10a	1
GO:0072521	purine-containing compound metabolic process	469/21092	2.65E-02	1.94E-01	0.153083885	Guca1b/Adcy1/Nt5e/Shmt1	4
GO:0009165	nucleotide biosynthetic process	267/21092	2.67E-02	1.94E-01	0.153083885	Guca1b/Adcy1/Shmt1	3
GO:0006986	response to unfolded protein	106/21092	2.72E-02	1.94E-01	0.153083885	Hspa1l/Chac1	2
GO:0046474	glycerophospholipid biosynthetic process	106/21092	2.72E-02	1.94E-01	0.153083885	Pgap2/Pigf	2
GO:0042752	regulation of circadian rhythm	107/21092	2.77E-02	1.94E-01	0.153083885	Drd2/Adcy1	2
GO:0051209	release of sequestered calcium ion into cytosol	107/21092	2.77E-02	1.94E-01	0.153083885	Drd2/Ryr1	2
GO:0030072	peptide hormone secretion	271/21092	2.78E-02	1.94E-01	0.153083885	Hmgn3/Drd2/Cyb5r4	3
GO:0070588	calcium ion transmembrane transport	271/21092	2.78E-02	1.94E-01	0.153083885	Gnb5/Drd2/Ryr1	3
GO:0051656	establishment of organelle localization	476/21092	2.78E-02	1.94E-01	0.153083885	Snap91/Ntn1/Drd2/Adcy1	4

GO:1902803	regulation of synaptic vesicle transport	108/21092	2.81E-02	1.94E-01	0.153083885	Drd2/Adcy1	2
GO:1901293	nucleoside phosphate biosynthetic process	274/21092	2.86E-02	1.94E-01	0.153083885	Guca1b/Adcy1/Shmt1	3
GO:0007052	mitotic spindle organization	109/21092	2.86E-02	1.94E-01	0.153083885	Parp3/Ripor2	2
GO:0030516	regulation of axon extension	109/21092	2.86E-02	1.94E-01	0.153083885	Ntn1/Nrg1	2
GO:0051283	negative regulation of sequestering of calcium ion	109/21092	2.86E-02	1.94E-01	0.153083885	Drd2/Ryr1	2
GO:0000963	mitochondrial RNA processing	12/21092	2.86E-02	1.94E-01	0.153083885	Mto1	1
GO:0007195	adenylate cyclase-inhibiting dopamine receptor signaling pathway	12/21092	2.86E-02	1.94E-01	0.153083885	Drd2	1
GO:0009265	2'-deoxyribonucleotide biosynthetic process	12/21092	2.86E-02	1.94E-01	0.153083885	Shmt1	1
GO:0014842	regulation of skeletal muscle satellite cell proliferation	12/21092	2.86E-02	1.94E-01	0.153083885	Ephb1	1
GO:0030432	peristalsis	12/21092	2.86E-02	1.94E-01	0.153083885	Drd2	1
GO:0032488	Cdc42 protein signal transduction	12/21092	2.86E-02	1.94E-01	0.153083885	Ntn1	1
GO:0046385	deoxyribose phosphate biosynthetic process	12/21092	2.86E-02	1.94E-01	0.153083885	Shmt1	1
GO:0071318	cellular response to ATP	12/21092	2.86E-02	1.94E-01	0.153083885	Ryr1	1
GO:0071468	cellular response to acidic pH	12/21092	2.86E-02	1.94E-01	0.153083885	Slc38a3	1
GO:0090494	dopamine uptake	12/21092	2.86E-02	1.94E-01	0.153083885	Drd2	1
GO:1900244	positive regulation of synaptic vesicle endocytosis	12/21092	2.86E-02	1.94E-01	0.153083885	Snap91	1
GO:2000146	negative regulation of cell motility	277/21092	2.94E-02	1.94E-01	0.153083885	Drd2/Ripor2/Nrg1	3
GO:0051282	regulation of sequestering of calcium ion	111/21092	2.96E-02	1.94E-01	0.153083885	Drd2/Ryr1	2
GO:0051208	sequestering of calcium ion	112/21092	3.01E-02	1.94E-01	0.153083885	Drd2/Ryr1	2
GO:0048568	embryonic organ development	490/21092	3.05E-02	1.94E-01	0.153083885	Ntn1/Tbx18/Ripor2/Hyal1	4
GO:0046467	membrane lipid biosynthetic process	113/21092	3.06E-02	1.94E-01	0.153083885	Pgap2/Pigf	2
GO:0006596	polyamine biosynthetic process	13/21092	3.10E-02	1.94E-01	0.153083885	Sms	1
GO:0009071	serine family amino acid catabolic process	13/21092	3.10E-02	1.94E-01	0.153083885	Shmt1	1
GO:0009219	pyrimidine deoxyribonucleotide metabolic process	13/21092	3.10E-02	1.94E-01	0.153083885	Shmt1	1
GO:0014841	skeletal muscle satellite cell proliferation	13/21092	3.10E-02	1.94E-01	0.153083885	Ephb1	1
GO:0030213	hyaluronan biosynthetic process	13/21092	3.10E-02	1.94E-01	0.153083885	Hyal1	1

GO:0031000	response to caffeine	13/21092	3.10E-02	1.94E-01	0.153083885	Ryr1	1
GO:0035810	positive regulation of urine volume	13/21092	3.10E-02	1.94E-01	0.153083885	Drd2	1
GO:0036270	response to diuretic	13/21092	3.10E-02	1.94E-01	0.153083885	Ryr1	1
GO:0060124	positive regulation of growth hormone secretion	13/21092	3.10E-02	1.94E-01	0.153083885	Drd2	1
GO:0060272	embryonic skeletal joint morphogenesis	13/21092	3.10E-02	1.94E-01	0.153083885	Hyal1	1
GO:0086067	AV node cell to bundle of His cell communication	13/21092	3.10E-02	1.94E-01	0.153083885	Scn10a	1
GO:0090493	catecholamine uptake	13/21092	3.10E-02	1.94E-01	0.153083885	Drd2	1
GO:0097202	activation of cysteine-type endopeptidase activity	13/21092	3.10E-02	1.94E-01	0.153083885	Cideb	1
GO:2001223	negative regulation of neuron migration	13/21092	3.10E-02	1.94E-01	0.153083885	Nrg1	1
GO:0051648	vesicle localization	283/21092	3.10E-02	1.94E-01	0.153083885	Snap91/Drd2/Adcy1	3
GO:1903828	negative regulation of cellular protein localization	114/21092	3.11E-02	1.94E-01	0.153083885	Ripor2/Dclk3	2
GO:1901136	carbohydrate derivative catabolic process	115/21092	3.16E-02	1.94E-01	0.153083885	Nt5e/Hyal1	2
GO:0051963	regulation of synapse assembly	117/21092	3.26E-02	1.94E-01	0.153083885	Ntn1/Ephb1	2
GO:0009416	response to light stimulus	290/21092	3.30E-02	1.94E-01	0.153083885	Guca1b/Drd2/Hyal1	3
GO:0071214	cellular response to abiotic stimulus	290/21092	3.30E-02	1.94E-01	0.153083885	Slc38a3/Ripor2/Hyal1	3
GO:0104004	cellular response to environmental stimulus	290/21092	3.30E-02	1.94E-01	0.153083885	Slc38a3/Ripor2/Hyal1	3
GO:0051604	protein maturation	291/21092	3.33E-02	1.94E-01	0.153083885	Ctsh/Cideb/Chac1	3
GO:0001771	immunological synapse formation	14/21092	3.33E-02	1.94E-01	0.153083885	Ephb1	1
GO:0006544	glycine metabolic process	14/21092	3.33E-02	1.94E-01	0.153083885	Shmt1	1
GO:0007194	negative regulation of adenylate cyclase activity	14/21092	3.33E-02	1.94E-01	0.153083885	Drd2	1
GO:0015802	basic amino acid transport	14/21092	3.33E-02	1.94E-01	0.153083885	Slc38a3	1
GO:0021781	glial cell fate commitment	14/21092	3.33E-02	1.94E-01	0.153083885	Nrg1	1
GO:0021984	adenohypophysis development	14/21092	3.33E-02	1.94E-01	0.153083885	Drd2	1
GO:0031223	auditory behavior	14/21092	3.33E-02	1.94E-01	0.153083885	Drd2	1
GO:0031987	locomotion involved in locomotory behavior	14/21092	3.33E-02	1.94E-01	0.153083885	Drd2	1
GO:0035815	positive regulation of renal sodium excretion	14/21092	3.33E-02	1.94E-01	0.153083885	Drd2	1

GO:0046033	AMP metabolic process	14/21092	3.33E-02	1.94E-01	0.153083885	Nt5e	1
GO:0046058	cAMP metabolic process	14/21092	3.33E-02	1.94E-01	0.153083885	Adcy1	1
GO:0048755	branching morphogenesis of a nerve	14/21092	3.33E-02	1.94E-01	0.153083885	Drd2	1
GO:0086069	bundle of His cell to Purkinje myocyte communication	14/21092	3.33E-02	1.94E-01	0.153083885	Scn10a	1
GO:0097154	GABAergic neuron differentiation	14/21092	3.33E-02	1.94E-01	0.153083885	Drd2	1
GO:0051952	regulation of amine transport	119/21092	3.36E-02	1.94E-01	0.153083885	Slc38a3/Drd2	2
GO:0014902	myotube differentiation	120/21092	3.41E-02	1.94E-01	0.153083885	Ripor2/Ryr1	2
GO:0060996	dendritic spine development	120/21092	3.41E-02	1.94E-01	0.153083885	Ephb1/Nrg1	2
GO:0042157	lipoprotein metabolic process	121/21092	3.47E-02	1.94E-01	0.153083885	Pgap2/Pigf	2
GO:0051153	regulation of striated muscle cell differentiation	121/21092	3.47E-02	1.94E-01	0.153083885	Ripor2/Nrg1	2
GO:0060048	cardiac muscle contraction	121/21092	3.47E-02	1.94E-01	0.153083885	Scn10a/Tnnt1	2
GO:0060326	cell chemotaxis	298/21092	3.53E-02	1.94E-01	0.153083885	Ephb1/Ackr4/Ripor2	3
GO:0009263	deoxyribonucleotide biosynthetic process	15/21092	3.57E-02	1.94E-01	0.153083885	Shmt1	1
GO:0014733	regulation of skeletal muscle adaptation	15/21092	3.57E-02	1.94E-01	0.153083885	Tnnt1	1
GO:0014857	regulation of skeletal muscle cell proliferation	15/21092	3.57E-02	1.94E-01	0.153083885	Ephb1	1
GO:0031280	negative regulation of cyclase activity	15/21092	3.57E-02	1.94E-01	0.153083885	Drd2	1
GO:0043129	surfactant homeostasis	15/21092	3.57E-02	1.94E-01	0.153083885	Ctsh	1
GO:0051974	negative regulation of telomerase activity	15/21092	3.57E-02	1.94E-01	0.153083885	Parp3	1
GO:0060134	prepulse inhibition	15/21092	3.57E-02	1.94E-01	0.153083885	Drd2	1
GO:0060192	negative regulation of lipase activity	15/21092	3.57E-02	1.94E-01	0.153083885	Snap91	1
GO:0072189	ureter development	15/21092	3.57E-02	1.94E-01	0.153083885	Tbx18	1
GO:0072498	embryonic skeletal joint development	15/21092	3.57E-02	1.94E-01	0.153083885	Hyal1	1
GO:0098926	postsynaptic signal transduction	15/21092	3.57E-02	1.94E-01	0.153083885	Nrg1	1
GO:0099527	postsynapse to nucleus signaling pathway	15/21092	3.57E-02	1.94E-01	0.153083885	Nrg1	1
GO:1903423	positive regulation of synaptic vesicle recycling	15/21092	3.57E-02	1.94E-01	0.153083885	Snap91	1
GO:2000369	regulation of clathrin-dependent endocytosis	15/21092	3.57E-02	1.94E-01	0.153083885	Snap91	1
GO:0015837	amine transport	123/21092	3.57E-02	1.94E-01	0.153083885	Slc38a3/Drd2	2

GO:0061387	regulation of extent of cell growth	124/21092	3.62E-02	1.94E-01	0.153083885	Ntn1/Nrg1	2
GO:0009582	detection of abiotic stimulus	125/21092	3.68E-02	1.94E-01	0.153083885	Guca1b/Ephb1	2
GO:0034763	negative regulation of transmembrane transport	125/21092	3.68E-02	1.94E-01	0.153083885	Gnb5/Drd2	2
GO:0046677	response to antibiotic	303/21092	3.69E-02	1.94E-01	0.153083885	Drd2/Cyb5r4/Hyal1	3
GO:0009581	detection of external stimulus	126/21092	3.73E-02	1.94E-01	0.153083885	Guca1b/Ephb1	2
GO:0006836	neurotransmitter transport	306/21092	3.78E-02	1.94E-01	0.153083885	Snap91/Drd2/Adcy1	3
GO:0035966	response to topologically incorrect protein	127/21092	3.79E-02	1.94E-01	0.153083885	Hspa1l/Chac1	2
GO:0097553	calcium ion transmembrane import into cytosol	127/21092	3.79E-02	1.94E-01	0.153083885	Drd2/Ryr1	2
GO:0002031	G protein-coupled receptor internalization	16/21092	3.80E-02	1.94E-01	0.153083885	Drd2	1
GO:0002098	tRNA wobble uridine modification	16/21092	3.80E-02	1.94E-01	0.153083885	Mto1	1
GO:0014856	skeletal muscle cell proliferation	16/21092	3.80E-02	1.94E-01	0.153083885	Ephb1	1
GO:0043968	histone H2A acetylation	16/21092	3.80E-02	1.94E-01	0.153083885	Morf4l1	1
GO:0046112	nucleobase biosynthetic process	16/21092	3.80E-02	1.94E-01	0.153083885	Shmt1	1
GO:0072672	neutrophil extravasation	16/21092	3.80E-02	1.94E-01	0.153083885	Ripor2	1
GO:2001015	negative regulation of skeletal muscle cell differentiation	16/21092	3.80E-02	1.94E-01	0.153083885	Ephb1	1
GO:0044282	small molecule catabolic process	308/21092	3.84E-02	1.94E-01	0.153083885	Glb1/Hyal1/Shmt1	3
GO:0051271	negative regulation of cellular component movement	311/21092	3.93E-02	1.94E-01	0.153083885	Drd2/Ripor2/Nrg1	3
GO:0007189	adenylate cyclase-activating G protein-coupled receptor signaling pathway	130/21092	3.95E-02	1.94E-01	0.153083885	Drd2/Adcy1	2
GO:0008037	cell recognition	131/21092	4.00E-02	1.94E-01	0.153083885	Ephb1/Hspa1l	2
GO:1902850	microtubule cytoskeleton organization involved in mitosis	131/21092	4.00E-02	1.94E-01	0.153083885	Parp3/Ripor2	2
GO:0007638	mechanosensory behavior	17/21092	4.03E-02	1.94E-01	0.153083885	Drd2	1
GO:0009070	serine family amino acid biosynthetic process	17/21092	4.03E-02	1.94E-01	0.153083885	Shmt1	1
GO:0010224	response to UV-B	17/21092	4.03E-02	1.94E-01	0.153083885	Hyal1	1
GO:0032225	regulation of synaptic transmission, dopaminergic	17/21092	4.03E-02	1.94E-01	0.153083885	Drd2	1
GO:0042754	negative regulation of circadian rhythm	17/21092	4.03E-02	1.94E-01	0.153083885	Drd2	1
GO:0042756	drinking behavior	17/21092	4.03E-02	1.94E-01	0.153083885	Drd2	1

GO:0048875	chemical homeostasis within a tissue	17/21092	4.03E-02	1.94E-01	0.153083885	Ctsh	1
GO:0051350	negative regulation of lyase activity	17/21092	4.03E-02	1.94E-01	0.153083885	Drd2	1
GO:0097091	synaptic vesicle clustering	17/21092	4.03E-02	1.94E-01	0.153083885	Snap91	1
GO:0010821	regulation of mitochondrion organization	132/21092	4.06E-02	1.94E-01	0.153083885	Cideb/Hspa1l	2
GO:0017158	regulation of calcium ion-dependent exocytosis	132/21092	4.06E-02	1.94E-01	0.153083885	Drd2/Adcy1	2
GO:0046488	phosphatidylinositol metabolic process	133/21092	4.12E-02	1.94E-01	0.153083885	Pgap2/Pigf	2
GO:0050905	neuromuscular process	133/21092	4.12E-02	1.94E-01	0.153083885	Drd2/Nrg1	2
GO:0007204	positive regulation of cytosolic calcium ion concentration	317/21092	4.12E-02	1.94E-01	0.153083885	Drd2/Ackr4/Ryr1	3
GO:0030010	establishment of cell polarity	134/21092	4.17E-02	1.94E-01	0.153083885	Ephb1/Ripor2	2
GO:0048675	axon extension	134/21092	4.17E-02	1.94E-01	0.153083885	Ntn1/Nrg1	2
GO:0006595	polyamine metabolic process	18/21092	4.27E-02	1.94E-01	0.153083885	Sms	1
GO:0009309	amine biosynthetic process	18/21092	4.27E-02	1.94E-01	0.153083885	Sms	1
GO:0031643	positive regulation of myelination	18/21092	4.27E-02	1.94E-01	0.153083885	Nrg1	1
GO:0033604	negative regulation of catecholamine secretion	18/21092	4.27E-02	1.94E-01	0.153083885	Drd2	1
GO:0036120	cellular response to platelet-derived growth factor stimulus	18/21092	4.27E-02	1.94E-01	0.153083885	Hyal1	1
GO:0042219	cellular modified amino acid catabolic process	18/21092	4.27E-02	1.94E-01	0.153083885	Chac1	1
GO:0042401	cellular biogenic amine biosynthetic process	18/21092	4.27E-02	1.94E-01	0.153083885	Sms	1
GO:0043278	response to morphine	18/21092	4.27E-02	1.94E-01	0.153083885	Drd2	1
GO:0048268	clathrin coat assembly	18/21092	4.27E-02	1.94E-01	0.153083885	Snap91	1
GO:0050650	chondroitin sulfate proteoglycan biosynthetic process	18/21092	4.27E-02	1.94E-01	0.153083885	Pxylp1	1
GO:0050961	detection of temperature stimulus involved in sensory perception	18/21092	4.27E-02	1.94E-01	0.153083885	Ephb1	1
GO:0050965	detection of temperature stimulus involved in sensory perception of pain	18/21092	4.27E-02	1.94E-01	0.153083885	Ephb1	1
GO:0051481	negative regulation of cytosolic calcium ion concentration	18/21092	4.27E-02	1.94E-01	0.153083885	Drd2	1
GO:0060088	auditory receptor cell stereocilium organization	18/21092	4.27E-02	1.94E-01	0.153083885	Ripor2	1
GO:0070886	positive regulation of calcineurin-NFAT signaling cascade	18/21092	4.27E-02	1.94E-01	0.153083885	Nrg1	1
GO:0106058	positive regulation of calcineurin-mediated signaling	18/21092	4.27E-02	1.94E-01	0.153083885	Nrg1	1

GO:1904424	regulation of GTP binding	18/21092	4.27E-02	1.94E-01	0.153083885	Ripor2	1
GO:0046928	regulation of neurotransmitter secretion	137/21092	4.34E-02	1.95E-01	0.153818291	Drd2/Adcy1	2
GO:0009267	cellular response to starvation	139/21092	4.46E-02	1.95E-01	0.153818291	Nprl2/Slc38a3	2
GO:0040013	negative regulation of locomotion	328/21092	4.49E-02	1.95E-01	0.153818291	Drd2/Ripor2/Nrg1	3
GO:0001975	response to amphetamine	19/21092	4.50E-02	1.95E-01	0.153818291	Drd2	1
GO:0002097	tRNA wobble base modification	19/21092	4.50E-02	1.95E-01	0.153818291	Mto1	1
GO:0006027	glycosaminoglycan catabolic process	19/21092	4.50E-02	1.95E-01	0.153818291	Hyal1	1
GO:0010447	response to acidic pH	19/21092	4.50E-02	1.95E-01	0.153818291	Slc38a3	1
GO:0010996	response to auditory stimulus	19/21092	4.50E-02	1.95E-01	0.153818291	Drd2	1
GO:0014072	response to isoquinoline alkaloid	19/21092	4.50E-02	1.95E-01	0.153818291	Drd2	1
GO:0014808	release of sequestered calcium ion into cytosol by sarcoplasmic reticulum	19/21092	4.50E-02	1.95E-01	0.153818291	Ryr1	1
GO:0036119	response to platelet-derived growth factor	19/21092	4.50E-02	1.95E-01	0.153818291	Hyal1	1
GO:0043931	ossification involved in bone maturation	19/21092	4.50E-02	1.95E-01	0.153818291	Ryr1	1
GO:1903214	regulation of protein targeting to mitochondrion	19/21092	4.50E-02	1.95E-01	0.153818291	Hspa1l	1
GO:0007613	memory	141/21092	4.57E-02	1.95E-01	0.153818291	Drd2/Adcy1	2
GO:0045017	glycerolipid biosynthetic process	141/21092	4.57E-02	1.95E-01	0.153818291	Pgap2/Pigf	2
GO:0010634	positive regulation of epithelial cell migration	142/21092	4.63E-02	1.95E-01	0.153818291	Ctsh/Hyal1	2
GO:0019233	sensory perception of pain	142/21092	4.63E-02	1.95E-01	0.153818291	Ephb1/Scn10a	2
GO:0016079	synaptic vesicle exocytosis	143/21092	4.69E-02	1.95E-01	0.153818291	Drd2/Adcy1	2
GO:0002693	positive regulation of cellular extravasation	20/21092	4.73E-02	1.95E-01	0.153818291	Ripor2	1
GO:0010560	positive regulation of glycoprotein biosynthetic process	20/21092	4.73E-02	1.95E-01	0.153818291	Pxylp1	1
GO:0014075	response to amine	20/21092	4.73E-02	1.95E-01	0.153818291	Drd2	1
GO:0042451	purine nucleoside biosynthetic process	20/21092	4.73E-02	1.95E-01	0.153818291	Nt5e	1
GO:0046129	purine ribonucleoside biosynthetic process	20/21092	4.73E-02	1.95E-01	0.153818291	Nt5e	1
GO:0046653	tetrahydrofolate metabolic process	20/21092	4.73E-02	1.95E-01	0.153818291	Shmt1	1
GO:0060123	regulation of growth hormone secretion	20/21092	4.73E-02	1.95E-01	0.153818291	Drd2	1

GO:0070977	bone maturation	20/21092	4.73E-02	1.95E-01	0.153818291	Ryr1	1
GO:1903514	release of sequestered calcium ion into cytosol by endoplasmic reticulum	20/21092	4.73E-02	1.95E-01	0.153818291	Ryr1	1
GO:2000010	positive regulation of protein localization to cell surface	20/21092	4.73E-02	1.95E-01	0.153818291	Nrg1	1
GO:2000114	regulation of establishment of cell polarity	20/21092	4.73E-02	1.95E-01	0.153818291	Ripor2	1
GO:0010769	regulation of cell morphogenesis involved in differentiation	336/21092	4.76E-02	1.96E-01	0.154394136	Snap91/Ntn1/Nrg1	3
GO:0001976	neurological system process involved in regulation of systemic arterial blood pressure	21/21092	4.96E-02	1.99E-01	0.157260746	Drd2	1
GO:0007190	activation of adenylate cyclase activity	21/21092	4.96E-02	1.99E-01	0.157260746	Adcy1	1
GO:0007625	grooming behavior	21/21092	4.96E-02	1.99E-01	0.157260746	Drd2	1
GO:0015012	heparan sulfate proteoglycan biosynthetic process	21/21092	4.96E-02	1.99E-01	0.157260746	Pxylp1	1
GO:0031290	retinal ganglion cell axon guidance	21/21092	4.96E-02	1.99E-01	0.157260746	Ephb1	1
GO:0043501	skeletal muscle adaptation	21/21092	4.96E-02	1.99E-01	0.157260746	Tnnt1	1
GO:1901673	regulation of mitotic spindle assembly	21/21092	4.96E-02	1.99E-01	0.157260746	Ripor2	1
GO:0060402	calcium ion transport into cytosol	148/21092	4.99E-02	2.00E-01	0.157614938	Drd2/Ryr1	2

Supp Table S7. List of Differentially Expressed genes at FDR 5% in *Gnb5+/-* mice - atria

Ensembl ID	Gene Symbol	Gene name	baseMean	log2FoldChange	lfcSE	stat	pvalue	padj
ENSMUSG00000032224	Fam81a	family with sequence similarity 81, member A	292.8574685	2.335882638	0.253579957	9.211621721	3.21234E-20	6.22167E-16
ENSMUSG00000032192	Gnb5	guanine nucleotide binding protein (G protein), beta 5	588.3942165	-0.927754237	0.10834755	-8.562761538	1.10196E-17	1.06714E-13
ENSMUSG00000033419	Snap91	synaptosomal-associated protein 91	593.4008865	-0.644595104	0.121995504	-5.283761128	1.26558E-07	0.00081706
ENSMUSG00000051378	Kif18b	kinesin family member 18B	20.36546888	2.054560276	0.444055668	4.626807909	3.71345E-06	0.014384406
ENSMUSG00000078137	Ankrd63	ankyrin repeat domain 63	231.3397505	0.696118485	0.148990179	4.672244111	2.97927E-06	0.014384406
ENSMUSG00000053093	Myh7	myosin, heavy polypeptide 7, cardiac muscle, beta	251.3134444	-0.96720691	0.212994578	-4.540993103	5.59899E-06	0.018073528
ENSMUSG00000023979	Guca1b	guanylate cyclase activator 1B	58.67765502	0.974404672	0.217497591	4.480071111	7.46182E-06	0.020645783

Supp Table S8. List of Differentially Expressed genes at FDR 5% in *Gnb5+/-* mice - ventricle

Ensembl ID	Gene Symbol	Gene name	baseMean	log2FoldChange	lfcSE	stat	pvalue	padj
ENSMUSG00000032192	Gnb5	guanine nucleotide binding protein (G protein), beta 5	313.5699776	-0.960435275	0.123650627	-7.767330392	8.01576E-15	1.39723E-10
ENSMUSG00000032224	Fam81a	family with sequence similarity 81, member A	535.3572241	1.099542929	0.159014957	6.914713879	4.68809E-12	4.0859E-08

Supp Table S9. List of Differentially Expressed genes at FDR 5% in *Gnb5-/-* mice - cerebellum

Ensembl ID	Gene Symbol	Gene name	baseMean	log2FoldChange	lfcSE	stat	pvalue	padj
ENSMUSG00000032192	Gnb5	guanine nucleotide binding protein (G protein), beta 5	3776.684327	-2.827640286	0.055298441	-51.13417754	0.00E+00	< 2.00E-308
ENSMUSG00000023979	Guca1b	guanylate cyclase activator 1B	437.4550876	3.711107472	0.099175263	37.41968881	1.8697E-306	1.5621E-302
ENSMUSG00000032232	Cgnl1	cingulin-like 1	5161.732469	1.318444731	0.078033577	16.89586428	4.8259E-64	2.69E-60
ENSMUSG00000048758	Rpl29	ribosomal protein L29	167.003666	-2.662526944	0.179928843	-14.79766612	1.51654E-49	6.34E-46
ENSMUSG00000032556	Bfsp2	beaded filament structural protein 2, phakinin	65.92606322	-3.710156999	0.343429245	-10.8032646	3.32179E-27	1.11E-23
ENSMUSG00000043587	Pxylp1	2-phosphoxylose phosphatase 1	2090.786713	-0.93940513	0.089637192	-10.48008205	1.06651E-25	2.97E-22
ENSMUSG00000023277	Twf2	twinfilin actin binding protein 2	931.2249327	-0.527947875	0.052457731	-10.06425304	7.94884E-24	1.90E-20
ENSMUSG00000032498	Mlh1	mutL homolog 1	668.627558	-0.704540452	0.072809837	-9.676445968	3.79686E-22	7.93E-19
ENSMUSG00000020253	Ppm1m	protein phosphatase 1M	736.854351	-0.583377557	0.062857481	-9.2809567	1.67964E-20	3.12E-17
ENSMUSG00000062270	Morf4l1	mortality factor 4 like 1	4272.079558	-0.455630844	0.050708541	-8.985288001	2.58058E-19	4.31E-16
ENSMUSG00000062270	Morf4l1b	mortality factor 4 like 1B	4272.079558	-0.455630844	0.050708541	-8.985288001	2.58058E-19	4.31E-16
ENSMUSG00000032500	Dclk3	doublecortin-like kinase 3	227.5683369	1.633993963	0.194019129	8.421818885	3.70684E-17	5.63E-14
ENSMUSG00000032563	Mrpl3	mitochondrial ribosomal protein L3	2535.527483	-0.354146675	0.043154236	-8.206533358	2.27666E-16	3.17E-13
ENSMUSG00000104282	Gm37460	predicted gene 37460	24.0513232	-3.989910368	0.490489586	-8.134546545	4.13483E-16	5.31E-13
ENSMUSG00000090626	Tex9	testis expressed gene 9	591.5495903	-0.682683678	0.084985708	-8.032923324	9.51772E-16	1.14E-12
ENSMUSG00000032567	Aste1	asteroid homolog 1	261.2643017	-0.726216234	0.103776418	-6.997892664	2.59841E-12	2.89E-09
ENSMUSG00000036545	Adamts2	a disintegrin-like and metallopeptidase (reprolysin type) with thrombospondin type 1 motif, 2	865.4646909	-0.444637534	0.063619194	-6.989046931	2.7676E-12	2.89E-09
ENSMUSG00000043719	Col6a6	collagen, type VI, alpha 6	86.23142466	1.431557776	0.205901274	6.952641647	3.58509E-12	3.52E-09

ENSMUSG00000103164	Gm38150	predicted gene 38150	75.50295187	1.856335622	0.270406058	6.864992725	6.64946E-12	6.17E-09
ENSMUSG00000104286	Gm37457	predicted gene 37457	83.69435181	-1.396799984	0.20663308	-6.759808188	1.38175E-11	1.22E-08
ENSMUSG00000032494	Tdgf1	teratocarcinoma-derived growth factor 1	88.70981041	-1.228803344	0.187927365	-6.53871426	6.20499E-11	5.18E-08
ENSMUSG00000020096	Tbata	thymus, brain and testes associated	1971.627299	0.271356344	0.041688236	6.509182673	7.55608E-11	6.01E-08
ENSMUSG00000032418	Me1	malic enzyme 1, NADP(+)-dependent, cytosolic	2486.718734	0.398420712	0.061534107	6.474794711	9.49409E-11	7.21E-08
ENSMUSG00000002020	Ltbp2	latent transforming growth factor beta binding protein 2	4421.817622	-0.490281841	0.076725482	-6.390078353	1.65801E-10	1.20E-07
ENSMUSG00000032554	Trf	transferrin	516.363827	-0.885336834	0.14025914	-6.312150725	2.75184E-10	1.92E-07
ENSMUSG00000032495	Lrrc2	leucine rich repeat containing 2	337.4958733	-0.80567915	0.129576646	-6.217780565	5.04236E-10	3.37E-07
ENSMUSG00000102225	Gm37983	predicted gene 37983	24.91169952	1.872814001	0.301640962	6.208752252	5.34069E-10	3.43E-07
ENSMUSG00000023495	Pcbp4	poly(rC) binding protein 4	9608.983245	0.438156046	0.070693682	6.197951952	5.72026E-10	3.54E-07
ENSMUSG00000111348	Gm19531	predicted gene 19531	50.79214136	-1.15586438	0.18808935	-6.145294146	7.98155E-10	4.76E-07
ENSMUSG00000032383	Ppib	peptidylprolyl isomerase B	5797.045453	0.340285278	0.056151123	6.060168681	1.35979E-09	7.84E-07
ENSMUSG00000032221	Mns1	meiosis-specific nuclear structural protein 1	56.59125716	-1.175230186	0.195568968	-6.009287647	1.8634E-09	1.00E-06
ENSMUSG00000059003	Grin2a	glutamate receptor, ionotropic, NMDA2A (epsilon 1)	4488.448054	-0.246141364	0.040933749	-6.013164469	1.81936E-09	1.00E-06
ENSMUSG00000032411	Tfdp2	transcription factor Dp 2	2502.966265	0.41235966	0.0699472	5.895299004	3.74004E-09	1.95E-06
ENSMUSG00000023345	Poc1a	POC1 centriolar protein A	91.35994109	-0.946728825	0.160973191	-5.881282596	4.07099E-09	2.06E-06
ENSMUSG00000034898	Filip1	filamin A interacting protein 1	217.3345229	1.070995942	0.185443542	5.775320789	7.68066E-09	3.77E-06
ENSMUSG00000010057	Nprl2	NPR2 like, GATOR1 complex subunit	1400.200434	0.277235707	0.048216138	5.749853009	8.93211E-09	4.15E-06
ENSMUSG00000051590	Map3k19	mitogen-activated protein kinase kinase kinase 19	151.7662179	-0.72256102	0.125662208	-5.75002643	8.92295E-09	4.15E-06
ENSMUSG00000091735	Gpr62	G protein-coupled receptor 62	313.5180019	0.686846592	0.119742794	5.736016061	9.69295E-09	4.38E-06
ENSMUSG00000040536	Necab1	N-terminal EF-hand calcium binding protein 1	1182.606983	-0.675042081	0.119629524	-5.642771587	1.67334E-08	7.36E-06
ENSMUSG00000087466	A330041J22Rik	RIKEN cDNA A330041J22 gene	74.58228965	1.434589369	0.256512536	5.592667679	2.23607E-08	9.58E-06
ENSMUSG00000044037	Als2cl	ALS2 C-terminal like	1028.642711	-0.418008066	0.075093528	-5.566499248	2.59908E-08	1.09E-05
ENSMUSG00000070469	Adamtsl3	ADAMTS-like 3	113.9892968	-0.662897133	0.122069091	-5.43050764	5.6194E-08	2.29E-05
ENSMUSG00000023868	Pde10a	phosphodiesterase 10A	6880.473669	-0.676534037	0.125581847	-5.387196095	7.15653E-08	2.85E-05

ENSMUSG00000057802	Gm10030	predicted gene 10030	21.42515066	-1.977535225	0.375457621	-5.266999825	1.38671E-07	5.39E-05
ENSMUSG00000032360	Hcrtr2	hypocretin (orexin) receptor 2	28.96765092	-1.487211303	0.285983133	-5.200346213	1.98918E-07	7.55E-05
ENSMUSG00000024403	Atp6v1g2	ATPase, H+ transporting, lysosomal V1 subunit G2	10912.75865	0.157684878	0.030688324	5.138269387	2.7728E-07	1.03E-04
ENSMUSG00000102568	Gm37040	predicted gene 37040	36.43245889	-1.278054894	0.249989747	-5.112429236	3.18042E-07	1.16E-04
ENSMUSG00000033590	Myo5c	myosin VC	265.6388649	-0.549651459	0.109058116	-5.039986752	4.65564E-07	1.66E-04
ENSMUSG00000032872	Cyb5r4	cytochrome b5 reductase 4	2148.279031	-0.43931008	0.087835518	-5.001508373	5.68835E-07	1.98E-04
ENSMUSG00000047021	Cfap65	cilia and flagella associated protein 65	28.70220643	-1.970744625	0.396179632	-4.974371384	6.54597E-07	2.23E-04
ENSMUSG00000042761	Mrap2	melanocortin 2 receptor accessory protein 2	223.3199552	1.820064844	0.366864164	4.961140998	7.00803E-07	2.34E-04
ENSMUSG00000090150	Acad11	acyl-Coenzyme A dehydrogenase family, member 11	1333.016891	-0.242690676	0.049029394	-4.949901548	7.4251E-07	2.43E-04
ENSMUSG00000056596	Trnp1	TMF1-regulated nuclear protein 1	2707.369654	0.257405668	0.052080717	4.942437138	7.7152E-07	2.48E-04
ENSMUSG00000074415	3110039I08Rik	RIKEN cDNA 3110039I08 gene	858.8892546	-0.347692944	0.071049825	-4.893649586	9.8983E-07	3.12E-04
ENSMUSG00000045414	1190002N15Rik	RIKEN cDNA 1190002N15 gene	9479.974493	0.203857188	0.041965151	4.857773243	1.18713E-06	3.67E-04
ENSMUSG00000019929	Dcn	decorin	945.0632883	-0.39965724	0.083620332	-4.77942659	1.75796E-06	5.34E-04
ENSMUSG00000018659	Pnpo	pyridoxine 5'-phosphate oxidase	1853.661258	0.24366376	0.051217163	4.757463036	1.96041E-06	5.64E-04
ENSMUSG00000021265	Slc25a29	solute carrier family 25 (mitochondrial carrier, palmitoylcarnitine transporter), member 29	1086.377437	0.293381215	0.061607831	4.762076706	1.91611E-06	5.64E-04
ENSMUSG00000041506	Rrp9	RRP9, small subunit (SSU) processome component, homolog (yeast)	633.4693325	-0.348737041	0.073351895	-4.754301764	1.99133E-06	5.64E-04
ENSMUSG00000032436	Cmtm7	CKLF-like MARVEL transmembrane domain containing 7	225.5308249	-0.784340082	0.165355327	-4.743361447	2.10201E-06	5.85E-04
ENSMUSG00000070720	Tmem200b	transmembrane protein 200B	879.3241942	0.237178838	0.050148875	4.729494708	2.25079E-06	6.17E-04
ENSMUSG00000029822	Osbpl3	oxysterol binding protein-like 3	2125.961608	-0.339350961	0.073793709	-4.598643542	4.25251E-06	1.15E-03
ENSMUSG00000010048	Ifrd2	interferon-related developmental regulator 2	562.5877885	0.365850749	0.080007846	4.572685919	4.81512E-06	1.28E-03
ENSMUSG00000045967	Gpr158	G protein-coupled receptor 158	12290.27869	-0.241962539	0.053293038	-4.540227925	5.61934E-06	1.47E-03
ENSMUSG00000032356	Rasgrf1	RAS protein-specific guanine nucleotide-releasing factor 1	15290.93068	0.499536916	0.110479983	4.521515126	6.13986E-06	1.58E-03

ENSMUSG00000036760	Kcnk9	potassium channel, subfamily K, member 9	13243.63708	-0.292027828	0.06499848	-4.492840872	7.02793E-06	1.76E-03
ENSMUSG00000049624	Slc17a5	solute carrier family 17 (anion/sugar transporter), member 5	892.3986237	-0.346728247	0.077198643	-4.491377501	7.0764E-06	1.76E-03
ENSMUSG00000032497	Lrrfip2	leucine rich repeat (in FLII) interacting protein 2	1954.49032	-0.165756146	0.037035569	-4.47559331	7.61994E-06	1.87E-03
ENSMUSG00000024830	Rps6kb2	ribosomal protein S6 kinase, polypeptide 2	2329.153627	0.177815047	0.039942537	4.451771506	8.51648E-06	2.06E-03
ENSMUSG00000042210	Abhd14a	abhydrolase domain containing 14A	685.2533565	-0.289047191	0.065636456	-4.403759862	1.06391E-05	2.50E-03
ENSMUSG00000032570	Atp2c1	ATPase, Ca++-sequestering	7634.149512	0.190293715	0.043395191	4.38513372	1.15915E-05	2.69E-03
ENSMUSG00000085564	Gm12198	predicted gene 12198	144.1003058	-0.655784624	0.1506718	-4.35240452	1.34653E-05	3.08E-03
ENSMUSG00000025189	Cnnm1	cyclin M1	9936.963016	0.171522867	0.03971572	4.318765082	1.56905E-05	3.54E-03
ENSMUSG00000026156	B3gat2	beta-1,3-glucuronyltransferase 2 (glucuronosyltransferase S)	1542.762622	0.40134508	0.093300587	4.301635111	1.69542E-05	3.78E-03
ENSMUSG00000018697	Aatf	apoptosis antagonizing transcription factor	909.2901189	0.207262888	0.048456521	4.277296095	1.89177E-05	4.11E-03
ENSMUSG00000029695	Aass	aminoadipate-semialdehyde synthase	502.5914013	-0.540371692	0.126482917	-4.272289917	1.93476E-05	4.14E-03
ENSMUSG00000032936	Camkv	CaM kinase-like vesicle-associated	155.6519028	0.645556244	0.151277644	4.267360514	1.97799E-05	4.18E-03
ENSMUSG00000031274	Col4a5	collagen, type IV, alpha 5	423.3176062	-0.339340123	0.079636924	-4.261090277	2.03432E-05	4.25E-03
ENSMUSG00000025422	Agap2	ArfGAP with GTPase domain, ankyrin repeat and PH domain 2	9075.763147	0.168987623	0.039938014	4.231247511	2.32399E-05	4.79E-03
ENSMUSG00000040929	Rfx3	regulatory factor X, 3 (influences HLA class II expression)	1948.279304	-0.227743173	0.053898976	-4.225371062	2.38547E-05	4.86E-03
ENSMUSG00000046378	Asphd1	aspartate beta-hydroxylase domain containing 1	600.4949404	0.321122754	0.076280176	4.209779938	2.5562E-05	5.15E-03
ENSMUSG00000010660	Plcd1	phospholipase C, delta 1	287.7365686	-0.438423508	0.104711926	-4.186949119	2.82729E-05	5.56E-03
ENSMUSG00000026676	Ccdc3	coiled-coil domain containing 3	194.3461266	-0.787253495	0.187973755	-4.188103256	2.81296E-05	5.56E-03
ENSMUSG00000049303	Syt12	synaptotagmin XII	4738.805298	0.171600731	0.041042568	4.181042741	2.90175E-05	5.64E-03
ENSMUSG00000007594	Hapln4	hyaluronan and proteoglycan link protein 4	7762.924373	0.20525169	0.049244469	4.168015088	3.07264E-05	5.90E-03
ENSMUSG00000053702	Nebl	nebulette	4122.080911	-0.200274445	0.048467616	-4.132129069	3.59418E-05	6.82E-03
ENSMUSG00000070866	Zfp804a	zinc finger protein 804A	529.6035357	-0.273660923	0.066470521	-4.117026906	3.83791E-05	7.14E-03
ENSMUSG00000103891	Gm37941	predicted gene 37941	90.25718563	-0.590766007	0.143506106	-4.116661118	3.84401E-05	7.14E-03

ENSMUSG00000033577	Myo6	myosin VI	7952.800259	-0.177308645	0.043222703	-4.102210917	4.09221E-05	7.51E-03
ENSMUSG00000032562	Gnai2	guanine nucleotide binding protein (G protein), alpha inhibiting 2	5695.835318	0.209104738	0.051108773	4.09136684	4.28838E-05	7.79E-03
ENSMUSG00000022548	Apod	apolipoprotein D	7327.803279	-0.302224918	0.074021475	-4.082935635	4.44703E-05	7.96E-03
ENSMUSG00000025889	Snca	synuclein, alpha	753.7428095	0.310662096	0.076126465	4.080868538	4.48677E-05	7.96E-03
ENSMUSG00000040003	Magi2	membrane associated guanylate kinase, WW and PDZ domain containing 2	3517.01469	-0.198280333	0.048611072	-4.078912966	4.52468E-05	7.96E-03
ENSMUSG00000032224	Fam81a	family with sequence similarity 81, member A	752.0267376	0.40135418	0.098857026	4.059945935	4.90841E-05	8.46E-03
ENSMUSG00000035941	Ibtk	inhibitor of Bruton agammaglobulinemia tyrosine kinase	2259.614768	-0.234174871	0.057652254	-4.061851089	4.86851E-05	8.46E-03
ENSMUSG00000053399	Adamts18	a disintegrin-like and metallopeptidase (reprolysin type) with thrombospondin type 1 motif, 18	1245.172925	-0.535900624	0.132150485	-4.055230107	5.0085E-05	8.54E-03
ENSMUSG00000031209	Heph	hephaestin	212.499617	-0.524851774	0.129709845	-4.046352637	5.20218E-05	8.78E-03
ENSMUSG00000045594	Glb1	galactosidase, beta 1	603.8171745	-0.251329503	0.062199	-4.040732209	5.32846E-05	8.90E-03
ENSMUSG00000039728	Slc6a5	solute carrier family 6 (neurotransmitter transporter, glycine), member 5	2131.525392	0.184557898	0.0457464	4.034369904	5.4749E-05	9.06E-03
ENSMUSG00000022816	Fstl1	follistatin-like 1	656.1358971	-0.313458386	0.077999396	-4.018728391	5.85131E-05	9.49E-03
ENSMUSG00000060961	Slc4a4	solute carrier family 4 (anion exchanger), member 4	26482.84028	-0.210742417	0.052420959	-4.020193892	5.81503E-05	9.49E-03
ENSMUSG00000032786	Alas1	aminolevulinic acid synthase 1	2264.965012	0.16544191	0.041256635	4.010067955	6.07013E-05	9.60E-03
ENSMUSG00000034780	B3galt1	UDP-Gal:betaGlcNAc beta 1,3-galactosyltransferase, polypeptide 1	1512.878245	-0.228990845	0.057113105	-4.009427354	6.08662E-05	9.60E-03
ENSMUSG00000042757	Tmem108	transmembrane protein 108	1743.966905	0.191530914	0.047761983	4.010112257	6.06899E-05	9.60E-03
ENSMUSG00000038540	Tmc3	transmembrane channel-like gene family 3	128.5246132	-0.635080101	0.158674431	-4.002409822	6.27006E-05	9.79E-03
ENSMUSG00000019899	Lama2	laminin, alpha 2	1767.500596	-0.307800775	0.077002817	-3.997266444	6.40782E-05	9.91E-03
ENSMUSG00000020331	Hcn2	hyperpolarization-activated, cyclic nucleotide-gated K+ 2	3684.614211	0.211210959	0.053011952	3.984213928	6.77039E-05	1.04E-02
ENSMUSG00000079470	Utp14b	UTP14B small subunit processome component	593.3329387	-0.43940743	0.110425779	-3.979210594	6.91445E-05	1.05E-02

ENSMUSG00000043873	Chil5	chitinase-like 5	569.1443709	-0.529904212	0.134141397	-3.950340648	7.804E-05	1.17E-02
ENSMUSG00000034891	Sncb	synuclein, beta	6033.619166	0.257865278	0.065369039	3.944761662	7.98794E-05	1.18E-02
ENSMUSG00000111874	Gm36539	predicted gene 36539	28.68067065	-1.151072889	0.2918086	-3.944616051	7.99279E-05	1.18E-02
ENSMUSG00000040813	Tex264	testis expressed gene 264	1627.318836	0.24003156	0.061051179	3.931644982	8.43666E-05	1.24E-02
ENSMUSG00000024145	Pigf	phosphatidylinositol glycan anchor biosynthesis, class F	527.8534165	0.269835764	0.068864084	3.918381649	8.91455E-05	1.30E-02
ENSMUSG00000056019	Zfp709	zinc finger protein 709	716.7501148	-0.221064446	0.05646221	-3.915263783	9.03054E-05	1.30E-02
ENSMUSG00000047793	Sned1	sushi, nidogen and EGF-like domains 1	5436.766785	-0.214764333	0.054903128	-3.911695799	9.16503E-05	1.31E-02
ENSMUSG00000054196	Cthrc1	collagen triple helix repeat containing 1	456.6616622	0.273577589	0.070468467	3.882269615	0.000103486	1.44E-02
ENSMUSG00000062296	Trank1	tetratricopeptide repeat and ankyrin repeat containing 1	8866.298066	-0.401596014	0.103457199	-3.881759962	0.000103703	1.44E-02
ENSMUSG00000032359	Ctsh	cathepsin H	293.9199692	-0.380690598	0.098160275	-3.878255222	0.000105208	1.45E-02
ENSMUSG00000044244	Il20rb	interleukin 20 receptor beta	4371.39349	-0.294150387	0.075956801	-3.872601062	0.00010768	1.47E-02
ENSMUSG00000022540	Rogdi	rogdi homolog	3549.588552	0.19537945	0.05061794	3.859885424	0.00011344	1.54E-02
ENSMUSG00000036875	Dna2	DNA replication helicase/nuclease 2	172.3546123	-0.491356217	0.128239542	-3.831550007	0.000127338	1.72E-02
ENSMUSG00000022131	Gpr180	G protein-coupled receptor 180	1001.298783	0.180560403	0.047197908	3.825601801	0.000130453	1.74E-02
ENSMUSG00000029304	Spp1	secreted phosphoprotein 1	314.3225449	-1.037931743	0.271691281	-3.820261514	0.00013331	1.77E-02
ENSMUSG00000032571	Pik3r4	phosphoinositide-3-kinase regulatory subunit 4	2100.770068	-0.151120322	0.039789316	-3.798012582	0.000145861	1.92E-02
ENSMUSG00000038665	Dgki	diacylglycerol kinase, iota	1078.595202	-0.375885813	0.099194535	-3.78938028	0.000151024	1.97E-02
ENSMUSG00000054976	Nyap2	neuronal tyrosine-phophorylated phosphoinositide 3-kinase adaptor 2	1169.835804	-0.298167703	0.078758509	-3.785847468	0.000153186	1.98E-02
ENSMUSG00000031865	Dctn1	dynactin 1	14438.60666	0.157031021	0.041575282	3.77702842	0.000158711	2.04E-02
ENSMUSG00000032344	Cgas	cyclic GMP-AMP synthase	20.25321073	-1.137586452	0.301649272	-3.771222276	0.00016245	2.07E-02
ENSMUSG00000085084	4930570G19Rik	RIKEN cDNA 4930570G19 gene	1161.071062	-0.278073956	0.073863903	-3.76467995	0.000166763	2.11E-02
ENSMUSG00000040138	Ndp	Norrie disease (pseudoglioma) (human)	707.6201088	0.219662722	0.058391047	3.761924736	0.000168611	2.12E-02
ENSMUSG00000055254	Ntrk2	neurotrophic tyrosine kinase, receptor, type 2	19030.20769	-0.126891755	0.033783148	-3.75606662	0.000172605	2.15E-02
ENSMUSG00000027425	Kat14	lysine acetyltransferase 14	1374.54001	0.198671813	0.053026405	3.746658187	0.000179206	2.22E-02

ENSMUSG00000002274	Metrn	meteorin, glial cell differentiation regulator	5167.733381	0.251300779	0.067293283	3.734411033	0.000188155	2.31E-02
ENSMUSG00000054555	Adam12	a disintegrin and metallopeptidase domain 12 (meltrin alpha)	250.2725205	-0.367994148	0.098586085	-3.73271897	0.000189424	2.31E-02
ENSMUSG00000020185	E2f7	E2F transcription factor 7	64.89049163	-0.647104213	0.173634674	-3.726814448	0.000193915	2.31E-02
ENSMUSG00000031558	Slit2	slit guidance ligand 2	128.0552607	-0.619583532	0.166242811	-3.726979397	0.000193788	2.31E-02
ENSMUSG00000032803	Cdv3	carnitine deficiency-associated gene expressed in ventricle 3	2963.464124	-0.225267786	0.060576528	-3.718730583	0.000200226	2.37E-02
ENSMUSG00000039033	Tasp1	taspase, threonine aspartase 1	555.9554491	0.22670657	0.061038063	3.714183568	0.000203861	2.40E-02
ENSMUSG00000032323	Cyp11a1	cytochrome P450, family 11, subfamily a, polypeptide 1	160.2036109	-0.54410811	0.146689928	-3.709239733	0.000207883	2.43E-02
ENSMUSG00000027737	Slc7a11	solute carrier family 7 (cationic amino acid transporter, y+ system), member 11	1540.871957	-0.358277877	0.0967587	-3.702797536	0.000213235	2.44E-02
ENSMUSG00000033152	Podxl2	podocalyxin-like 2	6112.985547	0.265277682	0.071596768	3.705162828	0.000211255	2.44E-02
ENSMUSG00000105230	Gm42433	predicted gene 42433	287.5596305	0.32790406	0.088599373	3.700974955	0.000214773	2.44E-02
ENSMUSG00000025780	Itih5	inter-alpha (globulin) inhibitor H5	3052.757631	-0.257421968	0.069613061	-3.697897575	0.000217393	2.45E-02
ENSMUSG00000062257	Opcml	opioid binding protein/cell adhesion molecule-like	5120.415454	0.229556926	0.062123271	3.695184118	0.000219728	2.46E-02
ENSMUSG00000002228	Ppm1j	protein phosphatase 1J	73.97859987	0.543936081	0.147487001	3.688027274	0.000225999	2.48E-02
ENSMUSG00000020467	Efemp1	epidermal growth factor-containing fibulin-like extracellular matrix protein 1	661.4773856	-0.246464103	0.066769489	-3.691268372	0.000223139	2.48E-02
ENSMUSG00000071793	2610005L07Rik	cadherin 11 pseudogene	499.0576741	-0.260764185	0.070694432	-3.688609945	0.000225483	2.48E-02
ENSMUSG00000037624	Kcnk2	potassium channel, subfamily K, member 2	546.4969263	-0.275003038	0.074638882	-3.684447469	0.000229199	2.50E-02
ENSMUSG00000032184	Lysmd2	LysM, putative peptidoglycan-binding, domain containing 2	1722.663597	0.179859137	0.048875377	3.679953949	0.000233276	2.52E-02
ENSMUSG00000053716	Dusp7	dual specificity phosphatase 7	851.3299296	-0.261817054	0.071153446	-3.67961174	0.000233589	2.52E-02
ENSMUSG00000001773	Folh1	folate hydrolase 1	417.0674349	-0.340484695	0.092777155	-3.669919545	0.000242627	2.60E-02
ENSMUSG00000058966	Fam57b	family with sequence similarity 57, member B	4089.571587	0.189611427	0.051728708	3.665497087	0.000246859	2.63E-02
ENSMUSG00000063382	Bcl9l	B cell CLL/lymphoma 9-like	2478.992746	0.160810433	0.043905694	3.662632777	0.000249636	2.64E-02
ENSMUSG00000039163	Cmc1	COX assembly mitochondrial protein 1	342.5573765	0.344219264	0.094239415	3.652603992	0.000259594	2.73E-02

ENSMUSG00000006611	Hfe	hemochromatosis	233.2512245	0.407642583	0.11167162	3.65036868	0.000261864	2.73E-02
ENSMUSG00000025666	Tmem47	transmembrane protein 47	6719.132151	-0.216149918	0.059318852	-3.643865528	0.000268574	2.79E-02
ENSMUSG00000043631	Ecm2	extracellular matrix protein 2, female organ and adipocyte specific	522.2468524	-0.450393032	0.124061234	-3.630409094	0.000282972	2.92E-02
ENSMUSG00000000168	Dlat	dihydrolipoamide S-acetyltransferase (E2 component of pyruvate dehydrogenase complex)	4583.776794	0.176427012	0.048640056	3.627195923	0.000286516	2.92E-02
ENSMUSG00000052353	Cemip	cell migration inducing protein, hyaluronan binding	1840.025575	-0.4649413	0.128287759	-3.624206261	0.00028985	2.94E-02
ENSMUSG00000010045	Tmem115	transmembrane protein 115	1344.974255	0.214213274	0.059281784	3.613475478	0.00030212	3.02E-02
ENSMUSG00000058571	Gpc6	glypican 6	1138.981461	-0.221737078	0.061346601	-3.614496551	0.000300932	3.02E-02
ENSMUSG00000021998	Lcp1	lymphocyte cytosolic protein 1	575.426901	-0.33184577	0.091996191	-3.607168583	0.000309557	3.06E-02
ENSMUSG00000099512	Gm28703	predicted gene 28703	42.47158017	-0.723172188	0.200554314	-3.605867029	0.000311112	3.06E-02
ENSMUSG00000026344	Lypd1	Ly6/Plaur domain containing 1	707.8577798	0.357304132	0.099205924	3.601641094	0.000316215	3.09E-02
ENSMUSG00000026875	Traf1	TNF receptor-associated factor 1	452.7246797	0.445913269	0.123949496	3.597539993	0.000321241	3.12E-02
ENSMUSG00000037685	Atp8a1	ATPase, aminophospholipid transporter (APLT), class I, type 8A, member 1	11419.74021	-0.152030474	0.042369287	-3.588223594	0.000332939	3.22E-02
ENSMUSG00000022551	Cyc1	cytochrome c-1	5969.488864	0.176594951	0.049237771	3.586574833	0.00033505	3.22E-02
ENSMUSG00000000881	Dlg3	discs large MAGUK scaffold protein 3	5293.782134	0.118328055	0.033009058	3.584714728	0.000337447	3.22E-02
ENSMUSG00000004187	Kifc2	kinesin family member C2	8872.227272	0.164258912	0.045857095	3.581973822	0.000341008	3.23E-02
ENSMUSG00000039252	Lgi2	leucine-rich repeat LGI family, member 2	6372.971886	0.318458404	0.088965961	3.579553376	0.000344182	3.23E-02
ENSMUSG00000046574	Prr12	proline rich 12	3312.873574	0.150871364	0.042148131	3.579550486	0.000344186	3.23E-02
ENSMUSG00000010054	Tusc2	tumor suppressor 2, mitochondrial calcium regulator	2502.522813	0.154214131	0.043214835	3.568546102	0.000358968	3.33E-02
ENSMUSG00000024777	Ppp2r5b	protein phosphatase 2, regulatory subunit B', beta	6579.099733	0.135258768	0.037954628	3.563696347	0.000365669	3.38E-02
ENSMUSG00000063428	Ddo	D-aspartate oxidase	1482.79067	-0.154868869	0.043574294	-3.554133786	0.000379226	3.48E-02
ENSMUSG00000042155	Klhl23	kelch-like 23	3422.227809	-0.108699883	0.03072909	-3.537360911	0.000404147	3.69E-02
ENSMUSG00000001227	Sema6b	sema domain, transmembrane domain (TM), and cytoplasmic domain, (semaphorin) 6B	1758.165062	0.156707228	0.044407639	3.528834961	0.000417393	3.79E-02

ENSMUSG00000037579	Kcnh3	potassium voltage-gated channel, subfamily H (eag-related), member 3	141.4872672	0.699261434	0.198678837	3.519556709	0.000432269	3.90E-02
ENSMUSG00000039838	Slc45a1	solute carrier family 45, member 1	2158.860514	0.248713208	0.070876463	3.509108621	0.000449611	4.04E-02
ENSMUSG00000029059	Fam213b	family with sequence similarity 213, member B	1756.94047	0.240099039	0.06861156	3.499396293	0.000466313	4.17E-02
ENSMUSG00000041695	Kcnj2	potassium inwardly-rectifying channel, subfamily J, member 2	142.9180509	-0.457228698	0.130737517	-3.497302913	0.000469988	4.18E-02
ENSMUSG00000018076	Med13l	mediator complex subunit 13-like	5781.01772	-0.173663194	0.049763156	-3.489794661	0.000483392	4.26E-02
ENSMUSG00000044134	Pheta1	PH domain containing endocytic trafficking adaptor 1	704.7746099	0.237777278	0.068167136	3.48815119	0.000486373	4.26E-02
ENSMUSG00000050511	Oprd1	opioid receptor, delta 1	20.04430459	-1.209406991	0.346726523	-3.488071752	0.000486517	4.26E-02
ENSMUSG00000030092	Cntn6	contactin 6	5331.154587	-0.182682189	0.052415205	-3.485289974	0.000491604	4.28E-02
ENSMUSG00000032295	Man2c1	mannosidase, alpha, class 2C, member 1	4727.558809	0.127253112	0.036673966	3.46984868	0.000520752	4.51E-02
ENSMUSG00000023764	Sfi1	Sfi1 homolog, spindle assembly associated (yeast)	1212.243325	0.224302065	0.064771647	3.462966855	0.000534254	4.59E-02
ENSMUSG00000024076	Vit	vitrin	66.44094499	-0.547881353	0.158244454	-3.462246786	0.000535686	4.59E-02
ENSMUSG00000028150	Rorc	RAR-related orphan receptor gamma	2262.687714	0.230559859	0.066619632	3.460839586	0.000538494	4.59E-02
ENSMUSG00000040651	Fam208a	family with sequence similarity 208, member A	4400.287323	-0.205270022	0.059351971	-3.458520737	0.00054315	4.61E-02
ENSMUSG00000032328	Tmem30a	transmembrane protein 30A	15615.31096	-0.114504148	0.033143918	-3.454755915	0.000550791	4.65E-02
ENSMUSG00000109724	Gm18194	predicted gene 18194	133.610084	-0.426838601	0.123598131	-3.45343896	0.000553488	4.65E-02
ENSMUSG00000033862	Cdk10	cyclin-dependent kinase 10	1241.950755	0.202461754	0.05868709	3.449851619	0.000560895	4.65E-02
ENSMUSG00000061046	Haghl	hydroxyacylglutathione hydrolase-like	3351.199806	0.194626781	0.056425654	3.449260539	0.000562124	4.65E-02
ENSMUSG00000078480	Mrpl48-ps	Mitochondrial ribosomal protein L48	27.58601781	-3.250561366	0.94190633	-3.451045249	0.00055842	4.65E-02
ENSMUSG00000032324	Tspan3	tetraspanin 3	9627.269076	0.132814628	0.03855294	3.44499351	0.000571073	4.70E-02
ENSMUSG00000023017	Asic1	acid-sensing (proton-gated) ion channel 1	5549.805749	0.176764615	0.051358748	3.441762535	0.000577937	4.73E-02
ENSMUSG00000099616	4932413F04Rik	RIKEN cDNA 4932413F04 gene	21.90064226	2.125104477	0.619335029	3.43126802	0.000600767	4.89E-02
ENSMUSG00000110945	Gm9856	predicted gene 9856	328.9491498	-0.365949833	0.106689059	-3.4300596	0.000603449	4.89E-02

Supp Table S10. List of Differentially Expressed genes at FDR 5% in *Gnb5-/-* mice - hippocampus

Ensembl ID	Gene Symbol	Gene name	baseMean	log2FoldChange	lfcSE	stat	pvalue	padj
ENSMUSG00000032192	Gnb5	guanine nucleotide binding protein (G protein), beta 5	2382.397101	-2.949092443	0.050530966	-58.36208266	0.00E+00	< 2.00E-308
ENSMUSG00000023979	Guca1b	guanylate cyclase activator 1B	267.9709549	3.578006541	0.118457105	30.20508174	2.03E-200	1.96E-196
ENSMUSG00000048758	Rpl29	ribosomal protein L29	186.1160919	-2.54505664	0.14267899	-17.83764128	3.61E-71	2.32E-67
ENSMUSG00000020253	Ppm1m	protein phosphatase 1M	677.7813768	-0.764173504	0.069114538	-11.05662471	2.04E-28	9.82E-25
ENSMUSG00000032556	Bfsp2	beaded filament structural protein 2, phakinin	72.5712779	-3.439485494	0.36690378	-9.374352839	6.96E-21	2.68E-17
ENSMUSG00000023345	Poc1a	POC1 centriolar protein A	290.9177971	-0.980344264	0.104992395	-9.337288312	9.88E-21	3.18E-17
ENSMUSG00000032221	Mns1	meiosis-specific nuclear structural protein 1	180.727792	1.133030106	0.149838879	7.56165631	3.98E-14	1.10E-10
ENSMUSG00000049624	Slc17a5	solute carrier family 17 (anion/sugar transporter), member 5	1358.227186	0.395134078	0.0552683	7.149379957	8.72E-13	2.10E-09
ENSMUSG00000032418	Me1	malic enzyme 1, NADP(+)-dependent, cytosolic	3220.61655	0.35094107	0.049212845	7.131086888	9.96E-13	2.13E-09
ENSMUSG00000032344	Cgas	cyclic GMP-AMP synthase	64.05394375	-1.297224737	0.183150018	-7.082853442	1.41E-12	2.48E-09
ENSMUSG00000087466	A330041J22Rik	RIKEN cDNA A330041J22 gene	106.9804268	1.041048682	0.146908797	7.086360423	1.38E-12	2.48E-09
ENSMUSG00000032383	Ppib	peptidylprolyl isomerase B	7246.634387	0.323390812	0.046451328	6.961928182	3.36E-12	5.39E-09
ENSMUSG00000034910	Pygo1	pygopus 1	4535.707067	0.296843044	0.042829899	6.930743563	4.19E-12	6.21E-09
ENSMUSG00000057802	Gm10030	predicted gene 10030	24.02046494	-2.238670246	0.325437036	-6.878965819	6.03E-12	8.31E-09
ENSMUSG00000103164	Gm38150	predicted gene 38150	26.51357105	1.792662303	0.27409376	6.540325124	6.14E-11	7.89E-08
ENSMUSG00000047257	Prss45	protease, serine 45	29.29370674	2.22072601	0.345290573	6.431470148	1.26E-10	1.52E-07
ENSMUSG00000042210	Abhd14a	abhydrolase domain containing 14A	1011.239637	-0.395645636	0.062995633	-6.280524786	3.37E-10	3.83E-07
ENSMUSG00000102225	Gm37983	predicted gene 37983	19.23587601	2.053502553	0.328382635	6.253383503	4.02E-10	4.30E-07
ENSMUSG00000113637	Gm7049	predicted gene 7049	22.35956108	2.599937147	0.417875517	6.221798223	4.91E-10	4.99E-07
ENSMUSG00000032498	Mlh1	mutL homolog 1	473.749797	-0.608376157	0.098140351	-6.199041977	5.68E-10	5.48E-07
ENSMUSG00000032349	Elovl5	ELOVL family member 5, elongation of long chain fatty acids (yeast)	3448.449111	0.266712933	0.043182619	6.176395514	6.56E-10	6.02E-07
ENSMUSG00000032872	Cyb5r4	cytochrome b5 reductase 4	1427.463459	-0.552583779	0.097467466	-5.669417721	1.43E-08	1.26E-05

ENSMUSG00000062270	Morf4l1	mortality factor 4 like 1	4261.150376	-0.370709156	0.066751219	-5.553593847	2.80E-08	2.35E-05
ENSMUSG00000062270	Morf4l1b	mortality factor 4 like 1B	4261.150376	-0.370709156	0.066751219	-5.553593847	2.80E-08	2.35E-05
ENSMUSG00000032232	Cgnl1	cingulin-like 1	716.6625714	-0.674264189	0.126477175	-5.331113623	9.76E-08	7.55E-05
ENSMUSG00000032563	Mrpl3	mitochondrial ribosomal protein L3	2653.667229	-0.241906517	0.045381018	-5.330566088	9.79E-08	7.55E-05
ENSMUSG00000029471	Camkk2	calcium/calmodulin-dependent protein kinase kinase 2, beta	7986.908004	0.28842287	0.055844882	5.164714513	2.41E-07	1.79E-04
ENSMUSG00000111348	Gm19531	predicted gene 19531	60.80809486	-0.967537	0.190133025	-5.088737203	3.60E-07	2.57E-04
ENSMUSG00000032363	Adamts7	a disintegrin-like and metallopeptidase (reprolysin type) with thrombospondin type 1 motif, 7	60.02830454	1.253658417	0.250364087	5.007341231	5.52E-07	3.79E-04
ENSMUSG00000034898	Filip1	filamin A interacting protein 1	818.7049445	1.116876389	0.2236231	4.994458936	5.90E-07	3.79E-04
ENSMUSG00000046186	Cd109	CD109 antigen	440.3239799	0.744000787	0.14896346	4.994518707	5.90E-07	3.79E-04
ENSMUSG00000032184	Lysmd2	LysM, putative peptidoglycan-binding, domain containing 2	1535.062665	0.192736213	0.039007063	4.941059295	7.77E-07	4.83E-04
ENSMUSG00000032567	Aste1	asteroid homolog 1	258.6818556	-0.411147502	0.08364275	-4.915518725	8.85E-07	5.34E-04
ENSMUSG00000004366	Sst	somatostatin	4564.046349	-0.619153137	0.128391349	-4.822389825	1.42E-06	8.05E-04
ENSMUSG00000086296	D030055H07Rik	RIKEN cDNA 030055H07 gene	30.05950376	1.958950704	0.408226916	4.798680896	1.60E-06	8.80E-04
ENSMUSG00000029819	Npy	neuropeptide Y	939.2650548	-0.512512486	0.107467639	-4.768993613	1.85E-06	9.92E-04
ENSMUSG00000042208	0610010F05Rik	RIKEN cDNA 0610010F05 gene	2105.523782	0.161358008	0.034019647	4.743082913	2.10E-06	1.10E-03
ENSMUSG00000042073	Abhd14b	abhydrolase domain containing 14b	680.5734956	-0.292955368	0.061980538	-4.726570277	2.28E-06	1.16E-03
ENSMUSG00000028681	Ptch2	patched 2	163.9075961	0.837619832	0.177967416	4.706590954	2.52E-06	1.21E-03
ENSMUSG00000064023	Klk8	kallikrein related-peptidase 8	472.905183	0.558842709	0.118652722	4.709902128	2.48E-06	1.21E-03
ENSMUSG00000039474	Wfs1	wolframin ER transmembrane glycoprotein	6619.822236	0.444546447	0.094628776	4.6977935	2.63E-06	1.24E-03
ENSMUSG00000021680	Crhbp	corticotropin releasing hormone binding protein	811.9965294	-0.700244123	0.150359765	-4.657124341	3.21E-06	1.47E-03
ENSMUSG00000049303	Syt12	synaptotagmin XII	1361.722132	0.338352088	0.072743355	4.651312622	3.30E-06	1.48E-03
ENSMUSG00000104586	4921539H07Rik	RIKEN cDNA 4921539H07	315.8272611	0.702883487	0.151686402	4.633793656	3.59E-06	1.57E-03
ENSMUSG00000041506	Rrp9	RRP9, small subunit (SSU) processome component, homolog (yeast)	673.6407763	-0.305170804	0.066043718	-4.620739307	3.82E-06	1.64E-03

ENSMUSG00000032420	Nt5e	5' nucleotidase, ecto	175.8655902	0.583004051	0.126570941	4.606144538	4.10E-06	1.72E-03
ENSMUSG00000023982	Guca1a	guanylate cyclase activator 1a (retina)	10.42051793	2.196823203	0.478445803	4.591582138	4.40E-06	1.81E-03
ENSMUSG00000060935	Tmem263	transmembrane protein 263	1125.137161	0.21083974	0.045978252	4.585640582	4.53E-06	1.82E-03
ENSMUSG00000010054	Tusc2	tumor suppressor 2, mitochondrial calcium regulator	2669.280548	0.150507457	0.033050594	4.553850268	5.27E-06	2.03E-03
ENSMUSG00000016942	Tmprss6	transmembrane serine protease 6	39.72576369	1.593037625	0.349843922	4.553566674	5.27E-06	2.03E-03
ENSMUSG00000030966	Trim21	tripartite motif-containing 21	113.3212122	-0.693400583	0.152836079	-4.536890679	5.71E-06	2.16E-03
ENSMUSG00000030688	Stard10	START domain containing 10	541.7897091	-0.295630626	0.065426937	-4.518484851	6.23E-06	2.31E-03
ENSMUSG00000029361	Nos1	nitric oxide synthase 1, neuronal	8256.593264	-0.261130979	0.059373749	-4.398088118	1.09E-05	3.97E-03
ENSMUSG00000063297	Luzp2	leucine zipper protein 2	6275.556935	0.268145569	0.061330761	4.372122009	1.23E-05	4.39E-03
ENSMUSG00000032570	Atp2c1	ATPase, Ca++-sequestering	10045.80105	0.188841067	0.043261344	4.365122496	1.27E-05	4.46E-03
ENSMUSG00000043719	Col6a6	collagen, type VI, alpha 6	118.7663673	1.69637505	0.390171056	4.347772659	1.38E-05	4.74E-03
ENSMUSG00000032332	Col12a1	collagen, type XII, alpha 1	629.8618523	-0.433906638	0.100352904	-4.32380748	1.53E-05	5.02E-03
ENSMUSG00000053040	Aph1c	aph1 homolog C, gamma secretase subunit	494.1347982	-0.311844717	0.072119583	-4.323995034	1.53E-05	5.02E-03
ENSMUSG00000058587	Tmod3	tropomodulin 3	1118.986474	-0.281319427	0.065066984	-4.323535703	1.54E-05	5.02E-03
ENSMUSG00000043587	Pxylp1	2-phosphoxylose phosphatase 1	545.5374077	-0.597492552	0.139927712	-4.270008748	1.95E-05	6.28E-03
ENSMUSG00000037089	Slc35b2	solute carrier family 35, member B2	868.1670288	0.238115051	0.05583839	4.264360995	2.00E-05	6.34E-03
ENSMUSG00000054204	Alkal2	ALK and LTK ligand 2	136.1426888	-0.81219183	0.191945922	-4.231357575	2.32E-05	7.23E-03
ENSMUSG00000032572	Col6a4	collagen, type VI, alpha 4	126.9727054	-2.511414656	0.595871353	-4.214692722	2.50E-05	7.66E-03
ENSMUSG00000085007	Gm11549	predicted gene 11549	231.5328462	0.4463464	0.106199532	4.202903639	2.64E-05	7.94E-03
ENSMUSG00000000805	Car4	carbonic anhydrase 4	2357.367529	0.308419263	0.073606666	4.19009963	2.79E-05	8.27E-03
ENSMUSG00000032330	Cox7a2	cytochrome c oxidase subunit 7A2	3013.00797	0.125559116	0.030057148	4.177346281	2.95E-05	8.49E-03
ENSMUSG00000110814	Gm38661	predicted gene 38661	14.96083878	-1.561989653	0.373750415	-4.179231894	2.92E-05	8.49E-03
ENSMUSG00000091345	Col6a5	collagen, type VI, alpha 5	174.2352851	1.016652505	0.244067905	4.165449379	3.11E-05	8.81E-03
ENSMUSG00000068428	Gmnc	geminin coiled-coil domain containing	264.2827313	-0.336898445	0.080973307	-4.160611156	3.17E-05	8.87E-03
ENSMUSG00000024883	Rin1	Ras and Rab interactor 1	4208.394122	0.206174191	0.049688679	4.149319198	3.33E-05	9.19E-03

ENSMUSG00000105230	Gm42433	predicted gene 42433	436.7842918	0.246770538	0.059606745	4.139976749	3.47E-05	9.44E-03
ENSMUSG00000071252	2210408I21Rik	RIKEN cDNA 2210408I21 gene	389.615445	0.264361422	0.064174253	4.119431228	3.80E-05	1.02E-02
ENSMUSG00000041923	Nol4	nucleolar protein 4	3286.050462	0.140254784	0.034100943	4.112929765	3.91E-05	1.03E-02
ENSMUSG00000019947	Arid5b	AT rich interactive domain 5B (MRF1-like)	1885.967968	-0.260157537	0.06335511	-4.106338656	4.02E-05	1.03E-02
ENSMUSG00000037104	Socs5	suppressor of cytokine signaling 5	5886.68313	0.107574506	0.026251141	4.097898351	4.17E-05	1.06E-02
ENSMUSG00000028971	Cort	cortistatin	67.60807817	-0.724694391	0.178109095	-4.068823039	4.73E-05	1.18E-02
ENSMUSG00000010057	Nprl2	NPR2 like, GATOR1 complex subunit	1429.63198	0.202997062	0.050049486	4.055927008	4.99E-05	1.23E-02
ENSMUSG00000032497	Lrrfip2	leucine rich repeat (in FLII) interacting protein 2	1294.793986	-0.201517371	0.049816198	-4.045217774	5.23E-05	1.26E-02
ENSMUSG00000040875	Osbpl10	oxysterol binding protein-like 10	644.5691274	-0.352970362	0.087207161	-4.047492849	5.18E-05	1.26E-02
ENSMUSG00000031209	Heph	hephaestin	349.4145748	-0.441492572	0.109271656	-4.040321062	5.34E-05	1.27E-02
ENSMUSG00000112441	Gm48898	predicted gene 48898	20.14550056	1.319734025	0.326804115	4.03830296	5.38E-05	1.27E-02
ENSMUSG00000014601	Strip1	striatin interacting protein 1	4618.315049	0.121491804	0.030263161	4.014511357	5.96E-05	1.37E-02
ENSMUSG00000040936	Ulk4	unc-51-like kinase 4	201.3074905	-0.524730265	0.132061386	-3.973381479	7.09E-05	1.61E-02
ENSMUSG00000038859	Baiap2l1	BAI1-associated protein 2-like 1	49.0839138	-1.306916288	0.331538163	-3.941978429	8.08E-05	1.81E-02
ENSMUSG00000016763	Scube1	signal peptide, CUB domain, EGF-like 1	1726.279322	0.426222434	0.108205935	3.93899311	8.18E-05	1.81E-02
ENSMUSG00000103133	Gm37303	predicted gene 37303	77.94310654	0.522106934	0.133550723	3.909427989	9.25E-05	2.03E-02
ENSMUSG00000004951	Hspb1	heat shock protein 1	151.4367051	-0.835319314	0.213951004	-3.904255167	9.45E-05	2.05E-02
ENSMUSG00000090877	Hspa1b	heat shock protein 1B	392.1558983	-0.763255749	0.19636514	-3.88692082	1.02E-04	2.18E-02
ENSMUSG00000029462	Vps29	VPS29 retromer complex component	3845.833264	0.14493881	0.037518194	3.863160675	1.12E-04	2.32E-02
ENSMUSG00000042444	Mindy2	MINDY lysine 48 deubiquitinase 2	3612.316289	-0.152283466	0.039398177	-3.865241432	1.11E-04	2.32E-02
ENSMUSG00000108325	NA	NA	93.73890629	0.5200387	0.134475044	3.867176279	1.10E-04	2.32E-02
ENSMUSG00000035941	Ibtk	inhibitor of Bruton agammaglobulinemia tyrosine kinase	1211.17404	-0.205862348	0.053432389	-3.852763275	1.17E-04	2.40E-02
ENSMUSG00000045327	6330549D23Rik	RIKEN cDNA 6330549D23 gene	49.6841459	-0.674934781	0.1754258	-3.847408893	1.19E-04	2.42E-02
ENSMUSG00000032012	Nectin1	nectin cell adhesion molecule 1	2017.659804	0.237274266	0.061873515	3.834827627	1.26E-04	2.52E-02

ENSMUSG00000051910	Sox6	SRY (sex determining region Y)-box 6	1109.249799	-0.210449817	0.054915382	-3.832256303	1.27E-04	2.52E-02
ENSMUSG00000033644	Piwil2	piwi-like RNA-mediated gene silencing 2	81.66252996	-0.533317618	0.139890545	-3.812392175	1.38E-04	2.71E-02
ENSMUSG00000006522	Itih3	inter-alpha trypsin inhibitor, heavy chain 3	1084.136711	-0.295092903	0.078005203	-3.782990024	1.55E-04	2.99E-02
ENSMUSG00000107092	Gm7993	predicted gene 7993	27.55659689	3.745229986	0.998444348	3.751065337	1.76E-04	3.36E-02
ENSMUSG00000038370	Pcp4l1	Purkinje cell protein 4-like 1	1329.318487	-0.232791453	0.063060501	-3.69155731	2.23E-04	4.17E-02
ENSMUSG00000048001	Hes5	hes family bHLH transcription factor 5	210.1360801	0.574406535	0.155524959	3.693339899	2.21E-04	4.17E-02
ENSMUSG00000051590	Map3k19	mitogen-activated protein kinase kinase kinase 19	332.5326268	-0.512141061	0.138814957	-3.689379518	2.25E-04	4.17E-02
ENSMUSG00000032265	Tent5a	terminal nucleotidyltransferase 5A	327.0098402	-0.714753787	0.195490594	-3.656205511	2.56E-04	4.70E-02

Supp Table S11. List of Differentially Expressed genes at FDR 5% in *Gnb5-/-* mice - cerebral cortex

Ensembl ID	Gene Symbol	Gene name	baseMean	log2FoldChange	lfcSE	stat	pvalue	padj
ENSMUSG00000032192	Gnb5	guanine nucleotide binding protein (G protein), beta 5	3593.342841	-3.062918872	0.090085387	-34.0001745	2.21E-253	4.84E-249
ENSMUSG00000023979	Guca1b	guanylate cyclase activator 1B	263.8918466	3.835511755	0.13316811	28.80202898	2.0231E-182	2.209E-178
ENSMUSG00000048758	Rpl29	ribosomal protein L29	264.164767	-2.731697404	0.15217746	-17.95073601	4.73586E-72	3.44739E-68
ENSMUSG00000020253	Ppm1m	protein phosphatase 1M	894.8693801	-1.212158437	0.086719969	-13.97784672	2.1283E-44	1.16195E-40
ENSMUSG00000032221	Mns1	meiosis-specific nuclear structural protein 1	116.3525616	1.634839206	0.147435847	11.08847841	1.42694E-28	6.23231E-25
ENSMUSG00000023345	Poc1a	POC1 centriolar protein A	386.6670779	-1.089635159	0.121899515	-8.938798156	3.93426E-19	1.43194E-15
ENSMUSG00000032332	Col12a1	collagen, type XII, alpha 1	887.9004528	-0.885695463	0.103581894	-8.550678424	1.22367E-17	3.8175E-14
ENSMUSG00000111765	Gm10635	predicted gene 10635	51.20226751	-3.314939998	0.393896818	-8.415757245	3.90365E-17	1.0656E-13
ENSMUSG00000111348	Gm19531	predicted gene 19531	101.5467041	-1.241020024	0.148741013	-8.343495822	7.2126E-17	1.7501E-13
ENSMUSG00000047257	Prss45	protease, serine 45	34.35647461	2.296734155	0.277403272	8.279405412	1.23792E-16	2.70337E-13
ENSMUSG00000042210	Abhd14a	abhydrolase domain containing 14A	1032.445648	-0.613596969	0.083391587	-7.358020052	1.86658E-13	3.70567E-10
ENSMUSG00000102225	Gm37983	predicted gene 37983	19.57885383	2.58186601	0.362084881	7.130554587	9.99653E-13	1.8192E-09
ENSMUSG00000043719	Col6a6	collagen, type VI, alpha 6	105.0713081	1.589103099	0.247685384	6.41581298	1.40073E-10	2.35302E-07

ENSMUSG00000032349	Elovl5	ELOVL family member 5, elongation of long chain fatty acids (yeast)	3648.481725	0.321846446	0.051309014	6.272707688	3.54823E-10	5.53473E-07
ENSMUSG00000032418	Me1	malic enzyme 1, NADP(+)-dependent, cytosolic	2016.009287	0.340643445	0.054688731	6.228768528	4.70116E-10	6.84426E-07
ENSMUSG00000010044	Zmynd10	zinc finger, MYND domain containing 10	228.8723475	0.730365544	0.120958409	6.038154333	1.55887E-09	1.79172E-06
ENSMUSG00000032498	Mlh1	mutL homolog 1	521.8321994	-0.490752727	0.081153472	-6.047217911	1.47368E-09	1.79172E-06
ENSMUSG00000032872	Cyb5r4	cytochrome b5 reductase 4	1413.346395	-0.564165726	0.093231634	-6.051226418	1.43747E-09	1.79172E-06
ENSMUSG00000087466	A330041J22 Rik	RIKEN cDNA A330041J22 gene	81.90474134	1.204927988	0.202332849	5.955177308	2.5979E-09	2.83665E-06
ENSMUSG00000049555	Tmie	transmembrane inner ear	241.8759334	0.63716907	0.114389213	5.570184912	2.54469E-08	2.64624E-05
ENSMUSG00000032556	Bfsp2	beaded filament structural protein 2, phakinin	85.4861346	-2.94717596	0.53990551	-5.458688424	4.79665E-08	4.63913E-05
ENSMUSG00000057802	Gm10030	predicted gene 10030	22.31636754	-1.9157509	0.351165297	-5.45541065	4.88598E-08	4.63913E-05
ENSMUSG00000062270	Morf4l1	mortality factor 4 like 1	3862.642941	-0.355532571	0.066892551	-5.314979978	1.06669E-07	9.706E-05
ENSMUSG00000062270	Morf4l1b	mortality factor 4 like 1B	3862.642941	-0.355532571	0.066892551	-5.314979978	1.06669E-07	9.706E-05
ENSMUSG00000103164	Gm38150	predicted gene 38150	23.78691025	1.84771035	0.366887132	5.036181944	4.74909E-07	0.000414843
ENSMUSG00000032383	Ppib	peptidylprolyl isomerase B	6545.594919	0.317038174	0.064051057	4.949772724	7.43002E-07	0.000624064
ENSMUSG00000059146	Ntrk3	neurotrophic tyrosine kinase, receptor, type 3	10681.1642	-0.195870941	0.040335881	-4.855997647	1.19782E-06	0.000968816
ENSMUSG00000059146	E430016F16 Rik	RIKEN cDNA E430016F16 gene	10681.1642	-0.195870941	0.040335881	-4.855997647	1.19782E-06	0.000968816
ENSMUSG00000032497	Lrrfip2	leucine rich repeat (in FLII) interacting protein 2	1541.136996	-0.220140185	0.04568305	-4.81885913	1.44381E-06	0.001126072
ENSMUSG00000109975	Gm19196	predicted gene 19196	76.97292567	-0.83775478	0.179372068	-4.670486274	3.00488E-06	0.002262775
ENSMUSG00000097099	Gm9917	predicted gene 9917	87.59711317	-0.72766991	0.158976579	-4.577214553	4.71208E-06	0.003334375
ENSMUSG00000110996	Gm36251	predicted gene, 36251	83.08922865	-2.301491121	0.502918057	-4.576274579	4.73329E-06	0.003334375
ENSMUSG00000024143	Rhoq	ras homolog family member Q	1994.563327	0.27220004	0.059757079	4.555109551	5.23583E-06	0.003573126
ENSMUSG00000055125	M5C1000l18 Rik	RIKEN cDNA M5C1000l18	169.1051477	-0.512026751	0.116302137	-4.4025567	1.06983E-05	0.007079656
ENSMUSG00000043587	Pxylp1	2-phosphoxylose phosphatase 1	541.0845473	-0.522547059	0.12057503	-4.333791642	1.46563E-05	0.009413649
ENSMUSG00000032370	Lactb	lactamase, beta	508.7191939	-0.370527801	0.086670063	-4.275153232	1.91006E-05	0.011586629
ENSMUSG00000063953	Amd2	S-adenosylmethionine decarboxylase 2	13.33707831	2.326043682	0.551895854	4.214642425	2.50174E-05	0.014765689

ENSMUSG00000041506	Rrp9	RRP9, small subunit (SSU) processome component, homolog (yeast)	741.5546544	-0.371086466	0.089204231	-4.159964852	3.18297E-05	0.018292002
ENSMUSG00000034910	Pygo1	pygopus 1	2350.941427	0.238237403	0.057597268	4.13626219	3.53009E-05	0.019766684
ENSMUSG00000033208	S100b	S100 protein, beta polypeptide, neural	4168.970089	0.202698353	0.049322006	4.109693985	3.96184E-05	0.021252459
ENSMUSG00000042073	Abhd14b	abhydrolase domain containing 14b	685.2510238	-0.305729814	0.074452684	-4.106363902	4.01936E-05	0.021252459
ENSMUSG00000091735	Gpr62	G protein-coupled receptor 62	243.7985731	0.456204569	0.111202042	4.102483748	4.08739E-05	0.021252459
ENSMUSG00000033730	Egr3	early growth response 3	6887.681122	-0.476370365	0.117456133	-4.055730036	4.9978E-05	0.025381829
ENSMUSG00000041460	Cacna2d4	calcium channel, voltage-dependent, alpha 2/delta subunit 4	115.497014	0.560303026	0.139981496	4.002693509	6.26254E-05	0.031082129
ENSMUSG00000039943	Plcb4	phospholipase C, beta 4	2966.652641	-0.243003116	0.061111924	-3.976361751	6.99776E-05	0.033959376
ENSMUSG00000032184	Lysmd2	LysM, putative peptidoglycan-binding, domain containing 2	1379.081352	0.192652009	0.049069682	3.926090417	8.63377E-05	0.04098789
ENSMUSG00000107092	Gm7993	predicted gene 7993	24.59807194	3.811634628	0.974363079	3.911924324	9.15636E-05	0.042543958
ENSMUSG00000032563	Mrpl3	mitochondrial ribosomal protein L3	2663.113172	-0.178171707	0.045609773	-3.906437045	9.3667E-05	0.042614597

Supp. Table S12. List of Biological Processes (BP) at FDR 5% - cerebellum

GO ID	Description	BgRatio	pvalue	p.adjust	qvalue	geneID	Count
GO:0042391	regulation of membrane potential	430/21092	7.30339E-05	0.164189734	0.156177167	Grin2a/Dcn/Snca/Tmem108/Hcn2/Dgki/Ntrk2/Kcnk2/Tusc2/Kcnh3/Kcnj2/Oprd1/Asic1	13
GO:0043949	regulation of cAMP-mediated signaling	64/21092	0.000200911	0.164189734	0.156177167	Gpr62/Pde10a/Mrap2/Gnai2/Cgas	5
GO:0006865	amino acid transport	145/21092	0.000227254	0.164189734	0.156177167	Slc25a29/Slc17a5/Myo6/Snca/Slc6a5/Ntrk2/Slc7a11	7
GO:0050808	synapse organization	427/21092	0.000271612	0.164189734	0.156177167	Filip1/Camkv/Col4a5/Zfp804a/Myo6/Snca/Magi2/Tmem108/Sncb/Dctn1/Ntrk2/Slc7a11	12
GO:0010039	response to iron ion	20/21092	0.000596278	0.288360066	0.274287904	Trf/Snca/Hfe	3
GO:0046928	regulation of neurotransmitter secretion	137/21092	0.001064507	0.3155174	0.300119942	Syt12/Myo6/Snca/Dgki/Ntrk2/Asic1	6
GO:0006022	aminoglycan metabolic process	99/21092	0.00148897	0.3155174	0.300119942	Pxylp1/Dcn/Chil5/Itih5/Cemip	5
GO:0043951	negative regulation of cAMP-mediated signaling	28/21092	0.001631142	0.3155174	0.300119942	Pde10a/Mrap2/Gnai2	3

GO:0050654	chondroitin sulfate proteoglycan metabolic process	29/21092	0.0018082	0.3155174	0.300119942	Pxylp1/Dcn/B3gat2	3
GO:0015800	acidic amino acid transport	63/21092	0.001941813	0.3155174	0.300119942	Myo6/Snca/Ntrk2/Slc7a11	4
GO:0015711	organic anion transport	404/21092	0.002251239	0.3155174	0.300119942	Slc25a29/Slc17a5/Myo6/Snca/Slc6a5/Slc4a4/Ntrk2/Slc7a11/Atp8a1/Tmem30a	10
GO:0006855	drug transmembrane transport	66/21092	0.002304207	0.3155174	0.300119942	Slc25a29/Slc6a5/Slc7a11/Tmem30a	4
GO:0051648	vesicle localization	283/21092	0.00275487	0.3155174	0.300119942	Myo5c/1190002N15Rik/Syt12/Myo6/Snca/Magi2/Dgki/Dctn1	8
GO:0098739	import across plasma membrane	114/21092	0.002763843	0.3155174	0.300119942	Slc6a5/Hcn2/Slc7a11/Hfe/Kcnj2	5
GO:0014047	glutamate secretion	34/21092	0.002871685	0.3155174	0.300119942	Myo6/Snca/Ntrk2	3
GO:0007612	learning	168/21092	0.002988362	0.3155174	0.300119942	Grin2a/Dgki/Ntrk2/Slc7a11/Atp8a1/Asic1	6
GO:0006826	iron ion transport	35/21092	0.003121703	0.3155174	0.300119942	Trf/Heph/Hfe	3
GO:1990089	response to nerve growth factor	35/21092	0.003121703	0.3155174	0.300119942	Magi2/Tmem108/Ntrk2	3
GO:1990090	cellular response to nerve growth factor stimulus	35/21092	0.003121703	0.3155174	0.300119942	Magi2/Tmem108/Ntrk2	3
GO:0043950	positive regulation of cAMP-mediated signaling	36/21092	0.003384682	0.3155174	0.300119942	Gpr62/Mrap2/Cgas	3
GO:1902475	L-alpha-amino acid transmembrane transport	37/21092	0.003660829	0.3155174	0.300119942	Slc25a29/Slc6a5/Slc7a11	3
GO:0042983	amyloid precursor protein biosynthetic process	11/21092	0.003664453	0.3155174	0.300119942	Necab1/Aatf	2
GO:0042984	regulation of amyloid precursor protein biosynthetic process	11/21092	0.003664453	0.3155174	0.300119942	Necab1/Aatf	2
GO:0106072	negative regulation of adenylate cyclase-activating G protein-coupled receptor signaling pathway	11/21092	0.003664453	0.3155174	0.300119942	Mrap2/Gnai2	2
GO:0014065	phosphatidylinositol 3-kinase signaling	122/21092	0.003699283	0.3155174	0.300119942	1190002N15Rik/Dcn/Agap2/Nyap2/Ntrk2	5
GO:1905475	regulation of protein localization to membrane	180/21092	0.004190431	0.3155174	0.300119942	Mrap2/Magi2/Slc7a11/Cemip/Gpc6/Lypd1	6
GO:0042762	regulation of sulfur metabolic process	12/21092	0.004373164	0.3155174	0.300119942	Snca/Slc7a11	2
GO:0071281	cellular response to iron ion	12/21092	0.004373164	0.3155174	0.300119942	Trf/Hfe	2

GO:0006836	neurotransmitter transport	306/21092	0.004413778	0.3155174	0.300119942	Syt12/Myo6/Snca/Slc6a5/Dgki/Ntrk2/Slc7a11/Asic1	8
GO:0006835	dicarboxylic acid transport	79/21092	0.004416017	0.3155174	0.300119942	Myo6/Snca/Ntrk2/Slc7a11	4
GO:0050805	negative regulation of synaptic transmission	79/21092	0.004416017	0.3155174	0.300119942	Gnai2/Snca/Dgki/Asic1	4
GO:0010559	regulation of glycoprotein biosynthetic process	40/21092	0.004570232	0.3155174	0.300119942	Pxylp1/Necab1/Aatf	3
GO:0001505	regulation of neurotransmitter levels	376/21092	0.004597278	0.3155174	0.300119942	Grin2a/Syt12/Myo6/Snca/Slc6a5/Dgki/Ntrk2/Slc7a11/Asic1	9
GO:0051588	regulation of neurotransmitter transport	184/21092	0.004661041	0.3155174	0.300119942	Syt12/Myo6/Snca/Dgki/Ntrk2/Asic1	6
GO:0030203	glycosaminoglycan metabolic process	81/21092	0.004827159	0.3155174	0.300119942	Pxylp1/Dcn/Itih5/Cemip	4
GO:0038179	neurotrophin signaling pathway	41/21092	0.004900965	0.3155174	0.300119942	Magi2/Tmem108/Ppp2r5b	3
GO:0009068	aspartate family amino acid catabolic process	13/21092	0.005139884	0.3155174	0.300119942	Aass/Ddo	2
GO:0042417	dopamine metabolic process	42/21092	0.005245786	0.3155174	0.300119942	Grin2a/Snca/Sncb	3
GO:0070838	divalent metal ion transport	457/21092	0.005365327	0.3155174	0.300119942	Gnb5/Grin2a/Atp2c1/Gnai2/Snca/Ibtk/Cemip/Kcnj2/Oprd1/Asic1	10
GO:0007269	neurotransmitter secretion	190/21092	0.005438454	0.3155174	0.300119942	Syt12/Myo6/Snca/Dgki/Ntrk2/Asic1	6
GO:0099643	signal release from synapse	190/21092	0.005438454	0.3155174	0.300119942	Syt12/Myo6/Snca/Dgki/Ntrk2/Asic1	6
GO:0060079	excitatory postsynaptic potential	84/21092	0.005490883	0.3155174	0.300119942	Grin2a/Snca/Tmem108/Dgki	4
GO:0072511	divalent inorganic cation transport	460/21092	0.005610938	0.3155174	0.300119942	Gnb5/Grin2a/Atp2c1/Gnai2/Snca/Ibtk/Cemip/Kcnj2/Oprd1/Asic1	10
GO:0060732	positive regulation of inositol phosphate biosynthetic process	14/21092	0.005963602	0.320444194	0.304806305	Plcd1/Snca	2
GO:0106070	regulation of adenylate cyclase-activating G protein-coupled receptor signaling pathway	14/21092	0.005963602	0.320444194	0.304806305	Mrap2/Gnai2	2
GO:1903018	regulation of glycoprotein metabolic process	45/21092	0.006366345	0.327535356	0.311551413	Pxylp1/Necab1/Aatf	3
GO:0050807	regulation of synapse organization	259/21092	0.006366485	0.327535356	0.311551413	Camkv/Zfp804a/Snca/Magi2/Dctn1/Ntrk2/Slc7a11	7
GO:0000041	transition metal ion transport	89/21092	0.006727861	0.328072847	0.312062675	Trf/Atp2c1/Heph/Hfe	4

GO:0010642	negative regulation of platelet-derived growth factor receptor signaling pathway	15/21092	0.006843317	0.328072847	0.312062675	Apod/Snca	2
GO:0097286	iron ion import	15/21092	0.006843317	0.328072847	0.312062675	Trf/Hfe	2
GO:0051650	establishment of vesicle localization	265/21092	0.00718333	0.328072847	0.312062675	Myo5c/1190002N15Rik/Syt12/Myo6/Snca/Dgki/Dctn1	7
GO:0001504	neurotransmitter uptake	47/21092	0.007186592	0.328072847	0.312062675	Snca/Slc6a5/Slc7a11	3
GO:0014066	regulation of phosphatidylinositol 3-kinase signaling	91/21092	0.007270244	0.328072847	0.312062675	1190002N15Rik/Dcn/Agap2/Ntrk2	4
GO:0050803	regulation of synapse structure or activity	266/21092	0.007326689	0.328072847	0.312062675	Camkv/Zfp804a/Snca/Magi2/Dctn1/Ntrk2/Slc7a11	7
GO:0098696	regulation of neurotransmitter receptor localization to postsynaptic specialization membrane	16/21092	0.007778044	0.331220927	0.315057127	Magi2/Gpc6	2
GO:0006816	calcium ion transport	409/21092	0.007827052	0.331220927	0.315057127	Gnb5/Grin2a/Atp2c1/Gnai2/Snca/Ibtk/Cemip/Oprd1/Asic1	9
GO:0048015	phosphatidylinositol-mediated signaling	146/21092	0.007844937	0.331220927	0.315057127	1190002N15Rik/Dcn/Agap2/Nyap2/Ntrk2	5
GO:0070588	calcium ion transmembrane transport	271/21092	0.008075514	0.331220927	0.315057127	Gnb5/Grin2a/Atp2c1/Snca/Ibtk/Cemip/Asic1	7
GO:0099565	chemical synaptic transmission, postsynaptic	94/21092	0.008136677	0.331220927	0.315057127	Grin2a/Snca/Tmem108/Dgki	4
GO:0046916	cellular transition metal ion homeostasis	95/21092	0.008439869	0.331220927	0.315057127	Trf/Atp2c1/Heph/Hfe	4
GO:0048017	inositol lipid-mediated signaling	149/21092	0.008525244	0.331220927	0.315057127	1190002N15Rik/Dcn/Agap2/Nyap2/Ntrk2	5
GO:0015893	drug transport	210/21092	0.008719811	0.331220927	0.315057127	Slc25a29/Syt12/Snca/Slc6a5/Slc7a11/Tmem30a	6
GO:0010919	regulation of inositol phosphate biosynthetic process	17/21092	0.008766807	0.331220927	0.315057127	Plcd1/Snca	2
GO:0051386	regulation of neurotrophin TRK receptor signaling pathway	17/21092	0.008766807	0.331220927	0.315057127	Tmem108/Ppp2r5b	2
GO:0071248	cellular response to metal ion	151/21092	0.009000841	0.334046503	0.317744812	Trf/Grin2a/Syt12/Snca/Hfe	5
GO:0007528	neuromuscular junction development	52/21092	0.009500864	0.334046503	0.317744812	Col4a5/Dctn1/Ntrk2	3

GO:0006898	receptor-mediated endocytosis	214/21092	0.009516311	0.334046503	0.317744812	Trf/Myo6/Snca/Magi2/Tmem108/Hfe	6
GO:0099072	regulation of postsynaptic membrane neurotransmitter receptor levels	99/21092	0.009726387	0.334046503	0.317744812	Myo6/Magi2/Gpc6/Dlg3	4
GO:0002710	negative regulation of T cell mediated immunity	18/21092	0.009808644	0.334046503	0.317744812	Il20rb/Hfe	2
GO:0010752	regulation of cGMP-mediated signaling	18/21092	0.009808644	0.334046503	0.317744812	Pde10a/Cgas	2
GO:0050650	chondroitin sulfate proteoglycan biosynthetic process	18/21092	0.009808644	0.334046503	0.317744812	Pxylp1/B3gat2	2
GO:0006879	cellular iron ion homeostasis	54/21092	0.010534313	0.353777329	0.336512761	Trf/Heph/Hfe	3
GO:0001975	response to amphetamine	19/21092	0.010902606	0.355799583	0.338436328	Grin2a/Asic1	2
GO:0048260	positive regulation of receptor-mediated endocytosis	55/21092	0.011074497	0.355799583	0.338436328	Trf/Magi2/Hfe	3
GO:0014075	response to amine	20/21092	0.012047753	0.355799583	0.338436328	Grin2a/Asic1	2
GO:0006584	catecholamine metabolic process	57/21092	0.012202184	0.355799583	0.338436328	Grin2a/Snca/Sncb	3
GO:0009712	catechol-containing compound metabolic process	57/21092	0.012202184	0.355799583	0.338436328	Grin2a/Snca/Sncb	3
GO:0045744	negative regulation of G protein-coupled receptor signaling pathway	57/21092	0.012202184	0.355799583	0.338436328	Mrap2/Gnai2/Snca	3
GO:1903510	mucopolysaccharide metabolic process	57/21092	0.012202184	0.355799583	0.338436328	Dcn/Itih5/Cemip	3
GO:1903539	protein localization to postsynaptic membrane	57/21092	0.012202184	0.355799583	0.338436328	Grin2a/Magi2/Gpc6	3
GO:0018958	phenol-containing compound metabolic process	106/21092	0.012271653	0.355799583	0.338436328	Grin2a/Snca/Sncb/Slc7a11	4
GO:0016311	dephosphorylation	367/21092	0.012532008	0.355799583	0.338436328	Ppm1m/Gnai2/Magi2/Ppm1j/Dusp7/Dlg3/Ppp2r5b/Sfi1	8
GO:0099504	synaptic vesicle cycle	228/21092	0.01271371	0.355799583	0.338436328	Syt12/Myo6/Snca/Magi2/Sncb/Dgki	6
GO:0046942	carboxylic acid transport	297/21092	0.012907908	0.355799583	0.338436328	Slc25a29/Slc17a5/Myo6/Snca/Slc6a5/Ntrk2/Slc7a11	7
GO:0015849	organic acid transport	298/21092	0.013127784	0.355799583	0.338436328	Slc25a29/Slc17a5/Myo6/Snca/Slc6a5/Ntrk2/Slc7a11	7

GO:0003433	chondrocyte development involved in endochondral bone morphogenesis	21/21092	0.013243161	0.355799583	0.338436328	Poc1a/Vit	2
GO:0095500	acetylcholine receptor signaling pathway	21/21092	0.013243161	0.355799583	0.338436328	Gnai2/Lypd1	2
GO:1903831	signal transduction involved in cellular response to ammonium ion	21/21092	0.013243161	0.355799583	0.338436328	Gnai2/Lypd1	2
GO:1905144	response to acetylcholine	21/21092	0.013243161	0.355799583	0.338436328	Gnai2/Lypd1	2
GO:1905145	cellular response to acetylcholine	21/21092	0.013243161	0.355799583	0.338436328	Gnai2/Lypd1	2
GO:0015807	L-amino acid transport	59/21092	0.013393424	0.355882404	0.338515107	Slc25a29/Slc6a5/Slc7a11	3
GO:0060078	regulation of postsynaptic membrane potential	111/21092	0.014328207	0.368755538	0.350760024	Grin2a/Snca/Tmem108/Dgki	4
GO:0003418	growth plate cartilage chondrocyte differentiation	22/21092	0.014487914	0.368755538	0.350760024	Poc1a/Vit	2
GO:0015874	norepinephrine transport	22/21092	0.014487914	0.368755538	0.350760024	Plcd1/Snca	2
GO:1902683	regulation of receptor localization to synapse	22/21092	0.014487914	0.368755538	0.350760024	Magi2/Gpc6	2
GO:0015672	monovalent inorganic cation transport	458/21092	0.015501344	0.378545307	0.360072046	Atp6v1g2/Kcnk9/Slc4a4/Hcn2/Kcnk2/Cyc1/Kcnh3/Kcnj2/Asic1	9
GO:1903828	negative regulation of cellular protein localization	114/21092	0.015660773	0.378545307	0.360072046	Dclk3/Mrap2/Apod/Lypd1	4
GO:1903077	negative regulation of protein localization to plasma membrane	23/21092	0.015781111	0.378545307	0.360072046	Mrap2/Lypd1	2
GO:0006801	superoxide metabolic process	63/21092	0.015968412	0.378545307	0.360072046	Cyb5r4/Aatf/Gnai2	3
GO:0030330	DNA damage response, signal transduction by p53 class mediator	63/21092	0.015968412	0.378545307	0.360072046	Pcbp4/Myo6/E2f7	3
GO:0042440	pigment metabolic process	63/21092	0.015968412	0.378545307	0.360072046	Cyb5r4/Alas1/Slc7a11	3
GO:0043113	receptor clustering	63/21092	0.015968412	0.378545307	0.360072046	Magi2/Slc7a11/Dlg3	3
GO:0031346	positive regulation of cell projection organization	462/21092	0.016310554	0.379822529	0.361286939	Twf2/Mns1/Zfp804a/Magi2/Ntrk2/Metrn/Efemp1/Ppp2r5b/Tmem30a	9
GO:0006470	protein dephosphorylation	242/21092	0.016599944	0.379822529	0.361286939	Ppm1m/Gnai2/Magi2/Ppm1j/Dusp7/Ppp2r5b	6

GO:0010640	regulation of platelet-derived growth factor receptor signaling pathway	24/21092	0.017121859	0.379822529	0.361286939	Apod/Snca	2
GO:0032928	regulation of superoxide anion generation	24/21092	0.017121859	0.379822529	0.361286939	Aatf/Gnai2	2
GO:0035384	thioester biosynthetic process	24/21092	0.017121859	0.379822529	0.361286939	Snca/Dlat	2
GO:0071616	acyl-CoA biosynthetic process	24/21092	0.017121859	0.379822529	0.361286939	Snca/Dlat	2
GO:0098810	neurotransmitter reuptake	24/21092	0.017121859	0.379822529	0.361286939	Snca/Slc6a5	2
GO:0051193	regulation of cofactor metabolic process	65/21092	0.017352887	0.381448013	0.362833097	Me1/Snca/Slc7a11	3
GO:0019933	cAMP-mediated signaling	179/21092	0.017689275	0.385339341	0.366534526	Gpr62/Pde10a/Mrap2/Gnai2/Cgas	5
GO:0099010	modification of postsynaptic structure	25/21092	0.01850928	0.38858238	0.369619302	Filip1/Camkv	2
GO:0120033	negative regulation of plasma membrane bounded cell projection assembly	25/21092	0.01850928	0.38858238	0.369619302	Slit2/Cdk10	2
GO:1902473	regulation of protein localization to synapse	25/21092	0.01850928	0.38858238	0.369619302	Magi2/Gpc6	2
GO:1904376	negative regulation of protein localization to cell periphery	25/21092	0.01850928	0.38858238	0.369619302	Mrap2/Lypd1	2
GO:0006029	proteoglycan metabolic process	67/21092	0.018802373	0.38858238	0.369619302	Pxylp1/Dcn/B3gat2	3
GO:0014068	positive regulation of phosphatidylinositol 3-kinase signaling	67/21092	0.018802373	0.38858238	0.369619302	Dcn/Agap2/Ntrk2	3
GO:0051668	localization within membrane	183/21092	0.019265243	0.394676759	0.375416272	Myo6/Magi2/Slc7a11/Gpc6/Dlg3	5
GO:0048168	regulation of neuronal synaptic plasticity	68/21092	0.019551554	0.394676759	0.375416272	Grin2a/Rasgrf1/Snca	3
GO:0010921	regulation of phosphatase activity	122/21092	0.019586936	0.394676759	0.375416272	Gnai2/Magi2/Dlg3/Sfi1	4
GO:0030212	hyaluronan metabolic process	26/21092	0.019942505	0.395253915	0.375965263	Itih5/Cemip	2
GO:0045332	phospholipid translocation	26/21092	0.019942505	0.395253915	0.375965263	Atp8a1/Tmem30a	2
GO:0031589	cell-substrate adhesion	325/21092	0.020133669	0.395798462	0.376483235	Rpl29/Tdgf1/Apod/Sned1/Spp1/Ecm2/Vit	7
GO:0010811	positive regulation of cell-substrate adhesion	125/21092	0.021202155	0.402000363	0.382382479	Tdgf1/Spp1/Ecm2/Vit	4

GO:0006026	aminoglycan catabolic process	27/21092	0.021420677	0.402000363	0.382382479	Chil5/Cemip	2
GO:0034204	lipid translocation	27/21092	0.021420677	0.402000363	0.382382479	Atp8a1/Tmem30a	2
GO:1902932	positive regulation of alcohol biosynthetic process	27/21092	0.021420677	0.402000363	0.382382479	Plcd1/Snca	2
GO:0007631	feeding behavior	126/21092	0.021758176	0.402000363	0.382382479	Hcrtr2/Mrap2/Ntrk2/Oprd1	4
GO:0050433	regulation of catecholamine secretion	71/21092	0.021897022	0.402000363	0.382382479	Plcd1/Syt12/Snca	3
GO:0097120	receptor localization to synapse	71/21092	0.021897022	0.402000363	0.382382479	Magi2/Gpc6/Dlg3	3
GO:0042177	negative regulation of protein catabolic process	127/21092	0.022323059	0.402000363	0.382382479	Grin2a/Agap2/Snca/Hfe	4
GO:0097553	calcium ion transmembrane import into cytosol	127/21092	0.022323059	0.402000363	0.382382479	Grin2a/Snca/Ibtk/Cemip	4
GO:0010959	regulation of metal ion transport	410/21092	0.022737662	0.402000363	0.382382479	Gnb5/Trf/Gnai2/Snca/Hfe/Cemip/Kcnj2/Oprd1	8
GO:0003413	chondrocyte differentiation involved in endochondral bone morphogenesis	28/21092	0.022942949	0.402000363	0.382382479	Poc1a/Vit	2
GO:0045780	positive regulation of bone resorption	28/21092	0.022942949	0.402000363	0.382382479	Trf/Spp1	2
GO:0046852	positive regulation of bone remodeling	28/21092	0.022942949	0.402000363	0.382382479	Trf/Spp1	2
GO:0089718	amino acid import across plasma membrane	28/21092	0.022942949	0.402000363	0.382382479	Slc6a5/Slc7a11	2
GO:1902668	negative regulation of axon guidance	28/21092	0.022942949	0.402000363	0.382382479	Slit2/Sema6b	2
GO:0097479	synaptic vesicle localization	192/21092	0.023141781	0.402567096	0.382921555	Syt12/Myo6/Snca/Magi2/Dgki	5
GO:0071804	cellular potassium ion transport	193/21092	0.023601378	0.40313958	0.383466102	Kcnk9/Hcn2/Kcnk2/Kcnh3/Kcnj2	5
GO:0071805	potassium ion transmembrane transport	193/21092	0.023601378	0.40313958	0.383466102	Kcnk9/Hcn2/Kcnk2/Kcnh3/Kcnj2	5
GO:0055076	transition metal ion homeostasis	130/21092	0.024071178	0.40313958	0.383466102	Trf/Atp2c1/Heph/Hfe	4
GO:0003333	amino acid transmembrane transport	74/21092	0.024389498	0.40313958	0.383466102	Slc25a29/Slc6a5/Slc7a11	3
GO:0032272	negative regulation of protein polymerization	74/21092	0.024389498	0.40313958	0.383466102	Twf2/Snca/Slit2	3
GO:0050432	catecholamine secretion	74/21092	0.024389498	0.40313958	0.383466102	Plcd1/Syt12/Snca	3

GO:0042168	heme metabolic process	29/21092	0.024508486	0.40313958	0.383466102	Cyb5r4/Alas1	2
GO:0051589	negative regulation of neurotransmitter transport	29/21092	0.024508486	0.40313958	0.383466102	Snca/Asic1	2
GO:0051881	regulation of mitochondrial membrane potential	75/21092	0.025252981	0.412579103	0.392444969	Dcn/Tusc2/Oprd1	3
GO:0043112	receptor metabolic process	198/21092	0.025987788	0.417990687	0.397592465	Myo6/Snca/Magi2/Pik3r4/Pheta1	5
GO:0010038	response to metal ion	269/21092	0.026268205	0.417990687	0.397592465	Trf/Grin2a/Plcd1/Syt12/Snca/Hfe	6
GO:0090287	regulation of cellular response to growth factor stimulus	269/21092	0.026268205	0.417990687	0.397592465	Tdgf1/Dcn/Tmem108/Slit2/Bcl9l/Ppp2r5b	6
GO:1904375	regulation of protein localization to cell periphery	134/21092	0.0265278	0.417990687	0.397592465	Mrap2/Magi2/Gpc6/Lypd1	4
GO:0044272	sulfur compound biosynthetic process	77/21092	0.027028868	0.417990687	0.397592465	Snca/Slc7a11/Dlat	3
GO:0032958	inositol phosphate biosynthetic process	31/21092	0.027766067	0.417990687	0.397592465	Plcd1/Snca	2
GO:0045920	negative regulation of exocytosis	31/21092	0.027766067	0.417990687	0.397592465	Gnai2/Snca	2
GO:0099563	modification of synaptic structure	31/21092	0.027766067	0.417990687	0.397592465	Filip1/Camkv	2
GO:0099633	protein localization to postsynaptic specialization membrane	31/21092	0.027766067	0.417990687	0.397592465	Magi2/Gpc6	2
GO:0099645	neurotransmitter receptor localization to postsynaptic specialization membrane	31/21092	0.027766067	0.417990687	0.397592465	Magi2/Gpc6	2
GO:1905476	negative regulation of protein localization to membrane	31/21092	0.027766067	0.417990687	0.397592465	Mrap2/Lypd1	2
GO:0048167	regulation of synaptic plasticity	348/21092	0.027881899	0.417990687	0.397592465	Grin2a/Rasgrf1/Syt12/Myo6/Snca/Dgki/Ntrk2	7
GO:0010923	negative regulation of phosphatase activity	78/21092	0.027941239	0.417990687	0.397592465	Gnai2/Dlg3/Sfi1	3
GO:0050770	regulation of axonogenesis	202/21092	0.028004339	0.417990687	0.397592465	Twf2/Ntrk2/Metrn/Slit2/Sema6b	5
GO:0043090	amino acid import	32/21092	0.029456493	0.434303664	0.413109358	Slc6a5/Slc7a11	2
GO:0048011	neurotrophin TRK receptor signaling pathway	32/21092	0.029456493	0.434303664	0.413109358	Tmem108/Ppp2r5b	2

GO:0098659	inorganic cation import across plasma membrane	81/21092	0.030775784	0.438771595	0.417359251	Hcn2/Hfe/Kcnj2	3
GO:0099587	inorganic ion import across plasma membrane	81/21092	0.030775784	0.438771595	0.417359251	Hcn2/Hfe/Kcnj2	3
GO:0031333	negative regulation of protein complex assembly	141/21092	0.031176982	0.438771595	0.417359251	Twf2/Snca/Slit2/Oprd1	4
GO:0090288	negative regulation of cellular response to growth factor stimulus	141/21092	0.031176982	0.438771595	0.417359251	Tdgf1/Dcn/Slit2/Bcl9l	4
GO:0032733	positive regulation of interleukin-10 production	33/21092	0.03118695	0.438771595	0.417359251	Il20rb/Tusc2	2
GO:0042554	superoxide anion generation	33/21092	0.03118695	0.438771595	0.417359251	Aatf/Gnai2	2
GO:1900181	negative regulation of protein localization to nucleus	33/21092	0.03118695	0.438771595	0.417359251	Dclk3/Apod	2
GO:0010810	regulation of cell-substrate adhesion	208/21092	0.031211214	0.438771595	0.417359251	Tdgf1/Apod/Spp1/Ecm2/Vit	5
GO:0010976	positive regulation of neuron projection development	357/21092	0.031400012	0.438874154	0.417456805	Twf2/Zfp804a/Magi2/Ntrk2/Metrn/Ppp2r5b/Tmem30a	7
GO:0007611	learning or memory	283/21092	0.032509909	0.445191004	0.423465388	Grin2a/Dgki/Ntrk2/Slc7a11/Atp8a1/Asic1	6
GO:0019935	cyclic-nucleotide-mediated signaling	211/21092	0.032897621	0.445191004	0.423465388	Gpr62/Pde10a/Mrap2/Gnai2/Cgas	5
GO:0007271	synaptic transmission, cholinergic	34/21092	0.032956654	0.445191004	0.423465388	Lama2/Lypd1	2
GO:0010737	protein kinase A signaling	34/21092	0.032956654	0.445191004	0.423465388	Pde10a/Lcp1	2
GO:0090322	regulation of superoxide metabolic process	34/21092	0.032956654	0.445191004	0.423465388	Aatf/Gnai2	2
GO:0097366	response to bronchodilator	34/21092	0.032956654	0.445191004	0.423465388	Grin2a/Asic1	2
GO:0010591	regulation of lamellipodium assembly	35/21092	0.034764833	0.459351728	0.43693506	Twf2/Slit2	2
GO:0033866	nucleoside bisphosphate biosynthetic process	35/21092	0.034764833	0.459351728	0.43693506	Snca/Dlat	2
GO:0034030	ribonucleoside bisphosphate biosynthetic process	35/21092	0.034764833	0.459351728	0.43693506	Snca/Dlat	2
GO:0034033	purine nucleoside bisphosphate biosynthetic process	35/21092	0.034764833	0.459351728	0.43693506	Snca/Dlat	2
GO:0042490	mechanoreceptor differentiation	86/21092	0.035822894	0.460779532	0.438293186	Myo6/Cthrc1/Ntrk2	3

GO:0060402	calcium ion transport into cytosol	148/21092	0.036276764	0.460779532	0.438293186	Grin2a/Snca/Ibtk/Cemip	4
GO:0071241	cellular response to inorganic substance	217/21092	0.036438489	0.460779532	0.438293186	Trf/Grin2a/Syt12/Snca/Hfe	5
GO:0003417	growth plate cartilage development	36/21092	0.036610724	0.460779532	0.438293186	Poc1a/Vit	2
GO:0006739	NADP metabolic process	36/21092	0.036610724	0.460779532	0.438293186	Me1/Cyb5r4	2
GO:0033238	regulation of cellular amine metabolic process	36/21092	0.036610724	0.460779532	0.438293186	Snca/Slc7a11	2
GO:0050919	negative chemotaxis	36/21092	0.036610724	0.460779532	0.438293186	Slit2/Sema6b	2
GO:0051181	cofactor transport	36/21092	0.036610724	0.460779532	0.438293186	Slc25a29/Slc7a11	2
GO:0072524	pyridine-containing compound metabolic process	149/21092	0.037042323	0.460779532	0.438293186	Me1/Cyb5r4/Pnpo/Dlat	4
GO:1901615	organic hydroxy compound metabolic process	453/21092	0.037758467	0.460779532	0.438293186	Grin2a/Pnpo/Plcd1/Snca/Sncb/Cyp11a1 /Slc7a11/Haghl	8
GO:0042737	drug catabolic process	150/21092	0.037817159	0.460779532	0.438293186	Aass/Snca/Chil5/Ctsh	4
GO:0035418	protein localization to synapse	88/21092	0.037953804	0.460779532	0.438293186	Grin2a/Magi2/Gpc6	3
GO:0055072	iron ion homeostasis	88/21092	0.037953804	0.460779532	0.438293186	Trf/Heph/Hfe	3
GO:0006778	porphyrin-containing compound metabolic process	37/21092	0.038493575	0.460779532	0.438293186	Cyb5r4/Alas1	2
GO:0009311	oligosaccharide metabolic process	37/21092	0.038493575	0.460779532	0.438293186	B3galt1/Man2c1	2
GO:0032620	interleukin-17 production	37/21092	0.038493575	0.460779532	0.438293186	Tusc2/Rorc	2
GO:0048169	regulation of long-term neuronal synaptic plasticity	37/21092	0.038493575	0.460779532	0.438293186	Grin2a/Snca	2
GO:0048846	axon extension involved in axon guidance	37/21092	0.038493575	0.460779532	0.438293186	Slit2/Sema6b	2
GO:1902284	neuron projection extension involved in neuron projection guidance	37/21092	0.038493575	0.460779532	0.438293186	Slit2/Sema6b	2
GO:0019318	hexose metabolic process	221/21092	0.03892471	0.462775342	0.440191599	Apod/Glb1/Dlat/Man2c1/Rorc	5
GO:0051937	catecholamine transport	89/21092	0.039043081	0.462775342	0.440191599	Plcd1/Syt12/Snca	3

GO:0042770	signal transduction in response to DNA damage	90/21092	0.040148167	0.47355253	0.450442853	Pcbp4/Myo6/E2f7	3
GO:0002686	negative regulation of leukocyte migration	38/21092	0.040412644	0.474358121	0.45120913	Apod/Slit2	2
GO:0035305	negative regulation of dephosphorylation	91/21092	0.041269006	0.482069834	0.458544507	Gnai2/Dlg3/Sfi1	3
GO:0001881	receptor recycling	39/21092	0.042367197	0.484971177	0.461304263	Snca/Pheta1	2
GO:0002823	negative regulation of adaptive immune response based on somatic recombination of immune receptors built from immunoglobulin superfamily domains	39/21092	0.042367197	0.484971177	0.461304263	Il20rb/Hfe	2
GO:0019934	cGMP-mediated signaling	39/21092	0.042367197	0.484971177	0.461304263	Pde10a/Cgas	2
GO:0045807	positive regulation of endocytosis	157/21092	0.043501024	0.484971177	0.461304263	Trf/Snca/Magi2/Hfe	4
GO:0051188	cofactor biosynthetic process	228/21092	0.043519857	0.484971177	0.461304263	Pnpo/Snca/Alas1/Slc7a11/Dlat	5
GO:0033674	positive regulation of kinase activity	467/21092	0.043822185	0.484971177	0.461304263	Tdgf1/Trf/Map3k19/Agap2/Snca/Pik3r4 /Cemip/Dlg3	8
GO:1990573	potassium ion import across plasma membrane	40/21092	0.044356511	0.484971177	0.461304263	Hcn2/Kcnj2	2
GO:0009100	glycoprotein metabolic process	308/21092	0.045902873	0.484971177	0.461304263	Pxylp1/Necab1/Dcn/B3gat2/Aatf/B3galt 1	6
GO:0044282	small molecule catabolic process	308/21092	0.045902873	0.484971177	0.461304263	Acad11/Aass/Glb1/Cemip/Ddo/Haghl	6
GO:0007200	phospholipase C-activating G protein-coupled receptor signaling pathway	95/21092	0.045908647	0.484971177	0.461304263	Hcrtr2/Plcd1/Oprd1	3
GO:0060359	response to ammonium ion	95/21092	0.045908647	0.484971177	0.461304263	Gnai2/Snca/Lypd1	3
GO:0060401	cytosolic calcium ion transport	160/21092	0.04607626	0.484971177	0.461304263	Grin2a/Snca/Ibtk/Cemip	4
GO:0034105	positive regulation of tissue remodeling	41/21092	0.046379872	0.484971177	0.461304263	Trf/Spp1	2
GO:0051281	positive regulation of release of sequestered calcium ion into cytosol	41/21092	0.046379872	0.484971177	0.461304263	Snca/Cemip	2
GO:0043648	dicarboxylic acid metabolic process	96/21092	0.047107301	0.484971177	0.461304263	Me1/Slc7a11/Ddo	3
GO:0006813	potassium ion transport	234/21092	0.047707806	0.484971177	0.461304263	Kcnk9/Hcn2/Kcnk2/Kcnh3/Kcnj2	5

GO:1901215	negative regulation of neuron death	234/21092	0.047707806	0.484971177	0.461304263	Agap2/Snca/Sncb/Ntrk2/Slc7a11	5
GO:0006732	coenzyme metabolic process	311/21092	0.047709981	0.484971177	0.461304263	Me1/Cyb5r4/Pnpo/Snca/Folh1/Dlat	6
GO:0051656	establishment of organelle localization	476/21092	0.048042656	0.484971177	0.461304263	Mlh1/Myo5c/1190002N15Rik/Syt12/Myo6/Snca/Dgki/Dctn1	8
GO:0006140	regulation of nucleotide metabolic process	97/21092	0.048321314	0.484971177	0.461304263	Guca1b/Me1/Snca	3
GO:0002820	negative regulation of adaptive immune response	42/21092	0.048436576	0.484971177	0.461304263	Il20rb/Hfe	2
GO:0009066	aspartate family amino acid metabolic process	42/21092	0.048436576	0.484971177	0.461304263	Aass/Ddo	2
GO:0031644	regulation of neurological system process	163/21092	0.048734935	0.484971177	0.461304263	Trf/Grin2a/Tmem108/Oprd1	4
GO:0035303	regulation of dephosphorylation	163/21092	0.048734935	0.484971177	0.461304263	Gnai2/Magi2/Dlg3/Sfi1	4
GO:0051186	cofactor metabolic process	478/21092	0.049015382	0.484971177	0.461304263	Me1/Cyb5r4/Pnpo/Snca/Alas1/Slc7a11/Folh1/Dlat	8
GO:0050772	positive regulation of axonogenesis	98/21092	0.049550611	0.484971177	0.461304263	Twf2/Ntrk2/Metrn	3

Supp. Table S13. List of Biological Processes (BP) at FDR 5% - hippocampus

GO ID	Description	BgRatio	pvalue	p.adjust	qvalue	geneID	Count
GO:0031282	regulation of guanylate cyclase activity	10/21092	7.96591E-06	0.012386993	0.011663772	Guca1b/Guca1a/Nos1	3
GO:0006140	regulation of nucleotide metabolic process	97/21092	5.08445E-05	0.03953156	0.03722349	Guca1b/Me1/Guca1a/Nos1/Cox7a2	5
GO:1900542	regulation of purine nucleotide metabolic process	93/21092	0.000596112	0.140031904	0.13185607	Guca1b/Guca1a/Nos1/Cox7a2	4
GO:0031279	regulation of cyclase activity	41/21092	0.000645175	0.140031904	0.13185607	Guca1b/Guca1a/Nos1	3
GO:0010753	positive regulation of cGMP-mediated signaling	10/21092	0.00074076	0.140031904	0.13185607	Cgas/Guca1a	2
GO:0051339	regulation of lyase activity	43/21092	0.000742487	0.140031904	0.13185607	Guca1b/Guca1a/Nos1	3
GO:0007128	meiotic prophase I	11/21092	0.000902946	0.140031904	0.13185607	Mlh1/Piwil2	2
GO:0051324	prophase	11/21092	0.000902946	0.140031904	0.13185607	Mlh1/Piwil2	2
GO:0061448	connective tissue development	274/21092	0.000953328	0.140031904	0.13185607	Poc1a/Adamts7/Col12a1/Arid5b/Sox6/Hes5	6

GO:0000279	M phase	12/21092	0.001080632	0.140031904	0.13185607	Mlh1/Piwil2	2
GO:0098762	meiotic cell cycle phase	12/21092	0.001080632	0.140031904	0.13185607	Mlh1/Piwil2	2
GO:0098764	meiosis I cell cycle phase	12/21092	0.001080632	0.140031904	0.13185607	Mlh1/Piwil2	2
GO:0045604	regulation of epidermal cell differentiation	52/21092	0.00129456	0.15112002	0.1422968	Cd109/Ptch2/Hes5	3
GO:0002062	chondrocyte differentiation	116/21092	0.001360566	0.15112002	0.1422968	Poc1a/Adamts7/Col12a1/Sox6	4
GO:0021781	glial cell fate commitment	14/21092	0.001481992	0.153633144	0.144663194	Sox6/Hes5	2
GO:0051216	cartilage development	205/21092	0.001600836	0.155581213	0.146497524	Poc1a/Adamts7/Col12a1/Sox6/Hes5	5
GO:0010752	regulation of cGMP-mediated signaling	18/21092	0.002465137	0.198716323	0.187114169	Cgas/Guca1a	2
GO:0030808	regulation of nucleotide biosynthetic process	66/21092	0.002571542	0.198716323	0.187114169	Guca1b/Guca1a/Nos1	3
GO:1900371	regulation of purine nucleotide biosynthetic process	66/21092	0.002571542	0.198716323	0.187114169	Guca1b/Guca1a/Nos1	3
GO:0062012	regulation of small molecule metabolic process	340/21092	0.002836471	0.198716323	0.187114169	Guca1b/Me1/Elovl5/Guca1a/Nos1/Cox 7a2	6
GO:0022403	cell cycle phase	20/21092	0.003044935	0.198716323	0.187114169	Mlh1/Piwil2	2
GO:0031281	positive regulation of cyclase activity	20/21092	0.003044935	0.198716323	0.187114169	Guca1a/Nos1	2
GO:0051349	positive regulation of lyase activity	20/21092	0.003044935	0.198716323	0.187114169	Guca1a/Nos1	2
GO:0007601	visual perception	145/21092	0.003067004	0.198716323	0.187114169	Guca1b/Bfsp2/Wfs1/Guca1a	4
GO:0003433	chondrocyte development involved in endochondral bone morphogenesis	21/21092	0.003356461	0.202224923	0.190417917	Poc1a/Col12a1	2
GO:0050953	sensory perception of light stimulus	149/21092	0.003381253	0.202224923	0.190417917	Guca1b/Bfsp2/Wfs1/Guca1a	4
GO:0003418	growth plate cartilage chondrocyte differentiation	22/21092	0.003682244	0.212069962	0.199688148	Poc1a/Col12a1	2
GO:0045682	regulation of epidermis development	78/21092	0.004126127	0.229147391	0.215768503	Cd109/Ptch2/Hes5	3
GO:1903035	negative regulation of response to wounding	83/21092	0.004910303	0.263293819	0.247921275	Cd109/Klk8/Tmprss6	3
GO:0001822	kidney development	274/21092	0.005544714	0.287401017	0.270620961	Pygo1/Wfs1/Aph1c/Arid5b/Hes5	5

GO:0003413	chondrocyte differentiation involved in endochondral bone morphogenesis	28/21092	0.005929656	0.28974529	0.272828363	Poc1a/Col12a1	2
GO:0000041	transition metal ion transport	89/21092	0.005962604	0.28974529	0.272828363	Atp2c1/Heph/Nectin1	3
GO:0035066	positive regulation of histone acetylation	29/21092	0.006351912	0.299309808	0.281834451	Nos1/Piwil2	2
GO:2000272	negative regulation of signaling receptor activity	30/21092	0.006787485	0.310427604	0.292303129	Crhbp/Socs5	2
GO:0046916	cellular transition metal ion homeostasis	95/21092	0.00714002	0.31256615	0.294316814	Tmprss6/Atp2c1/Heph	3
GO:0007602	phototransduction	31/21092	0.007236258	0.31256615	0.294316814	Guca1b/Guca1a	2
GO:0072001	renal system development	296/21092	0.007626354	0.317723617	0.299173161	Pygo1/Wfs1/Aph1c/Arid5b/Hes5	5
GO:0030810	positive regulation of nucleotide biosynthetic process	33/21092	0.008172955	0.317723617	0.299173161	Guca1a/Nos1	2
GO:1900373	positive regulation of purine nucleotide biosynthetic process	33/21092	0.008172955	0.317723617	0.299173161	Guca1a/Nos1	2
GO:2000758	positive regulation of peptidyl-lysine acetylation	33/21092	0.008172955	0.317723617	0.299173161	Nos1/Piwil2	2
GO:0006826	iron ion transport	35/21092	0.009161101	0.334296956	0.314778857	Heph/Nectin1	2
GO:0006986	response to unfolded protein	106/21092	0.009634673	0.334296956	0.314778857	Wfs1/Hspb1/Hspa1b	3
GO:0003417	growth plate cartilage development	36/21092	0.009674188	0.334296956	0.314778857	Poc1a/Col12a1	2
GO:0006739	NADP metabolic process	36/21092	0.009674188	0.334296956	0.314778857	Me1/Cyb5r4	2
GO:0043950	positive regulation of cAMP-mediated signaling	36/21092	0.009674188	0.334296956	0.314778857	Cgas/Nos1	2
GO:0048821	erythrocyte development	37/21092	0.010199805	0.344797769	0.324666574	Tmod3/Sox6	2
GO:0032102	negative regulation of response to external stimulus	323/21092	0.01085927	0.359280116	0.338303362	Cd109/Klk8/Nt5e/Tmprss6/Socs5	5
GO:0019934	cGMP-mediated signaling	39/21092	0.011288189	0.364902962	0.343597915	Cgas/Guca1a	2
GO:0042326	negative regulation of phosphorylation	461/21092	0.012038113	0.364902962	0.343597915	Cd109/Nos1/Socs5/Nprl2/Hspb1/Ibtk	6
GO:0051701	interaction with host	116/21092	0.012291784	0.364902962	0.343597915	Tusc2/Trim21/Nectin1	3
GO:0042220	response to cocaine	42/21092	0.013012015	0.364902962	0.343597915	Crhbp/Nos1	2

GO:0045981	positive regulation of nucleotide metabolic process	42/21092	0.013012015	0.364902962	0.343597915	Guca1a/Nos1	2
GO:1900544	positive regulation of purine nucleotide metabolic process	42/21092	0.013012015	0.364902962	0.343597915	Guca1a/Nos1	2
GO:1901985	positive regulation of protein acetylation	42/21092	0.013012015	0.364902962	0.343597915	Nos1/Piwil2	2
GO:0001655	urogenital system development	339/21092	0.013163049	0.364902962	0.343597915	Pygo1/Wfs1/Aph1c/Arid5b/Hes5	5
GO:0001709	cell fate determination	43/21092	0.013610528	0.364902962	0.343597915	Ptch2/Hes5	2
GO:0003416	endochondral bone growth	43/21092	0.013610528	0.364902962	0.343597915	Poc1a/Col12a1	2
GO:0043616	keratinocyte proliferation	43/21092	0.013610528	0.364902962	0.343597915	Cd109/Klk8	2
GO:0002063	chondrocyte development	44/21092	0.014220818	0.372266453	0.350531485	Poc1a/Col12a1	2
GO:0072522	purine-containing compound biosynthetic process	227/21092	0.014511589	0.372266453	0.350531485	Guca1b/Nt5e/Guca1a/Nos1	4
GO:0044848	biological phase	45/21092	0.014842778	0.372266453	0.350531485	Mlh1/Piwil2	2
GO:0098868	bone growth	45/21092	0.014842778	0.372266453	0.350531485	Poc1a/Col12a1	2
GO:0030218	erythrocyte differentiation	126/21092	0.015329422	0.378369072	0.3562778	Tmod3/Heph/Sox6	3
GO:0035966	response to topologically incorrect protein	127/21092	0.015654387	0.380352676	0.35814559	Wfs1/Hspb1/Hspa1b	3
GO:0055076	transition metal ion homeostasis	130/21092	0.016652558	0.389337206	0.366605554	Tmprss6/Atp2c1/Heph	3
GO:0031641	regulation of myelination	48/21092	0.016777644	0.389337206	0.366605554	Klk8/Hes5	2
GO:0032330	regulation of chondrocyte differentiation	48/21092	0.016777644	0.389337206	0.366605554	Adamts7/Sox6	2
GO:0060351	cartilage development involved in endochondral bone morphogenesis	51/21092	0.01881383	0.389337206	0.366605554	Poc1a/Col12a1	2
GO:0034101	erythrocyte homeostasis	137/21092	0.019117914	0.389337206	0.366605554	Tmod3/Heph/Sox6	3
GO:0009791	post-embryonic development	138/21092	0.01948573	0.389337206	0.366605554	Pygo1/Arid5b/Sox6	3
GO:0016573	histone acetylation	138/21092	0.01948573	0.389337206	0.366605554	Morf4l1/Nos1/Piwil2	3
GO:0009583	detection of light stimulus	52/21092	0.019514601	0.389337206	0.366605554	Guca1b/Guca1a	2
GO:0006879	cellular iron ion homeostasis	54/21092	0.020948606	0.389337206	0.366605554	Tmprss6/Heph	2

GO:0035065	regulation of histone acetylation	54/21092	0.020948606	0.389337206	0.366605554	Nos1/Piwil2	2
GO:0046718	viral entry into host cell	54/21092	0.020948606	0.389337206	0.366605554	Trim21/Nectin1	2
GO:0061077	chaperone-mediated protein folding	54/21092	0.020948606	0.389337206	0.366605554	Hspb1/Hspa1b	2
GO:0007224	smoothened signaling pathway	143/21092	0.021383537	0.389337206	0.366605554	Ptch2/Scube1/Hes5	3
GO:0018393	internal peptidyl-lysine acetylation	143/21092	0.021383537	0.389337206	0.366605554	Morf4l1/Nos1/Piwil2	3
GO:0006475	internal protein amino acid acetylation	146/21092	0.022569246	0.389337206	0.366605554	Morf4l1/Nos1/Piwil2	3
GO:0030856	regulation of epithelial cell differentiation	146/21092	0.022569246	0.389337206	0.366605554	Cd109/Ptch2/Hes5	3
GO:0062013	positive regulation of small molecule metabolic process	146/21092	0.022569246	0.389337206	0.366605554	Elovl5/Guca1a/Nos1	3
GO:0006457	protein folding	147/21092	0.022972324	0.389337206	0.366605554	Ppib/Hspb1/Hspa1b	3
GO:0030260	entry into host cell	57/21092	0.02317929	0.389337206	0.366605554	Trim21/Nectin1	2
GO:0044409	entry into host	57/21092	0.02317929	0.389337206	0.366605554	Trim21/Nectin1	2
GO:0051806	entry into cell of other organism involved in symbiotic interaction	57/21092	0.02317929	0.389337206	0.366605554	Trim21/Nectin1	2
GO:0051828	entry into other organism involved in symbiotic interaction	57/21092	0.02317929	0.389337206	0.366605554	Trim21/Nectin1	2
GO:0072347	response to anesthetic	57/21092	0.02317929	0.389337206	0.366605554	Crhbp/Nos1	2
GO:1903902	positive regulation of viral life cycle	57/21092	0.02317929	0.389337206	0.366605554	Ppib/Trim21	2
GO:0018394	peptidyl-lysine acetylation	154/21092	0.025903624	0.389337206	0.366605554	Morf4l1/Nos1/Piwil2	3
GO:0051926	negative regulation of calcium ion transport	61/21092	0.026298186	0.389337206	0.366605554	Gnb5/Nos1	2
GO:0070206	protein trimerization	61/21092	0.026298186	0.389337206	0.366605554	Trim21/Col6a4	2
GO:0006816	calcium ion transport	409/21092	0.027100618	0.389337206	0.366605554	Gnb5/Wfs1/Nos1/Atp2c1/Ibtk	5
GO:2000736	regulation of stem cell differentiation	62/21092	0.027103103	0.389337206	0.366605554	Sox6/Hes5	2
GO:2000756	regulation of peptidyl-lysine acetylation	63/21092	0.027917909	0.389337206	0.366605554	Nos1/Piwil2	2
GO:0001933	negative regulation of protein phosphorylation	414/21092	0.028355965	0.389337206	0.366605554	Cd109/Nos1/Socs5/Hspb1/Ibtk	5

GO:0043949	regulation of cAMP-mediated signaling	64/21092	0.02874251	0.389337206	0.366605554	Cgas/Nos1	2
GO:1901264	carbohydrate derivative transport	64/21092	0.02874251	0.389337206	0.366605554	Slc17a5/Slc35b2	2
GO:0061035	regulation of cartilage development	66/21092	0.030420729	0.389337206	0.366605554	Adamts7/Sox6	2
GO:0090278	negative regulation of peptide hormone secretion	66/21092	0.030420729	0.389337206	0.366605554	Crhbp/Nos1	2
GO:1903034	regulation of response to wounding	165/21092	0.030897152	0.389337206	0.366605554	Cd109/Klk8/Tmprss6	3
GO:0061045	negative regulation of wound healing	67/21092	0.031274163	0.389337206	0.366605554	Cd109/Tmprss6	2
GO:0007051	spindle organization	166/21092	0.031374485	0.389337206	0.366605554	Poc1a/Mlh1/Hspa1b	3
GO:0006163	purine nucleotide metabolic process	426/21092	0.031518336	0.389337206	0.366605554	Guca1b/Nt5e/Guca1a/Nos1/Cox7a2	5
GO:0002262	myeloid cell homeostasis	171/21092	0.033819296	0.389337206	0.366605554	Tmod3/Heph/Sox6	3
GO:0002088	lens development in camera-type eye	70/21092	0.033890674	0.389337206	0.366605554	Bfsp2/Nectin1	2
GO:0043627	response to estrogen	72/21092	0.035680958	0.389337206	0.366605554	Crhbp/Nos1	2
GO:0051851	modification by host of symbiont morphology or physiology	72/21092	0.035680958	0.389337206	0.366605554	Ppib/Tusc2	2
GO:0060271	cilium assembly	301/21092	0.03599202	0.389337206	0.366605554	Poc1a/Mns1/Gmnc/Ulk4	4
GO:0071772	response to BMP	176/21092	0.036360604	0.389337206	0.366605554	Adamts7/Tmprss6/Hes5	3
GO:0071773	cellular response to BMP stimulus	176/21092	0.036360604	0.389337206	0.366605554	Adamts7/Tmprss6/Hes5	3
GO:0060350	endochondral bone morphogenesis	73/21092	0.036589618	0.389337206	0.366605554	Poc1a/Col12a1	2
GO:0034620	cellular response to unfolded protein	74/21092	0.037507172	0.389337206	0.366605554	Wfs1/Hspa1b	2
GO:1901983	regulation of protein acetylation	74/21092	0.037507172	0.389337206	0.366605554	Nos1/Piwil2	2
GO:0061515	myeloid cell development	75/21092	0.038433534	0.389337206	0.366605554	Tmod3/Sox6	2
GO:0051702	interaction with symbiont	77/21092	0.040312336	0.389337206	0.366605554	Ppib/Tusc2	2
GO:0002118	aggressive behavior	10/21092	0.040499085	0.389337206	0.366605554	Crhbp	1
GO:0002934	desmosome organization	10/21092	0.040499085	0.389337206	0.366605554	Nectin1	1
GO:0003091	renal water homeostasis	10/21092	0.040499085	0.389337206	0.366605554	Wfs1	1

GO:0006995	cellular response to nitrogen starvation	10/21092	0.040499085	0.389337206	0.366605554	Nprl2	1
GO:0007220	Notch receptor processing	10/21092	0.040499085	0.389337206	0.366605554	Aph1c	1
GO:0010825	positive regulation of centrosome duplication	10/21092	0.040499085	0.389337206	0.366605554	Poc1a	1
GO:0043562	cellular response to nitrogen levels	10/21092	0.040499085	0.389337206	0.366605554	Nprl2	1
GO:0044154	histone H3-K14 acetylation	10/21092	0.040499085	0.389337206	0.366605554	Piwil2	1
GO:0045607	regulation of inner ear auditory receptor cell differentiation	10/21092	0.040499085	0.389337206	0.366605554	Hes5	1
GO:0045631	regulation of mechanoreceptor differentiation	10/21092	0.040499085	0.389337206	0.366605554	Hes5	1
GO:0046085	adenosine metabolic process	10/21092	0.040499085	0.389337206	0.366605554	Nt5e	1
GO:0048149	behavioral response to ethanol	10/21092	0.040499085	0.389337206	0.366605554	Crhbp	1
GO:0051458	corticotropin secretion	10/21092	0.040499085	0.389337206	0.366605554	Crhbp	1
GO:0051764	actin crosslink formation	10/21092	0.040499085	0.389337206	0.366605554	Baiap2l1	1
GO:0072070	loop of Henle development	10/21092	0.040499085	0.389337206	0.366605554	Hes5	1
GO:0072173	metanephric tubule morphogenesis	10/21092	0.040499085	0.389337206	0.366605554	Hes5	1
GO:0090343	positive regulation of cell aging	10/21092	0.040499085	0.389337206	0.366605554	Cgas	1
GO:1905456	regulation of lymphoid progenitor cell differentiation	10/21092	0.040499085	0.389337206	0.366605554	Hes5	1
GO:2000980	regulation of inner ear receptor cell differentiation	10/21092	0.040499085	0.389337206	0.366605554	Hes5	1
GO:0006473	protein acetylation	184/21092	0.040625775	0.389337206	0.366605554	Morf4l1/Nos1/Piwil2	3
GO:0070838	divalent metal ion transport	457/21092	0.040686115	0.389337206	0.366605554	Gnb5/Wfs1/Nos1/Atp2c1/Ibtk	5
GO:0071277	cellular response to calcium ion	78/21092	0.041264605	0.389337206	0.366605554	Crhbp/Syt12	2
GO:0072511	divalent inorganic cation transport	460/21092	0.041650992	0.389337206	0.366605554	Gnb5/Wfs1/Nos1/Atp2c1/Ibtk	5
GO:0043279	response to alkaloid	79/21092	0.042225339	0.389337206	0.366605554	Crhbp/Nos1	2

GO:0048708	astrocyte differentiation	79/21092	0.042225339	0.389337206	0.366605554	Sox6/Hes5	2
GO:0007218	neuropeptide signaling pathway	80/21092	0.043194454	0.389337206	0.366605554	Npy/Cort	2
GO:0008544	epidermis development	321/21092	0.04385706	0.389337206	0.366605554	Cd109/Ptch2/Atp2c1/Hes5	4
GO:0015748	organophosphate ester transport	81/21092	0.044171866	0.389337206	0.366605554	Stard10/Slc35b2	2
GO:0030203	glycosaminoglycan metabolic process	81/21092	0.044171866	0.389337206	0.366605554	Pxylp1/Itih3	2
GO:0032436	positive regulation of proteasomal ubiquitin-dependent protein catabolic process	81/21092	0.044171866	0.389337206	0.366605554	Socs5/Hspa1b	2
GO:0002756	MyD88-independent toll-like receptor signaling pathway	11/21092	0.044458699	0.389337206	0.366605554	Lrrfip2	1
GO:0006527	arginine catabolic process	11/21092	0.044458699	0.389337206	0.366605554	Nos1	1
GO:0009125	nucleoside monophosphate catabolic process	11/21092	0.044458699	0.389337206	0.366605554	Nt5e	1
GO:0048664	neuron fate determination	11/21092	0.044458699	0.389337206	0.366605554	Hes5	1
GO:0070944	neutrophil mediated killing of bacterium	11/21092	0.044458699	0.389337206	0.366605554	Tusc2	1
GO:0086103	G protein-coupled receptor signaling pathway involved in heart process	11/21092	0.044458699	0.389337206	0.366605554	Nos1	1
GO:0097264	self proteolysis	11/21092	0.044458699	0.389337206	0.366605554	Tmprss6	1
GO:2000615	regulation of histone H3-K9 acetylation	11/21092	0.044458699	0.389337206	0.366605554	Piwil2	1
GO:0072521	purine-containing compound metabolic process	469/21092	0.044628846	0.389337206	0.366605554	Guca1b/Nt5e/Guca1a/Nos1/Cox7a2	5
GO:0048524	positive regulation of viral process	82/21092	0.045157492	0.389337206	0.366605554	Ppib/Trim21	2
GO:0019058	viral life cycle	193/21092	0.045713446	0.389337206	0.366605554	Ppib/Trim21/Nectin1	3
GO:0044782	cilium organization	326/21092	0.045963204	0.389337206	0.366605554	Poc1a/Mns1/Gmnc/Ulk4	4
GO:0048469	cell maturation	194/21092	0.046297442	0.389337206	0.366605554	Bfsp2/Tusc2/Hes5	3
GO:0006862	nucleotide transport	12/21092	0.048402159	0.389337206	0.366605554	Slc35b2	1
GO:0043970	histone H3-K9 acetylation	12/21092	0.048402159	0.389337206	0.366605554	Piwil2	1

GO:0045625	regulation of T-helper 1 cell differentiation	12/21092	0.048402159	0.389337206	0.366605554	Socs5	1
GO:0070986	left/right axis specification	12/21092	0.048402159	0.389337206	0.366605554	Mns1	1
GO:2000674	regulation of type B pancreatic cell apoptotic process	12/21092	0.048402159	0.389337206	0.366605554	Wfs1	1
GO:1902115	regulation of organelle assembly	199/21092	0.049272929	0.389337206	0.366605554	Mns1/Nprl2/Hspa1b	3

Supp. Table S14. List of Biological Processes (BP) at FDR 5% - cerebral cortex

GO ID	Description	BgRatio	pvalue	p.adjust	qvalue	geneID	Count
GO:0003433	chondrocyte development involved in endochondral bone morphogenesis	21/21092	0.000615719	0.139820453	0.11902696	Poc1a/Col12a1	2
GO:0003418	growth plate cartilage chondrocyte differentiation	22/21092	0.000676543	0.139820453	0.11902696	Poc1a/Col12a1	2
GO:0120034	positive regulation of plasma membrane bounded cell projection assembly	106/21092	0.000846561	0.139820453	0.11902696	Mns1/Zmynd10/Rhoq	3
GO:0003413	chondrocyte differentiation involved in endochondral bone morphogenesis	28/21092	0.001099759	0.139820453	0.11902696	Poc1a/Col12a1	2
GO:0045724	positive regulation of cilium assembly	28/21092	0.001099759	0.139820453	0.11902696	Mns1/Zmynd10	2
GO:0070306	lens fiber cell differentiation	29/21092	0.001179919	0.139820453	0.11902696	Bfsp2/Ntrk3	2
GO:0003417	growth plate cartilage development	36/21092	0.001816821	0.154604889	0.131612719	Poc1a/Col12a1	2
GO:0006739	NADP metabolic process	36/21092	0.001816821	0.154604889	0.131612719	Me1/Cyb5r4	2
GO:0007601	visual perception	145/21092	0.002083607	0.154604889	0.131612719	Guca1b/Bfsp2/Cacna2d4	3
GO:0050953	sensory perception of light stimulus	149/21092	0.002251264	0.154604889	0.131612719	Guca1b/Bfsp2/Cacna2d4	3
GO:0003416	endochondral bone growth	43/21092	0.002584086	0.154604889	0.131612719	Poc1a/Col12a1	2
GO:0002063	chondrocyte development	44/21092	0.002704155	0.154604889	0.131612719	Poc1a/Col12a1	2
GO:0098868	bone growth	45/21092	0.002826812	0.154604889	0.131612719	Poc1a/Col12a1	2
GO:0060351	cartilage development involved in endochondral bone morphogenesis	51/21092	0.003616605	0.173279586	0.147510196	Poc1a/Col12a1	2

GO:0009583	detection of light stimulus	52/21092	0.003757129	0.173279586	0.147510196	Guca1b/Cacna2d4	2
GO:0120032	regulation of plasma membrane bounded cell projection assembly	183/21092	0.004019105	0.173279586	0.147510196	Mns1/Zmynd10/Rhoq	3
GO:0060491	regulation of cell projection assembly	185/21092	0.004143112	0.173279586	0.147510196	Mns1/Zmynd10/Rhoq	3
GO:1902017	regulation of cilium assembly	58/21092	0.004652825	0.183786586	0.156454641	Mns1/Zmynd10	2
GO:1902115	regulation of organelle assembly	199/21092	0.005076661	0.189973992	0.161721882	Mns1/Zmynd10/Ntrk3	3
GO:0060348	bone development	220/21092	0.00669866	0.22492988	0.191479282	Poc1a/Col12a1/Ppib	3
GO:0002088	lens development in camera-type eye	70/21092	0.006708555	0.22492988	0.191479282	Bfsp2/Ntrk3	2
GO:0007422	peripheral nervous system development	73/21092	0.007276213	0.22492988	0.191479282	Ntrk3/Egr3	2
GO:0060350	endochondral bone morphogenesis	73/21092	0.007276213	0.22492988	0.191479282	Poc1a/Col12a1	2
GO:1902117	positive regulation of organelle assembly	78/21092	0.008268942	0.231551969	0.197116562	Mns1/Zmynd10	2
GO:0031346	positive regulation of cell projection organization	462/21092	0.00847536	0.231551969	0.197116562	Mns1/Zmynd10/Ntrk3/Rhoq	4
GO:0120031	plasma membrane bounded cell projection assembly	493/21092	0.010583125	0.231551969	0.197116562	Mns1/Poc1a/Zmynd10/Rhoq	4
GO:0006140	regulation of nucleotide metabolic process	97/21092	0.012556103	0.231551969	0.197116562	Guca1b/Me1	2
GO:0060271	cilium assembly	301/21092	0.015630743	0.231551969	0.197116562	Mns1/Poc1a/Zmynd10	3
GO:0060349	bone morphogenesis	115/21092	0.017332275	0.231551969	0.197116562	Poc1a/Col12a1	2
GO:0010825	positive regulation of centrosome duplication	10/21092	0.017408049	0.231551969	0.197116562	Poc1a	1
GO:0031282	regulation of guanylate cyclase activity	10/21092	0.017408049	0.231551969	0.197116562	Guca1b	1
GO:0002062	chondrocyte differentiation	116/21092	0.017617071	0.231551969	0.197116562	Poc1a/Col12a1	2
GO:0002756	MyD88-independent toll-like receptor signaling pathway	11/21092	0.019132549	0.231551969	0.197116562	Lrrfip2	1
GO:0007128	meiotic prophase I	11/21092	0.019132549	0.231551969	0.197116562	Mlh1	1
GO:0019227	neuronal action potential propagation	11/21092	0.019132549	0.231551969	0.197116562	Ntrk3	1
GO:0048680	positive regulation of axon regeneration	11/21092	0.019132549	0.231551969	0.197116562	Ntrk3	1

GO:0051324	prophase	11/21092	0.019132549	0.231551969	0.197116562	Mlh1	1
GO:0098870	action potential propagation	11/21092	0.019132549	0.231551969	0.197116562	Ntrk3	1
GO:0044782	cilium organization	326/21092	0.019289759	0.231551969	0.197116562	Mns1/Poc1a/Zmynd10	3
GO:0009582	detection of abiotic stimulus	125/21092	0.020269212	0.231551969	0.197116562	Guca1b/Cacna2d4	2
GO:0034763	negative regulation of transmembrane transport	125/21092	0.020269212	0.231551969	0.197116562	Gnb5/Rhoq	2
GO:0009581	detection of external stimulus	126/21092	0.020573645	0.231551969	0.197116562	Guca1b/Cacna2d4	2
GO:0000279	M phase	12/21092	0.020854104	0.231551969	0.197116562	Mlh1	1
GO:0070572	positive regulation of neuron projection regeneration	12/21092	0.020854104	0.231551969	0.197116562	Ntrk3	1
GO:0070986	left/right axis specification	12/21092	0.020854104	0.231551969	0.197116562	Mns1	1
GO:0098762	meiotic cell cycle phase	12/21092	0.020854104	0.231551969	0.197116562	Mlh1	1
GO:0098764	meiosis I cell cycle phase	12/21092	0.020854104	0.231551969	0.197116562	Mlh1	1
GO:0062012	regulation of small molecule metabolic process	340/21092	0.02152968	0.231551969	0.197116562	Guca1b/Elovl5/Me1	3
GO:0006596	polyamine biosynthetic process	13/21092	0.022572718	0.231551969	0.197116562	Amd2	1
GO:0016446	somatic hypermutation of immunoglobulin genes	13/21092	0.022572718	0.231551969	0.197116562	Mlh1	1
GO:0042492	gamma-delta T cell differentiation	13/21092	0.022572718	0.231551969	0.197116562	Egr3	1
GO:0042761	very long-chain fatty acid biosynthetic process	13/21092	0.022572718	0.231551969	0.197116562	Elovl5	1
GO:0045141	meiotic telomere clustering	13/21092	0.022572718	0.231551969	0.197116562	Mlh1	1
GO:0002566	somatic diversification of immune receptors via somatic mutation	14/21092	0.024288398	0.231551969	0.197116562	Mlh1	1
GO:0030497	fatty acid elongation	14/21092	0.024288398	0.231551969	0.197116562	Elovl5	1
GO:0036159	inner dynein arm assembly	14/21092	0.024288398	0.231551969	0.197116562	Zmynd10	1
GO:0046607	positive regulation of centrosome cycle	14/21092	0.024288398	0.231551969	0.197116562	Poc1a	1
GO:0070307	lens fiber cell development	14/21092	0.024288398	0.231551969	0.197116562	Bfsp2	1

GO:0090220	chromosome localization to nuclear envelope involved in homologous chromosome segregation	14/21092	0.024288398	0.231551969	0.197116562	Mlh1	1
GO:0099151	regulation of postsynaptic density assembly	14/21092	0.024288398	0.231551969	0.197116562	Ntrk3	1
GO:0046496	nicotinamide nucleotide metabolic process	142/21092	0.025701212	0.231551969	0.197116562	Me1/Cyb5r4	2
GO:0033089	positive regulation of T cell differentiation in thymus	15/21092	0.026001147	0.231551969	0.197116562	Egr3	1
GO:0034397	telomere localization	15/21092	0.026001147	0.231551969	0.197116562	Mlh1	1
GO:0044827	modulation by host of viral genome replication	15/21092	0.026001147	0.231551969	0.197116562	Ppib	1
GO:0048304	positive regulation of isotype switching to IgG isotypes	15/21092	0.026001147	0.231551969	0.197116562	Mlh1	1
GO:1901386	negative regulation of voltage-gated calcium channel activity	15/21092	0.026001147	0.231551969	0.197116562	Gnb5	1
GO:0019362	pyridine nucleotide metabolic process	144/21092	0.026375309	0.231551969	0.197116562	Me1/Cyb5r4	2
GO:0042552	myelination	146/21092	0.027056585	0.231551969	0.197116562	Ntrk3/S100b	2
GO:0003414	chondrocyte morphogenesis involved in endochondral bone morphogenesis	16/21092	0.027710971	0.231551969	0.197116562	Col12a1	1
GO:0003429	growth plate cartilage chondrocyte morphogenesis	16/21092	0.027710971	0.231551969	0.197116562	Col12a1	1
GO:0043968	histone H2A acetylation	16/21092	0.027710971	0.231551969	0.197116562	Morf4l1	1
GO:0044794	positive regulation by host of viral process	16/21092	0.027710971	0.231551969	0.197116562	Ppib	1
GO:0046629	gamma-delta T cell activation	16/21092	0.027710971	0.231551969	0.197116562	Egr3	1
GO:0090171	chondrocyte morphogenesis	16/21092	0.027710971	0.231551969	0.197116562	Col12a1	1
GO:1904889	regulation of excitatory synapse assembly	16/21092	0.027710971	0.231551969	0.197116562	Ntrk3	1
GO:2001015	negative regulation of skeletal muscle cell differentiation	16/21092	0.027710971	0.231551969	0.197116562	S100b	1
GO:0007272	ensheathment of neurons	149/21092	0.028091837	0.231551969	0.197116562	Ntrk3/S100b	2

GO:0008360	regulation of cell shape	149/21092	0.028091837	0.231551969	0.197116562	Rhoq/S100b	2
GO:0008366	axon ensheathment	149/21092	0.028091837	0.231551969	0.197116562	Ntrk3/S100b	2
GO:0072524	pyridine-containing compound metabolic process	149/21092	0.028091837	0.231551969	0.197116562	Me1/Cyb5r4	2
GO:0003422	growth plate cartilage morphogenesis	17/21092	0.029417874	0.231551969	0.197116562	Col12a1	1
GO:0036158	outer dynein arm assembly	17/21092	0.029417874	0.231551969	0.197116562	Zmynd10	1
GO:1904469	positive regulation of tumor necrosis factor secretion	17/21092	0.029417874	0.231551969	0.197116562	Lrrfip2	1
GO:0000712	resolution of meiotic recombination intermediates	18/21092	0.031121862	0.231551969	0.197116562	Mlh1	1
GO:0006595	polyamine metabolic process	18/21092	0.031121862	0.231551969	0.197116562	Amd2	1
GO:0009309	amine biosynthetic process	18/21092	0.031121862	0.231551969	0.197116562	Amd2	1
GO:0031643	positive regulation of myelination	18/21092	0.031121862	0.231551969	0.197116562	S100b	1
GO:0042401	cellular biogenic amine biosynthetic process	18/21092	0.031121862	0.231551969	0.197116562	Amd2	1
GO:0048302	regulation of isotype switching to IgG isotypes	18/21092	0.031121862	0.231551969	0.197116562	Mlh1	1
GO:0048712	negative regulation of astrocyte differentiation	18/21092	0.031121862	0.231551969	0.197116562	Ntrk3	1
GO:0050650	chondroitin sulfate proteoglycan biosynthetic process	18/21092	0.031121862	0.231551969	0.197116562	Pxylp1	1
GO:0099150	regulation of postsynaptic specialization assembly	18/21092	0.031121862	0.231551969	0.197116562	Ntrk3	1
GO:0150052	regulation of postsynapse assembly	18/21092	0.031121862	0.231551969	0.197116562	Ntrk3	1
GO:0006733	oxidoreduction coenzyme metabolic process	160/21092	0.03202188	0.231551969	0.197116562	Me1/Cyb5r4	2
GO:0048291	isotype switching to IgG isotypes	19/21092	0.032822939	0.231551969	0.197116562	Mlh1	1
GO:1905874	regulation of postsynaptic density organization	19/21092	0.032822939	0.231551969	0.197116562	Ntrk3	1
GO:2000251	positive regulation of actin cytoskeleton reorganization	19/21092	0.032822939	0.231551969	0.197116562	Ntrk3	1

GO:0007051	spindle organization	166/21092	0.034252067	0.231551969	0.197116562	Poc1a/Mlh1	2
GO:0043271	negative regulation of ion transport	166/21092	0.034252067	0.231551969	0.197116562	Gnb5/Plcb4	2
GO:0002755	MyD88-dependent toll-like receptor signaling pathway	20/21092	0.034521109	0.231551969	0.197116562	Lrrfip2	1
GO:0010560	positive regulation of glycoprotein biosynthetic process	20/21092	0.034521109	0.231551969	0.197116562	Pxylp1	1
GO:0022403	cell cycle phase	20/21092	0.034521109	0.231551969	0.197116562	Mlh1	1
GO:0032148	activation of protein kinase B activity	20/21092	0.034521109	0.231551969	0.197116562	Ntrk3	1
GO:0046325	negative regulation of glucose import	20/21092	0.034521109	0.231551969	0.197116562	Rhoq	1
GO:0050908	detection of light stimulus involved in visual perception	20/21092	0.034521109	0.231551969	0.197116562	Cacna2d4	1
GO:0050962	detection of light stimulus involved in sensory perception	20/21092	0.034521109	0.231551969	0.197116562	Cacna2d4	1
GO:0015012	heparan sulfate proteoglycan biosynthetic process	21/21092	0.036216379	0.24065276	0.204863923	Pxylp1	1
GO:0000289	nuclear-transcribed mRNA poly(A) tail shortening	22/21092	0.037908752	0.24065288	0.204864026	Mlh1	1
GO:0000413	protein peptidyl-prolyl isomerization	22/21092	0.037908752	0.24065288	0.204864026	Ppib	1
GO:0045723	positive regulation of fatty acid biosynthetic process	22/21092	0.037908752	0.24065288	0.204864026	Elovl5	1
GO:0097107	postsynaptic density assembly	22/21092	0.037908752	0.24065288	0.204864026	Ntrk3	1
GO:1903020	positive regulation of glycoprotein metabolic process	22/21092	0.037908752	0.24065288	0.204864026	Pxylp1	1
GO:0060972	left/right pattern formation	23/21092	0.039598233	0.244743578	0.208346372	Mns1	1
GO:1903077	negative regulation of protein localization to plasma membrane	23/21092	0.039598233	0.244743578	0.208346372	Rhoq	1
GO:0006298	mismatch repair	25/21092	0.042968541	0.244743578	0.208346372	Mlh1	1
GO:0007289	spermatid nucleus differentiation	25/21092	0.042968541	0.244743578	0.208346372	Pygo1	1

GO:0010829	negative regulation of glucose transmembrane transport	25/21092	0.042968541	0.244743578	0.208346372	Rhoq	1
GO:0044788	modulation by host of viral process	25/21092	0.042968541	0.244743578	0.208346372	Ppib	1
GO:1904376	negative regulation of protein localization to cell periphery	25/21092	0.042968541	0.244743578	0.208346372	Rhoq	1
GO:0006312	mitotic recombination	26/21092	0.044649377	0.244743578	0.208346372	Mlh1	1
GO:0030201	heparan sulfate proteoglycan metabolic process	26/21092	0.044649377	0.244743578	0.208346372	Pxylp1	1
GO:0048642	negative regulation of skeletal muscle tissue development	26/21092	0.044649377	0.244743578	0.208346372	S100b	1
GO:0050927	positive regulation of positive chemotaxis	26/21092	0.044649377	0.244743578	0.208346372	Ntrk3	1
GO:1901020	negative regulation of calcium ion transmembrane transporter activity	26/21092	0.044649377	0.244743578	0.208346372	Gnb5	1
GO:1904861	excitatory synapse assembly	26/21092	0.044649377	0.244743578	0.208346372	Ntrk3	1
GO:0035987	endodermal cell differentiation	27/21092	0.04632734	0.244743578	0.208346372	Col12a1	1
GO:0050926	regulation of positive chemotaxis	27/21092	0.04632734	0.244743578	0.208346372	Ntrk3	1
GO:0060536	cartilage morphogenesis	27/21092	0.04632734	0.244743578	0.208346372	Col12a1	1
GO:1904467	regulation of tumor necrosis factor secretion	27/21092	0.04632734	0.244743578	0.208346372	Lrrfip2	1
GO:1990774	tumor necrosis factor secretion	27/21092	0.04632734	0.244743578	0.208346372	Lrrfip2	1
GO:0051307	meiotic chromosome separation	28/21092	0.048002435	0.244743578	0.208346372	Mlh1	1
GO:0042168	heme metabolic process	29/21092	0.049674668	0.244743578	0.208346372	Cyb5r4	1
GO:0046039	GTP metabolic process	29/21092	0.049674668	0.244743578	0.208346372	Rhoq	1
GO:0050654	chondroitin sulfate proteoglycan metabolic process	29/21092	0.049674668	0.244743578	0.208346372	Pxylp1	1
GO:0098698	postsynaptic specialization assembly	29/21092	0.049674668	0.244743578	0.208346372	Ntrk3	1

GO:0006302	double-strand break repair	204/21092	0.049694819	0.244743578	0.208346372	Mlh1/Morf4l1	2

Discussion and future perspectives

High-throughput analysis of genomes and molecular phenotype characterization have driven in recent time the force of discovery of causative variants for a multitude of Mendelian diseases. Clinical implementation of methodologies like whole exome sequencing and whole genome sequencing, more in general defined as Next-Generation Sequencing (NGS) technologies, have enhanced a lot the successful discovery of novel genes responsible for intellectual disability (ID), thus providing a genetic diagnosis in 25-40% of individuals with ID and neurodevelopmental disorders[1-5]. Not only NGS has been advantageous in increasing the number of genes linked to a certain condition; as the technologies became more advanced they also decreased the time to diagnosis and provided more refined diagnoses than possible with previous approaches[6-8]. Comprehensively, the patients, and the scientific community in general, have benefited a lot of the NGS as a diagnostic practice[9-13]. Nonetheless, there is yet a discreet number of ID-affected subjects that remained with an unexplained etiology; studies report that majority of these may have a genetic basis in genes remaining to be discovered[1,14]. Recently, growing evidence pointed to genes encoding G-protein β subunits as causative of a group of disorders characterized by cognitive impairment, developmental delay, cardiac anomalies and vision problems[15-36].

The work I carried on during my doctorate focused on one of these G-protein β subunits; specifically, as reported in the three chapters of this thesis, it concerned the discovery of *GNB5* ($G\beta_5$) variants and addressed the question of interpreting the gene involvement into pathological mechanisms of IDDCA syndrome. The approach touched different, and sometimes complementary, layers of complexity spanning from human to fish to mouse, and from phenotyping to physiology to molecular aspects.

Chapters 1 and 2 reported the investigations concerning the novel identified syndrome, recently christened IDDCA (Intellectual Developmental Disorder with Cardiac Arrhythmia), and in particular the detection of variants in *GNB5* gene as causative of phenotypic manifestations. Chapter 3 addressed phenotypic and molecular characterization of a mouse model lacking *Gnb5* gene.

In Chapter 1 we presented the clinical and molecular characterization of a number of patients with an undiagnosed disease. We investigated these patients by whole exome sequencing

that lead to the identification of potentially causative variations in *GNB5* gene, encoding the subunit β_5 of the heterotrimeric GTP-binding proteins (G proteins). *GNB5* is primarily expressed in brain where it forms complexes with members of the R7 regulator family of RGS proteins (Regulators of G-protein Signaling)[37,38], and is essential for the structural integrity and proteolytic stability of R7 RGS complexes, which function as negative regulators of G protein-coupled receptor (GPCR) signaling.

When we performed exome sequencing very little was known about possible involvement of *GNB5* gene in human pathology. Reassuringly, data about genetically modified model organisms lacking the orthologue *GNB5* were available. Genetic manipulation of the gene *eat-11*, encoding GPB-2, an orthologue of the human Gβ_5 protein in *Caenorhabditis elegans*, resulted in behavioural defects, including delayed egg laying, locomotion, and pharyngeal pumping[39]. Moreover, two RGS homologues, EGL-10 and EAT-16, were shown to modulate the GPB-2 mediated signalling[40]. Knock-out of the mouse *Gnb5* gene was shown to affect brain development and to cause neurobehavioral abnormalities, including impaired gait, motor learning, and hyperactivity[41]. Other studies using *Gnb5* knock-out mice have supported the role of Gnb5 in stabilizing the RGS proteins in the context of defective visual adaptation and altered functioning of retinal bipolar cells[42-44]. Finally, using *Rgs6*-null mice Posokhova and colleagues showed that the cardiac Rgs6/Gβ5 complex modulates the timing of parasympathetic influence on atrial myocytes and heart rate in mice[45].

The challenge of this project, which was approached with a combination of literature mining, variants modelling through analysis of the 3D crystal structure, and *in vivo* zebrafish phenotyping, was in fact to determine the genetic contribution of *GNB5* gene to phenotypic manifestations. On one hand our results supported the variants pathogenicity through *in vitro* and *in silico* evidence. On the other hand, generation of zebrafish larvae lacking both *gnb5a* and *gnb5b* paralogs showed that fish have similar symptoms to those of the patients: the zebrafish had problems with eye movement and problems with their muscles. Moreover, pharmacological stimulation of the parasympathetic branch of the autonomic nervous system showed an abnormal response causing a strong reduction of the fish heartbeat. Altogether our findings provided functional evidence for a direct role of *GNB5* in IDDCA syndrome and its related phenotypic traits. Furthermore, the analysis revealed the existence of genotype-phenotype correlation: carriers of the S81L variant were affected by a milder form of IDDCA; in contrast loss of function alleles correlated with severe end of the disease spectrum.

In Chapter 2, the study of a 2 years-old boy led to the discovery of two yet-unreported loss of function variants, each inherited from one parent in compound heterozygosity. Besides expanding the number of individuals presenting with IDDCA syndrome and the disease spectrum, we described two novel variants and modeled the consequences of one of them using 3D structure of GNB5 complexed with RGS9. This report emphasizing the phenotypic consequences of GNB5 deficiency, further corroborates the association between loss of function alleles with severe manifestation of the syndrome.

The results outlined in Chapter 1 and 2 were further supported by additional studies analyzing extended consanguineous families and identifying a striking phenotypic overlap with the affected individuals we described[25,29,30,34]. One of these reports revealed that mutant form of Gβ5 (*GNB5*-S81L) resulted in decreased protein expression and had a significantly impaired activity in terminating dopamine-elicited responses[30].

Still we have little understanding about the disease mechanism underlying the syndrome and there are no treatment options available.

Our findings in *gnb5* zebrafish model provided some indications about pathological mechanism; concordantly, a recent study using induced pluripotent stem cells (iPSCs) differentiated towards cardiomyocytes and engineered to carry the S81L variant reported that augmented cholinergic response – through the action of gated inward rectifier potassium (GIRK) - underpins the cardiac manifestation of IDDCA patients[46]. Treatment of both iPSCs and zebrafish larvae with selective GIRK inhibitors rescued the pharmacological-induced bradycardia[46].

Considering all these evidences, and given the *GNB5* function, we hypothesized that the pathogenic mechanism, and thus the clinical manifestations, of IDDCA relies on the destabilization of the macromolecular complex composed of muscarinic receptors mediating GPCRs signaling in the sinoatrial node of the heart, GNB5, and R7-RGS (particularly RGS6) resulting in impaired activity of GIRK and other ion channels.

Veerman and colleagues [46] investigated the effect of the S81L *in vitro* and in a zebrafish model. In contrast, we reasoned that the mouse would be a better tool to study the consequences of a human neurodevelopmental syndrome. To address the effect of *Gnb5* loss, and to mimick the severe IDDCA form, we employed the previously established *Gnb5* knock-out mouse

model and characterized the cardiac phenotype – never studied before.

In Chapter 3 we presented the results of this characterization and we showed that *Gnb5* is very important in controlling the parasympathetic process that brings the heart rate down during rest. Our results demonstrated that when *Gnb5* is defective, cholinergic sensitivity is significantly enhanced and causes severe bradycardia upon parasympathetic stimulation. Loss of functional *Gnb5* also resulted in increased number of arrhythmias, emphasizing that *Gnb5* plays an important role in cardiac sinus conduction and in controlling the regular heartbeat. Finally, we showed that the smaller *Gnb5* knock-out mice, presenting a smaller heart, compensate this feature by increasing the cardiac function. These data were also strengthened at molecular level by the transcriptome profiling of atria and ventricles that demonstrated modifications of transcripts encoding for proteins important in cardiac contraction, along with reduced ventricular expression of genes required for development of pacemaker cells.

We are well aware that the admixture of many cell types – mainly neural and muscle cells - in the atria and ventricles might pose a challenge to our results interpretation. Also, we performed bulk transcriptomics which interrogates average gene expression, so with our approach we might have missed the stochasticity and specificity of expression patterns. However, we reason that the tissues we tested represent disease-relevant tissues, and even though we could not get cell-specific expression, at the level of sinus-atrial and atrioventricular nodes of the heart, which are involved in setting the rhythm of the heart for example, this work shed light in the understanding of global transcriptional changes and gene expression patterns across the whole tissues.

Our transcriptome data also suggested compensation mechanisms that could attenuate the symptoms of *GNB5* ablation. Specifically, we observed that some of the known *Gnb5* RGS partners, e.g. *Rgs6*, as well as some GNB subunits, e.g. *Gnb3*, were overexpressed in knock-out mice tissues. The above-cited link between *GNB5* and *RGS6* suggest that they could present overlapping phenotypes when their function is altered. Furthermore, the RGS/GNB5 interactions have a functionally-relevant nature at neural and cardiac levels; therefore, we researched for individuals with variations in the genes encoding the R7-RGS genes (*RGS6*, *RGS7*, *RGS9* and *RGS11*). Through literature search and data sharing with GeneMatcher[47] we have identified 2 individuals, one with mutation in *RGS6*[48] and one with mutation in *RGS11*. Neuropsychiatric (ID, ASD, developmental delay) and visual phenotypes overlapped with

IDDCA syndrome. Cardiac manifestations were never checked in those individuals, and we are currently collaborating with clinicians to possibly investigate whether any, even mild, cardiac phenotype is present in these individuals. The neuropsychiatric symptoms may represent a vague set of generalized symptoms *per se*; we reason that the co-occurrence of those with visual and cardiac manifestations represent a quite unique combination in disorders associated to Gβ proteins.

Mindful of the abovementioned transcriptome results, we very recently sequenced the RNAs from three different brain regions dissected from the same animals used for the heart transcriptomes. We focused on cortex, hippocampus, and cerebellum, involved in higher cognitive function, formation of long-term and spatial memories, motor control and language process, respectively, and representing disease-relevant tissues for the IDDCA pathology. Also, cerebellar and hippocampal anomalies were documented in *Gnb5* knock-out pups, and quantitative RT-PCR along with microarray data previously indicated altered expression levels of genes implicated in neuronal development and function, such as *Grid2* (glutamate ionotropic receptor, delta 2) and *Synpo* (synaptopodin), among others, respectively involved in motor coordination and Purkinje cell synapse formations, and synaptic plasticity, as well as *Guca1a* and *Guca1b*[41], calcium-binding protein activating photoreceptor guanylate cyclases. *Guca1a* and *Guca1b* were also significantly differentially expressed in our brain transcriptome, both in hippocampus and cerebellum of *Gnb5* knock-out mice. *Synpo* showed a trend of increased expression in the hippocampus. A subset of additional differentially expressed genes included *Grin2a*, *Snca*, *Kcnj2*, *Slc7a11*, and *Gnai2* (at FDR of 5%).
Overall, we observed that differentially expressed genes between knock-out and control mice enriched for categories like visual perception, phototransduction, guanylate cyclase activity, and regulator of signaling receptors (in hippocampus), regulation of excitatory postsynaptic membrane potential, regulation of neurotransmitters secretion, learning and synapse organization, regulation of inositol 3-phosphate, regulation of cAMP-mediated signaling (in cerebellum), and sensory perception of light stimuli and lens development (in cortex). This preliminary analysis reveals processes relevant to the neuropsychiatric phenotype observed in IDDCA individuals, suggesting that although more prominent changes may be expected at protein level, altered expression of relevant genes may play a role. Of note, in brain we do not observe a striking compensatory expression of *RGS* genes, possibly suggesting that the

brain is less able to compensate dysregulated mechanisms.

While the transcriptome results are very interesting to us, future studies will inspect, and possibly validate, those findings by looking at protein levels (differential proteomics by mass spectrometry) and investigate the changes that the loss of *Gnb5* activity may cause. This task will reveal whether more outstanding changes may be detected at protein level as well as whether the transcriptome changes are due to an indirect effect or not.

As reported in this thesis and in[46] we hypothesize that GIRK channels or components of the signaling regulating the GIRK channels may be potential IDDCA therapeutic targets. Veerman and colleagues, preliminary showed that GIRK channel blockers help to rescue the cardiac phenotype. Therefore, we plan to test in the *Gnb5* mouse model the effect of GIRK inhibitors, including Tertiapin Q[49], NTC-801[50] and NIP-142[51], on the cardiac manifestations and verify whether the same intervention might also rescue some of the neurological manifestations of IDDCA. Moreover, since strategies other than inhibiting GIRK channels could also be effective in resolving or ameliorating the neurological and heart symptoms of the IDDCA disorder, and given that a combination of drugs may be the best way of confronting with this disorder, another approach to follow could be testing a battery of drugs that act via the GPCRs, the most intensively studied drug target family. There are currently roughly 500 drugs (~34% of all drugs approved by the FDA, US Food and Drug Administration) that act on hundred unique GPCR targets. Approximately 321 agents are currently in clinical trials, of which ~20% target 66 potentially novel GPCR targets that do not currently have an approved drug[52]. For these tests, GPCR drug libraries, for examples the Prestwich collection (http://prestwickchemical.fr/libraries-screening-lib-pcl.html), would be needed and drug optimization program could be assessed in cells, fish and mice for further characterization and optimal dosing. The advantage of using a GPCR drug library including compounds already approved by the FDA and the EMA (European Medicines Agency), is that these compounds could be tested immediately in patients.

Finally, looking beyond the *Gnb5*-null model, our mouse study (Chapter 3) revealed that *Gnb5* heterozygous mice had bigger heart; consequently, their ventricles contained more blood and their stroke volume and cardiac output were higher (Figures 3F-G, Chapter 3). However, their cardiac function (ejection fraction and fractional shortening, Figures 3D-E, Chapter 3)

remained unchanged, suggesting that the higher cardiac function depended on animal size. Notably, heterozygous mice increased their body weight by 6 months of age (Figure 2C, Chapter 3), a result that confirms previous findings[53], showing that *Gnb5* haploinsufficiency is also linked to altered metabolism and behavior. Additionally, human genetics studies established a link between obesity and quantitative trait locus containing *RGS7* and *RGS6* genes[54-57].

Based on this, we questioned whether haploinsufficiency of the *GNB5* gene could be associated to some subtle phenotype mimicking partial loss of R7 protein expression or function in human. We prepared a survey aiming at assessing general health conditions, body weight, and metabolic features in human carriers of *GNB5* variants in the heterozygous state and extended it to all parents of the IDDCA-patients cohort. We collected information of 8 *GNB5* heterozygous carriers and found that their general health status was unremarkable; however, 5/8 had BMI (Body Mass Index) higher than 25, and so were classified as "pre-obese" (4/5) or with "obesity class I" (1/5) as in BMI classification (WHO). It is difficult to disentangle whether these overweight and obesity states are due to genetic determinant, e.g. *GNB5* contribution, or if they are environmental-related. Therefore, for the moment we are cautious in stating that *GNB5* haploinsufficiency is associated to increased body weight, but we retain this as an observation that would need more evidence. Being able to recruit more subjects in the study may be helpful to unravel a significant signal.

To conclude, IDDCA syndrome represents a unique combination of phenotypic manifestations. *De facto* co-morbidities of ID, vision and cardiac conduction anomalies are not well known. Expanding genetic and molecular data through NGS and gathering phenotypic information could be a starting point towards identification of frequencies of these pathogenic commonalities.

Thesis discussion's references

1. Anazi, S. *et al.* Clinical genomics expands the morbid genome of intellectual disability and offers a high diagnostic yield. *Mol Psychiatry* **22**, 615-624 (2017).
2. Lionel, A.C. *et al.* Improved diagnostic yield compared with targeted gene sequencing panels suggests a role for whole-genome sequencing as a first-tier genetic test. *Genet Med* **20**, 435-443 (2018).
3. Martinez, F. *et al.* High diagnostic yield of syndromic intellectual disability by targeted next-generation sequencing. *J Med Genet* **54**, 87-92 (2017).
4. Redin, C. *et al.* Efficient strategy for the molecular diagnosis of intellectual disability using targeted high-throughput sequencing. *J Med Genet* **51**, 724-36 (2014).
5. Vrijenhoek, T. *et al.* Whole-exome sequencing in intellectual disability; cost before and after a diagnosis. *Eur J Hum Genet* **26**, 1566-1571 (2018).
6. Dillon, O.J. *et al.* Exome sequencing has higher diagnostic yield compared to simulated disease-specific panels in children with suspected monogenic disorders. *Eur J Hum Genet* **26**, 644-651 (2018).
7. Dixon-Salazar, T.J. *et al.* Exome sequencing can improve diagnosis and alter patient management. *Sci Transl Med* **4**, 138ra78 (2012).
8. Lee, H. *et al.* Clinical exome sequencing for genetic identification of rare Mendelian disorders. *JAMA* **312**, 1880-7 (2014).
9. Farwell, K.D. *et al.* Enhanced utility of family-centered diagnostic exome sequencing with inheritance model-based analysis: results from 500 unselected families with undiagnosed genetic conditions. *Genet Med* **17**, 578-86 (2015).
10. Fernandez-Marmiesse, A., Gouveia, S. & Couce, M.L. NGS Technologies as a Turning Point in Rare Disease Research , Diagnosis and Treatment. *Curr Med Chem* **25**, 404-432 (2018).
11. Wright, C.F. *et al.* Genetic diagnosis of developmental disorders in the DDD study: a scalable analysis of genome-wide research data. *Lancet* **385**, 1305-14 (2015).
12. Yang, Y. *et al.* Clinical whole-exome sequencing for the diagnosis of mendelian disorders. *N Engl J Med* **369**, 1502-11 (2013).
13. Yang, Y. *et al.* Molecular findings among patients referred for clinical whole-exome sequencing. *JAMA* **312**, 1870-9 (2014).
14. Vissers, L.E., Gilissen, C. & Veltman, J.A. Genetic studies in intellectual disability and related disorders. *Nat Rev Genet* **17**, 9-18 (2016).
15. Arno, G. *et al.* Recessive Retinopathy Consequent on Mutant G-Protein beta Subunit 3 (GNB3). *JAMA Ophthalmol* **134**, 924-7 (2016).
16. Endo, W. *et al.* Phenotype-genotype correlations in patients with GNB1 gene variants, including the first three reported Japanese patients to exhibit spastic diplegia, dyskinetic quadriplegia, and infantile spasms. *Brain Dev* (2019).
17. Fukuda, T. *et al.* Exome reports A de novo GNB2 variant associated with global developmental delay, intellectual disability, and dysmorphic features. *Eur J Med Genet*, 103804 (2019).
18. Hemati, P. *et al.* Refining the phenotype associated with GNB1 mutations: Clinical data on 18 newly identified patients and review of the literature. *Am J Med Genet A* **176**, 2259-2275 (2018).

19. Jones, H.F. *et al.* Myoclonus-dystonia caused by GNB1 mutation responsive to deep brain stimulation. *Mov Disord* **34**, 1079-1080 (2019).
20. Kuss, J. *et al.* Familial Sinus Node Disease Caused by a Gain of GIRK (G-Protein Activated Inwardly Rectifying K(+) Channel) Channel Function. *Circ Genom Precis Med* **12**, e002238 (2019).
21. Lassuthova, P. *et al.* Confirmation of the GNB4 gene as causal for Charcot-Marie-Tooth disease by a novel de novo mutation in a Czech patient. *Neuromuscul Disord* **27**, 57-60 (2017).
22. Lodder, E.M. *et al.* GNB5 Mutations Cause an Autosomal-Recessive Multisystem Syndrome with Sinus Bradycardia and Cognitive Disability. *Am J Hum Genet* **99**, 786 (2016).
23. Lohmann, K. *et al.* Novel GNB1 mutations disrupt assembly and function of G protein heterotrimers and cause global developmental delay in humans. *Hum Mol Genet* **26**, 1078-1086 (2017).
24. Malerba, N., De Nittis, P. & Merla, G. The Emerging Role of Gbeta Subunits in Human Genetic Diseases. *Cells* **8**(2019).
25. Malerba, N. *et al.* A NGS-Targeted Autism/ID Panel Reveals Compound Heterozygous GNB5 Variants in a Novel Patient. *Front Genet* **9**, 626 (2018).
26. Miura, S. *et al.* A novel missense variant (Gln220Arg) of GNB4 encoding guanine nucleotide-binding protein, subunit beta-4 in a Japanese family with autosomal dominant motor and sensory neuropathy. *Eur J Med Genet* **60**, 474-478 (2017).
27. Peng, J. *et al.* Novel West syndrome candidate genes in a Chinese cohort. *CNS Neurosci Ther* **24**, 1196-1206 (2018).
28. Petrovski, S. *et al.* Germline De Novo Mutations in GNB1 Cause Severe Neurodevelopmental Disability, Hypotonia, and Seizures. *Am J Hum Genet* **98**, 1001-1010 (2016).
29. Poke, G. *et al.* The epileptology of GNB5 encephalopathy. *Epilepsia* **60**, e121-e127 (2019).
30. Shamseldin, H.E. *et al.* GNB5 mutation causes a novel neuropsychiatric disorder featuring attention deficit hyperactivity disorder, severely impaired language development and normal cognition. *Genome Biol* **17**, 195 (2016).
31. Soong, B.W. *et al.* Exome sequencing identifies GNB4 mutations as a cause of dominant intermediate Charcot-Marie-Tooth disease. *Am J Hum Genet* **92**, 422-30 (2013).
32. Steinrucke, S. *et al.* Novel GNB1 missense mutation in a patient with generalized dystonia, hypotonia, and intellectual disability. *Neurol Genet* **2**, e106 (2016).
33. Szczaluba, K. *et al.* Novel GNB1 de novo mutation in a patient with neurodevelopmental disorder and cutaneous mastocytosis: Clinical report and literature review. *Eur J Med Genet* **61**, 157-160 (2018).
34. Turkdogan, D., Usluer, S., Akalin, F., Agyuz, U. & Aslan, E.S. Familial early infantile epileptic encephalopathy and cardiac conduction disorder: A rare cause of SUDEP in infancy. *Seizure* **50**, 171-172 (2017).
35. Vernon, H. *et al.* Intellectual developmental disorder with cardiac arrhythmia syndrome in a child with compound heterozygous GNB5 variants. *Clin Genet* **93**, 1254-1256 (2018).

36. Vincent, A. *et al.* Biallelic Mutations in GNB3 Cause a Unique Form of Autosomal-Recessive Congenital Stationary Night Blindness. *Am J Hum Genet* **98**, 1011-1019 (2016).
37. Cabrera, J.L., de Freitas, F., Satpaev, D.K. & Slepak, V.Z. Identification of the Gbeta5-RGS7 protein complex in the retina. *Biochem Biophys Res Commun* **249**, 898-902 (1998).
38. Zhang, J.H. & Simonds, W.F. Copurification of brain G-protein beta5 with RGS6 and RGS7. *J Neurosci* **20**, RC59 (2000).
39. Robatzek, M., Niacaris, T., Steger, K., Avery, L. & Thomas, J.H. eat-11 encodes GPB-2, a G beta(5) ortholog that interacts with G(o)alpha and G(q)alpha to regulate C-elegans behavior. *Current Biology* **11**, 288-293 (2001).
40. Chase, D.L., Patikoglou, G.A. & Koelle, M.R. Two RGS proteins that inhibit Galpha(o) and Galpha(q) signaling in C. elegans neurons require a Gbeta(5)-like subunit for function. *Curr Biol* **11**, 222-31 (2001).
41. Zhang, J.H. *et al.* Knockout of G protein beta5 impairs brain development and causes multiple neurologic abnormalities in mice. *J Neurochem* **119**, 544-54 (2011).
42. Chen, C.K. *et al.* Instability of GGL domain-containing RGS proteins in mice lacking the G protein beta-subunit Gbeta5. *Proc Natl Acad Sci U S A* **100**, 6604-9 (2003).
43. Krispel, C.M., Chen, C.K., Simon, M.I. & Burns, M.E. Prolonged photoresponses and defective adaptation in rods of Gbeta5-/- mice. *J Neurosci* **23**, 6965-71 (2003).
44. Rao, A., Dallman, R., Henderson, S. & Chen, C.K. G beta 5 is required for normal light responses and morphology of retinal ON-bipolar cells. *Journal of Neuroscience* **27**, 14199-14204 (2007).
45. Posokhova, E., Wydeven, N., Allen, K.L., Wickman, K. & Martemyanov, K.A. RGS6/G beta 5 Complex Accelerates I-KACh Gating Kinetics in Atrial Myocytes and Modulates Parasympathetic Regulation of Heart Rate. *Circulation Research* **107**, 1350-1354 (2010).
46. Veerman, C.C. *et al.* Genetic variation in GNB5 causes bradycardia by augmenting the cholinergic response via increased acetylcholine-activated potassium current (I-K,I-ACh). *Disease Models & Mechanisms* **12**(2019).
47. Sobreira, N., Schiettecatte, F., Valle, D. & Hamosh, A. GeneMatcher: a matching tool for connecting investigators with an interest in the same gene. *Hum Mutat* **36**, 928-30 (2015).
48. Chograni, M., Alkuraya, F.S., Maazoul, F., Lariani, I. & Chaabouni-Bouhamed, H. RGS6: a novel gene associated with congenital cataract, mental retardation, and microcephaly in a Tunisian family. *Invest Ophthalmol Vis Sci* **56**, 1261-6 (2014).
49. Mesirca, P. *et al.* G protein-gated IKACh channels as therapeutic targets for treatment of sick sinus syndrome and heart block. *Proc Natl Acad Sci U S A* **113**, E932-41 (2016).
50. Machida, T. *et al.* Effects of a highly selective acetylcholine-activated K+ channel blocker on experimental atrial fibrillation. *Circ Arrhythm Electrophysiol* **4**, 94-102 (2011).
51. Tanaka, H. & Hashimoto, N. A multiple ion channel blocker, NIP-142, for the treatment of atrial fibrillation. *Cardiovasc Drug Rev* **25**, 342-56 (2007).
52. Hauser, A.S., Attwood, M.M., Rask-Andersen, M., Schioth, H.B. & Gloriam, D.E. Trends in GPCR drug discovery: new agents, targets and indications. *Nat Rev Drug Discov* **16**, 829-842 (2017).

53. Wang, Q. *et al.* Targeted deletion of one or two copies of the G protein beta subunit G beta 5 gene has distinct effects on body weight and behavior in mice. *Faseb Journal* **25**, 3949-3957 (2011).
54. Aissani, B. *et al.* A quantitative trait locus for body fat on chromosome 1q43 in French Canadians: linkage and association studies. *Obesity (Silver Spring)* **14**, 1605-15 (2006).
55. Aissani, B., Wiener, H.W. & Zhang, K. Fine Mapping of the Body Fat QTL on Human Chromosome 1q43. *PLoS One* **11**, e0153794 (2016).
56. Kim, H.J., Min, J.Y. & Min, K.B. Interaction between the RGS6 gene and psychosocial stress on obesity-related traits. *Endocr J* **64**, 357-362 (2017).
57. Sibbel, S.P. *et al.* RGS6 variants are associated with dietary fat intake in Hispanics: the IRAS Family Study. *Obesity (Silver Spring)* **19**, 1433-8 (2011).